Abstract

Bin-Salamon, Sofi. Synthesis and Characterization of Electronically Labile Molecules. (Under the direction of David A. Shultz and Daniel L. Feldheim.)

Valence tautomers are molecules that change electronic states as a function of an external stimulus such as temperature, pressure and light. The purpose of the dissertation research has been to explore different aspects of the behavior of valence tautomeric molecules. The research work is divided into three exploratory avenues: 1) Intermolecular contributions to the behavior of surface-confined valence tautomers, 2) the effects of structural changes to the intramolecular coupling in dinuclear valence tautomeric systems, and 3) the synthetic control of the intramolecular delocalization of the semiquinonate-catecholate donor-acceptor pair. For the first project it was discovered that intermolecular interactions in surface-confined valence tautomers change the thermodynamic parameters of the valence tautomeric conversion. The second project yielded results that conclusively demonstrated that large spin-density distribution on the ligands of valence tautomers and small through-bond distance between valence tautomeric centers are necessary in order to electronically couple multinuclear valence tautomers. Finally, it was shown that it is possible to synthetically control the delocalization of the semiquinate-catecholate donor-acceptor pair of the low-temperature mixed-valent valence tautomeric state by substituting the bipyridine counterligand with different functional groups.

Synthesis and Characterization of Electronically Labile Molecules

By

Sofi Bin-Salamon

A dissertation submitted to the graduate faculty of North Carolina State University in partial fulfillment of the requirements for the degree of Doctor of Philosophy

Chemistry

Raleigh, North Carolina
2005

Approved by:

David A. Shultz Chair of the Advisory Committee	Daniel L. Feldheim Co-Chair of the Advisory Committee
Mike H. Whangbo	T. Brent Gunnoe
James D. Martin	

Dedication

To all the women I've ever loved.

Biography

Dr. Sofi Bin-Salamon

Sofi Bin-Salamon is an American born abroad in Kuala Lumpur, Malaysia, and was educated to Form 12 in the British educational system before migrating to the US. Once there he discovered that American teenage life was nothing like Beverly Hills 90210 and thus he worked really hard through Charlotte County High School in Virginia and in 1996 graduated with high honors. He then enrolled in Hampden-Sydney College in Virginia and "discovered" his place in life. In 2000 Sofi graduated with a bachelors of science in chemistry and was accepted as a graduate student at North Carolina State University. Sofi led an *interesting* existence at NC State that culminated with a masterful defense of his doctoral dissertation in chemistry. Currently the National Academies has seen fit to award Sofi an associateship to pursue research in chemistry at the US Naval Research Laboratory in Washington D.C. May his journey never grow dull.

Sofi's favorite inspirational quote has and always will be: "Been there, crushed that."

Acknowledgements

Truly there is not enough space to mention everyone who deserves acknowledgement. First and foremost I would like to thank my advisors David A. Shultz and Daniel L. Feldheim for their research support and guidance. I would like to express my gratitude to the following individuals who have helped me grow intellectually and professionally at NC State University: Edmond Bowden, Carl L. Bumgardner, Mike H. Whangbo, James D. Martin, T. Brent Gunnoe, Jerry L. Whitten, Dennis Wertz, Stefan Franzen, Robert Warren, Scott H. Brewer, Simon Lappi, Kathryn E. Preuss and Marty Lemaire.

The following individuals provided the foundation for my professional success at Hampden-Sydney, NC State and beyond: Herbert J. Sipe, Kevin M. Dunn, Paul H. Mueller, Bill Anderson, William Porterfield, the late Andrew Prophett, and especially my high school guidance counselor Mrs. Kelsaw, who more than any of the individuals mentioned provided the greatest foundation by helping me get started on my journey.

Thirdly I would like to thank the friends that have helped me along the way. On the top of that list are Chiamaka Agbasi-Porter and Angela Allen. Then there is Tashni-Ann Coote, Crissy Williams, Brenda Burgess, Lina Gugliotti, Dana DiDonato and my best friends Paul Sparzak and Seth Sanusi.

Finally I must thank the most important individuals of all, my family. *Terima kasih ibu dan bapa*, for if it weren't for you then truly I would not be where I am today. I would like to thank Majdah, whom I am very proud of, for putting up with me and supporting me through my time at NC State. Furthermore I would like to thank little Kareem, whom I am also proud of, for doing his part in helping me out.

Table of Contents

List of Figures ix

List of Tables xiv

List of Schemes xv

General Introduction 1

Chapter 1: General Introduction to Electron Behavior and Electronic States

1.1 Introduction 2

1.2 Classical Description of Spin-Magnetic Dipole Moment 3

1.3 Classical Description of Orbital Magnetic Dipole Moment 5

1.4 Brief Quantum Mechanical Description of Angular Momenta and Magnetic Moments 6

1.5 Coupling Between Spin and Orbital Angular Momenta 12

1.6 Pauli's Exclusion Principle 12

1.7 Hund's Rules 13

1.8 Crystal Field Splitting and Spin-orbit Coupling in Transition Metals 21

1.9 Jahn-Teller Instability and The Origin of Zero-Field Splitting in Transition Metals 26

1.10 Detailed Treatment of Second-Order Spin-orbit Coupling in Mn^{3+} 29

1.11 Different Perturbations in Context 37

1.12 References 39

Chapter 2: Molecule-Based Magnetism

2.1 Description of Different Magnetic Behavior in the Bulk 40

2.2 Intramolecular Exchange Coupling in Molecular Systems 41

2.3 Mixing Closed-Shell Excited States through Configuration Interaction 45
2.4 Exchange Coupling in Transition Metal Complexes 55
2.5 Magnetic Susceptibility of a System with a Single Unpaired Spin 58
2.6 The Van-Vleck Relationship 61
2.7 References 65

Chapter 3: Valence-Tautomerism

3.1 Ortho-Quinones as Organic Spin-Carriers 66
3.2 Intramolecular Donor-Acceptor Model of Valence-Tautomeric Behavior 68
3.3 Observed Thermodynamic Changes 71
3.4 Observed Magnetic Changes 76
3.5 Influences of the Counterligand on Valence Tautomerism 77
3.6 Influences of the Chemical Environment on Valence Tautomerism 80
3.7 Valence Tautomerism as an Electronic Transition and Comparisons to Fe Spin-Crossover Behavior 80
3.8 Intervalence Charge-Transfer (The Robin-Day Model and the Hush Prediction) 82
3.9 References 86

Chapter 4: Does Surface Confinement Affect Valence Tautomerism?

4.1 Introduction 87
4.2 Synthesis of Surface Bound Valence Tautomer 90
4.3 Nanoparticle Characterization 92
4.4 Characterization of Surface Bound Valence Tautomer 93
4.5 Infrared Spectroscopy Comparisons 96

4.6 Variable Temperature IR and SVD Analysis 98

4.7 Attempted Alternate Pathways 106

4.8 Surface Monolayer Cluster Synthesis 106

4.9 Surface Monolayer Synthesis and Characterization 109

4.10 Conclusion 111

4.11 Experimental 112

4.12 References 118

Chapter 5: Controlling Donor-Acceptor Interactions through Back Bonding

5.1 Introduction 119

5.2 Synthesis of **1** 129

5.3 Synthesis of **2** 130

5.4 Synthesis of **4** 131

5.5 Synthesis of **5** 132

5.6 Magnetic Susceptibility 133

5.7 Variable-Temperature Infrared Spectroscopy 135

5.8 Conclusion 142

5.9 Experimental 145

5.10 References 158

Chapter 6: Does Connectivity Affect Valence-Tautomerism?

6.1 Introduction 159

6.2 Synthesis of Para-isomer 165

6.3 Synthesis of Meta-isomer 167

6.4 Magnetic Susceptibility 169

6.5 Variable Temperature IR 170

6.6 Conclusion 177

6.7 Experimental 179

6.8 References 189

General Conclusion 190

Appendix 192

List of Figures

Figure 1.1. Classical description of an electron as a spinning charged particle with associated magnetic field lines. 5

Figure 1.2. Orbital angular momentum vectors of an L = 2 system. 10

Figure 1.3. Vectors of a S = ½ spin. 11

Figure 1.4. Two unpaired electrons in a doubly degenerate orbital set. 14

Figure 1.5 Possible configurations of two unpaired spins in two orbitals. 15

Figure 1.6. Symmetric and antisymmetric spin functions. 15

Figure 1.7. Vectorial depiction of symmetric and antisymmetric wavefunctions. 16

Figure 1.8. Singlet-triplet gap of two unpaired spins. 19

Figure 1.9. Overlap region. 20

Figure 1.10. Orbital state change as a function of octahedral field. 21

Figure 1.11. Electronic state change as a function of octahedral field. 22

Figure 1.12. First-order spin-orbit coupling. 23

Figure 1.13. *LS* coupling in a d^7 ion. 25

Figure 1.14. *j*-*j* coupling in a d^7 ion. 26

Figure 1.15. Jahn-Teller distortion in a d^4 ion. 27

Figure 1.16. Second-order spin-orbit coupling in a d^4 ion. 28

Figure 1.17. Effect of crystal field and second-order spin-orbit coupling in Mn^{3+} in C_{4v}. 29

Figure 1.18. Mn^{3+} MO scheme. 30

Figure 1.19. Different perturbations experienced by a d^1 in an octahedral field. 38

Figure 2.1. Commonly encountered magnetic behaviors. 41

Figure 2.2. SOMO of TMM. 42

Figure 2.3. Spin-polarization in TMM. 43

Figure 2.4. singet-triplet gap. 43

Figure 2.5. SOMO of TME. 44

Figure 2.6. Spin-polarization in TME. 45

Figure 2.7. Spin ladder without CI. 48

Figure 2.8. CI contribution to the spin-ladder energies. 53

Figure 2.9. Metal-ligand exchange. 55

Figure 2.10. Direct exchange pathways. 56

Figure 2.11. Antiferromagnetic (a) and ferromagnetic coupling (b) through diamagnetic ligand. 57

Figure 2.12. Ferromagnetic coupling through two ligand orbitals. 58

Figure 3.1. Quinone redox changes. 66

Figure 3.2. Metal ligand bonding in semiquinone complexes. 66

Figure 3.3. (A) Hückel coefficients for semiquinone SOMO (B) Hückel coefficients squared to yield SOMO electron's spin-densities. 67

Figure 3.4. Difference in structural parameters of SQ and Cat in the Co(SQ)(Cat)bpy. 68

Figure 3.5. Donor-acceptor interaction between metals and the dioxolene ligand. 68

Figure 3.6. Valence tautomerism in Co(SQ)(Cat)bpy. 69

Figure 3.7. Variable temperature solid state electronic absorption of Co(SQ)(Cat)biphenyl. 70

Figure 3.8. Idealized orbital changes with respect to valence tautomeric conversion. 72

Figure 3.9. Sketch of harmonic potentials of *ls*-Co^{III} and *hs*-Co^{II} states. 73

Figure 3.10. Spin ladder ladders of *ls*-Co^{III}(SQ)(Cat) and *hs*-$Co^{II}(SQ)_2$. 74

Figure 3.11. Spin-polarized energy diagrams depicting *ls* to *hs* change. 78

Figure 3.12. Electronic excitation of *ls*-Fe^{II} to *hs*-Fe^{II}. 81

Figure 4.1. Proposed surface-bound valence tautomer. 89

Figure 4.2. TEM image of **5**. 92

Figure 4.3. Electronic absorption spectrum of **5** in CH_2Cl_2. 93

Figure 4.4. 300 MHz ^{1}H-NMR spectrum of **4** in $CDCl_3$. 94

Figure 4.5. 300 MHz ^{1}H-NMR spectrum of **5** in $CDCl_3$. 95

Figure 4.6. Room temperature IR spectral overlay of **4** and **5**. 96

Figure 4.7. 4, 4´ - Dimethylbipyridine valence tautomer. 96

Figure 4.8. Room temperature IR spectral overlay of **5** and **6**. 97

Figure 4.9. Room temperature IR spectral overlay of **5** and **7**. 98

Figure 4.10. Variable temperature IR of **5** between 10 – 400 K. 99

Figure 4.11. SVD analysis of **5**. 100

Figure 4.12. SVD analysis of **6**. 100

Figure 4.13. SVD comparison of **5** and **6**. 101

Figure 4.14. Room temperature IR spectral overlay of **5** (lacks IVCT) and **6**. 103

Figure 4.15. Room temperature IR spectral overlay of **5** (lacks IVCT) and **7**. 103

Figure 4.16. Mixed-monolayer gold cluster. 107

Figure 4.17. ^{1}H-NMR of **9** 300 MHz in $CDCl_3$. 109

Figure 4.18. Surface Infrared of surface-bound **3**. 110

Figure 4.19. Surface Infrared of surface-bound valence tautomer. 110

Figure 4.20. SVD analysis of **5** and **6**. 115

Figure 5.1. The Creutz-Taube ion. 119

Figure 5.2. (**A**) Electron exchange and (**B**) hole exchange. 120

Figure 5.3. SQ and Cat as a donor-acceptor pair. 121

Figure 5.4. Description of the IVCT using MO theory. 122

Figure 5.5. MO diagram of SQ-Cat and dπ. 124

Figure 5.6. (**A**) and (**B**) Exaggerated orbital contributions of dπ to SQ-Cat π*. 126

Figure 5.7. Proposed synthetic systems. 127

Figure 5.8. Group theory derived LUMO of bipyridine. 128

Figure 5.9. Variable temperature magnetic susceptibility of **1**, **2**, **4** and **5** (2 – 400 K). 134

Figure 5.10. Enthalpy change with respect to π-acidity and σ-donation. 134

Figure 5.11. Variable temperature IR of **1** (10 – 300 K). 135

Figure 5.12. Variable temperature IR of **2** (100 – 400 K). 136

Figure 5.13. Variable temperature IR of **4** (100 – 400 K). 136

Figure 5.14. Variable temperature IR of **5** (100 – 400 K). 137

Figure 5.15. Sketch of the harmonic potentials of the ground and excited states of a mixed-valent system. 138

Figure 5.16. ΔE_{th} plotted as a function of σ^{+}_{para}. 139

Figure 5.17. $\Delta E(\Delta\nu_{Hush}-\Delta\nu_{Obs})$ plotted as a function of σ^{+}_{para}. 141

Figure 5.18. (**A**) resonance with cationic center, (**B**) resonance with anionic center. 142

Figure 5.19. Relative mixing of dπ with SQ-Cat π* with respect to the relative energy of the bipyridne LUMO (π*). 144

Figure 5.20. Saturation magnetization of **1**. 150

Figure 5.21. Saturation magnetization of **2**. 150

Figure 5.22. Saturation magnetization of **3**. 151

Figure 5.23. Saturation magnetization of **4**. 151

Figure 5.24. Crystal Structure of **2**. 153

Figure 5.25 Crystal structure of **4**. 156

Figure 6.1. Pyrazine-bridged valence tautomer polymer. 160

Figure 6.2. *Bis*-dioxolene ligand. 161

Figure 6.3. Tetraoxolene dinuclear valence tautomer. 162

Figure 6.4. Proposed dinuclear valence tautomers. 163

Figure 6.5. Magnetic susceptibility of para and meta isomers. 169

Figure 6.6. Variable Temp IR of para-isomer (100 – 400 K). 172

Figure 6.7. Variable-Temp IR of meta-isomer (100 – 400 K). 172

Figure 6.8. Variable Temp IR of para-isomer (100 – 400 K). 173

Figure 6.9. Variable Temp IR of meta-isomer (100 – 400 K). 173

Figure 6.10. SVD analysis of para and meta isomers. 175

Figure 6.11. Temperature-dependences of IVCT band intensity for **1** and **2**. 176

Figure 6.12. Crystal structure of **1**. 184

Figure 6.13. Crystal structure of **2**. 187

List of Tables

Table 3.1. Thermodynamic parameters of various valence tautomers. 77

Table 4.1. Thermodynamic parameters of **5** and **6**. 101

Table 5.1. E_{th} as a function of substituent. 138

Table 5.2. Calculated ΔE (Hush-Obs) values. 141

Table 5.3. Selected bond lengths of **2**. 153

Table 5.4. Crystal data and structure refinement of **4**. 154

Table 5.5. Selected bond lengths of **2**. 156

Table 5.6. Crystal data and structure refinement of **4**. 157

Table 6.1. Thermodynamic parameters from SVD fits of **1** and **2**. 175

Table 6.2. Thermodynamic parameters from IVCT intensity change. 176

Table 6.3. Selected bond lengths of **1**. 184

Table 6.4. Crystal data and Structure Refinement of **1**. 185

Table 6.5. Selected bond lengths of **2**. 187

Table 6.6. Crystal data and Structure Refinement of **2**. 188

List of Schemes

Scheme 4.1. Chemical synthesis of **5**. 91

Scheme 4.2. Chemical synthesis of **7**. 98

Scheme 4.3. Attempted chemical exchange reaction. 107

Scheme 4.4. Synthesis of **9**. 108

Scheme 5.1. Synthesis of **1**. 130

Scheme 5.2. Synthesis of **2**. 131

Scheme 5.3. Synthesis of **4**. 131

Scheme 5.4. Synthesis of **5**. 133

Scheme 6.1. Synthetic scheme for para-isomer. 166

Scheme 6.2. Synthetic scheme for meta-isomer. 168

General Introduction

The research presented in this thesis is an effort of discovery in a very small subset of molecular magnetism involving valence tautomerism. The thesis is meant to be self-contained and the concepts and theories of in the experimental chapters are described in Chapters 1 through 3. Chapter 1 begins with the brief classical and quantum mechanical treatments of the behavior of a single electron. The discourse continues with the consequences of multi-electron interactions in atomic and molecular systems. Chapter 2 is a brief introduction in molecular magnetism. The differences and similarities of magnetic behavior in the bulk and in the molecular regime are described. Furthermore, simple treatments of how the electronic state of different magnetic systems contributes to the magnetic moment are provided. Chapter 3 introduces the reader to valence tautomerism and valence tautomeric behavior. The chapter contains the underlying theory and factors that provide for the experimental observations in the valence tautomerism.

Chapters 4 – 6 are the actual experimental work of the dissertation. Each of the experimental chapters tackles a different fundamental aspect of valence tautomeric behavior. Chapter 4 is the attempt to uncover the effects of surface confinement on valence tautomerism and the results discussed help define the role of intermolecular interactions in valence tautomers. Chapter 5 describes how the degree of delocalization of the mixed-valent low-temperature state of valence tautomers can be controlled through synthetic methods. Chapter 6 is the attempt to create electronically-coupled dinuclear valence tautomers which establishes the intramolecular parameters that aids in the rational development of strongly-coupled multinuclear valence tautomeric systems.

Chapter 1: General Introduction to Electron Behavior

1.1 Introduction

Magnetism is ultimately a behavior that arises from the interactions amongst unpaired electrons. The view of magnetism and magnetic behavior is different depending on the emphasis of the particular *weltanschauung* of the practicing scientist. Magnetic behavior can be looked upon from a purely quantum mechanical perspective of the behavior of isolated unpaired electrons or it can be seen from the solid-state interactions in the bulk. Despite the many advances in the field of magnetism in the past century, our understanding of magnetic phenomena is still in its infancy for the manifestations of magnetic behavior in nature remain complex and our models are still relatively primitive. Magnetochemistry is a field of magnetism where the emphasis in perceiving magnetic behavior lies in the chemical manipulation and chemical understanding from a molecular perspective. Thus, many chemists over the years have developed a method of study of magnetic behavior using a sense of chemical "intuition" that involves a qualitative use of physics and chemical awareness of the electronic behavior of the elements. From the perspective of chemists, the magnetic moment of a system arises out of the chemical environment of the magnetic center. The chemical environment is a function of the molecular structure as well as the inter- and intramolecular interactions that are present. Thus, depending on the structure and symmetry of the molecule in question, the internal magnetic environment can change dramatically. Also, the external environment may also contribute to the magnetic moment.

The brief treatment of molecular magnetic behavior in this chapter is qualitative and will shift in depth and perspective depending on the nature of the explanation sought.

Truth is subjective. In science what is "true" depends on the level of theory that we are willing to use. Consequently the treatment of the behavior of the unpaired electron itself begins using qualitative classical physics. The picture of the unpaired electron in classical physics is ultimately incorrect since the behavior of the electron is best-explained using quantum mechanics. However, the depiction in classical physics is useful because the images are more intuitive to understand. Furthermore, to a limited extent the results obtained using classical physics will yield the same results as the quantum mechanical treatment.

1.2 Spin Magnetic Dipole Moment

An electron has an intrinsic angular momentum called its spin angular momentum (or just spin) *S*. By intrinsic it is meant that it is a basic characteristic of an electron like its mass and electric charge. Associated with this spin is an intrinsic spin magnetic dipole moment μ_s. *S* and μ_s are related by the following equation:

$$\mu_s = -\frac{e}{m} S \tag{1.1}$$

in which e is the elementary charge and m is the mass of the electron. *S* itself is a quantity that cannot be measured, rather only its component along an axis can be measured. Also, a measured component of *S* is quantized so it always has the same magnitude no matter which axis is chosen. If the component of spin *S* is measured along the z-axis of a coordinate system then the measured component (S_z) can only have two values given by:

$$S_z = m_s \hbar \tag{1.2}$$

for m_s = +/- ½ where m_s is the spin magnetic quantum number and $\hbar$ is $h/2\pi$. When S_z is parallel to the z-axis, m_s is + ½ and the electron is typically expressed as "spin up." When S_z is antiparallel to the z-axis, m_s is – ½ and the electron is "spin down." Just like S the spin magnetic dipole moment us of an electron itself also cannot be measured. Thus only a component can be measured and the component also is quantized and always has the same magnitude. The component $\mu_{s,z}$ can be related on the z-axis to S_z by rewriting equation 1.1 in component form for the z-axis as:

$$\mu_{s,z} = -\frac{e}{m} S_z \tag{1.3}$$

By substituting S_z from equation 1.2 into above equation the following relationship is formed:

$$\mu_{s,z} = \pm \frac{eh}{4\pi m} = \beta \tag{1.4}$$

The quantity on the right of the equation is the Bohr magneton β. For the electron, the magnitude of the measured component of μ_s is $\mu_{s,z} = 1\ \beta$ in classical mechanics.

When an electron is placed in an external magnetic field H_{ext}, a potential energy U can be associated with the orientation of the electron's spin magnetic moment μ_s just as a potential energy can be associated with the orientation of the magnetic moment u of a current loop placed in H_{ext}. The potential energy for the electron is then:

$$U = -\mu_s \bullet H_{ext} = -\beta H_{ext} \tag{1.5}$$

Therefore, although it is incorrect to do so, the electron can be imagined as a microscopic sphere and the spin (S), the spin magnetic moment μ_s, and the associated magnetic

moment field can be represented in the following figure where the magnetic field lines of the electron are also shown (**Figure 1.1**).[1]

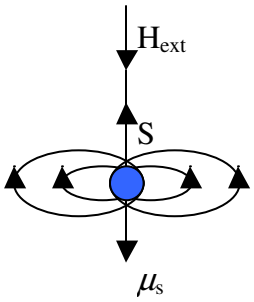

Figure 1.1. Classical description of an electron as a spinning charged particle with associated magnetic field lines.

1.3 Orbital Magnetic Dipole Moment

The electron in an atom has an additional angular momentum called its orbital angular momentum *L*. Associated with L is an orbital magnetic dipole moment μ_L. The two quantities are related similarly to the relationship between *S* and μ_S:

$$\mu_L = -\frac{e}{2m} L \tag{1.6}$$

Just like electron spin, orbital angular momentum cannot be directly measured, rather only components along an axis can be measured and those components are quantized. The components along the z-axis can have only the values given by:

$$L_z = m_l \hbar \tag{1.7}$$

where m_l = 0, +/- 1, +/- 2,…,+/-(limit).

m_l is the orbital magnetic quantum number and the limit refers to the largest allowed integer value for m_l. Just like the other quantum numbers μ_L of an electron cannot itself

be measured and that only its component can be measured and that the component is quantized. By writing equation 1.6 in component form along the z-axis and then substituting for L_z the z-component ($\mu_{L,z}$) of the orbital magnetic moment can be written as:

$$\mu_{L,z} = -m_l \frac{eh}{4\pi m} \tag{1.8}$$

and in terms of the Bohr magneton as: $\mu_{L,z} = -m_l\beta$.

Thus, just as the case with electron spin when an electron is placed in an external magnetic field, H_{ext}, a potential energy U can be associated with the orientation of the orbital magnetic moment of the electron. Its value is:

$$U = -\mu_L \bullet H_{ext} = -\mu_{L,z} H_{ext} \tag{1.9}$$

where the z-axis is taken in the direction of H_{ext}.

1.4 Brief Quantum Description of Angular Momenta and Magnetic Moments

The classical description to spin and orbital momenta provides a good introduction to the origins of spin and orbital contributions to the magnetic moment of an individual electron by imagining the electron as a moving charge. Quantum mechanics predicts many of the same results as classical mechanics with a few "extras."

In classical mechanics orbital angular momentum is treated for a single particle in a manner where the vector of angular projection (L) is expressed in terms of the cross product of the particle's position vector (r) and its linear momentum (p) vector[2]:

$$L = r \times p \tag{1.10}$$

The L vector can be described using a determinant:

$$L = \begin{vmatrix} i & j & k \\ x & y & z \\ px & py & pz \end{vmatrix} \tag{1.11}$$

where i, j and k are the unit vectors of L and x, y and z are the particle's coordinate at a given instant and p_x, p_y and p_z are the linear momentum vectors in the x, y and z directions respectively. From the determinant the angular momentum components of L are then: [2-5]

$$\begin{aligned} L_x &= yp_z - zp_y, \\ L_y &= zp_x - xp_z, \\ L_z &= xp_y - yp_x \end{aligned} \tag{1.12}$$

in which L_x, L_y and L_z are simply linear combinations of the product of the position vector components and the linear momentum components. Since the classical analog can still be used for a moving particle in quantum mechanics the operators of the orbital angular momentum vector components can still be expressed in the same classical fashion. The difference is that now the coordinates and momenta are replaced by their corresponding operators and that the components of the L operator are now scaled by h:

$$\begin{aligned} \hat{L}_x &= -i\hbar\left(y\frac{\partial}{\partial z} - x\frac{\partial}{\partial y} \right) \\ \hat{L}_x &= -i\hbar\left(z\frac{\partial}{\partial x} - x\frac{\partial}{\partial z} \right) \\ \hat{L}_x &= -i\hbar\left(x\frac{\partial}{\partial y} - y\frac{\partial}{\partial x} \right) \end{aligned} \tag{1.13}$$

The L component operators serve a useful purpose in that they can be used to express the result of the orbital motion for a particle. However there are certain commutative rules that the angular momentum operators must abide by that are a direct result of working in the quantum regime. The commutation relationships determine which physical quantities can be simultaneously assigned definite values. For the orbital angular momentum operators:

$$\begin{aligned}\left[\hat{L}_x, \hat{L}_y\right] &= i\hbar\hat{L}_z \\ \left[\hat{L}_y, \hat{L}_z\right] &= i\hbar\hat{L}_x \\ \left[\hat{L}_z, \hat{L}_x\right] &= i\hbar\hat{L}_y\end{aligned} \tag{1.14}$$

The commutation relationships above mean that there is no function that is an eigenfunction of any two combinations of L_x, L_y and L_z. As a result for a given wavefunction eigenvalues cannot be obtained from the orbital component operators and simultaneous measurements of any combination of L_x, L_y and L_z will not yield definite values. Only averages or expectation values can be extracted from these measurements. On the other hand:

$$\begin{aligned}\left[\hat{L}^2, \hat{L}_x\right] &= 0 \\ \left[\hat{L}^2, \hat{L}_y\right] &= 0 \\ \left[\hat{L}^2, \hat{L}_z\right] &= 0\end{aligned} \tag{1.15}$$

in which:

$$\hat{L}^2 = \left|\hat{L}\right|^2 = \hat{L} \bullet \hat{L} = \hat{L}_x^2 + \hat{L}_y^2 + \hat{L}_z^2 \tag{1.16}$$

Since the square of the orbital angular momentum vector commutes with each of its components the exact value for L^2 and any one of its components can be deduced. In

keeping with the restrictions of the quantum regime L^2 only signifies the magnitude of L and does not specify the L vector itself. Therefore by operating on an eigenfunction of L^2:

$$\hat{L}^2\psi = l(l+1)\hbar^2\psi \tag{1.17}$$

in which $l(l+1)\hbar^2$ are the eigenvalues of the operator and l is the orbital quantum number. For an electron in an isolated atom there is no preferred direction with respect to the orientation in space of the vector L and all directions are equivalent. However, magnets line up with magnetic fields, and the orbital angular momentum of a quantum state is tightly coupled to its orbital magnetic dipole moment. Thus, if an atom is immersed in a uniform magnetic field the direction of the field can then be taken as the z-axis to discuss the orientations of the electron's orbital magnetic dipole moment μ_L and its orbital angular momentum L. The quantized values of μ_L are the same as derived using the classical picture: [2-5]

$$\mu_L = -m_l\beta \tag{1.18}$$

Where m_l is the orbital magnetic quantum number. Furthermore, the quantized values of L are given by $L_z = m_l\hbar$. Thus for an electron with $l = 2$ there are associated orientations of the angular momentum L and correspondingly L_z (Figure 1.2). For a given value of l, there are $2l+1$ different values of m_l and for $l = 2$ there are five quantized projections of L_z (orbital angular momentum).

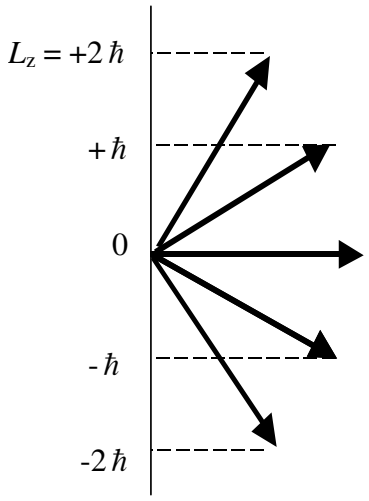

Figure 1.2. Orbital angular momentum vectors of an L = 2 system.

For electron spin the spin angular momentum operators are in a sense analogous to the orbital angular momentum operators. The difference between the orbital angular momentum and spin angular momentum operators is that there is no expression that describes spin angular momentum since the intrinsic property of electron spin has no classical analog. However, the same commutative relationships hold for electron spin: [2-5]

$$\begin{aligned} \left[\hat{S}_x, \hat{S}_y\right] &= i\hbar\hat{S}_z \\ \left[\hat{S}_y, \hat{S}_z\right] &= i\hbar\hat{S}_x \\ \left[\hat{S}_z, \hat{S}_x\right] &= i\hbar\hat{S}_y \end{aligned} \tag{1.20}$$

and

$$\left[\hat{S}^2, \hat{S}_x\right] = \left[\hat{S}^2, \hat{S}_y\right] = \left[\hat{S}^2, \hat{S}_z\right] = 0 \tag{1.21}$$

Furthermore, for a given eigenfunction of the square of the spin operator the following results:

$$\hat{S}^2\psi = s(s+1)\hbar^2\psi \tag{1.22}$$

where $s(s+1)\hbar^2$ are the eigenvalues of S^2. The quantized values of S are $S_z = m_s\hbar$ in which m_s is the spin magnetic quantum number. For a given S there are $2S + 1$ different values of m_s. One would expect the spin magnetic dipole moment μ_s would be the same as the classical derivation. However, this is where quantum mechanics predicts a slightly different result:

$$\mu_{s,z} = -gm_s\beta \tag{1.23}$$

where m_s is the spin magnetic quantum number and g is the electron g-factor. The electron g-factor has a very specific relativistic quantum mechanical meaning. However, in this case it will be treated as a constant with a value of 2 for a single free electron. For an S = ½ system the relationship between the quantized projections of $\mu_{s,z}$ and S_z can be described using vectors (**Figure 1.3**).

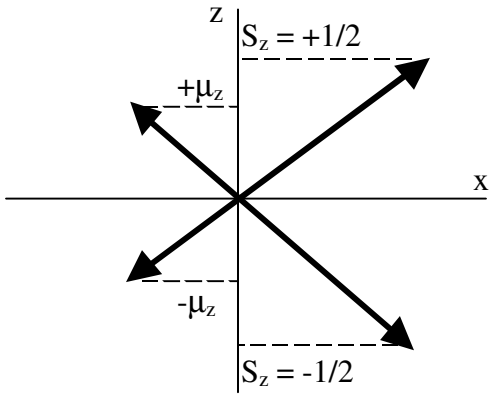

Figure 1.3. Vectors of a S = ½ spin.

1.5 Coupling between Spin and Orbital Angular Momenta

When the spin and orbital angular momenta couple a new vector results (J), which is the total angular momentum vector. The total angular momentum vector is the vector sum of the angular momenta of the individual electron:

$$J = L + S \tag{1.24}$$

For multiple electrons the J vector is the sum of all of the individual spin and angular momenta:

$$J_{tot} = (L_1 + L_2 + L_3 ... + L_n) + (S_1 + S_2 + S_3 + ... + S_n) \tag{1.25}$$

Similarly the total magnetic dipole moment is obtained by vectorially adding the magnetic dipole moments. In classical physics the effective magnetic dipole moment μ_{eff} for an electron is the vector component of the vector sum of the total magnetic dipole moments in the direction of –J.

1.6 The Pauli Exclusion Principle

In chemical systems the electrons are not free and are bound to individual nuclei. For a system with multiple unpaired electrons the relative orientations of the unpaired electrons with respect to each other in determines the relative energies of the spin states. The reason is simply inter-electron repulsion. Depending on the relative orientations of the unpaired electrons with respect to each other, their wavefunctions will interact with each other differently. In order to discuss the energies of spin states the electron wavefunctions must first be described. Electrons have half-integer spin and thus are fermions. It is commonly stated that a fermion's wavefunction is antisymmetric with respect to exchange of identical particles. The antisymmetry requirement means that: [2]

$$\psi(q_1, q_2, q_3..., q_n) = -\psi(q_2, q_1, q_3..., q_n) \tag{1.26}$$

Thus if there is a wavefunction where electrons 1 and 2 have the same coordinates, i.e., $x_1 = x_2$, $x_1 = x_2$, $x_1 = x_2$ and $m_{s1} = m_{s2}$, then by putting $q_1 = q_2$ the following results:

$$\begin{aligned} &\psi(q_1, q_1, q_3..., q_n) = -\psi(q_1, q_1, q_3..., q_n) \\ &2\psi = 0 \end{aligned} \tag{1.27}$$

Which means that:

$$\psi(q_1, q_1, q_3..., q_n) = 0 \tag{1.28}$$

For this reason two electrons with the same spin have zero probability of being found at the same point in space. The Pauli antisymmetry principle forces electrons of like spin to keep apart from one another and it is a reflection of the fact that the spin wavefunction must be antisymmetric with respect to exchange. The Pauli antisymmetry principle can be extended to spin-orbital functions, which are products of one-electron space orbital and one-electron spin functions. For two electrons in a single 1*s* orbital the spin-orbital function can be represented in determinant form as: [2]

$$\psi = \frac{1}{\sqrt{2}} \begin{vmatrix} 1s(1)\alpha(1) & 1s(1)\beta(1) \\ 1s(2)\alpha(2) & 1s(2)\beta(2) \end{vmatrix} \tag{1.29}$$

If both electrons had the same spin quantum number then both columns in the determinant would be the same and the determinant would vanish. This leads to the Pauli Exclusion Principle: No two electrons can occupy the same spin-orbital function. In other words no two electrons can have the same values for all of their quantum numbers.

1.7 Hund's Rules

Now consider two electrons in two degenerate orbitals (**Figure 1.4**).

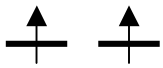

Figure 1.4. Two unpaired electrons in a doubly degenerate orbital set.

The wavefunction $\phi_a(1)\phi_b(2)$ that might describes the system is unacceptable because the wavefunction is neither symmetric nor antisymmetric with respect to exchange of identical particles, i.e., $\phi_a(1)\phi_b(2) \neq \phi_a(2)\phi_b(1)$. In other words, In order to resolve this dilemma the symmetrized and anti-symmetrized wavefunctions must be constructed:

$$\psi_s = \frac{1}{\sqrt{2}}\left(\phi_a(1)\phi_b(2) + \phi_a(2)\phi_b(1)\right) \tag{1.30}$$

$$\psi_a = \frac{1}{\sqrt{2}}\left(\phi_a(1)\phi_b(2) - \phi_a(2)\phi_b(1)\right) \tag{1.31}$$

By operating on the two wavefunctions above with the permutation operator P_{12} brings about:

$$P_{12} = \frac{1}{\sqrt{2}}\left(\phi_a(2)\phi_b(1) + \phi_a(1)\phi_b(2)\right) = \psi_s \tag{1.32}$$

$$P_{12} = \frac{1}{\sqrt{2}}\left(\phi_a(2)\phi_b(1) - \phi_a(1)\phi_b(2)\right) = \psi_a \tag{1.33}$$

The wavefunction ψ_s is symmetric with respect exchange and ψ_a is antisymmetric. To consider the spin wavefunctions there are four possibilities for two electrons to in two orbitals (**Figure 1.5**).

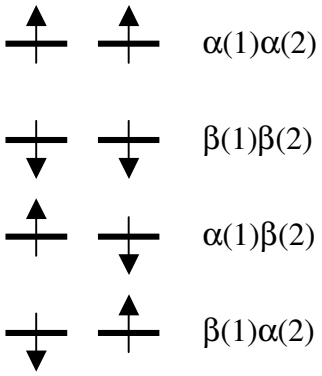

Figure 1.5 Possible configurations of two unpaired spins in two orbitals.

Both $\alpha(1)\alpha(2)$ and $\beta(1)\beta(2)$ are symmetric with respect to exchange. However, $\alpha(1)\beta(2)$ and $\beta(1)\alpha(2)$ are neither symmetric nor antisymmetric with respect to exchange because they allow for distinction between the two electrons and thus are not acceptable spin functions. Linear combinations must be taken for these unacceptable wavefunctions:

$$\frac{1}{\sqrt{2}}\left(\alpha(1)\beta(2)+\alpha(2)\beta(1)\right) \tag{1.34}$$

$$\frac{1}{\sqrt{2}}\left(\alpha(1)\beta(2)-\alpha(2)\beta(1)\right) \tag{1.35}$$

Henceforth, the four acceptable spin functions and their symmetries with respect to exchange of identical particles are:

Symmetric spin functions	**Antisymmetric spin function**
$\alpha(1)\alpha(2)$, $\beta(1)\beta(2)$, $\frac{1}{\sqrt{2}}\left(\alpha(1)\beta(2)+\beta(1)\alpha(2)\right)$	$\frac{1}{\sqrt{2}}\left(\alpha(1)\beta(2)-\beta(1)\alpha(2)\right)$

Figure 1.6. Symmetric and antisymmetric spin functions.

Since the electronic wavefunction must be antisymmetric, the symmetric orbital wavefunction ψ_s must be combined with the antisymmetric spin function to form the singlet state. Hence, the antisymmetric orbital wavefunction ψ_a must be combined with the three symmetric spin functions to create the triplet state (**Figure 1.7**).

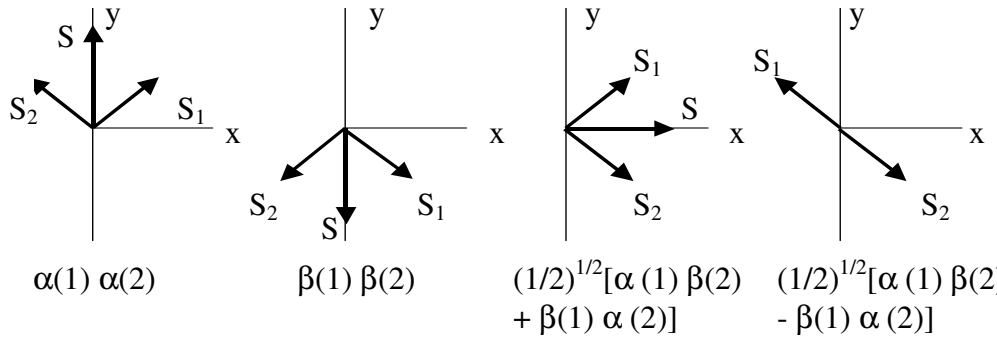

Figure 1.7. Vectorial depiction of symmetric and antisymmetric wavefunctions.

The relative energies of the singlet and triplet states are provided in the spatial wavefunctions. To simplify the notation the ϕ notation is dropped. Thus the antisymmetric spatial wavefunction (A) and the open-shell singlet spatial wavefunction (S, OS) can be described as:

$$\psi_A = \frac{1}{\sqrt{2}}\left(a(1)b(2) - b(1)a(2)\right) \qquad \text{(Triplet)} \qquad (1.36)$$

$$\psi_{S,OS} = \frac{1}{\sqrt{2}}\left(a(1)b(2) + b(1)a(2)\right) \qquad \text{(Open-shell singlet)} \qquad (1.37)$$

The energies of the two unperturbed states can now be evaluated using one-electron energy operators as part of the zeroth-order Hamiltonian:

$$\hat{H} = h(1) + h(2) \qquad (1.38)$$

The energy of the unperturbed the open-shell triplet:

$$
\begin{aligned}
E^{(0)}(\psi_A) &= \frac{1}{2}\big\langle a(1)b(2)-b(1)a(2)\big|h(1)+h(2)\big|a(1)b(2)-b(1)a(2)\big\rangle \\
&= \frac{1}{2}\begin{bmatrix}\big\langle a(1)b(2)\big|h(1)+h(2)\big|a(1)b(2)\big\rangle - \big\langle a(1)b(2)\big|h(1)+h(2)\big|b(1)a(2)\big\rangle \\ -\big\langle b(1)a(2)\big|h(1)+h(2)\big|a(1)b(2)\big\rangle + \big\langle b(1)a(2)\big|h(1)+h(2)\big|b(1)a(2)\big\rangle\end{bmatrix} \\
&= \frac{1}{2}\begin{bmatrix}\big\langle b(2)\big|b(2)\big\rangle\big\langle a(1)\big|h(1)\big|a(1)\big\rangle + \big\langle a(1)\big|a(1)\big\rangle\big\langle b(2)\big|h(2)\big|b(2)\big\rangle \\ -\big\langle b(2)\big|a(2)\big\rangle\big\langle a(1)\big|h(1)\big|b(1)\big\rangle - \big\langle a(1)\big|b(1)\big\rangle\big\langle b(2)\big|h(2)\big|a(2)\big\rangle \\ -\big\langle a(2)\big|b(2)\big\rangle\big\langle b(1)\big|h(1)\big|a(1)\big\rangle - \big\langle b(1)\big|a(1)\big\rangle\big\langle a(2)\big|h(2)\big|b(2)\big\rangle \\ +\big\langle a(2)\big|a(2)\big\rangle\big\langle b(1)\big|h(1)\big|b(1)\big\rangle + \big\langle b(1)\big|b(1)\big\rangle\big\langle a(2)\big|h(2)\big|a(2)\big\rangle\end{bmatrix} \\
&= \frac{1}{2}(\alpha+\alpha-0-0-0-0+\alpha+\alpha) = 2\alpha
\end{aligned}
\tag{1.39}
$$

The energy of the unperturbed open-shell singlet:

$$
\begin{aligned}
E^{(0)}(\psi_{S,OS}) &= \frac{1}{2}\big\langle a(1)b(2)+b(1)a(2)\big|h(1)+h(2)\big|a(1)b(2)+b(1)a(2)\big\rangle \\
&= \frac{1}{2}\begin{bmatrix}\big\langle a(1)b(2)\big|h(1)+h(2)\big|a(1)b(2)\big\rangle + \big\langle a(1)b(2)\big|h(1)+h(2)\big|b(1)a(2)\big\rangle \\ +\big\langle b(1)a(2)\big|h(1)+h(2)\big|a(1)b(2)\big\rangle + \big\langle b(1)a(2)\big|h(1)+h(2)\big|b(1)a(2)\big\rangle\end{bmatrix} \\
&= \frac{1}{2}\begin{bmatrix}\big\langle b(2)\big|b(2)\big\rangle\big\langle a(1)\big|h(1)\big|a(1)\big\rangle + \big\langle a(1)\big|a(1)\big\rangle\big\langle b(2)\big|h(2)\big|b(2)\big\rangle \\ +\big\langle b(2)\big|a(2)\big\rangle\big\langle a(1)\big|h(1)\big|b(1)\big\rangle + \big\langle a(1)\big|b(1)\big\rangle\big\langle b(2)\big|h(2)\big|a(2)\big\rangle \\ +\big\langle a(2)\big|b(2)\big\rangle\big\langle b(1)\big|h(1)\big|a(1)\big\rangle + \big\langle b(1)\big|a(1)\big\rangle\big\langle a(2)\big|h(2)\big|b(2)\big\rangle \\ +\big\langle a(2)\big|a(2)\big\rangle\big\langle b(1)\big|h(1)\big|b(1)\big\rangle + \big\langle b(1)\big|b(1)\big\rangle\big\langle a(2)\big|h(2)\big|a(2)\big\rangle\end{bmatrix} \\
&= \frac{1}{2}(\alpha+\alpha-0-0-0-0+\alpha+\alpha) = 2\alpha
\end{aligned}
\tag{1.40}
$$

Thus the unperturbed spin states of two electrons in two orbitals are degenerate with an energy of 2α. By taking into account interelectron repulsion the first order correction to the Hamiltonian is added:

$$\hat{H} = \hat{H}^{(0)} + \hat{H}^{(1)} \tag{1.41}$$

Where the first-order correction to the Hamiltonian is equal to $1/r_{12}$. The corrected energy of the triplet to first-order is now:

$$
\begin{aligned}
E^1(\psi_A) &= \frac{1}{2}\left\langle a(1)b(2)-b(1)a(2)\left|H^0+\frac{1}{r_{12}}\right|a(1)b(2)-b(1)a(2)\right\rangle \\
&= 2\alpha+\frac{1}{2}\left\langle a(1)b(2)-b(1)a(2)\left|\frac{1}{r_{12}}\right|a(1)b(2)-b(1)a(2)\right\rangle \\
&= 2\alpha+\frac{1}{2}\left[\begin{array}{l}\left\langle a(1)b(2)\left|\frac{1}{r_{12}}\right|a(1)b(2)\right\rangle-\left\langle a(1)b(2)\left|\frac{1}{r_{12}}\right|b(1)a(2)\right\rangle \\ -\left\langle b(1)a(2)\left|\frac{1}{r_{12}}\right|a(1)b(2)\right\rangle+\left\langle b(1)a(2)\left|\frac{1}{r_{12}}\right|b(1)a(2)\right\rangle\end{array}\right] \\
&= 2\alpha+\frac{1}{2}\left[\begin{array}{l}\left\langle a(1)a(1)\left|\frac{1}{r_{12}}\right|b(2)b(2)\right\rangle-\left\langle a(1)b(1)\left|\frac{1}{r_{12}}\right|a(2)b(2)\right\rangle \\ -\left\langle b(1)a(2)\left|\frac{1}{r_{12}}\right|a(2)b(2)\right\rangle+\left\langle b(1)b(1)\left|\frac{1}{r_{12}}\right|a(2)a(2)\right\rangle\end{array}\right] \\
&= 2\alpha+\frac{1}{2}\left[j-k-k+j\right]=2\alpha+j-k
\end{aligned}
\tag{1.42}
$$

And the corrected energy of the open-shell singlet to first order:

$$
\begin{aligned}
E^1(\psi_{S,OS}) &= \frac{1}{2}\left\langle a(1)b(2)+b(1)a(2)\left|H^0+\frac{1}{r_{12}}\right|a(1)b(2)+b(1)a(2)\right\rangle \\
&= 2\alpha+\frac{1}{2}\left\langle a(1)b(2)+b(1)a(2)\left|\frac{1}{r_{12}}\right|a(1)b(2)+b(1)a(2)\right\rangle \\
&= 2\alpha+\frac{1}{2}\left[\begin{array}{l}\left\langle a(1)b(2)\left|\frac{1}{r_{12}}\right|a(1)b(2)\right\rangle+\left\langle a(1)b(2)\left|\frac{1}{r_{12}}\right|b(1)a(2)\right\rangle \\ +\left\langle b(1)a(2)\left|\frac{1}{r_{12}}\right|a(1)b(2)\right\rangle+\left\langle b(1)a(2)\left|\frac{1}{r_{12}}\right|b(1)a(2)\right\rangle\end{array}\right] \\
&= 2\alpha+\frac{1}{2}\left[\begin{array}{l}\left\langle a(1)a(1)\left|\frac{1}{r_{12}}\right|b(2)b(2)\right\rangle+\left\langle a(1)b(1)\left|\frac{1}{r_{12}}\right|a(2)b(2)\right\rangle \\ +\left\langle b(1)a(2)\left|\frac{1}{r_{12}}\right|a(2)b(2)\right\rangle+\left\langle b(1)b(1)\left|\frac{1}{r_{12}}\right|a(2)a(2)\right\rangle\end{array}\right] \\
&= 2\alpha+\frac{1}{2}\left[j+k+k+j\right] = 2\alpha+j+k
\end{aligned}
\tag{1.43}
$$

For corrected energies of the singlet and triplet j is known as the Coulomb integral and represents the Coulombic repulsion between electron 1 and 2 in orbitals ϕ_a and ϕ_b. The k term is the exchange integral and represents the exchange energy of electrons 1 and 2 in the overlap region of orbitals ϕ_a and ϕ_b. Thus the difference in energy of the two states is:

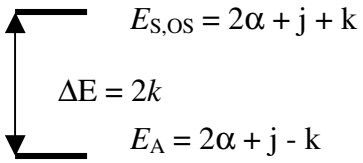

$$
\begin{aligned}
\Delta E &= E_{S,OS} - E_A \\
&= \left(2\alpha+j+k\right)-\left(2\alpha+j-k\right) \\
&= 2k
\end{aligned}
\tag{1.44}
$$

Figure 1.8. Singlet-triplet gap of two unpaired spins.

If electron 1 and 2 are in two degenerate and orthogonal p-orbitals ϕ_a and ϕ_b then the energy difference between the electrons pairing in the same direction (triplet state) and against each other (singlet state) is the repulsion in the overlap region of the two orbitals. According to the Pauli Exclusion Principle no two electrons can have all the same quantum numbers and since both electrons have the same quantum numbers in the triplet state, their electron densities are not shared in the overlap region and there is less repulsion (j - k). In the singlet both electrons can share the common space of the overlap region thus increasing the electronic repulsion (j + k) (**Figure 1.9**). This conclusion leads to Hund's first rule: In the absence of any other perturbation, the state with highest spin multiplicity will be the most stable. Hund's first rule works very well in the ground-state, however the model can fail when dealing with excited states.

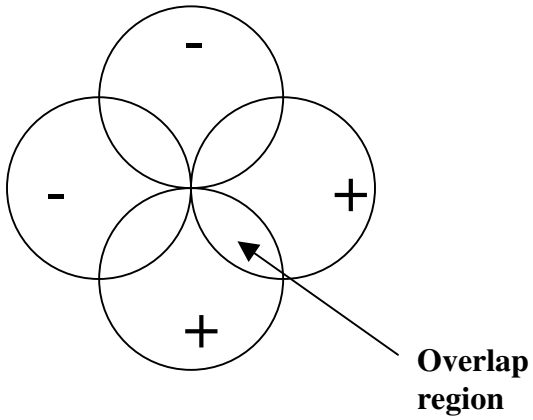

Figure 1.9. Overlap region.

Hund's second rule states that in the event that multiple states have the same spin-multiplicity the state with the highest orbital degeneracy is the most stabilized. Finally Hund's third rule states that if both the spin and orbital degeneracies are equal the state with the highest total angular momentum is the most stabilized.

1.8 Crystal Field Splitting and Spin-Orbit Coupling in Transition Metals

In transition metal complexes the electrons of transition metals interact with the electrons of the coordinating ligands. In crystal field theory, it is assumed that the interaction between metal and ligand is purely electrostatic where the metal acts as a cation and is surrounded by ionic or dipolar ligands that are electrostatically attracted to the metal cation. The interaction between the electrons of the cation and the electrons of the ligands is entirely repulsive and is known as the crystal field. This repulsive interaction perturbs the electron containing orbitals in the metal. Imagine a metal ion going from a spherical free ion environment to an octahedrally coordinated one. The electrons in the d orbitals experience the repulsive force from the ligand electrons and this perturbation splits the degenerate free ion d orbitals into two sets, e and t_2 (**Figure1.10**):

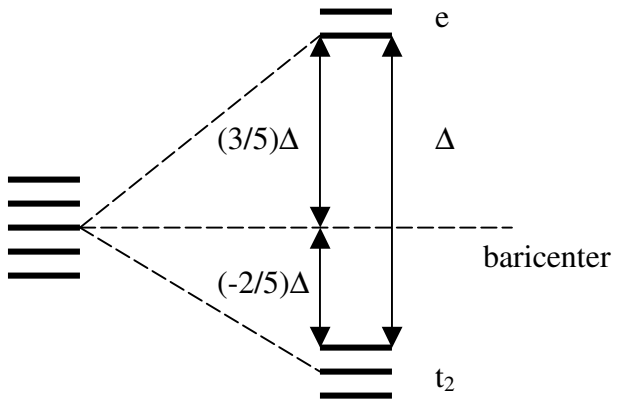

Figure 1.10. Orbital state change as a function of octahedral field.

where Δ is the crystal field splitting energy and the triply degenerate t_2 orbital set is lowered by (–2/5)Δ and the doubly degenerate e set is increased by (3/5)Δ from the baricenter respectively. If the crystal field environment is tetrahedral the relative energies of the t_2 and e sets are reversed.

Just as the crystal field environment determines the d orbital level splitting, so does the crystal field determine the relative energies of the electronic states of the metal system. For a d^1 metal ion in an octahedral ligand environment, the states that are formed from the free ion form are the ^{2}T and ^{2}E states (**Figure 1.11**). The states are split by the crystal field energy in which the ground state is the ^{2}T and the nearest excited state is ^{2}E.

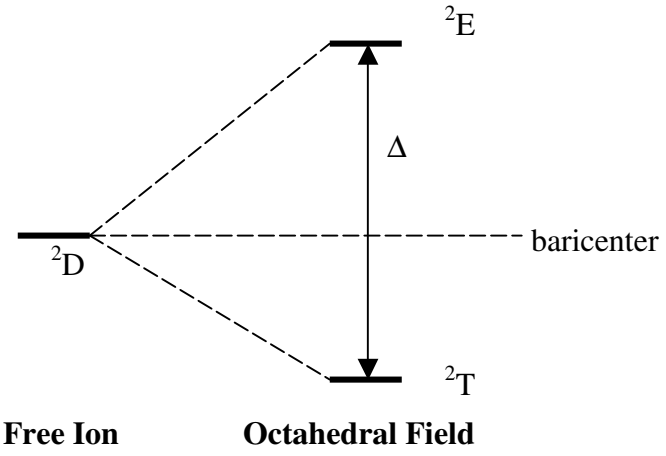

Figure 1.11. Electronic state change as a function of octahedral field.

The electronic state term symbols describe the total degeneracy of the state in which each term is [(2*S*+1)(2*L*+1)] degenerate. The ^{2}T ground state is six-fold degenerate (2 × 3) while the nearest ^{2}E excited state is four-fold degenerate (2 × 2). It is implicit in the symmetry notation that the spin and orbital degeneracies are uncoupled. Understanding the state splitting of the metal allows one to understand the electronic

structure of the metal. However, the above picture is for a very special case for it does not take into account the role of spin-orbit coupling.

Spin-orbit coupling is the interaction between the electron spin and its orbital angular momentum. Just as described with the free electron picture, the effect of the spin-orbit interaction creates a new resultant vector from the coupling of the spin and orbital angular momentum vectors (*J*). Consider a free ion with an unpaired electron in two degenerate and orthogonal p-orbitals (**Figure 1.12**).[5] Qualitatively it can be argued that the electron is not in one of the two orbitals because both orbitals are degenerate. Rather the electron is in both orbitals because it can freely "travel" between them. This electron motion appears circular and creates an orbital component to the electron motion. In addition, if the orbital motion is coupled to the electron spin then both spin and orbital angular momentum vectors can combine.

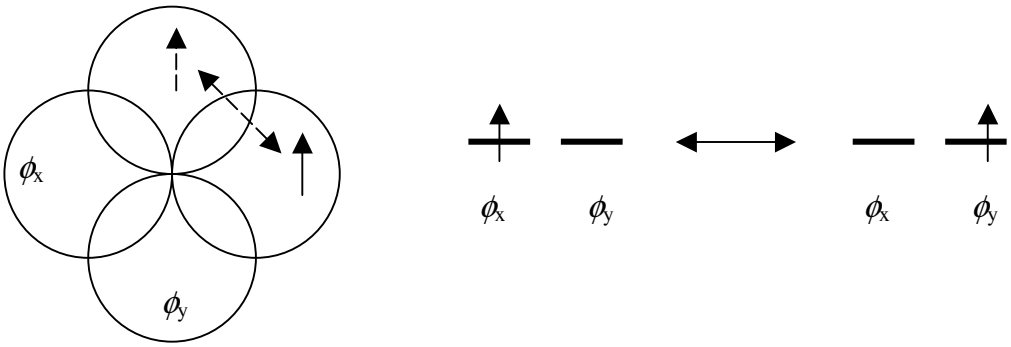

Figure 1.12. First-order spin-orbit coupling.[5]

As described previously just as *L* and *S* create their respective magnetic moments, so does *J*. Thus, the spin-orbit perturbation creates an internal magnetic field that perturbs the states of a transition metal ion. The picture described is a ground state

interaction and is described in quantum chemistry notation as a first-order perturbation in which the first-order correction to the energy is:

$$E_{SO}^{(1)} = \left\langle \psi_n \left| \lambda L \bullet S \right| \psi_m \right\rangle \qquad (1.45)$$
$$\lambda L \bullet S \propto L, S, m_l, m_s$$

where $\lambda L \cdot S$ is the spin-orbit operator and λ is the multi-electron spin-orbit coupling constant. The magnitude of λ is dependent on the individual elements of the periodic table and in general increases with the size and relativistic effects of the elements. The spin-orbit operator is proportional to the operators of the orbital angular momentum and it's z-component and the spin angular momentum and it's respective z-component. In group theory terminology the spin-orbit operator transforms as the rotations (R_x, R_y and R_z) of the irreducible representations of the point group.

Depending on the magnitude of the spin-orbit interaction with respect to the crystal field the states of a transition metal ion will be split differently. There are two general cases to consider: The crystal field is larger than the spin-orbit coupling and when the crystal field is smaller than the spin-orbit interaction.

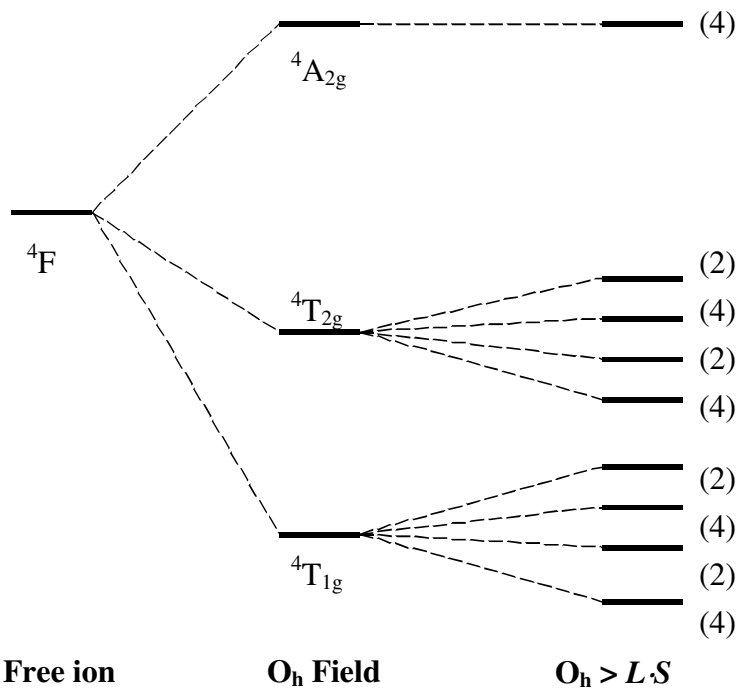

Figure 1.13. *LS* coupling in a d^7 ion.

The *Russell-Saunders* coupling (*LS* coupling) scheme is used when the crystal field is large and the spin-orbit interaction acts as a perturbation to the crystal field.[6] For a d^7 ion the effects of an octahedral crystal field and spin-orbit coupling in the *Russell-Saunders* scheme are shown (**Figure 1.13**). Since the spin-orbit interaction creates an internal magnetic field, the field splits the crystal field terms into the spin-orbit states in which each state is either four-fold or two-fold degenerate respectively. The *LS* coupling scheme can be applied to first row transition metal ions where the crystal field energies are greater than the spin-orbit interaction. However, as the relativistic effects increase with the second through third row transition metals and especially with the rare earth

elements the spin-orbit interaction becomes larger than the crystal field and *j*·*j* coupling scheme must used.

In *j*·*j* coupling the crystal field is treated as a perturbation to the spin-orbit coupling.[6] By using the same d^7 ion example, the effects of the octahedral crystal field perturbing the spin-orbit states can be shown (**Figure 1.14**):

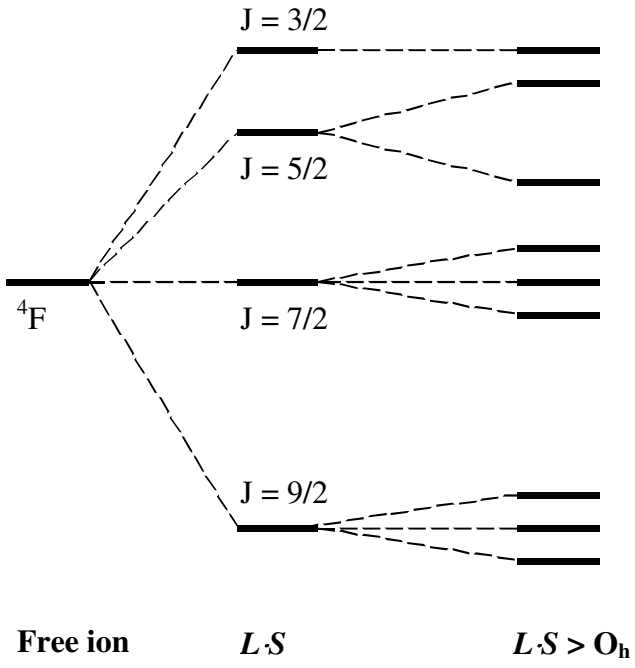

Figure 1.14. *j*·*j*coupling in a d^7 ion.

1.9 Jahn-Teller Instability and the Origin of Zero-field Splitting in Transition Metals

The picture that describes the perturbations of the electronic states of metal ions is still incomplete. First-order spin-orbit coupling is symmetry dependent. High symmetry environments allow for the electron motion in ground states with nonzero orbital angular momentum. However, low symmetry fields can disrupt first-order spin-orbit coupling.

The same electronic states that experience first-order spin-orbit coupling are also susceptible to the *Jahn-Teller* instability. The *Jahn-Teller* instability predicts that electronic states with nonzero orbital angular momentum experience a perturbation that lowers the energy of the system by reducing the electronic state to lower symmetry terms. In molecular systems this perturbation occurs by distorting the molecule to lower symmetry through a non-totally symmetric vibrational mode. For transition metal systems, low symmetry crystal fields can change the d orbital ordering from the usual e and t_2 orbital levels and consequently the electronic state terms as well. This can be shown by considering a high-spin d^4 ion (**Figure 1.15**).

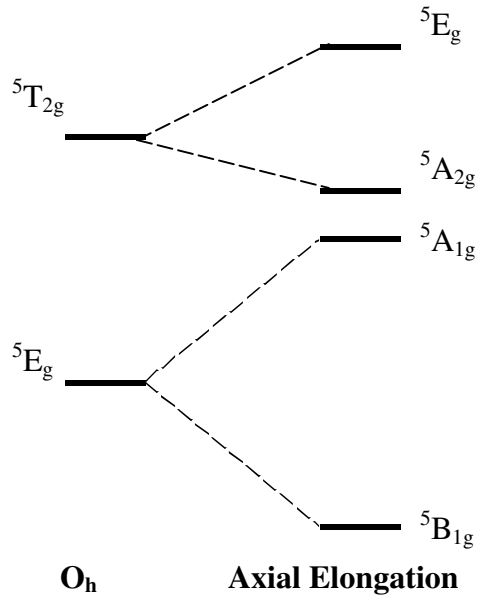

Figure 1.15. Jahn-Teller distortion in a d^4 ion.

The ultimate effect of *Jahn-Teller* distortion is to quench first-order orbital angular momentum in the spin-orbit active states of metal ions, which reduces spin-orbit coupling as a first order perturbation. However, if there are excited states low in energy with

respect to the distorted orbital singlet ground state, these excited states can mix with the ground state provided that the spin-orbit coupling constant is large and the excited states possess the correct symmetry. In the case of the distorted d^4 ion the $^5A_{2g}$ and ^5E_g are the nearest excited states that can mix with the ground state term (**Figure 1.16**).

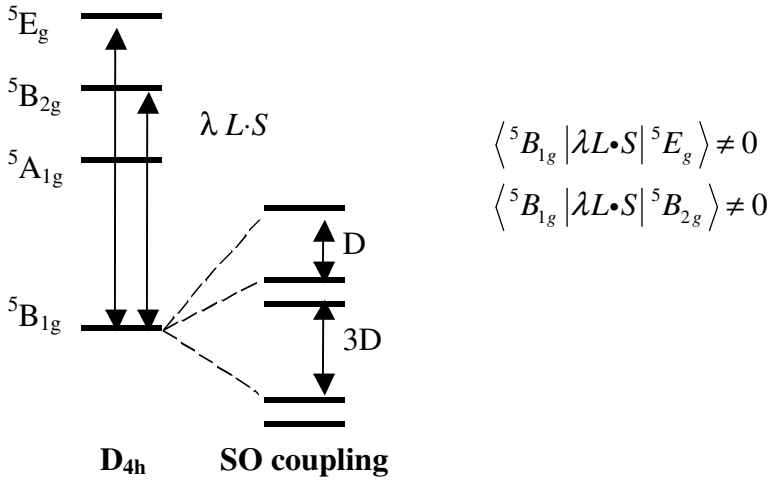

Figure 1.16. Second-order spin-orbit coupling in a d^4 ion.

The excited state mixing allows for a small orbital angular momentum component to build into the ground state term that in turn creates a small internal magnetic field. Since the L = 0 for the ground state term, only m_s spin-states of the ground state term are perturbed by the resulting field which splits them. In the case of the d^4 ion example the m_s states are split into a singlet and two kramer's doublets. Kramer theorized that in a ground-state configuration with half-integral spin there exists a degeneracy that a low-symmetry ligand field cannot remove.[8] The energy difference between the split m_s levels is proportional to the zero-field parameter (D). Spin-orbit coupling that occurs via

excited states is a second-order perturbation and the following notation can represent the energy of the second-order spin-orbit coupled state:

$$E_{SO}^{(2)} = \frac{\left\langle \psi_m \left| \lambda L \bullet S \right| \psi_n \right\rangle^2}{E_m - E_n} \tag{1.46}$$

In transition metal complexes spin-orbit coupling is the primary method by which zero-field splitting occurs because transition metals tend to have low-lying excited states that allow for mixing and possess relatively large spin-orbit coupling constants, λ.

1.10 Detailed Treatment of Second-Order Spin-Orbit Coupling in Mn^{3+}

The second-order spin-orbit perturbation can be treated in more detail by using the specific example of five-coordinate Mn^{3+} in the C_{4v} point group. The electronic states of C_{4v} Mn^{3+} can be extracted from the free ion terms:

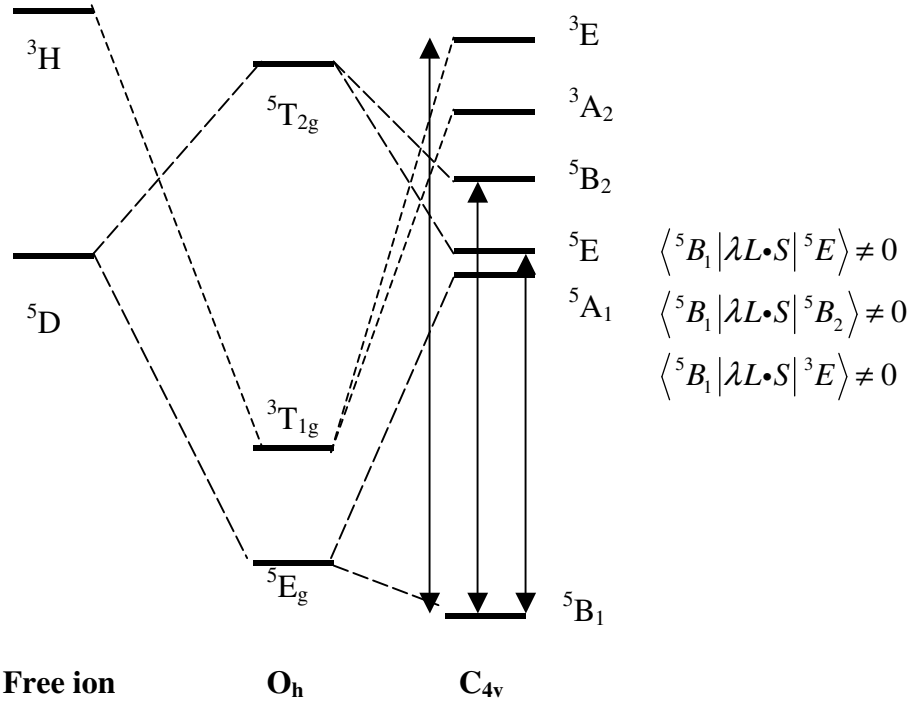

Figure 1.17. Effect of crystal field and second-order spin-orbit coupling in Mn^{3+} in C_{4v}.

Three of the five nearest excited states can mix with the $^5B_1$ ground state because they possess the correct symmetry. However, to be brief only the wavefunctions belonging to ^3E will be evaluated. First the spin-orbital states for the ground and excited state terms must be defined since spin-orbital wavefunctions are eigenfunctions of the spin-orbit operator. In this case the spin-orbital wavefunctions are treated as Slater-type determinants in which the matrix elements of the determinants are ordered by the MO scheme that describes the Mn^{3+} ion (**Figure 1.18**).[7]

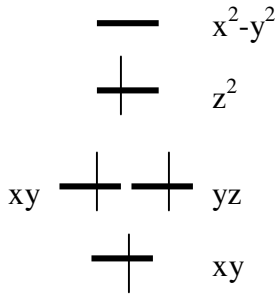

Figure 1.18. Mn^{3+} MO scheme.

From the orbital picture the ground state term wavefunctions can be constructed:

$$^5B_1(M_s=2)=d^+_{xy}d^+_{xz}d^+_{yz}d^+_{z^2}$$

$$^5B_1(M_s=1)=\left(1/2\right)\left(d^-_{xy}d^+_{xz}d^+_{yz}d^+_{z^2}+d^+_{xy}d^-_{xz}d^+_{yz}d^+_{z^2}+d^+_{xy}d^+_{xz}d^-_{yz}d^+_{z^2}+d^+_{xy}d^+_{xz}d^+_{yz}d^-_{z^2}\right)$$

$$^5B_1(M_s=0)=\left(1/6\right)^{1/2}\begin{pmatrix} d^-_{xy}d^-_{xz}d^+_{yz}d^+_{z^2}+d^-_{xy}d^+_{xz}d^-_{yz}d^+_{z^2}+d^-_{xy}d^+_{xz}d^+_{yz}d^-_{z^2} \\ +d^+_{xy}d^-_{xz}d^-_{yz}d^+_{z^2}+d^+_{xy}d^-_{xz}d^+_{yz}d^-_{z^2}+d^+_{xy}d^+_{xz}d^-_{yz}d^-_{z^2}\end{pmatrix}$$

For the ^3E excited term the following is defined:

$$^3E_a(M_s=1)=d^+_{xy}d^+_{xz}d^+_{yz}d^-_{yz}$$

$$^3E_a(M_s=0)=\left(1/2\right)^{1/2}\left(d^+_{xy}d^-_{xz}d^+_{yz}d^-_{yz}+d^-_{xy}d^+_{xz}d^+_{yz}d^-_{yz}\right)$$

$$^3E_b(M_s=1) = d_{xy}^+ d_{xz}^+ d_{xz}^- d_{yz}^+$$

$$^3E_b(M_s=0) = \left(1/2\right)^{1/2}\left(d_{xy}^+ d_{xz}^+ d_{xz}^- d_{yz}^- + d_{xy}^- d_{xz}^+ d_{xz}^- d_{yz}^+\right)$$

The spin-orbit operator H_{LS} that will be used is:[7]

$$H_{LS} = \xi \sum_i l_{zi}s_{zi} + l_{xi}s_{xi} + l_{yi}s_{yi}$$

where ξ is the spin-orbit coupling constant for a single electron and $l_{zi}s_{zi}$, $l_{zi}s_{zi}$ and $l_{zi}s_{zi}$ are the x, y and z spin-orbital operators for each electron. ξ is related to the multi-electron spin-orbit coupling constant (λ):[7]

$$\lambda = \frac{\xi}{2S}$$

where S is the spin quantum number. Finally, in order to evaluate the wavefunctions the following relationships will be used:[7]

$$l_z d_{xy} = -2i d_{x^2-y^2}$$
$$l_z d_{xz} = i d_{yz}$$
$$l_z d_{yz} = -i d_{xz}$$
$$l_x d_{xy} = i d_{xz}$$
$$l_x d_{xz} = -i d_{xy}$$
$$l_x d_{yz} = (3)^{1/2} i d_{z^2} + i d_{x^2-y^2}$$
$$l_y d_{xy} = -i d_{yz}$$
$$l_y d_{xz} = (3)^{1/2} - i d_{z^2} + i d_{x^2-y^2}$$
$$l_y d_{yz} = i d_{xy}$$

And the spin operators are defined as:[5]

$$s_z|+\rangle = \frac{1}{2}|+\rangle$$
$$s_z|-\rangle = -\frac{1}{2}|-\rangle$$

$$s_x|+\rangle = \frac{1}{2}|-\rangle$$

$$s_x|-\rangle = -\frac{1}{2}|+\rangle$$

$$s_y|+\rangle = \frac{i}{2}|-\rangle$$

$$s_y|-\rangle = -\frac{i}{2}|+\rangle$$

Thus H_{LS} components operating on each of the $^3E_a(M_s = 1)$ determinants gives the following:

$$l_{zi}s_{zi}\left|{}^3E_a(1)\right\rangle = \left(\frac{1}{2}\right)(-2i)\left(d^+_{x^2-y^2}d^+_{xz}d^+_{yz}d^-_{yz}\right)+\left(\frac{1}{2}\right)(i)\left(d^+_{xy}d^+_{yz}d^+_{yz}d^-_{yz}\right)+\left(\frac{1}{2}\right)(-i)\left(d^+_{xy}d^+_{xz}d^+_{xz}d^-_{yz}\right)$$
$$+\left(-\frac{1}{2}\right)(-i)\left(d^+_{xy}d^+_{xz}d^+_{yz}d^-_{xz}\right)$$

$$l_{xi}s_{xi}\left|{}^3E_a(1)\right\rangle = \left(\frac{1}{2}\right)(i)\left(d^-_{xz}d^+_{xz}d^+_{yz}d^-_{yz}\right)+\left(\frac{1}{2}\right)(-i)\left(d^+_{xy}d^-_{xy}d^+_{yz}d^-_{yz}\right)+\left(\frac{1}{2}\right)\left(i\sqrt{3}\right)\left(d^+_{xy}d^+_{xz}d^-_{z^2}d^-_{yz}\right)$$
$$+\left(-\frac{1}{2}\right)\left(i\sqrt{3}\right)\left(d^+_{xy}d^+_{xz}d^+_{yz}d^+_{z^2}\right)$$

$$l_{yi}s_{yi}\left|{}^3E_a(1)\right\rangle = \left(\frac{i}{2}\right)(-i)\left(d^-_{yz}d^+_{xz}d^+_{yz}d^-_{yz}\right)+\left(\frac{i}{2}\right)\left(-i\sqrt{3}\right)\left(d^+_{xy}d^-_{z^2}d^+_{yz}d^-_{yz}\right)+\left(\frac{i}{2}\right)(i)\left(d^+_{xy}d^+_{xz}d^-_{xy}d^-_{yz}\right)$$
$$+\left(-\frac{i}{2}\right)(i)\left(d^+_{xy}d^+_{xz}d^+_{yz}d^+_{xy}\right)$$

Although there are 12 terms the real answer involves 15 since some of the orbital operations on the excited state determinants creates a linear combination of d_z^2 and d_x^2-$_y^2$ (i.e., $l_x d_{yz}$ and $l_y d_{xz}$). However only the d_z^2 component of the linear combination is considered. Of the 12 terms above by considering only the terms that belong to $^5B_1$ the following results:

$$H_{LS}\left|{}^3E_a(1)\right\rangle = \left(\frac{i\sqrt{3}}{2}\right)\left(d_{xy}^{+}d_{xz}^{+}d_{z^2}^{-}d_{yz}^{-}\right)+\left(\frac{\sqrt{3}}{2}\right)\left(d_{xy}^{+}d_{xz}^{+}d_{yz}^{+}d_{z^2}^{+}\right)$$

The order of the determinant matrix elements is changed to reflect the fact that the excited state functions must be identical to the ground state functions. By changing the order of the d orbitals the determinants change sign since it is an exchange in two columns or rows in the determinant matrix.

$$H_{LS}\left|{}^3E_a(1)\right\rangle = \left(\frac{\sqrt{3}}{2}\right)\left(d_{xy}^{+}d_{xz}^{+}d_{yz}^{-}d_{z^2}^{-}\right)+\left(\frac{\sqrt{3}}{2}\right)\left(d_{xy}^{+}d_{xz}^{+}d_{yz}^{+}d_{z^2}^{+}\right)$$

$$=\frac{\sqrt{3}}{2}\left(d_{xy}^{+}d_{xz}^{+}d_{yz}^{-}d_{z^2}^{-}+d_{xy}^{+}d_{xz}^{+}d_{yz}^{+}d_{z^2}^{+}\right)$$

The same operations can be used to determine the rest of the spin-orbit operated excited state determinants.

For ${}^3E_b(M_s = 1)$:

$$l_{zi}s_{zi}\left|{}^3E_b(1)\right\rangle = \left(\frac{1}{2}\right)(-2i)\left(d_{x^2-y^2}^{+}d_{xz}^{+}d_{xz}^{-}d_{yz}^{+}\right)+\left(\frac{1}{2}\right)(i)\left(d_{xy}^{+}d_{yz}^{+}d_{xz}^{-}d_{yz}^{+}\right)+\left(-\frac{1}{2}\right)(i)\left(d_{xy}^{+}d_{xz}^{+}d_{yz}^{-}d_{yz}^{+}\right)$$
$$+\left(\frac{1}{2}\right)(-i)\left(d_{xy}^{+}d_{xz}^{+}d_{xz}^{-}d_{xz}^{+}\right)$$

$$l_{xi}s_{xi}\left|{}^3E_b(1)\right\rangle = \left(\frac{1}{2}\right)(i)\left(d_{xz}^{-}d_{xz}^{+}d_{xz}^{-}d_{yz}^{+}\right)+\left(\frac{1}{2}\right)(-i)\left(d_{xy}^{+}d_{xy}^{-}d_{xz}^{-}d_{yz}^{+}\right)+\left(-\frac{1}{2}\right)(-i)\left(d_{xy}^{+}d_{xz}^{+}d_{xy}^{+}d_{z^2}^{+}\right)$$
$$+\left(\frac{1}{2}\right)\left(i\sqrt{3}\right)\left(d_{xy}^{+}d_{xz}^{+}d_{xz}^{-}d_{z^2}^{-}\right)$$

$$l_{yi}s_{yi}\left|{}^3E_b(1)\right\rangle = \left(\frac{i}{2}\right)(-i)\left(d_{yx}^{-}d_{xz}^{+}d_{xz}^{-}d_{yz}^{+}\right)+\left(\frac{i}{2}\right)\left(-i\sqrt{3}\right)\left(d_{xy}^{+}d_{z^2}^{-}d_{xz}^{-}d_{yz}^{+}\right)$$
$$+\left(-\frac{i}{2}\right)\left(-i\sqrt{3}\right)\left(d_{xy}^{+}d_{xz}^{+}d_{z^2}^{+}d_{yz}^{+}\right)+\left(\frac{i}{2}\right)(i)\left(d_{xy}^{+}d_{xz}^{+}d_{xz}^{-}d_{xy}^{-}\right)$$

$$H_{LS}\left|{}^3E_b(1)\right\rangle=\left(\frac{i\sqrt{3}}{2}\right)\left(d^+_{xy}d^-_{z^2}d^-_{xz}d^+_{yz}\right)+\left(-\frac{i\sqrt{3}}{2}\right)\left(d^+_{xy}d^+_{xz}d^+_{z^2}d^+_{yz}\right)$$

$$=\left(\frac{i\sqrt{3}}{2}\right)\left(d^+_{xy}d^-_{xz}d^+_{yz}d^-_{z^2}\right)+\left(\frac{i\sqrt{3}}{2}\right)\left(d^+_{xy}d^+_{xz}d^+_{yz}d^+_{z^2}\right)$$

$$=\frac{i\sqrt{3}}{2}\left(d^+_{xy}d^-_{xz}d^+_{yz}d^-_{z^2}+d^+_{xy}d^+_{xz}d^+_{yz}d^+_{z^2}\right)$$

For ${}^3E_a(M_s = 0)$:

$$l_{zi}s_{zi}\left|{}^3E_a(0)\right\rangle=$$

$$\left(\frac{1}{2}\right)^{1/2}\left[\begin{array}{l}\left(\frac{1}{2}\right)(-2i)\left(d^+_{x^2-y^2}d^-_{xz}d^+_{yz}d^-_{yz}\right)+\left(\frac{1}{2}\right)(i)\left(d^+_{xy}d^-_{yz}d^+_{yz}d^-_{yz}\right)+\left(\frac{1}{2}\right)(i)\left(d^+_{xy}d^-_{xz}d^+_{yz}d^-_{yz}\right)\\+\left(-\frac{1}{2}\right)(-i)\left(d^+_{xy}d^-_{xz}d^+_{yz}d^-_{xz}\right)+\left(-\frac{1}{2}\right)(-2i)\left(d^-_{x^2-y^2}d^+_{xz}d^+_{yz}d^-_{yz}\right)+\left(\frac{1}{2}\right)(i)\left(d^-_{xy}d^+_{yz}d^+_{yz}d^-_{yz}\right)\\\left(\frac{1}{2}\right)(i)\left(d^-_{xy}d^+_{xz}d^+_{yz}d^-_{yz}\right)+\left(-\frac{1}{2}\right)(-i)\left(d^-_{xy}d^+_{xz}d^+_{yz}d^-_{xz}\right)\end{array}\right]$$

$$l_{xi}s_{xi}\left|{}^3E_a(0)\right\rangle=$$

$$\left(\frac{1}{2}\right)^{1/2}\left[\begin{array}{l}\left(\frac{1}{2}\right)(i)\left(d^-_{xz}d^-_{xz}d^+_{yz}d^-_{yz}\right)+\left(-\frac{1}{2}\right)(-i)\left(d^+_{xy}d^+_{xy}d^+_{yz}d^-_{yz}\right)+\left(\frac{1}{2}\right)\left(i\sqrt{3}\right)\left(d^+_{xy}d^-_{xz}d^-_{z^2}d^-_{yz}\right)\\+\left(-\frac{1}{2}\right)\left(i\sqrt{3}\right)\left(d^+_{xy}d^-_{xz}d^+_{yz}d^+_{z^2}\right)+\left(-\frac{1}{2}\right)(i)\left(d^+_{xz}d^+_{xy}d^+_{yz}d^-_{yz}\right)+\left(\frac{1}{2}\right)(-i)\left(d^-_{xy}d^-_{xy}d^+_{yz}d^-_{yz}\right)\\\left(\frac{1}{2}\right)\left(i\sqrt{3}\right)\left(d^-_{xy}d^+_{xz}d^-_{z^2}d^-_{yz}\right)+\left(-\frac{1}{2}\right)\left(i\sqrt{3}\right)\left(d^-_{xy}d^+_{xz}d^+_{yz}d^+_{z^2}\right)\end{array}\right]$$

$$l_{yi}s_{yi}\left|{}^3E_a(0)\right\rangle=$$

$$\left(\frac{1}{2}\right)^{1/2}\left[\begin{array}{l}\left(\frac{i}{2}\right)(i)\left(d^-_{yz}d^-_{xz}d^+_{yz}d^-_{yz}\right)+\left(-\frac{i}{2}\right)\left(-i\sqrt{3}\right)\left(d^+_{xy}d^+_{z^2}d^+_{yz}d^-_{yz}\right)+\left(\frac{i}{2}\right)(i)\left(d^+_{xy}d^-_{xz}d^-_{xy}d^-_{yz}\right)\\+\left(-\frac{i}{2}\right)(i)\left(d^+_{xy}d^-_{xz}d^+_{yz}d^+_{xy}\right)+\left(-\frac{i}{2}\right)(i)\left(d^+_{yz}d^+_{xy}d^+_{yz}d^-_{yz}\right)+\left(\frac{i}{2}\right)\left(-i\sqrt{3}\right)\left(d^-_{xy}d^-_{z^2}d^+_{yz}d^-_{yz}\right)\\\left(\frac{i}{2}\right)(i)\left(d^-_{xy}d^+_{xz}d^-_{xy}d^-_{yz}\right)+\left(-\frac{i}{2}\right)(i)\left(d^-_{xy}d^+_{xz}d^+_{yz}d^+_{xy}\right)\end{array}\right]$$

$$H_{LS}\left|{}^3E_a(0)\right\rangle=\left(\frac{1}{2}\right)^{\frac{1}{2}}\left[\begin{array}{l}\frac{i\sqrt{3}}{2}\left(d^+_{xy}d^-_{xz}d^-_{z^2}d^-_{yz}\right)-\frac{i\sqrt{3}}{2}\left(d^+_{xy}d^-_{xz}d^+_{yz}d^+_{z^2}\right)\\+\frac{i\sqrt{3}}{2}\left(d^-_{xy}d^+_{xz}d^-_{z^2}d^-_{yz}\right)-\frac{i\sqrt{3}}{2}\left(d^-_{xy}d^+_{xz}d^+_{yz}d^+_{z^2}\right)\end{array}\right]$$

$$=\left(\frac{1}{2}\right)^{\frac{1}{2}}\left[\begin{array}{l}\frac{\sqrt{3}}{2}\left(d^+_{xy}d^-_{xz}d^-_{yz}d^-_{z^2}\right)+\frac{\sqrt{3}}{2}\left(d^+_{xy}d^-_{xz}d^+_{yz}d^+_{z^2}\right)+\frac{\sqrt{3}}{2}\left(d^-_{xy}d^+_{xz}d^-_{yz}d^-_{z^2}\right)\\+\frac{\sqrt{3}}{2}\left(d^-_{xy}d^+_{xz}d^+_{yz}d^+_{z^2}\right)\end{array}\right]$$

$$=\left(\frac{3}{8}\right)^{\frac{1}{2}}\left(d^+_{xy}d^-_{xz}d^-_{yz}d^-_{z^2}+d^+_{xy}d^-_{xz}d^+_{yz}d^+_{z^2}+d^-_{xy}d^+_{xz}d^-_{yz}d^-_{z^2}+d^-_{xy}d^+_{xz}d^+_{yz}d^+_{z^2}\right)$$

For ${}^3E_b(M_s = 0)$:

$$l_{zi}s_{zi}\left|{}^3E_b(0)\right\rangle=$$

$$\left(\frac{1}{2}\right)^{1/2}\left[\begin{array}{l}\left(\frac{1}{2}\right)(-2i)\left(d^+_{x^2-y^2}d^+_{xz}d^-_{xz}d^-_{yz}\right)+\left(\frac{1}{2}\right)(i)\left(d^+_{xy}d^+_{yz}d^-_{xz}d^-_{yz}\right)+\left(-\frac{1}{2}\right)(i)\left(d^+_{xy}d^+_{xz}d^-_{yz}d^-_{yz}\right)\\+\left(-\frac{1}{2}\right)(-i)\left(d^+_{xy}d^+_{xz}d^-_{xz}d^-_{xz}\right)+\left(-\frac{1}{2}\right)(-2i)\left(d^-_{x^2-y^2}d^+_{xz}d^-_{xz}d^+_{yz}\right)+\left(\frac{1}{2}\right)(i)\left(d^-_{xy}d^+_{yz}d^-_{xz}d^+_{yz}\right)\\\left(-\frac{1}{2}\right)(i)\left(d^-_{xy}d^+_{xz}d^-_{yz}d^+_{yz}\right)+\left(\frac{1}{2}\right)(-i)\left(d^-_{xy}d^+_{xz}d^-_{xz}d^-_{xz}\right)\end{array}\right]$$

$$l_{xi}s_{xi}\left|{}^3E_b(0)\right\rangle=$$

$$\left(\frac{1}{2}\right)^{1/2}\left[\begin{array}{l}\left(\frac{1}{2}\right)(i)\left(d^-_{xz}d^+_{xz}d^-_{xz}d^-_{yz}\right)+\left(\frac{1}{2}\right)(-i)\left(d^+_{xy}d^-_{xy}d^-_{xz}d^-_{yz}\right)+\left(-\frac{1}{2}\right)(-i)\left(d^+_{xy}d^+_{xz}d^+_{xy}d^-_{yz}\right)\\+\left(-\frac{1}{2}\right)(i)\left(d^+_{xy}d^+_{xz}d^-_{xz}d^+_{z^2}\right)+\left(-\frac{1}{2}\right)(i)\left(d^+_{xz}d^+_{xz}d^-_{xz}d^+_{yz}\right)+\left(\frac{1}{2}\right)(-i)\left(d^-_{xy}d^-_{xy}d^-_{xz}d^+_{yz}\right)\\\left(-\frac{1}{2}\right)(-i)\left(d^-_{xy}d^+_{xz}d^+_{xy}d^+_{yz}\right)+\left(\frac{1}{2}\right)(i)\left(d^-_{xy}d^+_{xz}d^-_{xz}d^-_{z^2}\right)\end{array}\right]$$

$$l_{yi}s_{yi}\left|{}^3E_b(0)\right\rangle=$$

$$\left(\frac{1}{2}\right)^{1/2}\left[\begin{array}{l}\left(\frac{i}{2}\right)(-i)\left(d^-_{yz}d^+_{xz}d^-_{xz}d^-_{yz}\right)+\left(\frac{i}{2}\right)\left(-i\sqrt{3}\right)\left(d^+_{xy}d^-_{z^2}d^-_{xz}d^-_{yz}\right)+\left(-\frac{i}{2}\right)\left(-i\sqrt{3}\right)\left(d^+_{xy}d^+_{xz}d^+_{z^2}d^-_{yz}\right)\\+\left(-\frac{i}{2}\right)(i)\left(d^+_{xy}d^+_{xz}d^-_{xz}d^+_{xy}\right)+\left(-\frac{i}{2}\right)(i)\left(d^+_{yz}d^+_{xz}d^-_{xz}d^+_{yz}\right)+\left(\frac{i}{2}\right)\left(-i\sqrt{3}\right)\left(d^-_{xy}d^-_{z^2}d^-_{xz}d^+_{yz}\right)\\\left(-\frac{i}{2}\right)\left(-i\sqrt{3}\right)\left(d^-_{xy}d^+_{xz}d^+_{z^2}d^+_{yz}\right)+\left(\frac{i}{2}\right)(i)\left(d^-_{xy}d^+_{xz}d^-_{xz}d^-_{xy}\right)\end{array}\right]$$

$$H_{LS}\left|{}^3E_b(0)\right\rangle=\left(\frac{1}{2}\right)^{\frac{1}{2}}\left[\begin{array}{l}\frac{i\sqrt{3}}{2}\left(d_{xy}^{+}d_{z^2}^{-}d_{xz}^{-}d_{yz}^{-}\right)-\frac{i\sqrt{3}}{2}\left(d_{xy}^{+}d_{xz}^{+}d_{z^2}^{+}d_{yz}^{-}\right)\\+\frac{i\sqrt{3}}{2}\left(d_{xy}^{-}d_{z^2}^{-}d_{xz}^{-}d_{yz}^{+}\right)-\frac{i\sqrt{3}}{2}\left(d_{xy}^{-}d_{xz}^{+}d_{z^2}^{+}d_{yz}^{+}\right)\end{array}\right]$$

$$=\left(\frac{1}{2}\right)^{\frac{1}{2}}\left[\begin{array}{l}\frac{i\sqrt{3}}{2}\left(d_{xy}^{+}d_{xz}^{-}d_{yz}^{-}d_{z^2}^{-}\right)+\frac{i\sqrt{3}}{2}\left(d_{xy}^{+}d_{xz}^{+}d_{yz}^{-}d_{z^2}^{+}\right)+\frac{i\sqrt{3}}{2}\left(d_{xy}^{-}d_{xz}^{-}d_{yz}^{+}d_{z^2}^{-}\right)\\+\frac{i\sqrt{3}}{2}\left(d_{xy}^{-}d_{xz}^{+}d_{yz}^{+}d_{z^2}^{+}\right)\end{array}\right]$$

$$=\left(\frac{3}{8}\right)^{\frac{1}{2}}i\left(d_{xy}^{+}d_{xz}^{-}d_{yz}^{-}d_{z^2}^{-}+d_{xy}^{+}d_{xz}^{+}d_{yz}^{-}d_{z^2}^{+}+d_{xy}^{-}d_{xz}^{-}d_{yz}^{+}d_{z^2}^{-}+d_{xy}^{-}d_{xz}^{+}d_{yz}^{+}d_{z^2}^{+}\right)$$

From the terms above the following nonzero matrix elements can be constructed:

$$\left\langle{}^5B_1(2)\left|H_{LS}\right|{}^3E_a(1)\right\rangle=\frac{\sqrt{3}}{2}\xi$$

$$\left\langle{}^5B_1(2)\left|H_{LS}\right|{}^3E_b(1)\right\rangle=\frac{\sqrt{3}}{2}i\xi$$

$$\left\langle{}^5B_1(1)\left|H_{LS}\right|{}^3E_a(0)\right\rangle=\left(\frac{3}{8}\right)^{\frac{1}{2}}\xi$$

$$\left\langle{}^5B_1(1)\left|H_{LS}\right|{}^3E_b(0)\right\rangle=\left(\frac{3}{8}\right)^{\frac{1}{2}}i\xi$$

$$\left\langle{}^5B_1(0)\left|H_{LS}\right|{}^3E_a(1)\right\rangle=\left(\frac{1}{8}\right)^{\frac{1}{2}}\xi$$

$$\left\langle{}^5B_1(0)\left|H_{LS}\right|{}^3E_b(1)\right\rangle=\left(\frac{1}{8}\right)^{\frac{1}{2}}i\xi$$

Accordingly, now the contribution of ^{3}E to ^{5}B$_1$ can be calculated:

$$\Delta E(2)=\frac{-\frac{3}{2}\xi^2}{\Delta E\left({}^3E-{}^5B_1\right)}$$

$$\Delta E(1) = \frac{-\frac{3}{4}\xi^2}{\Delta E\left({}^3E - {}^5B_1\right)}$$

$$\Delta E(0) = \frac{-\frac{1}{2}\xi^2}{\Delta E\left({}^3E - {}^5B_1\right)}$$

For an $S = 2$ system the zero-field splitting parameter is defined as:

$$3D = E\left(M_s = \pm 2\right) - E\left(M_s = \pm 1\right)$$
$$D = E\left(M_s = \pm 1\right) - E\left(M_s = \pm 0\right)$$

Then the zero-field splitting due solely to the ^{3}E contribution is the difference between $\Delta E(1)$ and $\Delta E(2)$:

$$D = \frac{-\frac{1}{4}\xi^2}{\Delta E\left({}^3E - {}^5B_1\right)} = \frac{-4\lambda^2}{\Delta E\left({}^3E - {}^5B_1\right)}$$

1.11 Different Perturbations in Context

The practicing magnetochemist must discern between multiple competing perturbations that transition metal ions experience in order to craft a sensible picture of the electronic structure of the system under study. Depending on whether the transition metal is experiencing weak or strong crystal fields determines the construction of the metal's electronic state. The *Jahn-Teller* instability and spin-orbit coupling are perturbations that act in opposing fashions. One acts to lower symmetry while the other acts to preserve it. However, in molecular systems most first row transition metals can be "well-behaved"—a subjective term —in which the crystal field, *Jahn-Teller* effect and spin-orbit coupling act in a relatively predictable manner in the first row transition metal elements. In general the magnitude of the perturbations in first row transition metals can

be described as follows: crystal field > *Jahn-Teller* > spin-orbit. For simplicity consider a d^1 ion in an octahedral field. The free ion has a total of 10 states (^5D). The crystal field splits the free ion degeneracy into the ^5E and ^5T terms. By assuming a simple tetragonal distortion from O_h symmetry to D_{4h} that follows splits the ground state term into an orbital singlet ground state ($^2B_{2g}$) and a doubly degenerate nearest excited state (^5E_g). Finally spin-orbit coupling lifts the remaining degeneracy in the ground state term (**Figure 1.19**).[8]

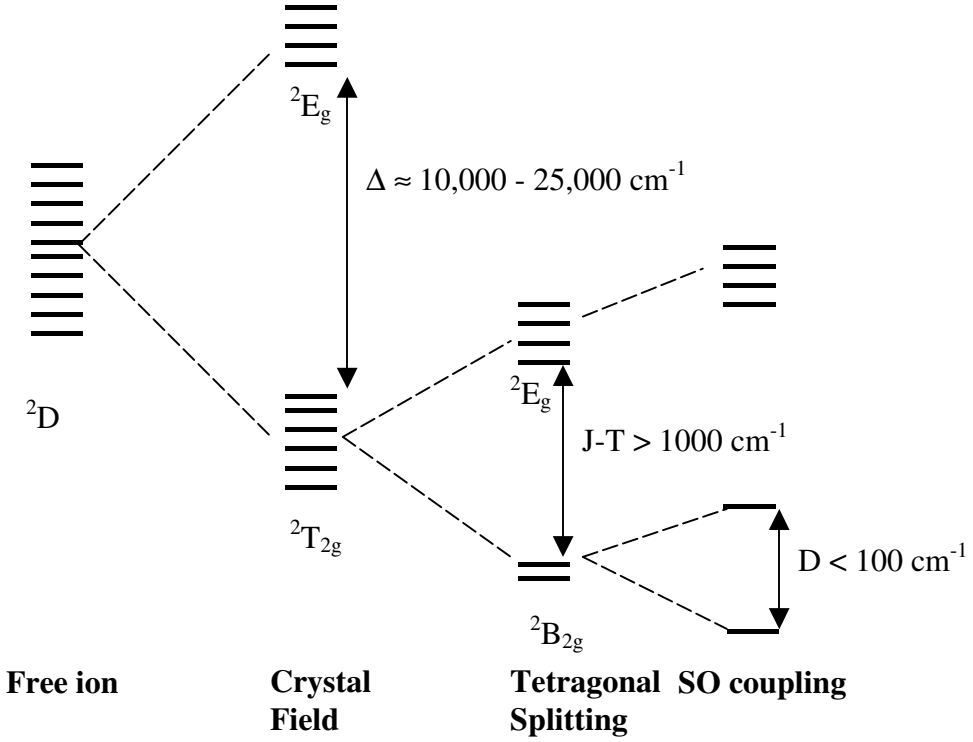

Figure 1.19. Different perturbations experienced by a d^1 in an octahedral field.

1.12 References

1. Halliday, D.; Resnick, R.; Walker, J. *Fundamentals of Physics Volume 2 (Fifth Edition)*. John Wiley & Sons, Inc. USA 1997.
2. Ira N. Levine. *Quantum Chemistry (Fourth Edition)*. Prentice-Hall, Inc. USA 1991.
3. Melvin W. Hanna. *Quantum Mechanics in Chemistry*. Benjamin/Cummings Pub Co. USA 1981.
4. Clifford E. Dykstra. *Introduction to Quantum Chemistry*. Prentice-Hall, Inc. USA 1993.
5. Gordon L. Squires. *Problems in Quantum Mechanics: With Solutions*. Cambridge University Press (1995).
6. Russell S. Drago. *Physical Methods for Chemists*. Saunders College Publishing (1997).
7. Krzystek J.; Telser, J.; Brunel, L. C. *Inorg. Chem.* **1999**, *38*, 6121.
8. S. F. A. Kettle. *Physical Inorganic Chemistry: A Coordination Chemistry Approach*. Oxford University Press (New York 1998).

Chapter 2: Molecule-Based Magnetism

2.1 Description of Different Magnetic Behavior in the Bulk

There are many different types of magnetic behavior.[1] The most common behaviors encountered are *diamagnetism*, *paramagnetism*, *ferromagnetism* and *antiferromagnetism*. Most common materials exhibit diamagnetism because their electrons are in closed shells. In *diamagnetism*, weak magnetic dipole moments are produced in the atoms of the material when the material is placed in an external magnetic field.[2] The induced magnetic moment is very small and the net field disappears when the external field is removed. Materials containing unpaired electrons exhibit *paramagnetism*. The magnetic centers of paramagnetic materials have a permanent magnetic dipole moment but the moments are weakly coupled and are magnetically dilute. The moments are randomly oriented in paramagnetic materials and the materials as a whole lacks a net magnetic field (**Figure 2.1**). However, an external field can align the magnetic dipole moments to give the material a net magnetic field. The alignment and thus its field disappear when the external field is removed. *Ferromagnetism* is a form of paramagnetism where the magnetic centers are strongly coupled and are thus magnetically concentrated. The electrons in ferromagnetic materials align their magnetic dipole moments parallel to each other to create a strong magnetic dipole moment. An external field can also align the magnetic moments to the external field producing a magnetic field for the material as a whole. The field persists when the external field is removed. *Antiferromagnetism* is another form of paramagnetism where the magnetic centers are magnetically concentrated and are strongly coupled. However, the electrons in antiferromagnetic materials align their dipole moments antiparallel with each other that

creates a zero net magnetic moment (**Figure 2.1**). In the presence of an external field the magnetic dipole moments align with the field producing a magnetic field for the material as a whole. When the field is removed the spins will revert to an antiparallel orientation.

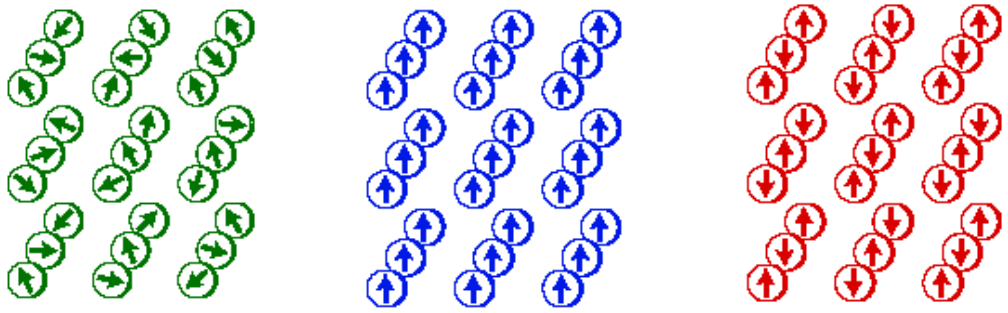

Paramagnetism Ferromagnetism Antiferromagnetism

Figure 2.1. Commonly encountered magnetic behaviors.

The descriptions of *ferromagnetism* and *antiferromagnetism* above are definitions that apply only in the bulk where there are domains of magnetic coupling and the interactions are intermolecular. Molecules with unpaired electrons only exhibit paramagnetism. However, they can have analogous behavior as the bulk in the sense that the spins within the molecule may exhibit ferromagnetic and antiferromagnetic intramolecular coupling. The ability of a paramagnetic molecule to exhibit magnetically concentrated behavior depends on the exchange coupling between the magnetic centers of the molecule. Exchange coupling is a purely repulsive phenomenon and it is rooted in Hund's first rule.

2.2 Intramolecular Exchange Coupling in Molecular Systems

As described previously Hund's first rule states that in the absence of any other perturbation, the state with highest spin multiplicity will be the most stable. This

reasoning is due to the fact that in a ground state where there are unpaired electrons in degenerate and orthogonal orbitals, the repulsion between the unpaired electrons is less when the electrons are paired in a parallel fashion than when the electrons are antiparallel to each other. Previously Hund's first rule was described using atomic orbitals however the model can be extended to molecular orbitals as well. Using simple organic biradicals as examples the exchange between the unpaired electrons can be described as a function of the interelectron repulsion. The singly occupied molecular orbitals (SOMO), or magnetic orbitals, of trimethylene methane (TMM) are doubly degenerate and orthogonal (**Figure 2.2**).[3]

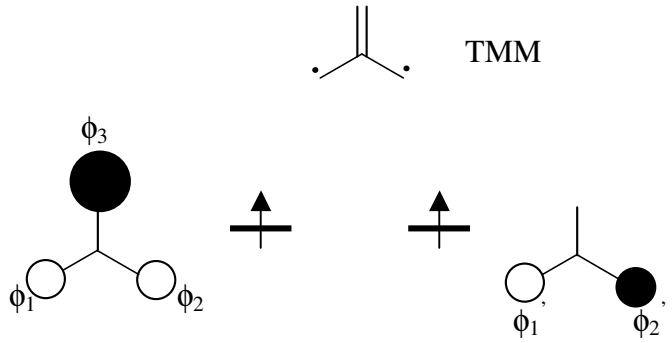

Figure 2.2. SOMO of TMM.

Despite the fact the orbitals of the doubly degenerate SOMOs are orthogonal to each other they share an overlap region at ϕ_1, ϕ_2 and ϕ_1', ϕ_2'. This overlap in the case of TMM is identical to the overlap discussed using the degenerate and orthogonal atomic p-orbitals. In organic radicals this interaction is known as disjoint.[3] Since there is less repulsion in the overlap region of the SOMOs of TMM for the triplet configuration due to the Pauli Exclusion Principle, the triplet state is lower in energy than the corresponding singlet state (**Figure 2.2**). The molecular orbital approach to constructing the ferromagnetic coupling in the TMM example can be distilled to a spin-polarized

depiction between the spin centers. Spin-polarization assumes that electron spin densities are distributed in an alternating fashion through the molecular framework. How one electron spin is oriented determines through the spin-polarization mechanism how the other spin will be oriented with respect to the first (**Figure 2.3**).[3]

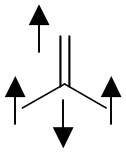

Figure 2.3. Spin-polarization in TMM.

The "negative" spin-density that's observed at the tertiary carbon of TMM comes from configuration interaction (CI) with singlet excited states.[3]

From both the molecular orbital and spin-polarization approaches the unpaired electrons in the TMM biradical are coupled ferromagnetically and the strength of the intermolecular exchange coupling is proportional to the exchange coupling energy (J) between the triplet ground state and the singlet excited state. Depending on how one constructs the spin-hamiltonian that describes the interelectron interaction between multiple unpaired spins the sign of the J parameter instructs on the type of exchange coupling that's observed. The spin-state arrangement shown is also known as a spin-ladder (**Figure 2.4**).[4]

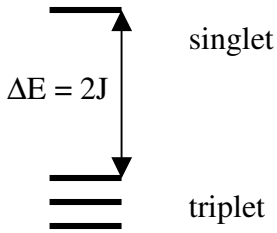

Figure 2.4. singet-triplet gap.

The tetramethylene ethane (TME) biradical can be used to describe how antiferromagnetic exchange coupling occurs in organic molecules. In order to illustrate the exchange coupling in TME it is easier to construct the SOMOs as degenerate fragment orbitals that "appear" non-orthogonal (**Figure 2.5**). In order to build the molecular orbitals of the TME SOMOs only linear combinations of the fragments need to be performed. The unpaired spins are shown as "spin-up" however the final ground state must still be described.

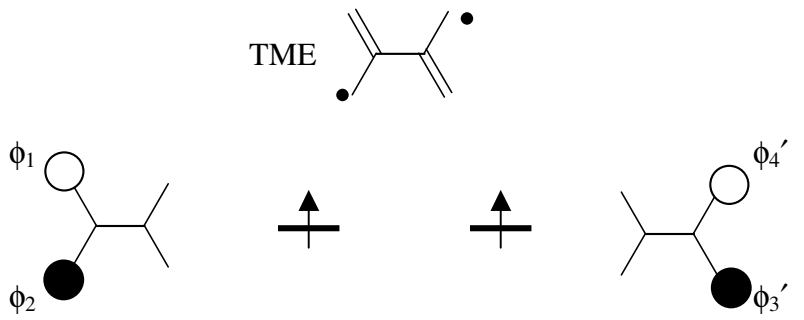

Figure 2.5. SOMO of TME.

In the fragment orbitals none of the orbital coefficients overlap each other. There is no difference in energy between the singlet and triplet states because there is no overlap region repulsion that would distinguish them. Thus at this level of theory the singlet is degenerate with triplet state. However, since the singlet is similar to a "bonding" interaction this provides further stabilization that the triplet does not have. Hence the TME biradical possesses a singlet ground state with a triplet excited state. The singlet ground state in TME is an example of antiferromagnetic exchange coupling in molecular systems. Using the spin-polarization picture one will arrive at the same result as the fragment orbital approach (**Figure 2.6**).

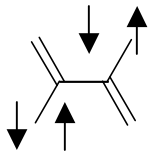

Figure 2.6. Spin-polarization in TME.

It appears from the TMM and TME examples that orthogonal SOMOs create ferromagnetic exchange coupling while non-orthogonal SOMOs do not. This is not always true because there are other perturbations that can take place that may change the expected spin-ladder such as excited state mixing through configuration interaction. For the biradicals shown, only the triplet and the lowest singlet states are shown. However, there are higher energy zwitter-ionic singlet states that can perturb the systems further.

2.3 Mixing Closed-Shell Excited States with Configuration Interaction: Antiferromagnetic Contribution to Exchange

In order to evaluate how the excited states perturb the ground state of simple biradicals the closed shell zwitterionic singlet states must be taken into account. There are two possible zwitterionic states possible in a biradical, $\psi_{S+,\,CS}$ and $\psi_{S-,\,CS}$. Thus by including the zwitterionic states in a biradical system the following states can be used to evaluate the state energies of the biradical:

$$\psi_A = \frac{1}{\sqrt{2}}\left(a(1)b(2) - b(1)a(2)\right) \qquad \text{(Triplet)}$$

$$\psi_{S,OS} = \frac{1}{\sqrt{2}}\left(a(1)b(2) + b(1)a(2)\right) \qquad \text{(Open-shell singlet)}$$

$$\psi_{S^+,CS} = \frac{1}{\sqrt{2}}\left(a(1)a(2) + b(1)b(2)\right) \qquad \text{(Closed-shell singlet)}$$

$$\psi_{S^-,CS} = \frac{1}{\sqrt{2}}\left(a(1)a(2) - b(1)b(2)\right) \qquad \text{(Closed-shell singlet)}$$

The energies of the open-shell triplet and singlet have already been evaluated to first-order. The energies of the unperturbed closed-shell excited states can be treated in the same way by first using the one-electron energy operators as part of the zeroth-order Hamiltonian. The energy of the unperturbed first closed-shell singlet:

$$
\begin{aligned}
E^{(0)}(\psi_{S+,CS}) &= \frac{1}{2}\left\langle a(1)a(2)+b(1)b(2)\middle|h(1)+h(2)\middle|a(1)a(2)+b(1)b(2)\right\rangle \\
&= \frac{1}{2}\left[\begin{array}{l}\left\langle a(1)a(2)\middle|h(1)+h(2)\middle|a(1)a(2)\right\rangle+\left\langle a(1)b(2)\middle|h(1)+h(2)\middle|b(1)b(2)\right\rangle \\ +\left\langle b(1)b(2)\middle|h(1)+h(2)\middle|a(1)a(2)\right\rangle+\left\langle b(1)b(2)\middle|h(1)+h(2)\middle|b(1)b(2)\right\rangle\end{array}\right] \\
&= \frac{1}{2}\left[\begin{array}{l}\left\langle a(2)\middle|a(2)\right\rangle\left\langle a(1)\middle|h(1)\middle|a(1)\right\rangle+\left\langle a(1)\middle|a(1)\right\rangle\left\langle a(2)\middle|h(2)\middle|a(2)\right\rangle \\ +\left\langle a(2)\middle|b(2)\right\rangle\left\langle a(1)\middle|h(1)\middle|b(1)\right\rangle+\left\langle a(1)\middle|b(1)\right\rangle\left\langle a(2)\middle|h(2)\middle|b(2)\right\rangle \\ +\left\langle b(2)\middle|a(2)\right\rangle\left\langle b(1)\middle|h(1)\middle|a(1)\right\rangle+\left\langle b(1)\middle|a(1)\right\rangle\left\langle b(2)\middle|h(2)\middle|a(2)\right\rangle \\ +\left\langle b(2)\middle|b(2)\right\rangle\left\langle b(1)\middle|h(1)\middle|b(1)\right\rangle+\left\langle b(1)\middle|b(1)\right\rangle\left\langle b(2)\middle|h(2)\middle|b(2)\right\rangle\end{array}\right] \\
&= \frac{1}{2}(\alpha+\alpha-0-0-0-0+\alpha+\alpha) = 2\alpha
\end{aligned}
\tag{2.1}
$$

The energy of the unperturbed second closed-shell singlet:

$$
\begin{aligned}
E^{(0)}(\psi_{S-,CS}) &= \frac{1}{2}\left\langle a(1)a(2)-b(1)b(2)\middle|h(1)+h(2)\middle|a(1)a(2)-b(1)b(2)\right\rangle \\
&= \frac{1}{2}\left[\begin{array}{l}\left\langle a(1)a(2)\middle|h(1)+h(2)\middle|a(1)a(2)\right\rangle-\left\langle a(1)b(2)\middle|h(1)+h(2)\middle|b(1)b(2)\right\rangle \\ -\left\langle b(1)b(2)\middle|h(1)+h(2)\middle|a(1)a(2)\right\rangle+\left\langle b(1)b(2)\middle|h(1)+h(2)\middle|b(1)b(2)\right\rangle\end{array}\right] \\
&= \frac{1}{2}\left[\begin{array}{l}\left\langle a(2)\middle|a(2)\right\rangle\left\langle a(1)\middle|h(1)\middle|a(1)\right\rangle+\left\langle a(1)\middle|a(1)\right\rangle\left\langle a(2)\middle|h(2)\middle|a(2)\right\rangle \\ -\left\langle a(2)\middle|b(2)\right\rangle\left\langle a(1)\middle|h(1)\middle|b(1)\right\rangle-\left\langle a(1)\middle|b(1)\right\rangle\left\langle a(2)\middle|h(2)\middle|b(2)\right\rangle \\ -\left\langle b(2)\middle|a(2)\right\rangle\left\langle b(1)\middle|h(1)\middle|a(1)\right\rangle-\left\langle b(1)\middle|a(1)\right\rangle\left\langle b(2)\middle|h(2)\middle|a(2)\right\rangle \\ +\left\langle b(2)\middle|b(2)\right\rangle\left\langle b(1)\middle|h(1)\middle|b(1)\right\rangle+\left\langle b(1)\middle|b(1)\right\rangle\left\langle b(2)\middle|h(2)\middle|b(2)\right\rangle\end{array}\right] \\
&= \frac{1}{2}(\alpha+\alpha-0-0-0-0+\alpha+\alpha) = 2\alpha
\end{aligned}
\tag{2.2}
$$

Again by taking into account interelectron repulsion the first order correction to the Hamiltonian can be added where the corrected energy of the first closed-shell singlet to first-order:

$$
\begin{aligned}
E^1(\psi_{S+,CS}) &= \frac{1}{2}\left\langle a(1)a(2)+b(1)b(2)\left|H^0+\frac{1}{r_{12}}\right|a(1)a(2)+b(1)b(2)\right\rangle \\
&= 2\alpha+\frac{1}{2}\left\langle a(1)a(2)+b(1)b(2)\left|\frac{1}{r_{12}}\right|a(1)a(2)+b(1)b(2)\right\rangle \\
&= 2\alpha+\frac{1}{2}\left[\begin{array}{l}\left\langle a(1)a(2)\left|\frac{1}{r_{12}}\right|a(1)a(2)\right\rangle+\left\langle a(1)a(2)\left|\frac{1}{r_{12}}\right|b(1)b(2)\right\rangle \\ +\left\langle b(1)b(2)\left|\frac{1}{r_{12}}\right|a(1)a(2)\right\rangle+\left\langle b(1)b(2)\left|\frac{1}{r_{12}}\right|b(1)b(2)\right\rangle\end{array}\right] \\
&= 2\alpha+\frac{1}{2}\left[\begin{array}{l}\left\langle a(1)a(1)\left|\frac{1}{r_{12}}\right|a(2)a(2)\right\rangle+\left\langle a(1)b(1)\left|\frac{1}{r_{12}}\right|a(2)b(2)\right\rangle \\ +\left\langle b(1)a(1)\left|\frac{1}{r_{12}}\right|a(2)b(2)\right\rangle+\left\langle b(1)b(1)\left|\frac{1}{r_{12}}\right|a(2)a(2)\right\rangle\end{array}\right] \\
&= 2\alpha+\frac{1}{2}\left[j^0+k+k+j^0\right]=2\alpha+j^0+k
\end{aligned}
\tag{2.3}
$$

The corrected energy of the second closed-shell singlet to first-order:

$$
\begin{aligned}
E^1(\psi_{S-,CS}) &= \frac{1}{2}\left\langle a(1)a(2)-b(1)b(2)\left|H^0+\frac{1}{r_{12}}\right|a(1)a(2)-b(1)b(2)\right\rangle \\
&= 2\alpha+\frac{1}{2}\left\langle a(1)a(2)-b(1)b(2)\left|\frac{1}{r_{12}}\right|a(1)a(2)-b(1)b(2)\right\rangle \\
&= 2\alpha+\frac{1}{2}\left[\begin{array}{l}\left\langle a(1)a(2)\left|\frac{1}{r_{12}}\right|a(1)a(2)\right\rangle-\left\langle a(1)a(2)\left|\frac{1}{r_{12}}\right|b(1)b(2)\right\rangle \\ -\left\langle b(1)b(2)\left|\frac{1}{r_{12}}\right|a(1)a(2)\right\rangle+\left\langle b(1)b(2)\left|\frac{1}{r_{12}}\right|b(1)b(2)\right\rangle\end{array}\right]
\end{aligned}
$$

$$= 2\alpha + \frac{1}{2}\left[\begin{array}{l} \left\langle a(1)a(1)\left|\frac{1}{r_{12}}\right|a(2)a(2)\right\rangle - \left\langle a(1)b(1)\left|\frac{1}{r_{12}}\right|a(2)b(2)\right\rangle \\ -\left\langle b(1)a(1)\left|\frac{1}{r_{12}}\right|a(2)b(2)\right\rangle + \left\langle b(1)b(1)\left|\frac{1}{r_{12}}\right|a(2)a(2)\right\rangle \end{array}\right]$$

$$= 2\alpha + \frac{1}{2}\left[j^0 + k + k + j^0 \right] = 2\alpha + j^0 - k \qquad (2.4)$$

The energy level diagram for the four states is now:

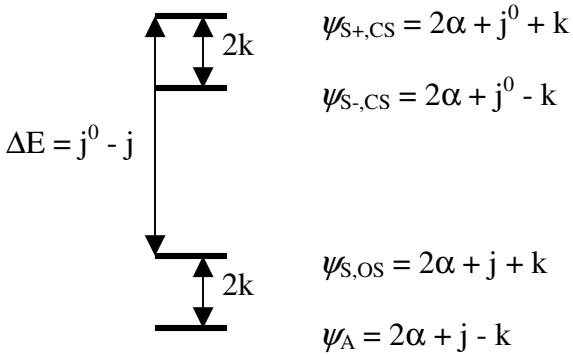

Figure 2.7. Spin ladder without CI.

The second order correction to the energy provides how the excited states perturb the ground state energies through configuration interaction:

$$E^{(2)} = \frac{\left\langle \psi_m \left| H^0 + H^1 \right| \psi_n \right\rangle^2}{E_n - E_m} \qquad (2.5)$$

By first evaluating the numerator, the second order correction for the mixing of $\psi_{S,OS}$ and $\psi_{S+,CS}$ is:

$$
\begin{aligned}
&\left\langle \psi_{S,OS} \left| h(1)+h(2)+\frac{1}{r_{12}} \right| \psi_{S+,CS} \right\rangle^2 \\
&= \left\langle \frac{1}{\sqrt{2}}\big(a(1)b(2)+b(1)a(2)\big) \left| h(1)+h(2)+\frac{1}{r_{12}} \right| \frac{1}{\sqrt{2}}\big(a(1)a(2)+b(1)b(2)\big) \right\rangle^2 \\
&= \frac{1}{\sqrt{2}} \left[\begin{array}{l}
\big\langle a(1)b(2)+b(1)a(2) \big| h(1) \big| a(1)a(2)+b(1)b(2) \big\rangle \\
+\big\langle a(1)b(2)+b(1)a(2) \big| h(2) \big| a(1)a(2)+b(1)b(2) \big\rangle \\
+\left\langle a(1)b(2)+b(1)a(2) \left| \frac{1}{r_{12}} \right| a(1)a(2)+b(1)b(2) \right\rangle
\end{array} \right]^2 \\
&= \frac{1}{2} \left[\begin{array}{l}
\big\langle a(1)b(2) \big| h(1) \big| a(1)a(2) \big\rangle + \big\langle a(1)b(2) \big| h(1) \big| b(1)b(2) \big\rangle + \big\langle b(1)a(2) \big| h(1) \big| a(1)a(2) \big\rangle \\
+\big\langle b(1)a(2) \big| h(1) \big| b(1)b(2) \big\rangle + \big\langle a(1)b(2) \big| h(2) \big| a(1)a(2) \big\rangle + \big\langle a(1)b(2) \big| h(2) \big| b(1)b(2) \big\rangle \\
+\big\langle b(1)a(2) \big| h(2) \big| a(1)a(2) \big\rangle + \big\langle b(1)a(2) \big| h(2) \big| b(1)b(2) \big\rangle + \left\langle a(1)b(2) \left| \frac{1}{r_{12}} \right| a(1)a(2) \right\rangle \\
\left\langle a(1)b(2) \left| \frac{1}{r_{12}} \right| b(1)b(2) \right\rangle + \left\langle b(1)a(2) \left| \frac{1}{r_{12}} \right| a(1)a(2) \right\rangle + \left\langle b(1)a(2) \left| \frac{1}{r_{12}} \right| b(1)b(2) \right\rangle
\end{array} \right]^2 \\
&= \frac{1}{2} \left[\begin{array}{l}
\big\langle b(2) \big| a(2) \big\rangle \big\langle a(1) \big| h(1) \big| a(1) \big\rangle + \big\langle b(2) \big| b(2) \big\rangle \big\langle a(1) \big| h(1) \big| b(1) \big\rangle \\
+\big\langle a(2) \big| a(2) \big\rangle \big\langle b(1) \big| h(1) \big| a(1) \big\rangle + \big\langle a(2) \big| b(2) \big\rangle \big\langle b(1) \big| h(1) \big| b(1) \big\rangle \\
+\big\langle a(1) \big| a(1) \big\rangle \big\langle b(2) \big| h(2) \big| a(2) \big\rangle + \big\langle a(1) \big| b(1) \big\rangle \big\langle b(2) \big| h(2) \big| b(2) \big\rangle \\
+\big\langle b(1) \big| a(1) \big\rangle \big\langle a(2) \big| h(2) \big| a(2) \big\rangle + \big\langle b(1) \big| b(1) \big\rangle \big\langle a(2) \big| h(2) \big| b(2) \big\rangle \\
+\left\langle a(1)a(1) \left| \frac{1}{r_{12}} \right| a(2)b(2) \right\rangle + \left\langle a(1)b(1) \left| \frac{1}{r_{12}} \right| b(2)b(2) \right\rangle \\
+\left\langle b(1)a(1) \left| \frac{1}{r_{12}} \right| a(2)a(2) \right\rangle + \left\langle b(1)b(1) \left| \frac{1}{r_{12}} \right| a(2)b(2) \right\rangle
\end{array} \right]^2 \qquad (2.6) \\
&= \left[\frac{1}{2}\big(0+\beta+\beta+0+\beta+0+0+\beta+l+l+l+l\big) \right]^2 \\
&= \left[\frac{1}{2}\big(4\beta+4l\big) \right]^2 = 4\big(\beta+l\big)^2
\end{aligned}
$$

The second-order correction to the energy of the $\psi_{S,OS}$ state then is:

$$E^{(2)}(\psi_{S,OS}) = \frac{4(\beta + l)^2}{j^0 - j} \tag{2.7}$$

By mixing $\psi_{S,OS}$ and $\psi_{S-,CS}$ the following is evaluated:

$$\left\langle \psi_{S,OS} \left| h(1) + h(2) + \frac{1}{r_{12}} \right| \psi_{S-,CS} \right\rangle^2$$

$$= \left\langle \frac{1}{\sqrt{2}}\big(a(1)b(2) + b(1)a(2)\big) \left| h(1) + h(2) + \frac{1}{r_{12}} \right| \frac{1}{\sqrt{2}}\big(a(1)a(2) - b(1)b(2)\big) \right\rangle^2$$

$$= \left[\frac{1}{\sqrt{2}} \begin{bmatrix} \langle a(1)b(2) + b(1)a(2) | h(1) | a(1)a(2) - b(1)b(2) \rangle \\ + \langle a(1)b(2) + b(1)a(2) | h(2) | a(1)a(2) - b(1)b(2) \rangle \\ + \left\langle a(1)b(2) + b(1)a(2) \left| \frac{1}{r_{12}} \right| a(1)a(2) - b(1)b(2) \right\rangle \end{bmatrix} \right]^2$$

$$= \left[\frac{1}{2} \begin{bmatrix} \langle a(1)b(2) | h(1) | a(1)a(2) \rangle - \langle a(1)b(2) | h(1) | b(1)b(2) \rangle + \langle b(1)a(2) | h(1) | a(1)a(2) \rangle \\ - \langle b(1)a(2) | h(1) | b(1)b(2) \rangle + \langle a(1)b(2) | h(2) | a(1)a(2) \rangle - \langle a(1)b(2) | h(2) | b(1)b(2) \rangle \\ + \langle b(1)a(2) | h(2) | a(1)a(2) \rangle - \langle b(1)a(2) | h(2) | b(1)b(2) \rangle + \left\langle a(1)b(2) \left| \frac{1}{r_{12}} \right| a(1)a(2) \right\rangle \\ - \left\langle a(1)b(2) \left| \frac{1}{r_{12}} \right| b(1)b(2) \right\rangle + \left\langle b(1)a(2) \left| \frac{1}{r_{12}} \right| a(1)a(2) \right\rangle - \left\langle b(1)a(2) \left| \frac{1}{r_{12}} \right| b(1)b(2) \right\rangle \end{bmatrix} \right]^2$$

$$= \left[\frac{1}{2} \begin{bmatrix} \langle b(2) | a(2) \rangle \langle a(1) | h(1) | a(1) \rangle + \langle b(2) | b(2) \rangle \langle a(1) | h(1) | b(1) \rangle \\ - \langle a(2) | a(2) \rangle \langle b(1) | h(1) | a(1) \rangle + \langle a(2) | b(2) \rangle \langle b(1) | h(1) | b(1) \rangle \\ - \langle a(1) | a(1) \rangle \langle b(2) | h(2) | a(2) \rangle + \langle a(1) | b(1) \rangle \langle b(2) | h(2) | b(2) \rangle \\ - \langle b(1) | a(1) \rangle \langle a(2) | h(2) | a(2) \rangle - \langle b(1) | b(1) \rangle \langle a(2) | h(2) | b(2) \rangle \\ + \left\langle a(1)a(1) \left| \frac{1}{r_{12}} \right| a(2)b(2) \right\rangle - \left\langle a(1)b(1) \left| \frac{1}{r_{12}} \right| b(2)b(2) \right\rangle + \left\langle b(1)a(1) \left| \frac{1}{r_{12}} \right| a(2)a(2) \right\rangle \\ - \left\langle b(1)b(1) \left| \frac{1}{r_{12}} \right| a(2)b(2) \right\rangle \end{bmatrix} \right]^2$$

$$= \left[\frac{1}{2} \left(0 - \beta + \beta - 0 + \beta - 0 + 0 - \beta + l - l + l - l \right) \right]^2$$

$$= \left[\frac{1}{2} (0) \right]^2 = 0 \tag{2.8}$$

The second-order correction to the energy of $\psi_{S-,CS}$ is zero.

For the mixing of $\psi_{+,CS}$ into ψ_A the second-order correction to the ψ_A state is:

$$\left\langle \psi_A \left| h(1) + h(2) + \frac{1}{r_{12}} \right| \psi_{S+,CS} \right\rangle^2$$

$$= \left\langle \frac{1}{\sqrt{2}} \left(a(1)b(2) - b(1)a(2) \right) \left| h(1) + h(2) + \frac{1}{r_{12}} \right| \frac{1}{\sqrt{2}} \left(a(1)a(2) + b(1)b(2) \right) \right\rangle^2$$

$$= \left[\frac{1}{\sqrt{2}} \left[\begin{array}{l} \left\langle a(1)b(2) - b(1)a(2) \left| h(1) \right| a(1)a(2) + b(1)b(2) \right\rangle \\ + \left\langle a(1)b(2) - b(1)a(2) \left| h(2) \right| a(1)a(2) + b(1)b(2) \right\rangle \\ + \left\langle a(1)b(2) - b(1)a(2) \left| \frac{1}{r_{12}} \right| a(1)a(2) + b(1)b(2) \right\rangle \end{array} \right] \right]^2$$

$$= \left[\frac{1}{2} \left[\begin{array}{l} \left\langle a(1)b(2) \left| h(1) \right| a(1)a(2) \right\rangle + \left\langle a(1)b(2) \left| h(1) \right| b(1)b(2) \right\rangle - \left\langle b(1)a(2) \left| h(1) \right| a(1)a(2) \right\rangle \\ - \left\langle b(1)a(2) \left| h(1) \right| b(1)b(2) \right\rangle + \left\langle a(1)b(2) \left| h(2) \right| a(1)a(2) \right\rangle + \left\langle a(1)b(2) \left| h(2) \right| b(1)b(2) \right\rangle \\ - \left\langle b(1)a(2) \left| h(2) \right| a(1)a(2) \right\rangle - \left\langle b(1)a(2) \left| h(2) \right| b(1)b(2) \right\rangle + \left\langle a(1)b(2) \left| \frac{1}{r_{12}} \right| a(1)a(2) \right\rangle \\ + \left\langle a(1)b(2) \left| \frac{1}{r_{12}} \right| b(1)b(2) \right\rangle - \left\langle b(1)a(2) \left| \frac{1}{r_{12}} \right| a(1)a(2) \right\rangle - \left\langle b(1)a(2) \left| \frac{1}{r_{12}} \right| b(1)b(2) \right\rangle \end{array} \right] \right]^2$$

$$
= \left[\frac{1}{2} \left[\begin{array}{l}
\langle b(2)|a(2)\rangle\langle a(1)|h(1)|a(1)\rangle + \langle b(2)|b(2)\rangle\langle a(1)|h(1)|b(1)\rangle \\
-\langle a(2)|a(2)\rangle\langle b(1)|h(1)|a(1)\rangle - \langle a(2)|b(2)\rangle\langle b(1)|h(1)|b(1)\rangle \\
+\langle a(1)|a(1)\rangle\langle b(2)|h(2)|a(2)\rangle + \langle a(1)|b(1)\rangle\langle b(2)|h(2)|b(2)\rangle \\
-\langle b(1)|a(1)\rangle\langle a(2)|h(2)|a(2)\rangle - \langle b(1)|b(1)\rangle\langle a(2)|h(2)|b(2)\rangle \\
+\left\langle a(1)a(1)\left|\frac{1}{r_{12}}\right|a(2)b(2)\right\rangle - \left\langle a(1)b(1)\left|\frac{1}{r_{12}}\right|b(2)b(2)\right\rangle - \left\langle b(1)a(1)\left|\frac{1}{r_{12}}\right|a(2)a(2)\right\rangle \\
-\left\langle b(1)b(1)\left|\frac{1}{r_{12}}\right|a(2)b(2)\right\rangle
\end{array} \right] \right]^2
$$

$$
= \left[\frac{1}{2} \left(0 + \beta - \beta - 0 + \beta + 0 - 0 - \beta + l + l - l - l \right) \right]^2
$$

$$
= \left[\frac{1}{2} (0) \right]^2 = 0 \tag{2.9}
$$

The second order correction to $\psi_{S+,CS}$ is zero.

For mixing $\psi_{S-,CS}$ into ψ_A the following is evaluated:

$$
\left\langle \psi_A \left| h(1) + h(2) + \frac{1}{r_{12}} \right| \psi_{S-,CS} \right\rangle^2
$$

$$
= \left\langle \frac{1}{\sqrt{2}} \left(a(1)b(2) - b(1)a(2) \right) \left| h(1) + h(2) + \frac{1}{r_{12}} \right| \frac{1}{\sqrt{2}} \left(a(1)a(2) - b(1)b(2) \right) \right\rangle^2
$$

$$
= \left[\frac{1}{\sqrt{2}} \left[\begin{array}{l}
\langle a(1)b(2) - b(1)a(2)|h(1)|a(1)a(2) - b(1)b(2)\rangle \\
+\langle a(1)b(2) - b(1)a(2)|h(2)|a(1)a(2) - b(1)b(2)\rangle \\
+\left\langle a(1)b(2) - b(1)a(2)\left|\frac{1}{r_{12}}\right|a(1)a(2) - b(1)b(2)\right\rangle
\end{array} \right] \right]^2
$$

$$
= \left[\frac{1}{2} \left[\begin{array}{l}
\langle a(1)b(2)|h(1)|a(1)a(2)\rangle - \langle a(1)b(2)|h(1)|b(1)b(2)\rangle - \langle b(1)a(2)|h(1)|a(1)a(2)\rangle \\
+\langle b(1)a(2)|h(1)|b(1)b(2)\rangle + \langle a(1)b(2)|h(2)|a(1)a(2)\rangle - \langle a(1)b(2)|h(2)|b(1)b(2)\rangle \\
-\langle b(1)a(2)|h(2)|a(1)a(2)\rangle + \langle b(1)a(2)|h(2)|b(1)b(2)\rangle + \left\langle a(1)b(2)\left|\frac{1}{r_{12}}\right|a(1)a(2)\right\rangle \\
-\left\langle a(1)b(2)\left|\frac{1}{r_{12}}\right|b(1)b(2)\right\rangle - \left\langle b(1)a(2)\left|\frac{1}{r_{12}}\right|a(1)a(2)\right\rangle + \left\langle b(1)a(2)\left|\frac{1}{r_{12}}\right|b(1)b(2)\right\rangle
\end{array} \right] \right]^2
$$

$$
\begin{aligned}
&= \left[\frac{1}{2} \left[\begin{array}{l}
\langle b(2)|a(2)\rangle\langle a(1)|h(1)|a(1)\rangle - \langle b(2)|b(2)\rangle\langle a(1)|h(1)|b(1)\rangle \\
-\langle a(2)|a(2)\rangle\langle b(1)|h(1)|a(1)\rangle + \langle a(2)|b(2)\rangle\langle b(1)|h(1)|b(1)\rangle \\
+\langle a(1)|a(1)\rangle\langle b(2)|h(2)|a(2)\rangle - \langle a(1)|b(1)\rangle\langle b(2)|h(2)|b(2)\rangle \\
-\langle b(1)|a(1)\rangle\langle a(2)|h(2)|a(2)\rangle + \langle b(1)|b(1)\rangle\langle a(2)|h(2)|b(2)\rangle \\
+\left\langle a(1)a(1)\left|\frac{1}{r_{12}}\right|a(2)b(2)\right\rangle - \left\langle a(1)b(1)\left|\frac{1}{r_{12}}\right|b(2)b(2)\right\rangle \\
-\left\langle b(1)a(1)\left|\frac{1}{r_{12}}\right|a(2)a(2)\right\rangle + \left\langle b(1)b(1)\left|\frac{1}{r_{12}}\right|a(2)b(2)\right\rangle
\end{array} \right] \right]^2 \\
&= \left[\frac{1}{2}\left(0 - \beta - \beta + 0 + \beta - 0 - 0 + \beta + l - l - l + l\right) \right]^2 \\
&= \left[\frac{1}{2}(0) \right]^2 = 0
\end{aligned}
\tag{2.10}
$$

Thus configuration interaction operates only on the singlet manifold and the corrections give rise the following corrected energy level diagram for the singlet-triplet spin-ladder:

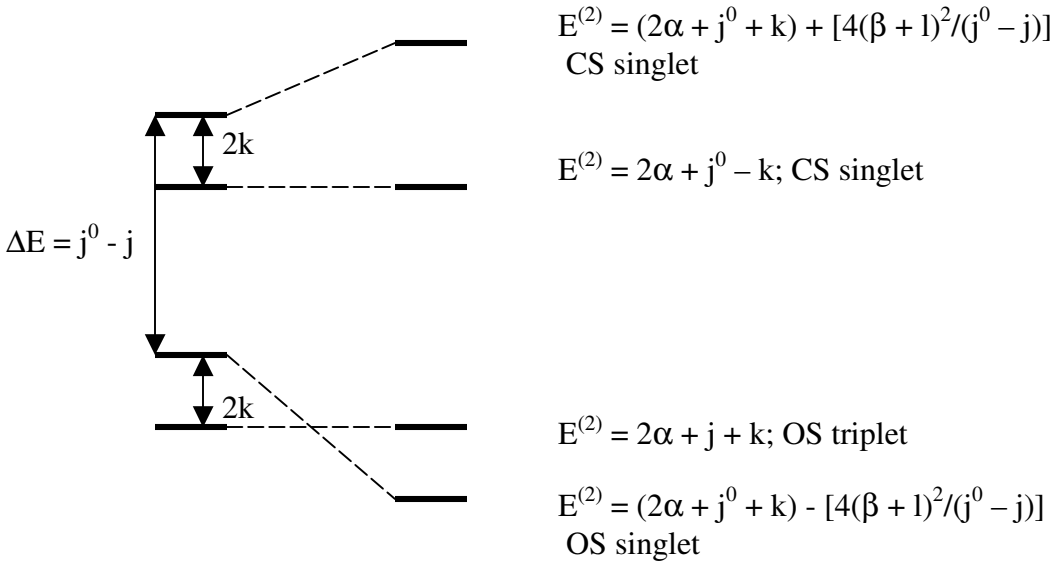

Figure 2.8. CI contribution to the spin-ladder energies.

Mixing of the singlet excited state terms lowers the energy of the open-shell singlet below the triplet despite the fact that Hund's first rule predicts otherwise. The revised exchange coupling parameter can now be expressed in terms of the second-order contributions of the excited states:

$$J = 2k - \frac{4(\beta + l)^2}{j^0 - j} \qquad (2.11)$$
$$= J_F + J_{AF}$$

Hund's rules were derived from first-order inter-electron interactions. By taking into account second order-effects such as CI the ultimate exchange coupling between two magnetic centers may differ from that predicted using simple orthogonality arguments.

2.4 Exchange Coupling in Transition Metal Complexes[5]

At very low levels of theory the exchange coupling in transition metal complexes can be viewed in terms of the orthogonality of the magnetic orbitals similarly to the models used in simple organic biradicals. To describe magnetic interactions in transition metal complexes two cases will be considered: 1) direct exchange between a metal ion and radical containing ligand and 2) superexchange coupling between transition metal ions through a diamagnetic ligand.

In the former case the examples that can be used are similar to the first-order treatment given for the organic biradicals. Consider a metal-ligand interaction where the magnetic orbital of the metal and ligand are orthogonal to each other (**Figure 2.9**).

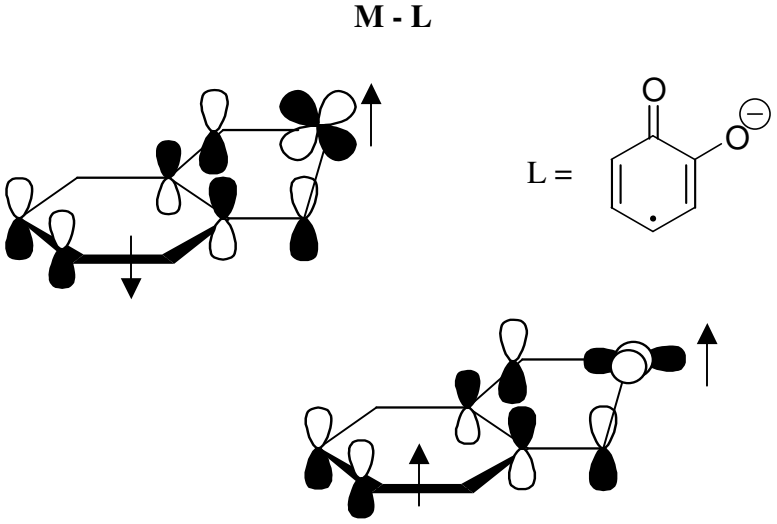

Figure 2.9. Metal-ligand exchange.

Just as Hund's first rule predicts the orthogonality of the two spin-containing orbitals prevents the unpaired electron densities to be distributed in the overlap region of the two magnetic orbitals thus the direct exchange stabilizes the ferromagnetically coupled state. If the magnetic orbitals are non-orthogonal then the direct exchange stabilizes the antiferromagnetically coupled state (**Figure 2.9**).

Unlike the simple organic biradicals there is an added complexity with direct exchange in metal complexes because metal magnetic orbitals can at the same time be both orthogonal and not with respect to the ligand magnetic orbital (**Figure 2.10**). This produces competing direct exchange pathways. In most cases the antiferromagnetic direct exchange pathway dominates due to the bonding stabilization the exchange pathway affords.

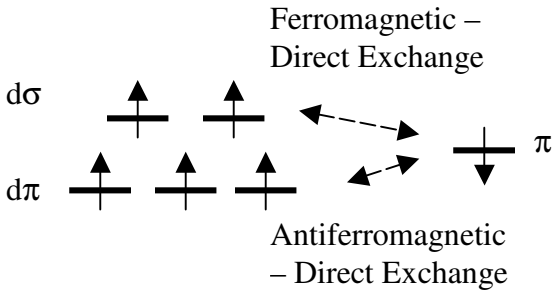

Figure 2.10. Direct exchange pathways.

In the superexchange case consider an example where there is bonding between the two transition metal ions through a pure ligand p-orbital. The magnetic orbitals of the transition metal ions are the same with the same number of unpaired electrons while the diamagnetic p-orbital contains two electrons (**Figure 2.11 A**).[1] If one of the metal magnetic orbitals contains a spin-up electron, the bonding interaction with the p-orbital is such that the pairing between the meta electron and the first p-orbital electron is "anti" with respect to each. Because the other p-orbital electron must be antiparallel to the first electron, pairing between the second p-orbital electron and the second d-orbital electron must be also be antiparallel. Overall the two transition metal magnetic orbitals are coupled antiferromagnetically through the diamagnetic ligand. The antiferromagnetic exchange is due primarily to the non-orthogonality of the metal magnetic orbitals with

respect to the diamagnetic ligand orbital. In order to discuss ferromagnetic exchange between metal magnetic orbitals a slightly different picture is needed (**Figure 2.11 B**).[1]

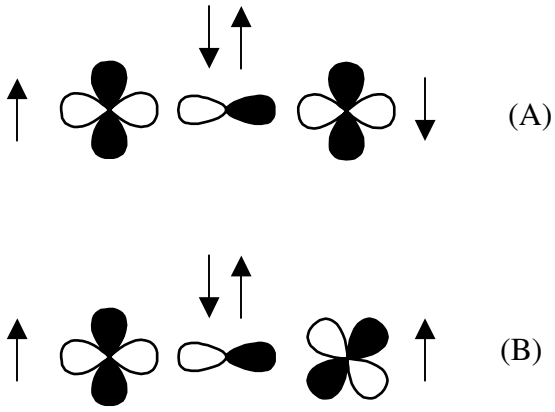

Figure 2.11. Antiferromagnetic (a) and ferromagnetic coupling (b) through diamagnetic ligand.

In this example the two magnetic orbitals are different in which one is a dσ orbital while the other is in dπ and they are both coupled through the same p-orbital as the antiferromagnetic example. Since the magnetic dσ orbital is non-orthogonal with respect to the bridging p-orbital, again the expected interaction is such that the dσ spin aligns antiparallel with the first p-orbital electron. However the interaction of the second p-orbital spin is parallel with respect to the dπ magnetic orbital because both the bridging p-orbital and the dπ orbitals are orthogonal to each other. Thus the two magnetic orbitals are coupled ferromagnetically through superexchange.

The key to the development of ferromagnetic coupling in the example above is the step involving the orthogonality of two orbitals. The orthogonality does not need to be between metal and ligand orbitals. If the superexchange pathway involves a bridge

that includes two p-orbitals on the same atom, these p-orbitals are mutually orthogonal and ferromagnetic coupling can result (**Figure 2.12**).[5]

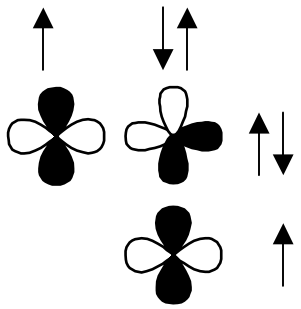

Figure 2.12. Ferromagnetic coupling through two ligand orbitals.

Clearly it seems that by using a choice of magnetic orbitals and bridging ligand one can select for ferromagnetic or antiferromagnetic superexchange coupling. However in most cases the coupling between two linked metal atoms, each with unpaired electrons, will contain at least one antiferromagnetic coupling pathway that involves non-orthogonal orbitals and perhaps a ferromagnetic coupling pathway through another orbital sequence. Just as with all the examples covered from the exchange coupling in organic biradicals to the direct exchange in metal and radical containing ligands, the antiferromagnetic coupling pathway almost always dominates because the bonding interaction stabilization of the antiferromagnetic exchange is so much greater.

2.5 Magnetic Susceptibility of a System with a Single Unpaired Spin

The observed magnetic behavior of systems with unpaired electrons can be related to the number and orbital arrangement of the unpaired electrons. The magnetic behavior is determined by measuring the magnetic polarization of the substance by a

magnetic field. In order to describe the behavior of a paramagnetic system the magnetic induction is typically defined as:[5,6]

$$\vec{B} = \vec{H}_0 + 4\pi\vec{M} \tag{2.12}$$

where $\vec{H}_0$ is the applied field strength and $\vec{M}$ is the magnetization per unit volume. By dividing the equation by $\vec{H}_0$ the following results:

$$\frac{B}{H_0} = 1 + 4\pi\frac{M'}{H_0} = 1 + 4\pi\chi_v \tag{2.13}$$

χ_v is the magnetic susceptibility per unit volume. By dividing χ_v by the density of the substance (d) produces the gram susceptibility χ_g and by multiplying χ_g with the molecular weight of the paramagnetic substance the molar susceptibility results, χ_m.

The paramagnetic contribution to the susceptibility arises from the spin and orbital angular momenta of the electrons interacting with the field. To begin it is easier to consider a single electron with no orbital contribution to the moment. Using the same relationships discussed in Chapter 1, the projection along the field direction of the magnetic moment of an electron in a quantum state n is described by the partial derivative of the energy of that state E_n with respect to the field, H:[6]

$$\mu_n = \mu_{s,z} = -\frac{\partial E_n}{\partial H} = -g\beta m_s \tag{2.14}$$

The bulk magnetic moment of a paramagnetic sample is described by the sum of the individual moments of the states weighted by their Boltzmann populations. Thus, the population-weighted sum of magnetic moments over the individual states (or the macroscopic magnetic moment) can be described for a mole of material with S = 1/2 as:

$$M = N\sum_{m_s} \mu_n P_n$$
$$= \frac{N\sum_{m_s=-1/2}^{+1/2} \mu_n \exp\left(\frac{-E_n}{kT}\right)}{\sum_{m_s=-1/2}^{+1/2} \mu_n \exp\left(\frac{-E_n}{kT}\right)} \qquad (2.15)$$

where N is Avogadro's number and P_n is the Boltzmann factor for calculating the probability. By substituting equation 2.14 for μ_n and $E = m_s g\beta H$ for E_n and summing over $m_s = \pm ½$ produces:[1]

$$M = \frac{Ng\beta}{2}\left[\frac{\exp\left(\frac{g\beta H}{2kT}\right) - \exp\left(\frac{-g\beta H}{2kT}\right)}{\exp\left(\frac{g\beta H}{2kT}\right) + \exp\left(\frac{-g\beta H}{2kT}\right)}\right] \qquad (2.16)$$

For very small values of $g\beta H/kT$ the following approximation can be used:

$$\exp\left(\frac{g\beta H}{2kT}\right) \approx \left(1 \pm \frac{g\beta H}{2kT}\right) \qquad (2.17)$$

which can be substituted into equation 2.16 and leads to:

$$M = \frac{Ng^2\beta^2 H}{4kT} \qquad (2.18)$$

Since the molar susceptibility can be related to M/H then χ_m can be written in terms of:

$$\chi_m = \frac{Ng^2\beta^2}{4kT} = \frac{C}{T} \qquad (2.19)$$

The above equation is the Curie law and predicts a straight-line relationship between the susceptibility and the inverse of the temperature to provide a zero intercept. However,

the Curie law approximation is not very accurate because for many systems the intercept is non-zero due to intermolecular interactions between neighboring magnetic moments that contribute to the value of the intercept. To account for the non-zero intercept the Curie-Weiss approximation can be used:

$$\chi = \frac{C}{T - \theta} \tag{2.20}$$

where θ is the Weiss correction that accounts for the susceptibility difference at 0 K.

Both χ and M are macroscopic properties and in describing the magnetic properties of transition metal complexes it is easier to use a microscopic quantity called the effective magnetic moment defined as:

$$\mu_{eff} = \left(\frac{3kT}{N\beta^2} \right)^{1/2} (\chi T)^{1/2} = 2.828 (\chi T)^{1/2} \tag{2.21}$$

And the spin-only magnetic moment can be calculated using:[1]

$$\mu_{eff}(spin-only) = g\left[S(S+1)) \right]^{1/2} = \left[n(n+1) \right]^{1/2} \tag{2.22}$$

where *n* is the number of unpaired electrons per molecule.

2.6 The Van-Vleck Relationship

The problem with the spin-only derivations is that the moments and temperature dependence of the susceptibility do not agree with predictions when dealing with systems that are electronically complex. Such complexity can arise from contributions of excited states to the magnetic moment. Two cases will be considered to explore more complex behavior in the magnetic susceptibility: 1) a low symmetry transition metal ion with

nonzero orbital angular momentum in the ground state and 2) an exchange coupled system.

For a single transition metal ion in a low-symmetry environment with spin-orbit coupling operative in the ground state the following Hamiltonian can be constructed:[6]

$$\hat{H} = \lambda \hat{L} \bullet \hat{S} + \beta(\hat{L} + g\hat{S}) \bullet H \tag{2.23}$$

The zeroth-order contribution to the Hamiltonian is the spin-orbit operator. The other contributions to the Hamiltonian are orbital and spin operators and are functions of the magnetic field. The field-induced terms allow for the mixing of excited zeeman terms into the ground state. Thus the contributions to the energy of a given state *n* are:[1,5,6]

$$E_n = E_n^{(0)} + HE_n^{(1)} + H^2 E_n^{(2)} \tag{2.24}$$

where the zeroth-order term is the spin-orbit coupling, which makes no contribution to the magnetic moment of a given state. The first-order term is the first-order zeeman interaction and is independent of the field strength. The second-order term is the second-order zeeman interaction and is field dependent.

To take into account the influence of these effects on the susceptibility the equation 2.15 can be rewritten by replacing $\exp(-E_n/kT)$ with:

$$\exp\left(\frac{-E_n^{(0)} - HE_n^{(1)} - H^2 E_n^{(2)}}{kT}\right) \cong \left(1 - \frac{HE_n^{(1)}}{kT}\right)\exp\left(\frac{-E_n^{(0)}}{kT}\right) \tag{2.25}$$

Furthermore μ_n can now be defined as:

$$\mu_n = \frac{-\partial E_n}{\partial H} = -E_n^{(1)} - 2HE_n^{(2)} \tag{2.26}$$

Hence:

$$M = N\frac{\sum_n \left(-E_n^{(1)} - 2HE_n^{(2)}\right)\left(1-\frac{HE_n^{(1)}}{kT}\right)\exp\left(\frac{-E_n^{(0)}}{kT}\right)}{\sum_n \left(1-\frac{HE_n^{(1)}}{kT}\right)\exp\left(\frac{-E_n^{(0)}}{kT}\right)} \tag{2.27}$$

The numerator can be expanded and the following results:

$$\psi_M = N\frac{\sum_n \left(\frac{\left(E_n^{(1)}\right)^2 H}{kT} - 2HE_n^{(2)} + \frac{2H^2 E_n^{(1)}}{kT}\right)\exp\left(\frac{-E_n^{(0)}}{kT}\right)}{\sum_n \exp\left(\frac{-E_n^{(0)}}{kT}\right)} \tag{2.28}$$

By canceling the H's and neglecting the term $2HE_n^{(1)}/kT$ the Van-Vleck expression results:

$$\psi_M = N\frac{\sum_n \left(\frac{\left(E_n^{(1)}\right)^2}{kT} - 2E_n^{(2)}\right)\exp\left(\frac{-E_n^{(0)}}{kT}\right)}{\sum_n \exp\left(\frac{-E_n^{(0)}}{kT}\right)} \tag{2.29}$$

In cases where the second order zeeman terms are ignored the expression simplifies to:

$$\psi_M = N\frac{\sum_n \left(\frac{\left(E_n^{(1)}\right)^2}{kT}\right)\exp\left(\frac{-E_n^{(0)}}{kT}\right)}{\sum_n \exp\left(\frac{-E_n^{(0)}}{kT}\right)} \tag{2.30}$$

Consequently the difference between the Van-Vleck expression and the spin-only expression is that the Van-Vleck takes into account the mixing of excited state zeeman terms using the magnetic field operators.

If the system in question contains two magnetic centers and they are exchanged-coupled the contributions to the energy of state n can expressed in the same manner as equation 2.23. The difference is that the zeroth-order term is now the exchange coupling interaction of the unperturbed states where the zeroth-order Hamiltonian is:

$$\hat{H}^{(0)} = -2J\hat{S}_1\hat{S}_2 \tag{2.31}$$

where J is the exchange coupling. The first and second order contributions to the energy remain the first and second order zeeman contributions. By using the following expressions:

$$\begin{aligned} E_n^{(1)} &= m_s g\beta \\ \sum_{-S}^{+S} m_s^2 &= \frac{1}{3}S\left(S+1\right)\left(2S+1\right) \end{aligned} \tag{2.32}$$

equation 2.30 can be expressed as:

$$\chi = \frac{Ng^2\beta^2}{3kT}\frac{\sum_S S(S+1)(2S+1)\exp\left(\frac{-E_S}{kT}\right)}{\sum_S (2S+1)\exp\left(\frac{-E_S}{kT}\right)} \tag{2.33}$$

Where E_s is the energy of the exchanged-coupled states determined by using the exchange coupled Hamiltonian.

2.7 References

1. S. F. A. Kettle. *Physical Inorganic Chemistry: A Coordination Chemistry Approach*. Oxford University Press (New York 1998).
1. Halliday, D.; Resnick, R.; Walker, J. *Fundamentals of Physics Volume 2 (Fifth Edition)*. John Wiley & Sons, Inc. USA 1997.
2. Borden, W. T.; Davidson, E .R. *J. Am. Chem.Soc*. **1977**, *99*, 4587.
3. Pei, Y.; Verdaguer, M.; Kahn, O.; Sletten, J.; Renard, J. P. *J. Am. Chem. Soc*. **1986**, *108*, 7428.
4. Oliver Kahn. *Molecular Magnetism*. Wiley-VCH, USA **1993**.
5. Halliday, D.; Resnick, R.; Walker, J. *Fundamentals of Physics Volume 2 (Fifth Edition)*. John Wiley & Sons, Inc. USA 1997.
6. Russell S. Drago. *Physical Methods for Chemists*. Saunders College Publishing (1997).

Chapter 3: Valence Tautomerism

3.1 Ortho-Quinones as Organic Spin Carriers

Ortho-quinones are molecules that form an important class of redox-active ligands that can exist in three different oxidation states.[1] The addition of one electron to the o-quinone π^* molecular orbital gives rise to a paramagnetic one-electron containing species (S = ½) called a semiquinone (SQ). Further reduction by another electron of the semiquinone will provide for the diamagnetic ligand known as the catecholate (Cat) (**Figure 3.1**).[1]

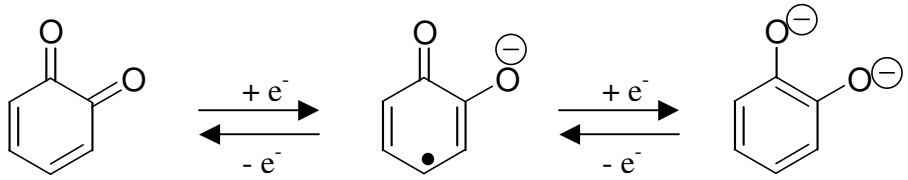

Figure 3.1. Quinone redox changes.

The semiquinone form of the o-quinone molecule is a fairly stable spin-carrier when the quinone molecule is sterically protected (**Figure 3.2**) and is coordinated to a metal ion or is formed as an alkali-metal salt.

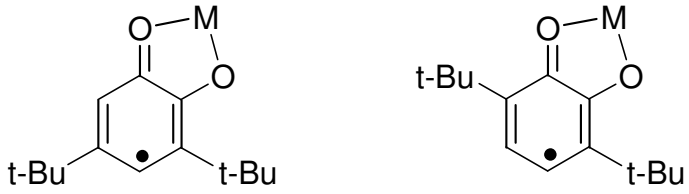

Figure 3.2. Metal ligand bonding in semiquinone complexes.

The semiquinone spin-carrier has several pronounced spectroscopic signatures. In the infrared spectrum the o-quinone ligand contains a signature vibrational C=O stretching transition at 1660 cm^{-1}.[1] Upon reduction to the semiquinone the C=O stretching band of quinone disappears and is instead replaced by a C=O stretching transition near 1450 cm^{-1}.[1] Semiquinone spin-carriers tend to be very colored materials, which indicate that semiquinones are strongly absorbing in the visible. The semiquinone chromophore can be identified in the electronic spectrum where the n (SOMO) $\rightarrow \pi^*$ transition that is characteristic of semiquinones appears near 800 nm (12,500 cm^{-1}).[1] The semiquinone SOMO is described in **Figure 3.3**. The coefficients of the semiquinone SOMO are squared to determine the unpaired electron's spin density, which is distributed along much of the ring and the two oxygen atoms.

A **B**

Figure 3.3. (A) Hückel coefficients for semiquinone SOMO (B) Hückel coefficients squared to yield SOMO electron's spin-densities.

Furthermore in the x-ray crystal structure, the semiquinone is identified from its dioxolene ring bond lengths. Below are the bond-lengths of the typical semiquinone (SQ) and catecholate (Cat) ligands in Co(SQ)(Cat)bpy (**Figure 3.4**).[3]

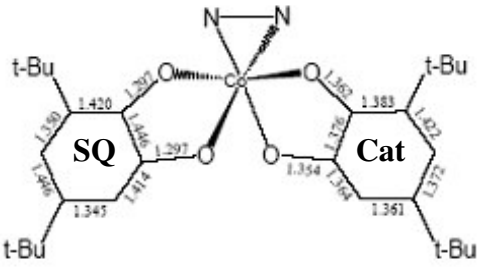

Figure 3.4. Difference in structural parameters of SQ and Cat in the Co(SQ)(Cat)bpy.[5]

3.2 Intramolecular Donor-Acceptor Model of Valence-Tautomeric Behavior

It has been shown that metal complexes composed of first row transition metals and quinone ligands have localized bonding descriptions where ligands and metals have idealized oxidation states and unpaired spin density resides in localized regions of the molecule. An interesting behavior of some particular metal quinone complexes is valence-tautomerism, which is a property by which a molecule changes its electronic state as a function of a change in its external environment.[3]

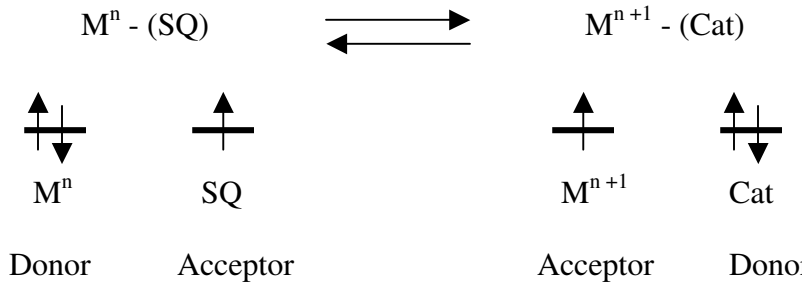

Figure 3.5. Donor-acceptor interaction between metals and the dioxolene ligand.

The electronic state change is a function of the donor-acceptor interactions between the metal and SQ ligand. The close proximity and orbital symmetry of both the frontier

orbitals of certain first-row transition metals and the SQ ligand allow for intramolecular electron-transfer to occur (**Figure 3.5**).

The valence-tautomeric behavior has been observed for metal quinone complexes containing Co, Mn, Fe, Rh, Ir and Cu.[3-8] The nature of the valence-tautomeric conversion is dependent on changes in temperature and pressure. In the case of the cobalt *bis*(dioxolene) valence-tautomer relatively small changes in temperature and pressure lead to an interconversion between two electronic states of the complex: low-spin $Co^{III}(SQ)(Cat)(bpy)$ and high-spin $Co^{II}(SQ)_2(bpy)$ (**Figure 3.6**). In the low-temperature Co^{III} state the Cat and SQ ligands constitute an asymmetric mixed-valent moiety and the system as a whole has one unpaired electron. In the higher temperature Co^{II} state, the inter-ligand mixed-valency is lost and the system as a whole contains five unpaired electrons.

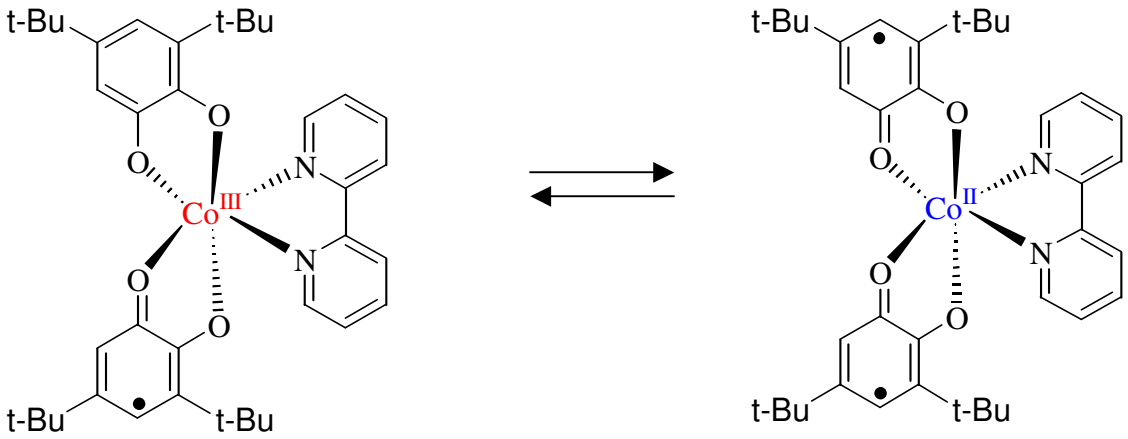

Figure 3.6. Valence tautomerism in Co(SQ)(Cat)bpy.

Although the mechanistic order has yet to be determined the process of changing the electronic state of the cobalt valence-tautomeric complex involves an intramolecular

electron transfer process between the metal and dioxolene ligands and spin-crossover of the metal ion to from high to low spin or vice versa. Typically the interconversion occurs in a 20-100 ^{0}C range depending on the medium the complex is in. Furthermore, it has been shown that the valence-tautomeric conversion can be photoinduced both in solution and in polymeric films.[9]

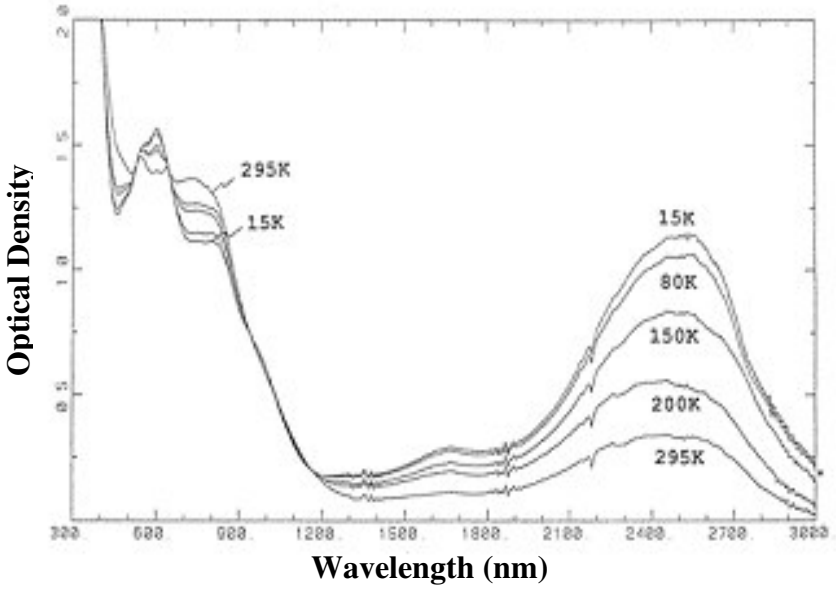

Figure 3.7. Variable temperature solid state electronic absorption of Co(SQ)(Cat)biphenyl.[8]

The variable-temperature spectra of the diphenyl bipyridine valence-tautomer in a polymer matrix is representative of all of the known cobalt bis(dioxolene) valence-tautomers (**Figure 3.7**).[10] At room temperature there is a band at 600 nm with a shoulder at 800 nm, which is characteristic of the *ls*-Co^{III} tautomeric form of the complex. As the temperature is increased from 298K the intensity of the 600 nm band decreases while a band at 770 nm increases in intensity. This new electronic band is characteristic of the *hs*-Co^{II} form of the complex. The spectrum of the Co^{II} form also has electronic

absorptions at 655 nm and 545 nm. The origin of the *hs*-Co^{II} charge transfer transition at 600 nm originates from transitions from filled molecular π-orbitals to the unoccupied SQ π*-orbital. This band also contains some contribution from a ligand to metal charge-transfer involving the Cat^{2-} ligand and the cobalt ion. The band at 770 nm is a metal to ligand charge transfer transition of the high-spin Co^{II} tautomer. The existence of isosbestic points also suggests that only two different species are present in solution.

There are large changes that occur in the optical spectrum in the near infrared region of the spectrum. At low temperatures, a band appears at 2500 nm with a shoulder at 1670 nm, which is only associated with the Co^{III} tautomer. It has been shown using theoretical calculations that the band at 2500 nm is an intervalence charge-transfer (IVCT) band involving excitation of an electron from the Cat^{2-} to the SQ^{1-} ligand.[11]

3.3 Observed Thermodynamic Changes

For the cobalt *bis*(dioxolene) complex there are at least three minima close in energy along the ground-state potential-energy surface of the shown complex in which the two extremes are the *ls*-Co^{III} and the *hs*-Co^{II}. The intermediate state is the *ls*-Co^{II} tautomer. Thus the presence of two or more electronic states close in energy can lead to large vibronic interactions and sensitivity to the environment.

In order to understand the thermodynamic bases of the valence-tautomeric conversion the change in electronic states must be understood. The electronic structure of the cobalt *bis*(dioxolene) system can be understood at least superficially using molecular orbitals in idealized symmetry arguments. The idealized electronic configurations of the *ls*-Co^{III} and *hs*-Co^{II} forms in the local O_h symmetry of the metal

center are respectively $(t_{2g})^6(e_g^*)^0(\pi^*Cat)^2(\pi^*SQ)^1$ and $(t_{2g})^5(e_g^*)^2(\pi^*SQ_1)^1(\pi^*SQ_2)^1$ (**Figure 3.8**).

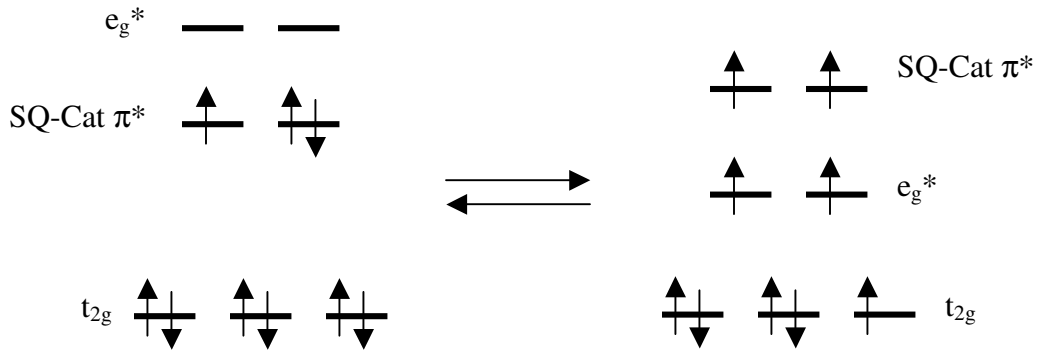

Figure 3.8. Idealized orbital changes with respect to valence tautomeric conversion.

The idealized d orbitals are split into the familiar t_{2g} and e_g^* sets and the ligand antibonding orbitals contain a single electron in the SQ^{1-} oxidation state and two electrons in the CAT^{2-} oxidation state. Since the electronic state change involves changing the occupation of the e_g^* dσ-antibonding orbitals of cobalt the conversion between the two valence-tautomeric states is typically characterized by an elongation in the metal to ligand bond lengths of an average of 0.2 Å.[3] As a comparison similar changes are observed in Fe^{II} spin-crossover complexes that undergo the transformation between *ls*-Fe^{II} $(t_{2g})^6(e_g^*)^0$ and *hs*-Fe^{II} $(t_{2g})^4(e_g^*)^2$ as a function of temperature, pressure and light.[11] Since valence tautomerism is an intramolecular electron transfer process the electronic interconversion involve not only large metal-ligand bond length changes but also smaller internal dioxolene ligand bond length changes due to the conversion between SQ and Cat.

The electronic interconversion process can be illustrated with the aid of a one-dimensional potential energy diagram, which contains two harmonic potential energy curves to represent the two valence-tautomeric states (**Figure 3.9**). Furthermore the surfaces are plotted with respect to the nuclear coordinate. Since the nuclear configurations of the two states differ mainly in the metal-ligand bond lengths it is then reasonable to assume for further discussion that to first approximation that the reaction coordinate for valence-tautomerism is equivalent to the totally symmetric metal-ligand breathing vibrational mode.[10-11]

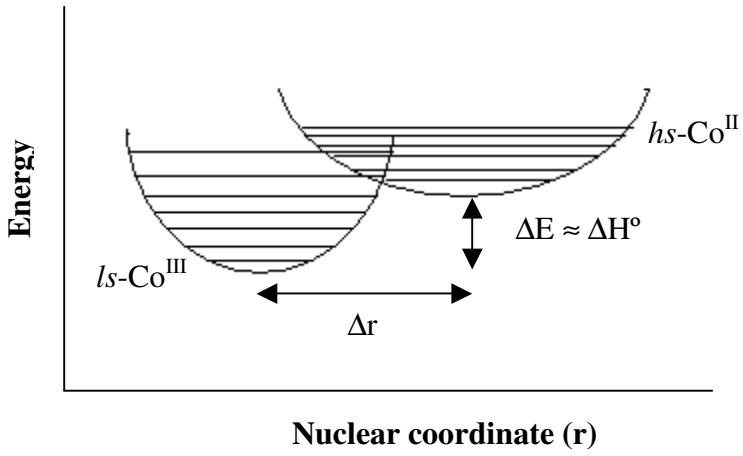

Figure 3.9. Sketch of harmonic potentials of *ls*-Co^{III} and *hs*-Co^{II} states.

The energy of the symmetric metal-ligand stretching vibration in *ls*-Co^{III} complexes is roughly between 450 cm^{-1} and for *hs*-Co^{II} complexes the value lies near to roughly 350 cm^{-1}.[13] Consequently the wells are shifted relative to each other by a value reflecting the average 0.2 Å metal-ligand bond length distance change. In addition ΔE, which

is the energy separation between the two lowest vibrational levels of the individual electronic states is positive since the high-spin Co^{II} state lies higher in energy:

$$\Delta E \approx \Delta H = \Delta H_{hs-Co^{II}} - \Delta H_{ls-Co^{III}} > 0$$

The valence-tautomeric interconversion occurs with contributions from electronic entropy (ΔS_{elec}) due to the higher spin-state degeneracy of the higher temperature Co^{II} form. At low temperatures, the low-spin state has an S = ½ (diamagnetic metal and one unpaired electron on one of the dioxolene ligands). The high temperature form spin ladder has one S = 5/2, one S = ½ and two S = 3/2 states thermally populated due to very weak magnetic exchange interactions (**Figure 3.10**).[14]

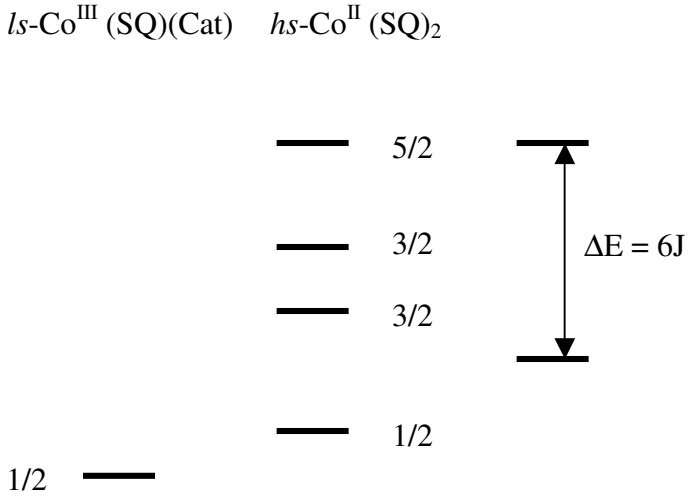

Figure 3.10. Spin ladder ladders of *ls*-Co^{III}(SQ)(Cat) and *hs*-$Co^{II}(SQ)_2$.

There is also vibrational entropy gain since the longer metal-ligand bond lengths of the high-spin Co^{II} tautomer has lower energy vibrations and higher density of vibrational

states than the low-spin state form. Thus, the thermal population of tautomeric states is dictated by the Gibbs free energy difference where:

$$\Delta G = \Delta G_{hs-Co^{II}} - \Delta G_{hs-Co^{II}} = \Delta H - T\Delta S$$

and:

$$\Delta H = \Delta H_{hs-Co^{II}} - \Delta H_{ls-Co^{III}}$$
$$\Delta S = \Delta S_{hs-Co^{II}} - \Delta H_{ls-Co^{III}} = \Delta S_{elec} + \Delta S_{vib}$$

The electronic entropy gain can be described by:

$$\Delta S_{elec} = R \ln\left(\frac{W_{Co^{II}}}{W_{Co^{III}}}\right)$$

where R is the gas constant and $W_{Co}{}^{II}$ and $W_{Co}{}^{III}$ are the electronic degeneracies of the high-spin Co^{II} and low-spin Co^{III} states. For the cobalt *bis*(dioxolene) complexes $W_{Co}{}^{II}$ = 16 due to the Co^{II} spin ladder (the degeneracy of each spin-state is 2S + 1) and for $W_{Co}{}^{II}$ = 4 due to the mixed-valency of the low-temperature form. As a consequence $\Delta S_{elec} = R \ln (16/4) = 11.53$ J mol^{-1} K^{-1}. Typically ΔS_{vib} values are estimated from comparisons with Fe spin-crossover complexes and it has been widely assumed that ΔS_{vib} in cobalt valence tautomers would be of similar or larger magnitude. In consequence ΔS_{vib} has been predicted to be in the range of 70-80 J mol^{-1} K^{-1} or greater.[10-11]

With this information at hand the process of the electronic state conversion can be briefly discussed. At low temperature the TΔS term is negligible compared to ΔH. Consequently the low-spin Co^{III} form is populated if ΔH > kT. At higher temperatures

$T\Delta S$ is no longer negligible and ΔG changes sign at the midpoint temperature $T_{1/2}$ where $\Delta G = 0$ and $\Delta H = T\Delta S$. If the entropy term is high enough the Co^{II} tautomeric state may be completely populated at higher temperatures. Accordingly by decreasing the energy separation of the two tautomeric states $T_{1/2}$ decreases.

3.4 Observed Magnetic Changes

Large changes in the magnetic behavior also accompany the valence-tautomeric interconversion. From the experimentally observed sigmoids, the values of $\chi_m T$ range from the low-temperature limit of 0.37 – 0.54 $\chi_m T$ ($\chi_m T$ = cm^3 K mol^{-1}) to 2.35 emu K mol^{-1} in the high temperature limit.[15] At low temperature the $\chi_m T$ values are close to the value expected for a single unpaired electron on the semiquinonate ligand of the low-spin complex. If there are no intramolecular magnetic exchange interactions present in the *hs*-Co^{II} and if the Co^{II} ion exhibited spin-only magnetism, then the value of $\chi_m T$ would be 2.62 (μ_{eff} = 4.58 μ_B).[16] However high-spin Co^{II} typically exhibits large nonzero orbital angular momentum due to spin-orbit interactions and the experimentally observed $\chi_m T$ values range from 2.9 to 3.1 emu K mol^{-1} (4.8 – 5.0 μ_B).[10] Furthermore another possible reasons for the low $\chi_m T$ values is the intramolecular magnetic exchange interactions between the SQ ligands and the Co^{II} ion. Because of the spin-orbit contribution to the magnetic moment it is not unusual to that there is a relatively small discrepancy in the observed and predicted values of the Co^{II} ion in valence-tautomers especially since the values are similar for the majority of the known cobalt *bis*(dioxolene) valence-tautomers reported in the literature.

The best-fit ΔH and ΔS values from the observed magnetic data of are listed for several of the complexes in Table 3.1 with different counterligands. The ΔH values for the complexes were found to be 2238, 3056, 3206 cm^{-1} respectively. The entropy gains for these systems range from 118.1 to 133.1 J mol^{-1} K^{-1}.[10] Several have theorized that the higher observed values of ΔS for some of the valence tautomeric complexes could be associated with a larger vibrational entropy gain. This hypothesis is rationalized from the fact that the interconversion is an electron transfer process and not only involves metal-ligand bond length changes as in Fe^{II} spin crossover complexes but also changes in the bond lengths and vibrational frequencies associated with the SQ and Cat ligands.[11]

Table 3.1. Thermodynamic parameters of various valence tautomers.

Complex	**$T_{1/2}$ (K)**	**ΔH^o (cm^{-1})**	**ΔH^o (kJ mol^{-1})**	**ΔS^o (J mol^{-1} K^{-1})**
Phenanthroline[9]	226.6	2238	26.77	118.1
Bipyridine[9]	277.0	3056	36.56	133.1
5, 5´ - Dimethyl bipyridine[9]	286.6	3206	38.36	133.8
5, 5´ - Diphenyl bipyridine[9]	350.0	1717	21.33	60.6

3.5 Influences of the Counterligand on Valence Tautomerism

There are several ways to address how the diiminium counterligand influences the properties of a given valence tautomeric cobalt complex. The most widely cited description treats the counterligand interactions using spin-unrestricted density functional theory in which the spin up (α) and spin down (β) electrons are treated separately.[10] Using this theory the frontier molecular orbitals for the S = ½ CoIII state and the

antiferromagnetic S = ½ high-spin Co^{II} state can be constructed (**Figure 3.11**). From the orbital construction the idealized energy level diagrams of the spin polarized ligand field splitting of the cobalt d orbitals and π*-energy levels of the two quinones can be seen. The vertical axis gives the orbital energies and the horizontal axis separates the levels according to their spin index, either α or β. The *ls*-Co^{III} state has the occupation scheme of Co^{III} is $d^3(\alpha)d^3(\beta)$ and the Co^{II} state is Co^{II} $d^5(\alpha)d^2(\beta)$.

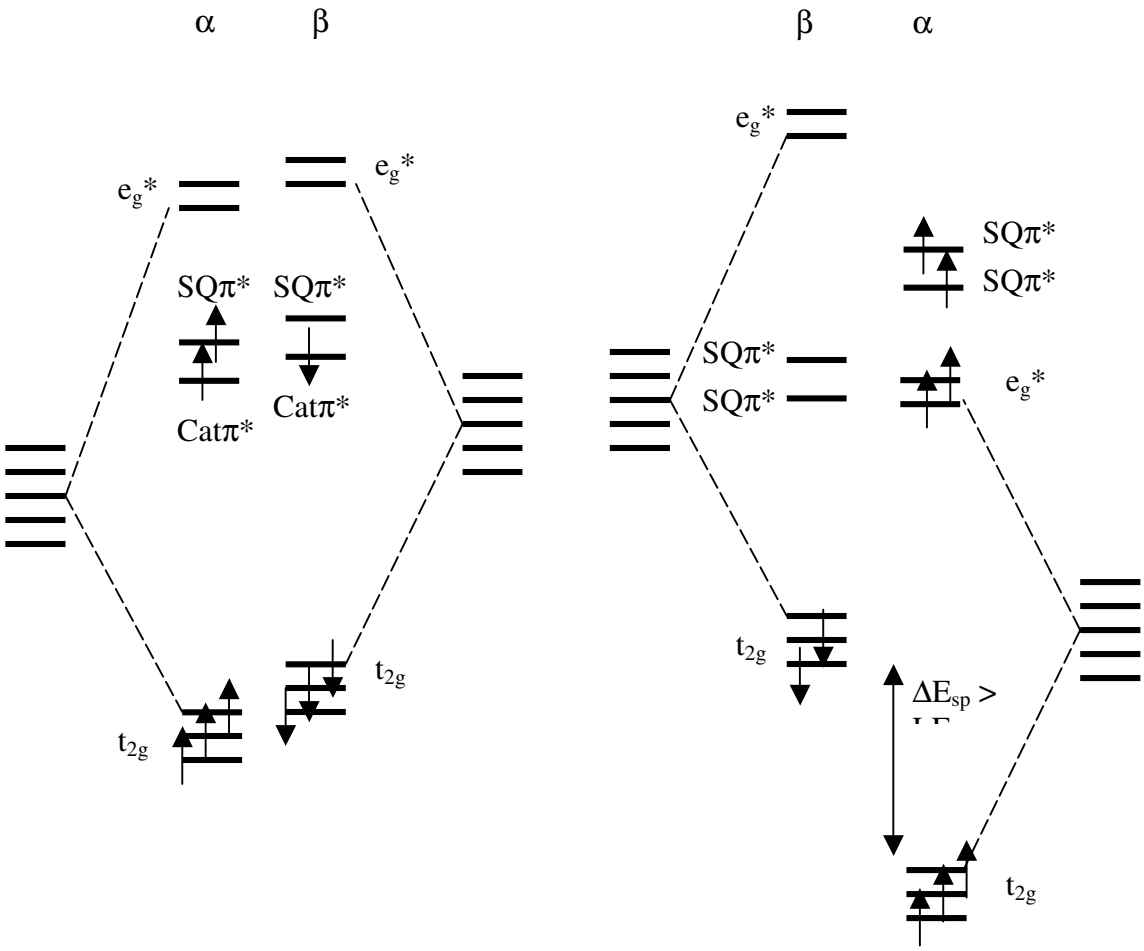

Figure 3.11. Spin-polarized energy diagrams depicting *ls* to *hs* change. [9]

In this model the *ls*-Co^{III} state the quinone π*-orbitals are the highest occupied and lie relatively close in energy to the unoccupied e_g* orbitals of the cobalt ion. For the *hs*-Co^{II} state the e_g* orbitals are lower in energy with respect to the low-spin state. Thus in the Co^{II} form there is a large spin polarization energy splitting between majority α-spin and minority β-spin 3d energy levels because the amount of unpaired spin has increased. Also, the ligand field splitting has been substantially reduced since the metal-ligand bond distances have increased by 0.2 Å. The spin polarization splitting for the high-spin Co^{II} state slightly exceeds the ligand field splitting, and consequently the competition favors the high-spin metal ion.

The σ-donating and π-accepting properties of the counterligand affects the ligand field splitting of the cobalt center which leads to modulation of the energy separations between valence-tautomeric states. Greater σ-donation stabilizes the low-spin Co^{III} state by changing the energies of the e_g* orbitals are removed further from the o-quinone π* orbitals. Decreasing the energy of the e_g* orbitals can lead to a situation in which the e_g* orbitals lie lower in energy than the π* ligand orbitals and electron transfer between ligand and metal orbitals. On the other hand, weaker σ-donation leads to the stabilization of the high-spin Co^{II} state. In summary if the ligand field splitting is smaller than the spin polarization energy splitting, the high-spin state is favored. In the *hs*-Co^{II} tautomer greater σ-donation places the occupied e_g* in α closer in energy proximity to the unoccupied π*-orbitals. If the ligand field is large, the e_g* orbitals may be higher in energy than the π*-orbitals resulting in electron transfer from the Co^{II} center to the SQ π*-orbitals.

3.6 Influences of the Chemical Environment on Valence Tautomerism

The environment about the valence tautomeric complex can also influence $T_{1/2}$ by contributing to the energy separation between the tautomeric forms. For example in the solid state the cobalt bipyridine valence tautomer displays the absorption characteristics of the low-spin valence-tautomer whereas at room temperature in toluene solution, the complex shows the characteristics of the *hs*-Co^{II} tautomer. Relative to the solution room temperature spectrum, the solid state matrix increases the energy separation between the valence-tautomeric states. This is due to the fact that the more compact solid-state polymeric medium that serves to favor the much smaller *ls*-Co^{III} tautomer. For crystalline samples the valence-tautomeric conversion can be influenced by how the complex is solvated.[17-18] Changes to the valence tautomeric conversion can also arise from surface confinement and it has been shown that the solvent dielectric can also shift $T_{1/2}$.[15, 19]

3.7 Valence Tautomerism as an Electronic Transition and Comparisons to Fe Spin Crossover Behavior

The valence tautomeric conversion can also be described in a similar manner to an electronic transition in spectroscopy by comparing the electronic conversion to that observed in Fe spin-crossover complexes. For the Fe spin-crossover conversion the low temperature form can be treated as a ground state with $^1A_1$ symmetry. The excited state term or the high-temperature high-spin Fe^{II} form is $^5T_2$ (**Figure 3.12**).[12]

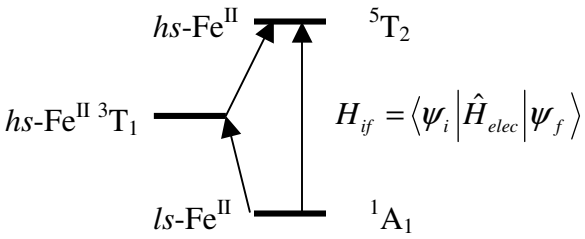

Figure 3.12. Electronic excitation of *ls*-Fe^{II} to *hs*-Fe^{II}.

The electronic coupling between the two states can be described by the electronic coupling matrix element H_{if} (**Figure 3.10**) where ψ_i and ψ_f are the initial and final states respectively and H_{elec} is the electronic Hamiltonian.[11] Symmetry and spin restrictions are important factors in the evaluation of the extent of electronic coupling. Consequently the magnitude of H_{if} depends on the spin multiplicity differences between the initial and final states, the symmetry of the donor and acceptor orbitals of the initial and final electronic states and the availability of electronic states that can mix with the donor and acceptor wavefunctions. H_{if} in Fe^{II} spin-crossover complexes is small since the $^5T_2$ to $^1A_1$ spin-crossover involves a $\Delta S = 2$ transition that is formally spin forbidden. Furthermore to first order $H_{if} = 0$ because the $^5T_2$ and $^1A_1$ states are orthogonal. From a spectroscopic standpoint in order to allow for the electronic state change to occur H_{if} is directed by a second-order spin-orbit interaction through the intermediate $^3T_1$ state.

The electronic coupling in valence tautomeric complexes results from a fundamentally different origin. Because magnetic exchange coupling in the cobalt valence-tautomeric complexes allows for a zero spin-change ($\Delta S = 0$) interconversion pathway the electronic interconversion is formally spin allowed. This spin allowed

interaction is because the high-spin Co^{II} complex is a magnetically exchanged coupled system having one S = 5/2, two S = 3/2 and one S = ½, states in close energy proximity. The *ls*-Co^{III} tautomer is an S = ½ complex. Hence the spin-allowed valence tautomeric interconversion involves the S = ½ state of the high-spin state Co^{II} tautomer. Because the cobalt valence tautomeric system is a donor-acceptor electron transfer system the molecular orbital symmetries of the donor and acceptor moieties contribute to the magnitude of H_{if}. Theoretical investigations of the electronic coupling in electron transfer systems have shown that the magnitude of electronic coupling H_{if} depends on the overlap integral $< \psi_i | \psi_f >$ where ψ_i and ψ_f are the molecular orbitals of the initial and final states which donate and accept electrons respectively.[20, 21] It has been shown from theory that the donor and acceptor orbitals are orthogonal in valence tautomeric complexes and the mixing between the ground *ls*-Co^{III} and excited *hs*-Co^{II} states are very small. Therefore H_{if} in valence tautomers is not large since the tunneling matrix element is limited due to poor orbital overlap.[11]

3.8 Intervalence Charge-Transfer (The Robin-Day Model and the Hush Prediction)[22, 23]

The low-spin Co^{III} valence-tautomer is a symmetric mixed valent complex due to the semiquinonate and catecholate ligands. The Robin and Day model can be used to describe the mixed-valency by making two simple assumptions to simplify the problem: interactions from the bridge that couples the donor and acceptor are ignored and intermolecular contributions are negligible.[22] For the low temperature cobalt valence

tautomer in which the metal wavefunctions are neglected the ground state wavefunction of the Cat-SQ system to zeroth-order is:

$$\Psi_0 = \psi_A^{2-}\psi_B^{1-} \tag{3.1}$$

where A and B refer to the cateholate and semiquinonate wavefunctions respectively and the charges are indicated for each site. On transferring one electron from the Cat center to the SQ the wavefunctions will change their charge state labels by +1 and -1 respectively yielding excited state wavefunctions. The excited state may be written as:

$$\Psi_k = \psi_A^{1-}\psi_B^{2-} \tag{3.2}$$

By assuming that the excited state function has the correct symmetry for mixing with the ground state wavefunction (e.g., both ground and excited states have the same symmetry) the ground state may then be taken as a linear combination of the ground and excited states:

$$\begin{aligned}\Psi_1 &= \sqrt{1-\alpha^2}\Psi_0 + \alpha\Psi_k \\ &= \sqrt{1-\alpha^2}\psi_A^{2-}\psi_B^{1-} + \alpha\psi_A^{1-}\psi_B^{2-}\end{aligned} \tag{3.3}$$

where α is proportional to the mixing between the ground and excited states:[22]

$$\alpha \propto \frac{\left\langle \Psi_0 \middle| H \middle| \Psi_k \right\rangle^2}{E_k - E_0} \tag{3.4}$$

Since the oxidized species contains one electron outside of a closed shell the following can be defined:

$$\begin{aligned}\psi_A^{2-} &= \phi_A^C \\ \psi_A^{1-} &= \phi_A^C\phi_A^* \\ \psi_B^{2-} &= \phi_B^C \\ \psi_B^{1-} &= \phi_B^C\phi_B^*\end{aligned} \tag{3.5}$$

where ϕ^C represents the wavefunction for the closed-shell core and ϕ^* is the only orbital outside the core. Using the relationship above:

$$\begin{aligned}\Psi_1 &= \sqrt{1-\alpha^2}\,\phi_A^C\phi_B^C\phi_B^* + \alpha\phi_A^C\phi_A^*\phi_B^C \\ &= \phi_A^C\phi_B^C\left(\sqrt{1-\alpha^2}\,\phi_B^* + \alpha\phi_A^*\right) \\ &= \kappa\left(\sqrt{1-\alpha^2}\,\phi_B^* + \alpha\phi_A^*\right)\end{aligned} \tag{3.6}$$

The prefactor (κ) is simply the product of all the closed-shell core functions. The resulting wavefunction describes the delocalized electron (the optical electron) in a molecular orbital written as a sum of the donor and acceptor orbitals in which the two fragments (ϕ_A^* and ϕ_B^*) must have the same symmetry in order to mix. Qualitatively this means on a very simple level that the electron is delocalized between the donor and acceptor sites as long as the donor and acceptor have the same symmetry. For both Cat and SQ the point group symmetry is C_{2v}. The α term determines the level of the delocalization. For large differences between ground and excited states α is small and the mixed-valent wavefunction reduces to the zeroth-order ground state wavefunction (Eq. 3.1). This is the definition of Class I behavior in the Robin and Day model. On the other hand if the ΔE is small or near zero then the system delocalized and is Class III. An intermediate state (Class II) implies that there is valence-trapping between the donor and acceptor sites. Since the difference in energy between the Cat and SQ fragments is very small it is expected that the degree of delocalization is large for the mixed valent Co^{III} valence tautomeric form.

It is possible to use Hush theory to qualitatively extract a rough level of the electronic coupling and measure the barrier to interconversion by inspecting the light-induced electron transfer band of the mixed-valent species:[23]

$$H_{ab} = \left(2.05\times10^{-2}\right)\left(\sqrt{\frac{\varepsilon\Delta\nu_{1/2}}{\nu_{\max}}}\right)\frac{\nu_{\max}}{r} \qquad (3.7)$$

where ε_{max} is the maximum extinction coefficient of the absorption band in M^{-1} cm^{-1}, $\Delta\nu_{1/2}$ is the band width at ε_{max}, ν_{max} is the energy of the absorption in cm^{-1} and r is the distance between donor (Cat) and acceptor (SQ). As an example by using the following values – r = 2.83 angstroms (shortest distance between oxygen atoms of the donor and acceptor), ε_{max} = 2200 M^{-1} cm^{-1}, $\Delta\nu_{1/2}$ = 1200 cm^{-1} and ν_{max} = 4000 cm^{-1}, the electronic coupling (H_{ab}) is calculated to be 752 cm^{-1}. In the case of a symmetrical one electron transfer the barrier height (E_{th}) can be related to ν_{max} (E_{op}) where:[23]

$$E_{op} = 4E_{th}$$
$$E_{th} = \frac{E_{op}}{4} \qquad (3.8)$$

For the cobalt bipyridine valence tautomer E_{th} = 1000 cm^{-1}. The values for the electronic coupling and barrier height are rough estimates since the Hush model was initially developed for intervalence charge-transfer for metal ions in solution.

References

1. Pierpont, C. G.; Buchanan, R. M. *Coord. Chem Rev*. **1981**, *38*, 45.
2. Pierpont, C. G.; Buchanan, R. M. *J. Am. Chem. Soc*. **1980**, *102*, 4951.
3. Adams, D. M.; Dei, A.; Rheingold, A. L; Hendrickson, D. N. *Angew. Chem. Int. Ed. Engl.* **1993**, *32*, 880.
4. Lynch, M. W.; Hendrickson, D. N.; Fitzgerald, B. J.; Pierpont, C. G. *J. Am. Chem. Soc*. **1984**, *106*, 2041.
5. Lynch, M. W.; Valentine, M.; Hendrickson, D. N. *J. Am. Chem. Soc*. **1982**, *104*, 6982.
6. Abakumov, G. A.; Razuvaev, G. A.; Nevodchikov, V. I.; Cherkasov, V. K. *J. Organomet. Chem*. **1988**, *341*, 485.
7. Abakumov, G. A.; Razuvaev, G. A.; Nevodchikov, V. I.; Cherkasov, V. K. *Dold. Akad. Nauk. SSR*. **1989**, *304*, 107.
8. Adams, D. M.; Li, B. L.; Simon, J. D.; Hendrickson, D. N. *Angew. Chem. Int. Ed. Engl*. **1995**, *34*, 1481.
9. Adams, D. M.; Hendrickson, D. N. *J. Am. Chem. Soc*. **1996**, *118*, 11515.
10. Adams, D. M.; Noodleman, L.; Hendrickson, D. N. *Inorg. Chem*. **1997**, *36*, 3966.
11. Osamu Sato. *Acc. Chem. Res*. **2003**, *36*, 692.
12. Buhks, E.; Bixon, M.; Jortner, J. *J. Phys. Chem*. **1981**, *85*, 3763.
13. Lynch, M. W.; Buchanan, R. M.; Pierpont, C. G.; Hendrickson, D. N. *Inorg. Chem*. **1981**, *20*, 1038.
14. Cordtland G. Pierpont. *Coord. Chem. Rev*. **2001**, *216-217*, 99.
15. Russell S. Drago. *Physical Methods for Chemists*. Saunders College Publishing, **1997**.
16. Adams, D. M.; Dei, A.; Rheingold, A. L.; Hendrickson, D. N. *J. Am. Chem. Soc*. **1993**, *115*, 8221.
17. Cador, O.; Dei, A.; Sangregorio, C. *Chem. Comm*. **2004**, 652.
18. Bin-Salamon, S.; Brewer, S.; Feldheim, D. L.; Franzen, S.; Lappi, S.; Shultz, D. A. *J. Am. Chem. Soc*. **2005**, *127*, 5328.
19. Koga, N.; Sameshima, K.; Morokuma, K. *J. Phys. Chem*. **1993**, *97*, 13117.
20. Newton, M. D. *Chem. Rev*. **1991**, *91*, 767.
21. Robin, M. B.; Day, P. *Adv. Inorg. Chem. Radiochem*. **1967**, *10*, 248.
22. N. S. Hush. *Prog. Inorg. Chem*. **1967**, *3*, 391.

Chapter 4: Does Surface Confinement Affect Valence Tautomerism?

4.1 Introduction

As discussed in sections 3.5 and 3.6 valence tautomeric behavior of cobalt *bis*(dioxolene) complexes can be also be influenced by intramolecular interactions such as changes in ΔH^{o} due to counterligand back bonding and intermolecular interactions such as solvation effects. [1] The intermolecular environment involves the molecular solvation sphere. The solvation environment contributes to the relative free energies of the valence tautomeric states. This is because the $Co^{III}(SQ)(Cat)$ and $Co^{II}(SQ)_2$ forms are different structural species for the average metal – ligand bond lengths, which are different by 0.2 Å for the two forms.[2] In essence the Co^{III} and Co^{II} states differ in size in which the $Co^{III}(SQ)(Cat)$ molecule is smaller than the $Co^{II}(SQ)_2$ molecule. Thus, for the valence tautomeric conversion to occur the chemical environment must accommodate the molecular change that accompanies the different state populations. As the valence tautomeric system converts from the Co^{III} to the Co^{II} form the molecular environment must contain the empty space needed to accommodate the larger Co^{II} system for if not, then there exists a substantial barrier to the interconversion to the Co^{II} state. This has been observed in the solid state for a series of crystalline systems where the $Co(diox)_2bpy$ molecule is solvated differently.[3] It was discovered that solvent molecules that "crowd" the molecular solvation sphere hindered and in some cases completely prevented the valence tautomeric conversion to occur.

Space is not an issue in the solution phase. Rather the rotating solvent dipole moments can easily accommodate both valence tautomeric forms. Solvents with low dielectric constants tend to increase the potential energy difference, while higher

dielectric solvents tend to decrease the relative divergence.[3] This is because the two tautomeric states have different molecular dipole moments. This is evident since the charge distribution for the two valence tautomer states is different.[4]

A previously unexplored avenue to understanding the intermolecular contribution to the valence tautomeric behavior is to measure the effect of surface confinement. Simple organic molecules that are confined to metal surfaces experience a distinctive environment where depending on the density of the surface molecules, the molecular surroundings may promote a "crystalline packing" of the surface molecules or a completely amorphous one.[5] Surface molecules can also experience electronic coupling to the bonded surface.[6]

A surface – attached valence tautomer may experience any of the above-mentioned interactions that could in turn influence the thermodynamic interconversion process. Understanding the dynamics of valence tautomer to surface interactions may also allow for a greater awareness of the intermolecular contributions to valence tautomeric behavior as a whole. Consequently our research goal is to gain a better understanding of the effect of surface confinement on valence tautomerism by synthesizing a valence tautomer chemically bonded to a nanometer – scale gold cluster and measure the thermodynamic changes, if any, which may possibly occur due to surface confinement (**Figure 4.1**).

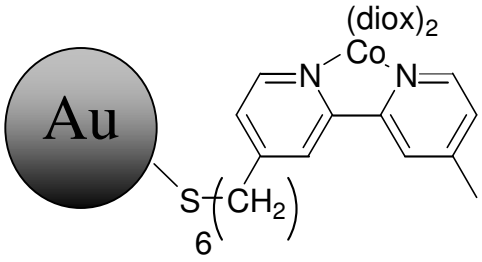

Figure 4.1. Proposed surface-bound valence tautomer.

The chemistry of nanometer – scale gold clusters is well established and there is substantial research that provides for a strong foundation to understanding the gold cluster to surface – molecule interaction.[7] Furthermore, synthetically, nanometer – scale gold clusters are fairly simple to make and this allows for ease of design. With gold clusters, an interesting possibility is that the gold surface charge may affect the surface bound valence tautomer. It has been shown that the surfaces of gold clusters are negatively charged.[7] Just as with solvent dipoles this surface dipole may affect a change in the enthalpic separation of the two valence tautomeric states given that the valence tautomer is close to the surface. The change in ΔH^{o} may be observed in the IR where the IVCT band may gain intensity at room temperature if ΔH^{o} increases and vice versa if the reverse occurs.

4.2 Synthesis of Surface Bound Valence Tatutomer (5)

Synthesis of the surface-attached valence tautomer is shown in **Scheme 4.1**. Synthesis of the nanoparticle confined valence tautomer begins with the synthesis of **1** from 4, 4´ -dimethylbipyridine using LDA and 1,5 - dibromopentane.[8] **1** was converted to **2** by reaction with potassium thioacetate.[8] **2** was reacted with NaOH to create the **3**.[8] **4** was synthesized using the standard Brust procedure[9] and the **4** was reacted with cobalt tetramer[10] to yield **5**.

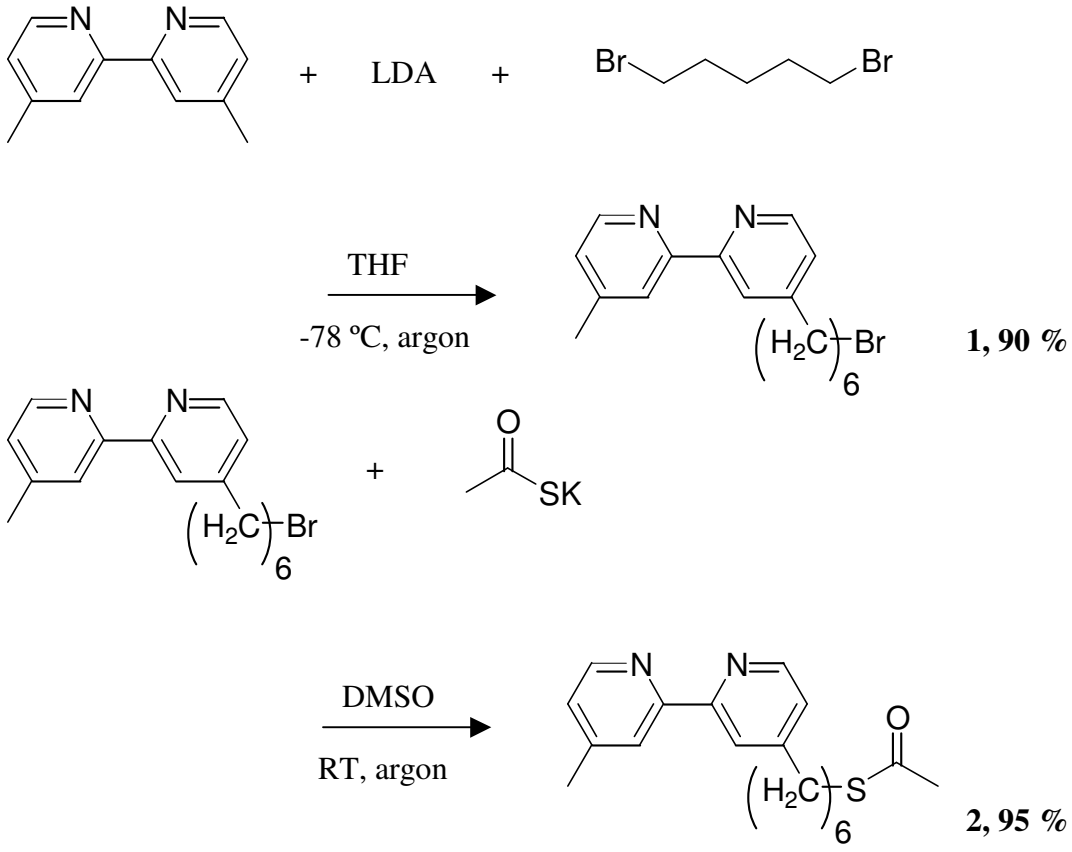

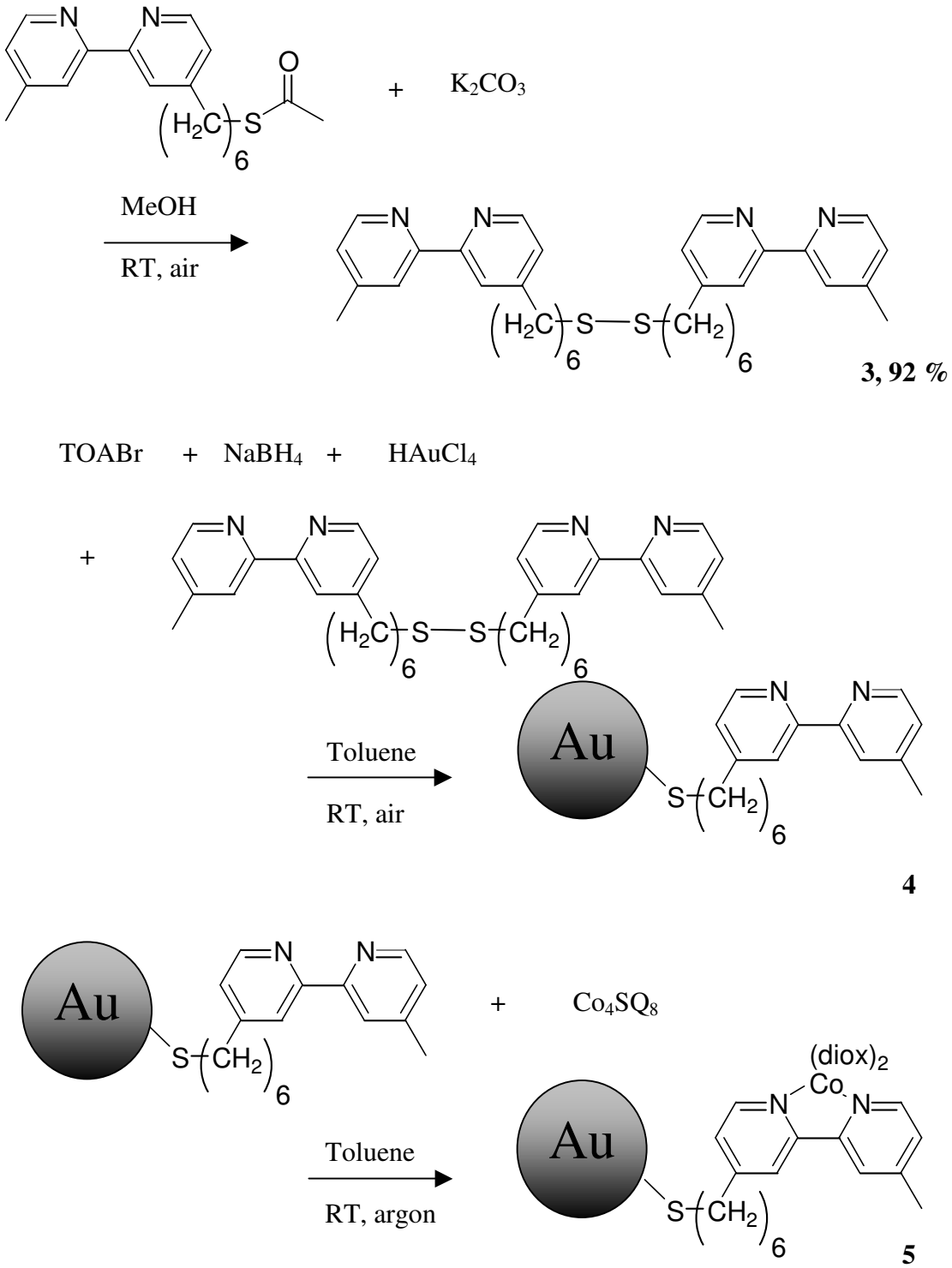

Scheme 4.1. Chemical synthesis of **5**.

4.3 Nanoparticle Characterization

The first order of business is to determine whether the surface bound complex was actually synthesized. First, transmission electron microscopy (TEM) shows that the gold clusters retained their colloidal and monodisperse properties. Furthermore, the TEM image shows clusters that are on the order of ~ 2 – 5 nanometers in diameter (**Figure 4.2**).

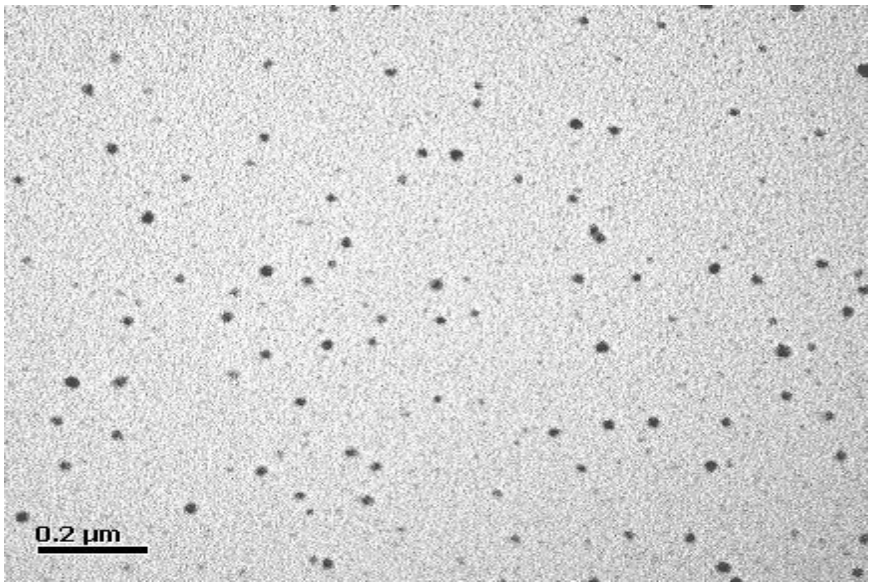

Figure 4.2. TEM image of **5**.

Second, electronic absorption spectroscopy supports the existence of gold clusters with the presence of the gold plasmon polariton absorption band.[9] This absorption band is the signature electronic absorption band of gold clusters and its shape and intensity can be used to extract the average size of the cluster being studied. The maximum absorption wavelength of the plasmon band is ~ 520 nm and the band shape is very broad (**Figure**

4.3). Based on established research both observations are consistent with small diameter clusters on the order of ~ 2 nm.[9]

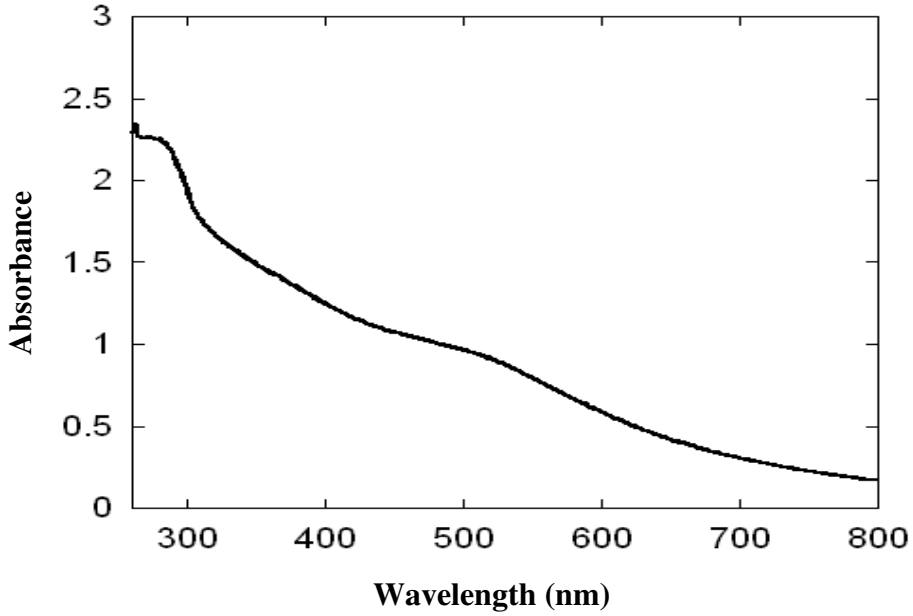

Figure 4.3. Electronic absorption spectrum of **5** in CH_2Cl_2.

4.4 Characterization of Surface Bound Valence Tautomer

TEM and electronic can be used to describe the *particle*, however, other spectroscopic tools are needed to describe the valence tautomer itself. For **4**, ^{1}H-NMR shows a spectrum that is identical with **3** molecule with the exception that all of the nuclear transitions are broadened due to the Au particles' electric field (**Figure 4.4**).[5, 9]

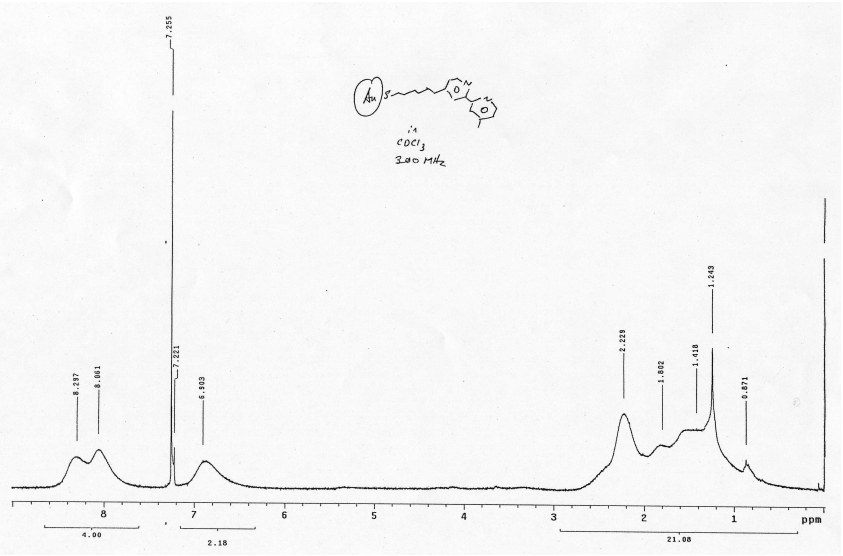

Figure 4.4. 300 MHz ^{1}H-NMR spectrum of **4** in $CDCl_3$.

5 on the other hand experiences an additional perturbation in that the system is now paramagnetic. The paramagnetic contribution to the ^{1}H-NMR experiment provides an added line broadening mechanism due to the changes in the T_1 and T_2 nuclear relaxation processes from the interaction of the nuclear spins with the magnetic field of the paramagnetic valence tautomer (**Figure 4.5**).[11-12] Thus many of the nuclear transitions of the surface bound valence tautomer are broadened into the baseline. There is a lack of signals in the of range of –50 – 100 ppm. Interestingly, the methylene protons are enhanced due to the paramagnetic perturbation. More importantly, the ^{1}H spectrum confirms that there are no free valence tautomer impurities since the free compound will exhibit an NMR spectrum consistent with the known spectrum of $Co(diox)_2bpy$.[13]

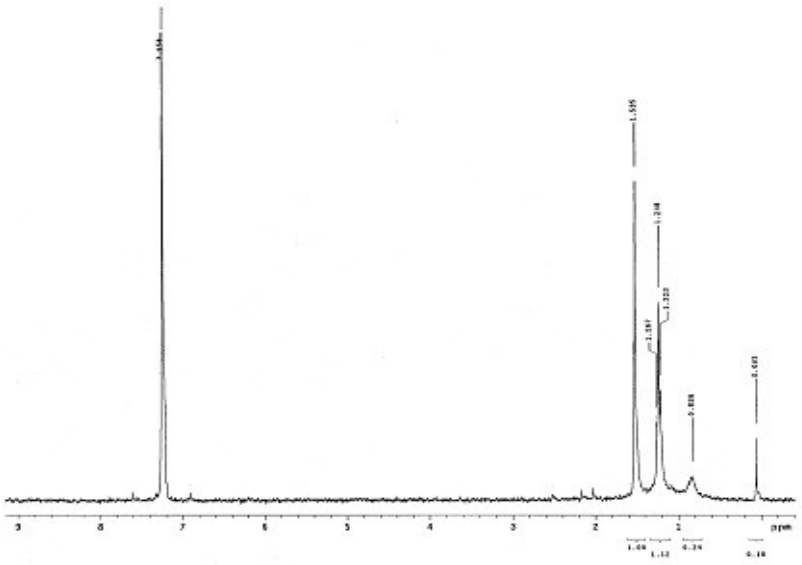

Figure 4.5. 300 MHz ^{1}H-NMR spectrum of **5** in $CDCl_3$.

Infrared spectroscopy experiments yield definitive evidence of the surface bound complex. Firstly the room temperature IR spectrum of **4** can be measured against **5** (**Figure 4.6**). The room temperature spectrum of **4** is consistent with that of the free bipyridine molecule in which the IR spectrum contains the aromatic breathing mode of the bipyridine molecule at 1590 cm^{-1}.[14] Upon coordination breathing mode shifts to 1620 cm^{-1}, a known shift of the bipyridine breathing mode to higher frequency due to coordination to the cobalt metal center.[14]

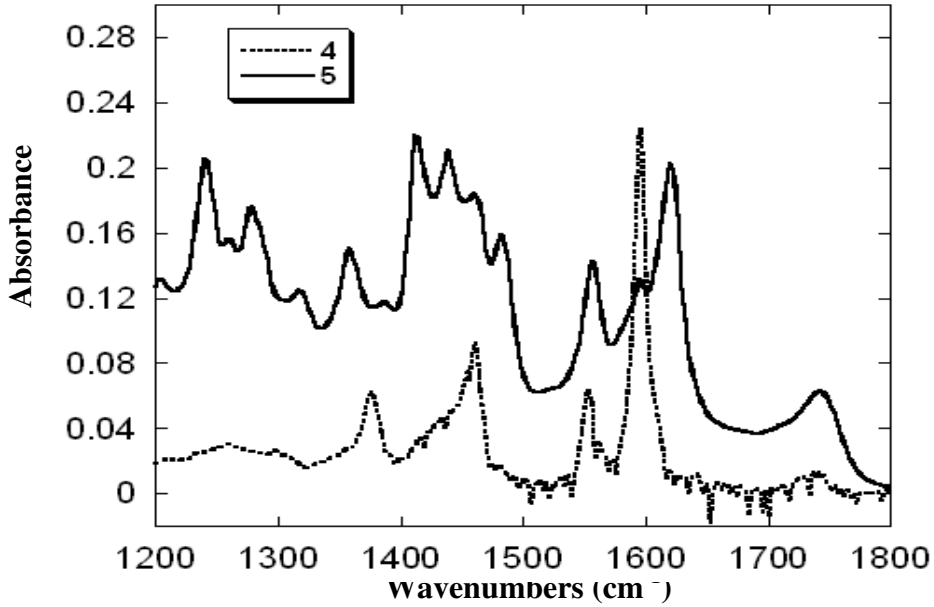

Figure 4.6. Room temperature IR spectral overlay of **4** and **5**.

4.5 Infrared Spectroscopy Comparisons

Comparisons of the room temperature infrared spectra of the **5** and its electronically and structurally comparable analog **6** (**Figure 4.7**) illustrate a striking similarity especially in the aromatic region (**Figure 4.8**). Disparities in the methylene region of the infrared spectrum are present but these differences are expected since **5** and **6** differ in the existence of the chain. Interestingly, the IVCT of **5** is not present (will be discussed later).

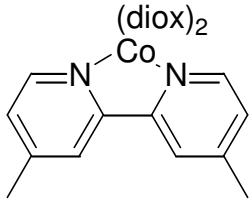

6

F**igure 4.7**. 4, 4´ - Dimethylbipyridine valence tautomer.

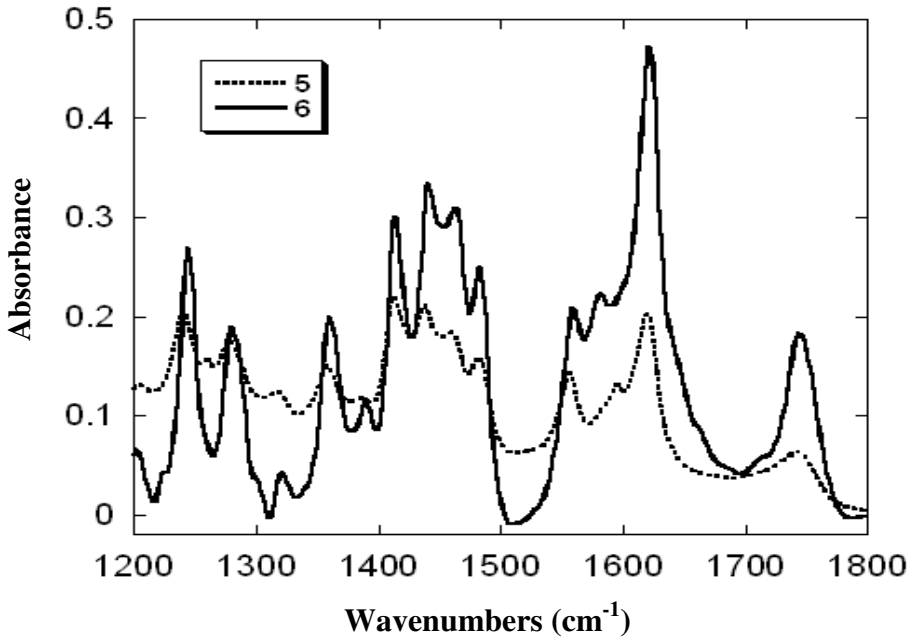

Figure 4.8. Room temperature IR spectral overlay of **5** and **6**.

A more accurate assessment can be made by evaluating the room temperature IR spectrum of the surface bound complex to the room temperature spectrum of **7** (**Figure 4.9**). Synthesis of **7** is detailed in **Scheme 4.2**. **5** shares a near-exact infrared spectrum to the electronically and structurally identical **7**. Thus all spectroscopic evidence describe the surface bound valence tautomer and the combination of room temperature NMR and IR experiments are consistent with the presence of the valence tautomer. Additional evidence for the valence tautomer is provided in the variable temperature infrared experiments.

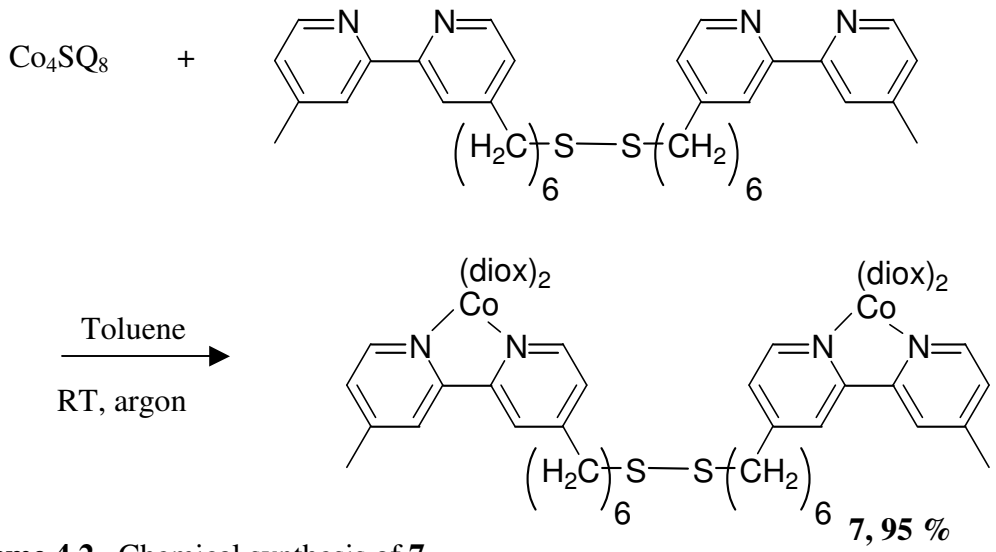

Scheme 4.2. Chemical synthesis of **7**.

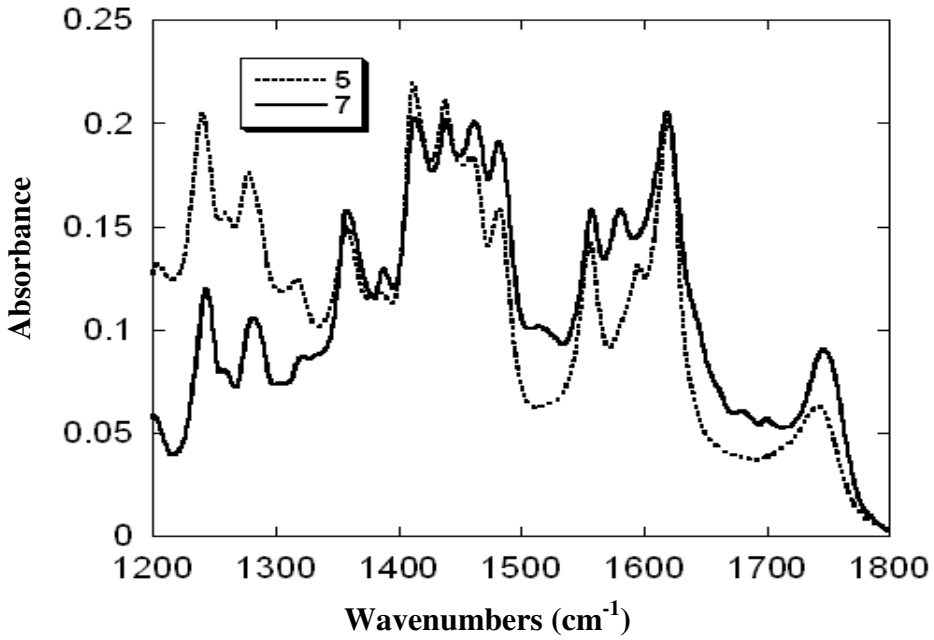

Figure 4.9. Room temperature IR spectral overlay of **5** and **7**.

4.6 Variable Temperature Infrared and Singular Value Decomposition Analysis

To complete the analysis of the effect of surface confinement to valence tautomerism it is necessary to observe the electronic state change of the system as a

function of temperature. Variable-temperature infrared spectroscopy is a convenient method that allows for the study of the electronic state change. Because the valence tautomeric equilibrium involves interconverting between two different states, the vibrational modes will change in both frequency and intensity as a function of temperature (**Figure 4.10**). Singular value decomposition (SVD) analysis is a method that permits the determination the vibrational change as the different states are populated.[15] From the SVD analysis, the sigmoid that describes the relative change of the vibrational modes with respect to temperature can be constructed (**Figure 4.11**). The complete description of the singular value decomposition method used is detailed in experimental section. As a comparison SVD analysis was also performed on **6** as well (**Figure 4.12**).

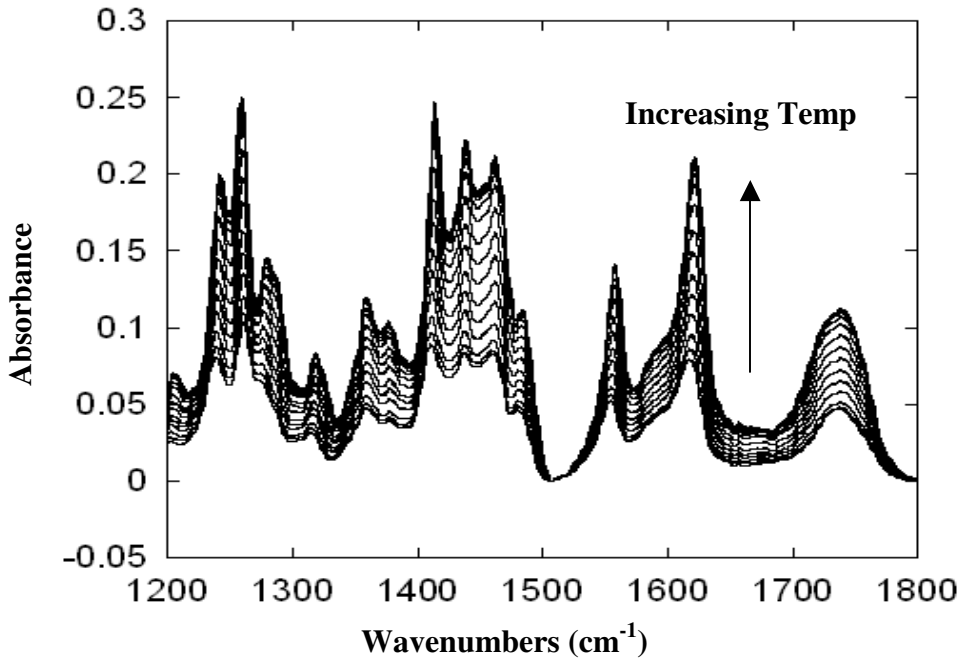

Figure 4.10. Variable temperature IR of **5** between 10 – 400 K.

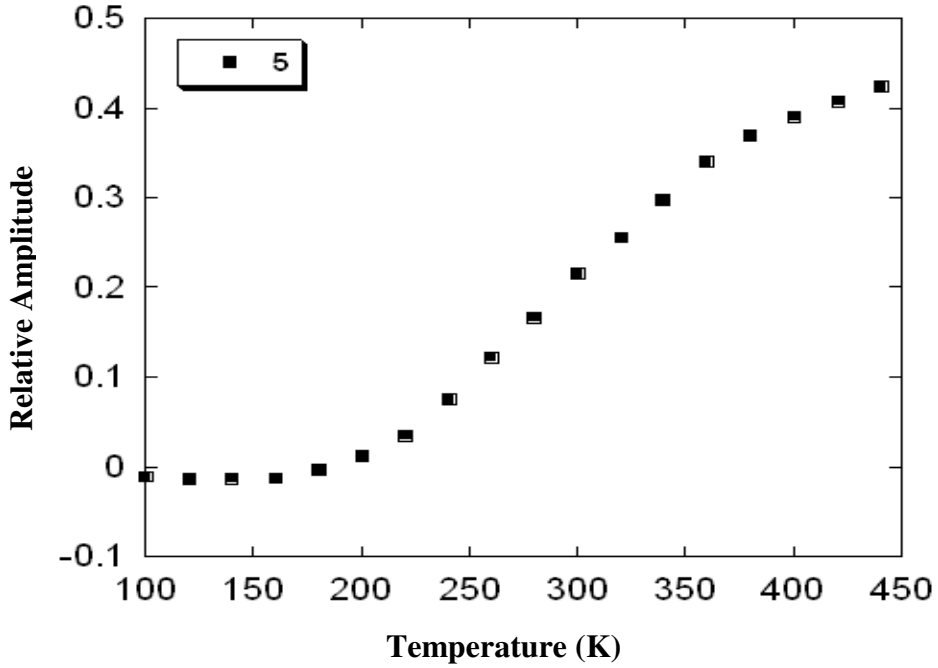

Figure 4.11. SVD analysis of **5**.

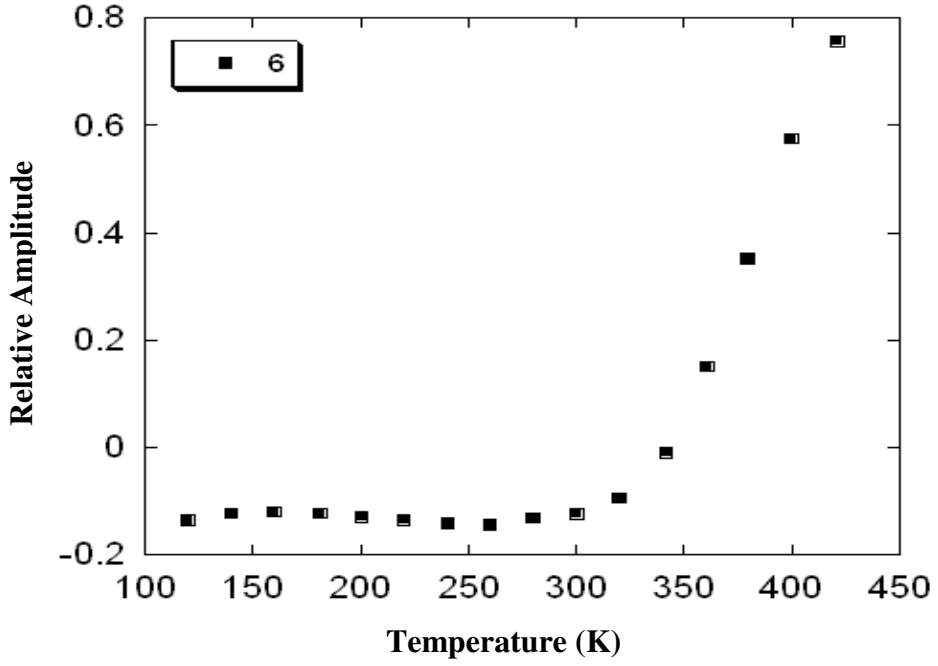

Figure 4.12. SVD analysis of **6**.

By fitting the sigmoids it was possible to extract the thermodynamic changes from the SVD analysis (**Figure 4.13** and **Table 4.1**). The relationships used to fit the data are detailed in the experimental section.

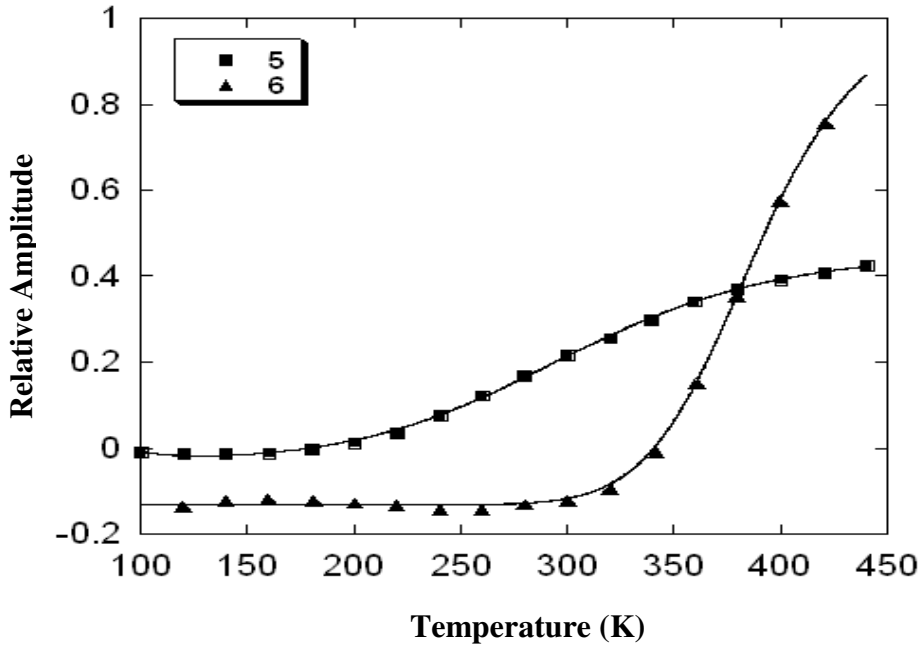

Figure 4.13. SVD comparison of **5** and **6**.

Table 4.1. Thermodynamic parameters of **5** and **6**.

Parameter	**5**	**6**
$T_{1/2}$ (K)	318	389
ΔH^{o} (kcal mol^{-1})	3.42	11.35
ΔS^{o} (cal mol^{-1} K^{-1})	10.7	29.2

The thermodynamic fits describe a striking difference between **5** and **6**. Both enthalpy and entropy values for the **5** are 1/3 of the values of the comparison molecule. Any attempt to explain the differences must begin by reflecting on the possible perturbations that may contribute to the change: 1) electronic coupling; 2) spin/vibrational effects; and 3) solvation.

Beginning with electronic coupling, there are two types of electronic perturbations the metal surface can exert[5-7] on the valence tautomeric change: 1) mixing of the orbital wavefunctions of the valence tautomer with the gold surface orbitals either through space or through bond, and 2) interaction of the valence tautomer dipole with the surface charge. In the former type the infrared experiments may provide additional insight. Although from the spectroscopic evidence by comparisons of **6** and **7** to **5** that it is abundantly clear that the surface bound valence tautomer was synthesized, there are some electronic differences that distinguish **5** from its free analogs. The intervalence charge-transfer band due to the mixed-valent Co^{III} state is largely quenched in the surface-bound complex. The quenching can be observed in the comparison of **5** with the other molecules (**Figures 4.14 – 4.15**). Quenching of electronic bands by surface interactions has precendent.[17] The molecule to surface interaction provides for the coupling of the surface metal orbitals to the electronic distribution of the electronic dipole moment change, which allows for the quenching perturbation to occur.

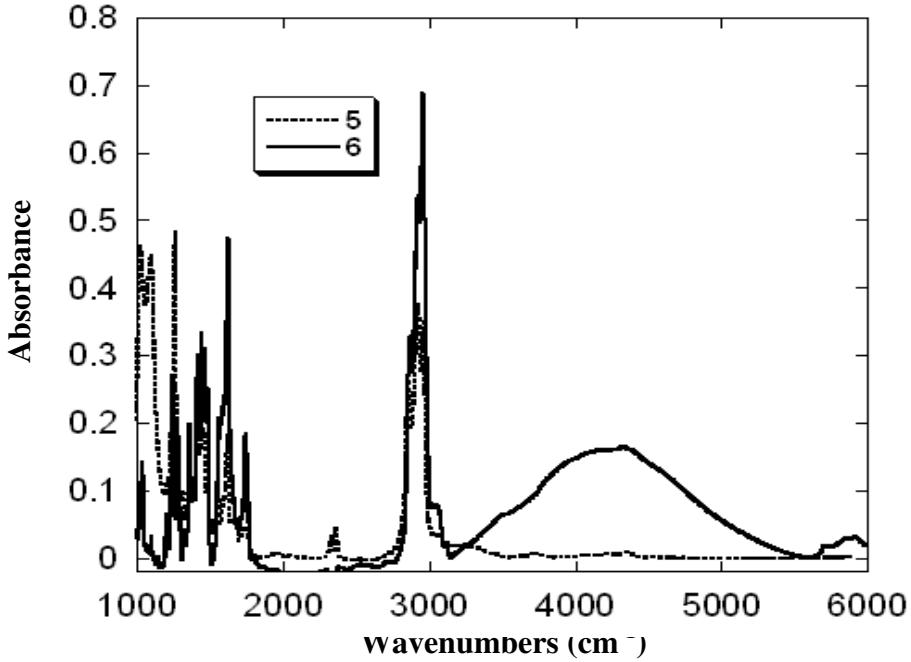

Figure 4.14. Room temperature IR spectral overlay of **5** (lacks IVCT) and **6**.

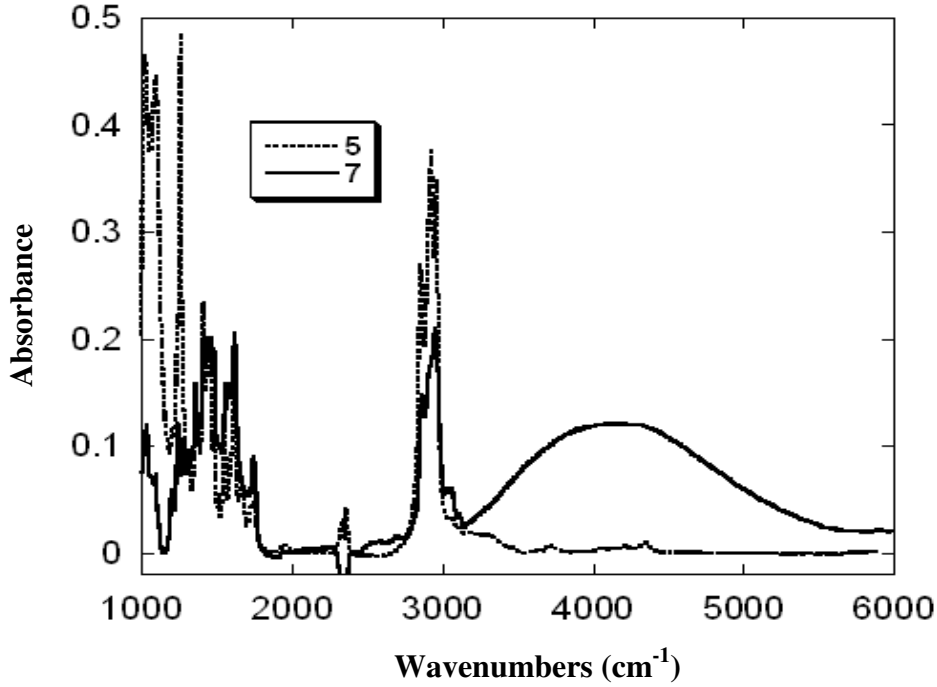

Figure 4.15. Room temperature IR spectral overlay of **5** (lacks IVCT) and **7**.

Orbital mixing may also explain the IVCT change. If orbital mixing is the culprit then it is unlikely that the coupling is occurring through the alkyl chain since the potential energy barrier of electron transfer through sigma bonds is relatively high. It is also unlikely that the valence tautomer is standing up from the surface since the Co bis(dioxolene) headgroup is very large.[5-7] This assumption makes it very likely that the valence tautomer head group lies very near to the surface. Gold is a third row transition metal ion and has very diffuse orbitals. Thus it is not hard to imagine that there may be some mixing of the surface bound valence tautomer orbitals with the gold surface orbitals. However, despite these seemingly reasonable arguments it is still not entirely clear that the quenching of the IVCT band is due entirely to surface coupling. Electron transfer between donors and acceptors is inherently a vibronic process unless the donor/acceptor systems are free ions.[16-17] Thus in order for the electron transfer to occur there must exist the vibrational freedom to allow for the process to occur. It is entirely possible that the packing of the surface bound valence tautomer prevents the necessary vibrational freedom and the system is vibronically – trapped. Vibronic trapping may explain the lack of the intervalence charge transfer band since the solid state crystal structure of the $Co(diox)_2bpy$ complex displays clear unsymmetric SQ and Cat moieties and not the delocalized groups expected from the predicted large coupling matrix that describes the mixing of SQ and Cat wavefunctions.[13]

In the latter possibility the valence tautomer system may experience the dipole interaction with the gold surface charge. From the IR analysis this possibility is also unlikely. Since the surface charge effect is described as the coupling of the molecular dipole moment to the surface dipole, this intermolecular coupling forms the basis of

surface selection rules.[18] Consider a simple metal – ligand (M – L) bond. A metal to ligand charge transfer is the redistribution of charge from the metal to the ligand. This charge orientation describes an electronic dipole moment change from the ground to the excited state. Surface selection rules dictate that the surface dipole can influence the nature of the dipole moment change and substantial changes may be observed in the metal to ligand charge transfer band. This may be the reason why the IVCT is quenched, however it is extremely unlikely since if surface selection rules are to be completely obeyed then the same perturbation is to be expected to occur in the vibrational region as well. The IR data does not show substantial changes between the surface bound complex and its free analogs and surface charge may be neglected as a possible major contributor to the thermodynamic change. The possible role of electronic coupling to the thermodynamic change can be expressed with a final addition. While electronic coupling clearly plays an important role in altering the electronic properties of molecular chromophores, it *cannot* strongly affect the entropy as would be required to account for the changes observed in the thermodynamic parameters since electronic coupling is an enthalpic process and not an entropic one. Consequently, electronic coupling can be effectively ruled out as a major contributor to the thermodynamic change.

The second possible contributor to the observed thermodynamic change is spin/vibrational effects. The spin contribution to the thermodynamic equilibrium is ΔS^{o} (spin) = R ln (16/4) = 11.5 J mol^{-1} K^{-1} and it can excluded as a major contribution to the overall entropy.[19] It has been proposed that the largest contribution to ΔS^{o} arises from changes in metal-ligand bond-stretching frequencies as the valence tautomer interconverts between the *ls*-Co^{III} and *hs*-Co^{II} forms.[20] This is because of the occupation

of the dσ* orbitals in the *hs*-Co^{II} form and the resultant lower metal-ligand vibrational frequencies. These low energy modes provide for greater vibrational entropy in the *hs*-Co^{II} form by analogy with Fe^{II} spin-crossover complexes.[19-22] From this analogy ΔS^{o} (vibration) from previous studies has been assumed to be reasonable. However, doubt has been cast on the magnitude of ΔS^{o} (vibration) by heat capacity measurements made by Abakumov[23] and by computational results reported by Cox.[24]

The remaining explanation is "solvation." The solvation sphere of the surface bound valence tautomer is composed of other surface valence tautomers and the gold surface. It is entirely possible that by anchoring the valence tautomer to the surface a large number of intermolecular interactions that arises from the solvation sphere has been eliminated thereby reducing ΔH^{o} and ΔS^{o}. This assumption has much merit since it has been shown that solvation plays a substantial role in the valence tautomeric process.[5]

4.7 Attempted Alternative Pathways

The next two sections outline the alternative paths taken to synthesize and characterize a surface-bound valence tautomer. Ultimately these synthetic efforts did not provide the conclusions needed to help understand the surface-bound valence tautomeric behavior, however, they are informative in the sense that they provide a more complete picture of the process needed to achieve the goals met in this project.

4.8 Mixed-Monolayer Cluster Synthesis

An attempt to synthesis the surface-bound complex involved the creation of a mixed-monolayer gold cluster and two methods of synthesizing the mixed-monolayer

compound were endeavored (**Figure 4.16**). The first method involves exchanging the dinuclear valence tautomer (**7**) with the clusters containing hexane thiolates as the stabilizing surface substituent (**Scheme 4.3**). However, the disulfide valence tautomer did not seem to provide observable exchange despite differing the molar ratios of the compounds and the lack of exchange is attributed to the unfavorable competition of the disulfide to gold reaction in the presence of surface thiolates.

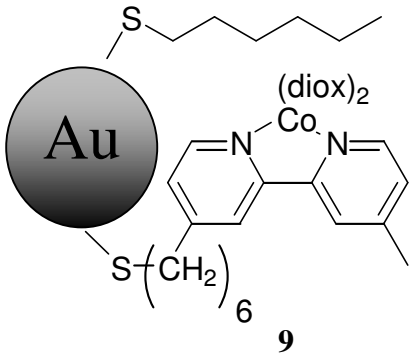

9

Figure 4.16. Mixed-monolayer gold cluster.

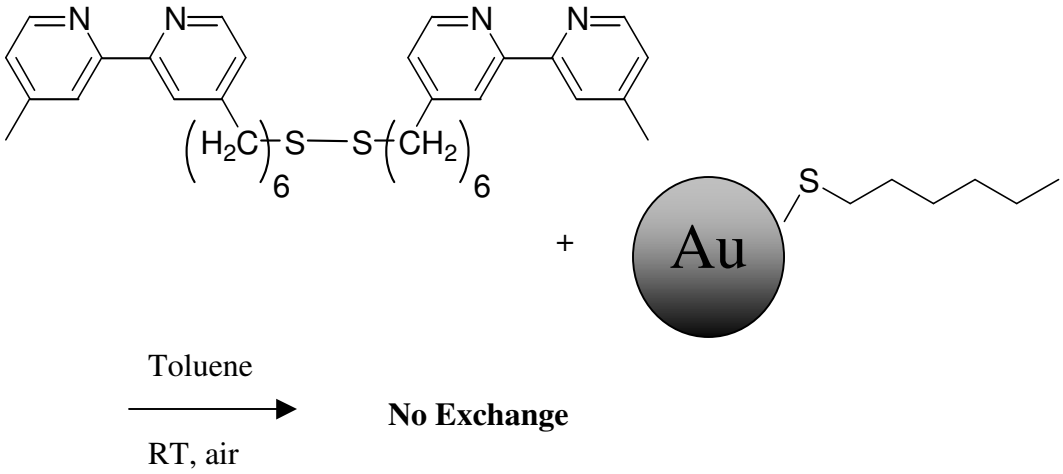

No Exchange

Scheme 4.3. Attempted chemical exchange reaction.

The successful synthesis of **8**[24] provides an avenue to successfully complete the exchange reaction (Scheme 4.4). The mixed-monolayer cluster was successfully synthesized and characterized by NMR (**Figure 4.17**). Regrettably the weak signal intensities and the presence of the hexane thiolate on the surface complicates the characterization methods, especially the variable temperature IR experiments and SVD analysis.

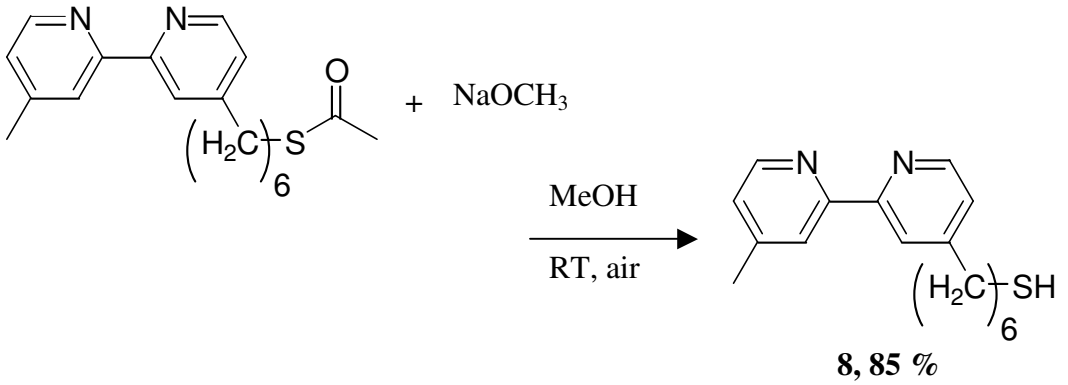

8, 85 %

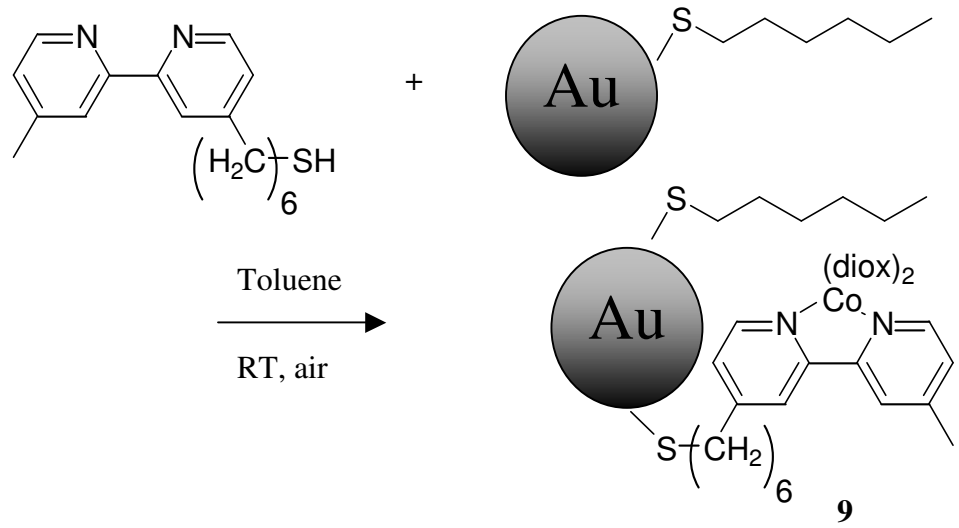

9

Scheme 4.4. Synthesis of **9**.

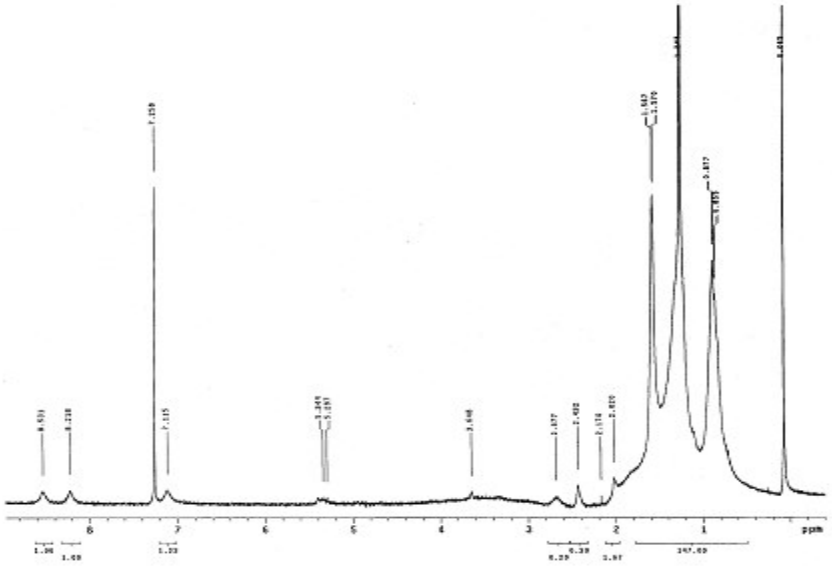

Figure 4.17. ^{1}H-NMR of **9** 300 MHz in $CDCl_3$.

4.9 Surface Monolayer Synthesis and Characterization

Synthesis and characterization of the valence tautomer on a flat surface was attempted. Synthesis was performed by submersing a flat gold slide in a solution containing a specific concentration of **3** and then re-subjecting the gold slide to a solution of cobalt tetramer. Surface IR indicates the presence of the coordinated species due to the shift of the bipyridine breathing mode (**Figure 4.18 – 4.19**). However, the poor quality of surface IR methodology prevented further characterization of the surface-bound system.

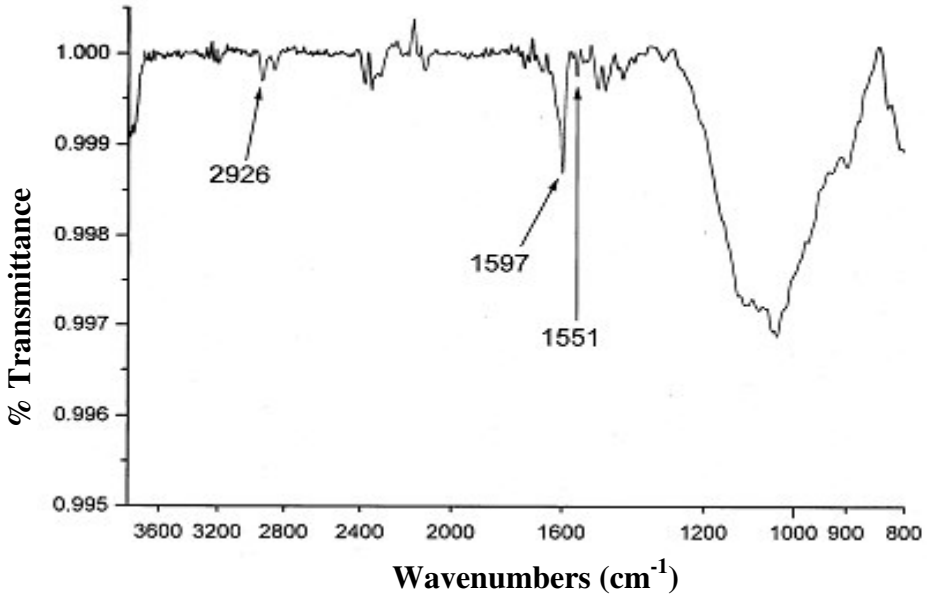

Figure 4.18. Surface Infrared of surface-bound **3**.

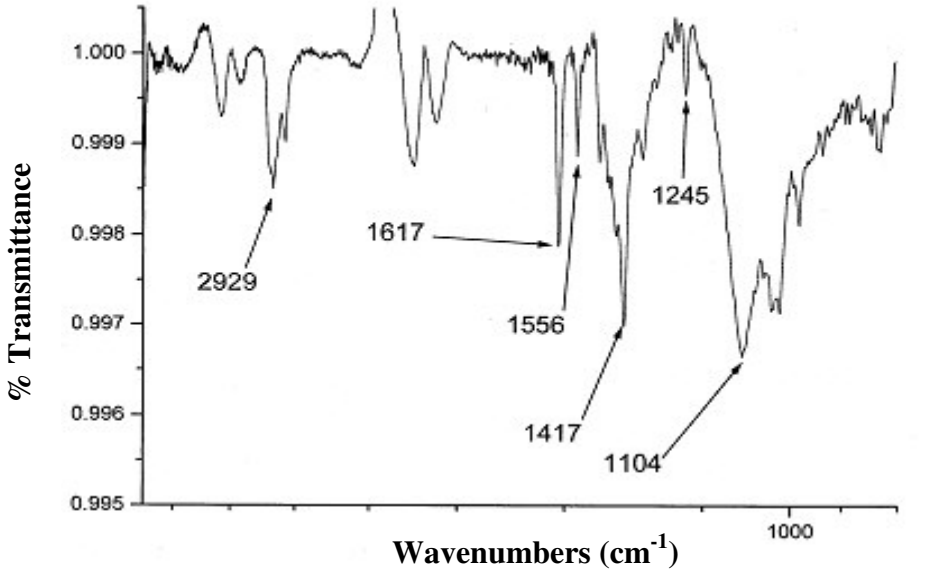

Figure 4.19. Surface Infrared of surface-bound valence tautomer.

4.10 Conclusion

The striking difference between the surface-bound complex and **6** could be attributed to a number of possibilities, including electronic coupling, spin/vibrational effects and solvation. However, experimental evidence indicate that solvation may play the dominant role in the thermodynamic change. This conclusion can be supported by further experiments. One possible method to explore this behavior is to "inflate" the solvation sphere of the valence tautomer with small solvent molecules during the IR experiment. This can be done by performing a solution – based variable temperature experiment. In solution the surface bound valence tautomer is fully solvated and the thermodynamic change may reflect the values typically reported in the literature. In any case, the experiments performed in this endeavor have opened a new avenue in valence tautomer research as it has been demonstrated that surface attachment can be used to tune valence tautomeric behavior.

4.11 Experimental

All syntheses were performed under inert conditions with anhydrous solvents unless stated otherwise. NMR spectra were recorded in *d*-chloroform at 300 MHz. Electronic absorption spectra were collected in CH_2Cl_2 on a Hewlett Packard 8452A Diode Array Scanning Spectrophotometer. IR experiments were performed on a Digilab FTS 3000 FTIR spectrometer equipped with a globar source, KBr beamsplitter and a liquid nitrogen cooled MCT detector. The spectra were the result of 64 scans at a spectral resolution of 2 cm^{-1}. The temprature dependent spectra were recorded using a helium cooled cryostat (MicrostatHe, Oxford Instruments). SQUID experiments were performed on a Quantum Design MPMS-XL7 SQUID magnetometer using a Delrin sample holder at an applied field of 4000G. Pascal's constants were used to calculate diamagnetic corrections.

Synthesis of 4´-(6-bromo-hexyl)-4-methyl-[2,2´]bipyridinyl (**1**). A 250 mL schlenk flask is charged with 3.8 mL diisopropylamine and 20 mL THF. The flask is cooled to –78 ºC and 13.6 mL 2.0 M n-butyllithium in hexanes is added to the reaction mixture. After stirring for 30 minutes the formed lithium diisopropyl amine mixture was cannulated into a separate schlenk flask containing 5 g of 4, 4´ – dimethylbipyridine dissolved in 20 mL THF. After stirring for 2 hours the reaction mixture was cannulated to a 250 mL schlenk flask containing 3.71 mL dibromopentane and 20 mL THF. The mixture was allowed to warm slowly overnight and finally quenched with deionized water. The product wa sextracted using methylene chloride and precipitated from acetonitrile (4.56 g, white solid). ^{1}H NMR: δ 8.55 (t, 2H, J = 5.4 Hz); 7.13 (d, 2H, J = 4.8 Hz); 3.4 (t, 2H, J = 6.6 Hz); 2.7 (t, 2H, J = 7.8 Hz); 2.4 (s, 4H); 1.8 (m, 2H); 1.7 (m, 2H).

Synthesis of thioacetic acid S-[6-(4´-methyl-[2,2']bipyridinyl-4-yl)-hexyl] ester (**2**). A 250 mL schlenk flask was charged with 0.530 g of **1** and 0.182 g of potassium thioacetate. The reagents are dissolved in 20 mL DMSO and allowed to stir at 70 ºC overnight. The reaction mixture was quenched with deionized water and the product was extracted using methylene chloride and purified by precipitation from absolute ethanol (0.284 g, white solid). ^{1}H-NMR: δ 8.5 (t, 2H, J = 4.5 Hz); 8.2 (d, 2H, J = 3.3 Hz); 7.12 (d, 2H, J = 3.0 Hz); 2.8 (t, 2H, J = 7.5); 2.7 (t, 2H, J = 8.1); 2.4 (s, 3H); 2.3 (s, 3H).

Synthesis of *bis*(6-(4´-methyl-[2,2']bipyridinyl-4-yl)-hex-1-yl-)disulfane (**3**). A 250 mL round bottom flask was charged with 0.100g of **2** and 1.165g K_2CO_3 and dissolved in 30 mL wet methanol. The reaction mixture was allowed to stir for 2 days in air until quenched with deionized water. The product was extracted using methylene chloride and precipitated from absolute ethanol (0.056 g, white solid). ^{1}H-NMR: δ 8.5 (s, 2H); 8.2 (s, 2H); 2.6 (q, 4H, J = 7.5);

Synthesis of Au-bpy (**4**). A 250 mL round bottom flask was charged with 30 mL of 0.03 M $HAuCl_4$ in water and 100 mL wet toluene. 2.19 g tetraoctyl ammonium bromide is added to the reaction mixture and allowed to stir for 10 minutes. 0.200 g of **3** is added and allowed to stir for an additional 10 minutes. Finally, 0.756 g $NaBH_4$ is added to the reaction mixture and the system was allowed to stir overnight. The product was collected in the toluene layer and precipitated in absolute ethanol (0.162 g, purple solid).

Synthesis of Au-VT (**5**). A 250 mL round bottom was charged with 0.100 g **4** and 0.020 g cobalt semiquinone tetramer. The reactants were dissolved in 20 mL toluene and allowed to stir for 2 hours. Toluene from the mixture was evaporated under vacuum until a superconcentrated mixture remained and the product was precipitated using hexanes. The product was collected on a filter stick (0.023 g, purple solid).

Synthesis of VT-SS-VT (**7**). A 250 mL Schlenk flask was charged with 0.025 g **4** and 0.039 g 3, 5 – di – tert – butylorthoquinone and dissolved in 15 mL toluene. In a separate flask 0.015 g of dicobalt octacarbonyl was dissolved in 10 mL toluene. The dicobalt octacarbonyl solution was cannulated to the disulfide/quinone reaction mixture and allowed to stir for 10 minutes. The solution was then allowed to sit overnight and the product was collected on a filter stick (0.026 g, green solid). Magnetic suscetiblity confirms the molecule since the low temperature χT value is 0.75 emu K mol^{-1}, which is consistent with two uncoupled unpaired electrons.

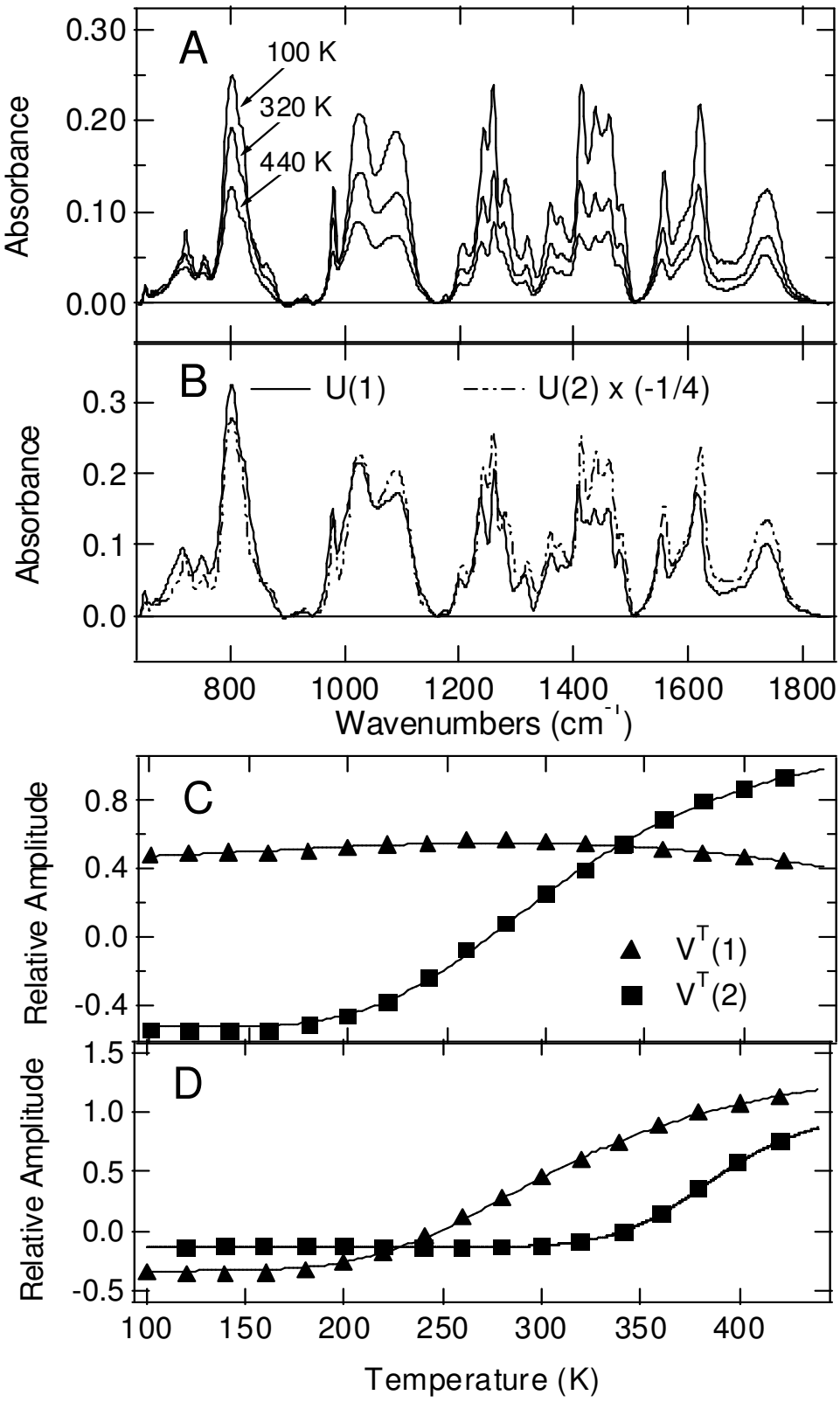

Figure 4.20. SVD analysis of **5** and **6**.

The SVD analysis refers to **Figure 4.20**. The first component represents the low temperature (*ls*-Co^{III} form) spectrum in the U matrix (wavenumber dimension) and a relatively constant term in the V matrix (temperature dimension). The second component represents the difference between the *ls*-Co^{III} and *hs*-Co^{II} forms in the wavenumber dimension (**Figure 4.20 B**). The familiar sigmoidal shape expected from a two-state equilibrium is observed for the temperature dimension of this component (**Figure 4.20 D**). The sigmoidal curves in **Figure 4.20 D** were least-squares fit to obtain the thermodynamic parameters as well as $T_{1/2}$ for both compounds. By using the following relationships the thermodynamic parameters for the SVD analysis sigmoids were constructed and fitted to the data (**Figure 4.20**).[20]

$$Co_{ls} \overset{K_{eq}}{\leftrightarrow} Co_{hs} \tag{5.1}$$

$$K_{eq} = \frac{[Co_{hs}]}{[Co_{ls}]} = \frac{f(Co_{hs})}{f(Co_{ls})} \tag{5.2}$$

$$A = f * (A_{Co_{ls}}) + (1 - f) * (A_{Co_{hs}}) \tag{5.3}$$

$$f = \frac{K_{eq}}{1 + K_{eq}} \tag{5.4}$$

$$A = \frac{K_{eq} * A_{Co_{ls}} + A_{Co_{hs}}}{1 + K_{eq}} \tag{5.5}$$

$$K_{eq} = \exp(-\frac{\Delta G^0}{RT}) \tag{5.6}$$

$$A(T) = \frac{\exp\left(-\frac{\Delta G^0}{RT}\right) * A_{Co_{ls}} + A_{Co_{hs}}}{1 + \exp\left(-\frac{\Delta G^0}{RT}\right)} \tag{5.7}$$

$$\Delta G^0 = \Delta H^0 \left(1 - \frac{T}{T_{1/2}}\right) \tag{5.8}$$

$$\Delta S^0_{T_{1/2}} = \frac{\Delta H^0_{T_{1/2}}}{T_{1/2}} \tag{5.9}$$

4.12 References

1. Adams, D. M.; Dei, A.; Rheingold, A. L.; Hendrickson, D. N. *J. Am. Chem. Soc*. **1993**, *115*, 8221.
2. Pierpont, C. G.; Buchanan, R. M. *J. Am. Chem. Soc*. **1980**, *102*, 4951.
3. Cador, O.; Dei, A.; Sangregorio, C. *Chem. Comm*. **2004**, 652.
4. Koga, N.; Sameshima, K.; Morokuma, K. *J. Phys. Chem*. **1993**, *97*, 13117.
5. Shenhar, R.; Rotello, V. *Acc. Chem. Res*. **2003**, *36*, 549.
6. Thomas, G. K; Kamat, P. V. Acc. Chem. Res. **2003**, *36*, 888.
7. Daniel, M – C.; Astruc, D. *Chem. Rev*. **2003**, *104*, 293.
8. Sato, Y.; Uosaki, K. *J. Electroanal. Chem.* **1995**, *384*, 57-66.
9. Brust, M.; Bethell, D.; Schiffrin, D. J.; Kiely, C. J. *Adv. Mater*. **1995**, *7*, 795.
10. Buchanan, R. M.; Fitzgerald, B. J.; Pierpont, C. G. *Inorg. Chem*. **1979**, *18*, 3439.
11. Gunther, NMR
12. Russell S. Drago. *Physical Methods for Chemists*. Saunders College Publishing, **1997**.
13. Pierpont, C. G.; Buchanan, R. M. *J. Am. Chem. Soc*. **1980**, *102*, 4951.
14. Bonomo, R. P.; Musumeci, S.; Rizzarelli, E.; Seminara, A. *Z. Anorg. Allg. Chem*. **1975**, *414*, 185.
15. Vetterling, W. T.; Flannery, B. P. *Numberical Recipes in C++: The Art of Scientific Computing*; Cambridge University Press: New York, 2002.
16. Robin, M. B.; Day, P. *Adv. Inorg. Chem. Radiochem*. **1967**, *10*, 248.
17. N. S. Hush. *Prog. Inorg. Chem*. **1967**, *3*, 391.
18. Franzen, S.; Folmer, J. C. W.; Glomm, W. R.; O'Neal, R. J. Phys. Chem. A. 2002, 106, 6533.
19. Gutlich, P. *Struct. Bonding* (Berlin). **1981**, *44*, 83.
20. Gutlich, P.; Hauser, A.; Spiering, H. *Angew. Chem., Int. Ed. Engl*. **1994**, *33*, 2024.
21. Adams, D. M.; Dei, A.; Rheingold, A. L.; Hendrickson, D. N. *J. Am. Chem. Soc*. **1993**, *115*, 8221.
22. Shultz, D. A. *Valence Tautomerism in Dioxolene Complexes of Cobalt*. In *Magnetism: Molecules to Materials II: Molecule-Based Materials*; Miller, J. S., Drillon, M., Eds.; Wiley-VCH: New York, **2001**.
23. Abakumov, G. A.; Cherkasov, V. K.; Bubnov, M. P.; Ellert, O. G.; Dobrokhotova, Z. V.; Zakharov, L. N.; Struchkov, Y. T. *Dokl. Akad. Nauk*. **1993**, *328*, 332.
24. LaBute, M. X.; Kulkarni, R. V.; Endres, R. G.; Cox, D. L. *J. Chem. Phys*. **2002**, *116*, 3681.
25. Yamada, S.; Koide, Y.; Matsuo, T. *J. Electroanal. Chem.* **1997**, *426*, 23-26.

Chapter 5: Controlling Donor-Acceptor Behavior through Back Bonding

5.1 Introduction

In chemistry a mixed valent system is a compound that contains atomic centers with different oxidation states.[1] Although the oldest known mixed valent system is Prussian Blue,[2] the most famous and the most widely studied is the Creutz Taube ion (**Figure 5.1**).[1]

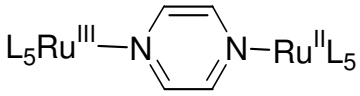

Acceptor **Donor**

Figure 5.1. The Creutz-Taube ion.

Mixed-valent molecules are very interesting to study because it has been shown that if the intramolecular interaction between the divergent oxidation state centers is large, then the mixed-valency behaves as an intramolecular donor-acceptor system. In the case of the Creutz-Taube ion the pyrazine ligand behaves as the electronic coupler between the two ruthenium centers. This is only feasible if there is strong back bonding into the pyrazine π^* that allows for electronic communication between the donor-acceptor pair.[3] Consequently it is possible for an intramolecular electron transfer process to occur between Ru^{II} to the Ru^{III} center. There are two equally valid ways to portray the electron transfer mechanism: electron exchange and hole exchange (**Figure 5.2**).[4] Electron exchange involves the low-lying π^* LUMO of the bridge for providing a communication

pathway between the donor-acceptor centers (**Figure 5.2 A**). Hole exchange involves the π HOMO of the bridge instead (**Figure 5.2 B**).

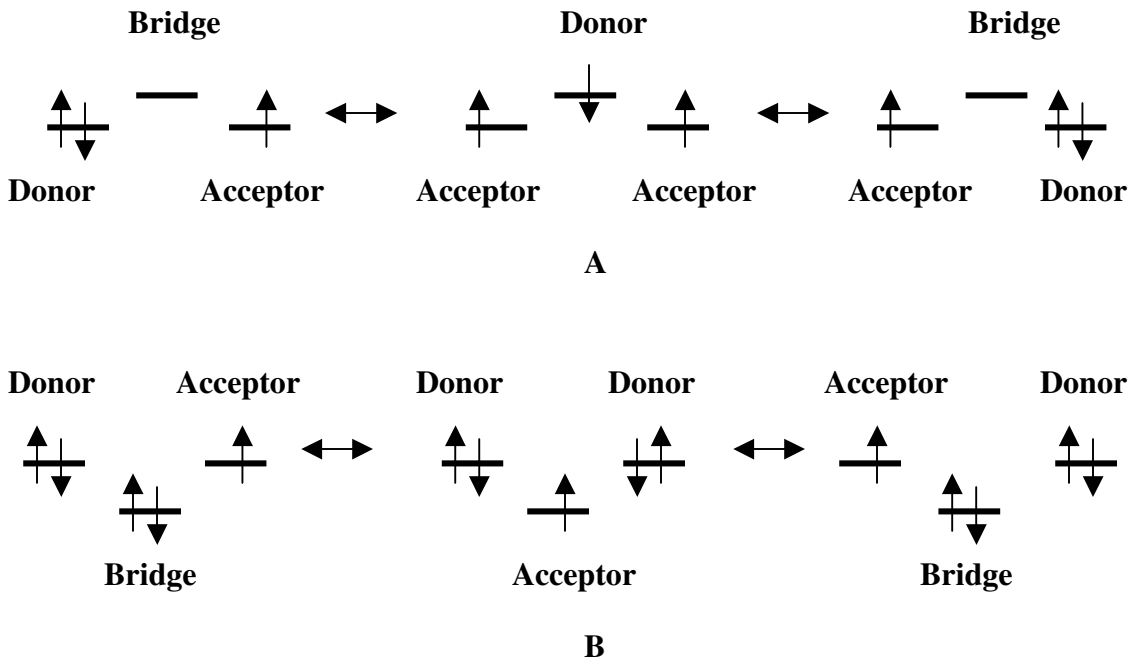

Figure 5.2. (**A**) Electron exchange and (**B**) hole exchange.

The degree of coupling between the donor and acceptor determines the level of delocalization of the electron that's shared between the two centers. As described in Chapter 3 mixed valent systems such as the Creutz-Taube ion are divided into three general classes as defined by the Robin-Day model and Hush theory.[5-6] Depending on how well the charge-transfer excited state mixes into the ground state term the mixed-valent system can be classified as Class I, II or III (section 3.8). Class I describes a behavior where the mixed valent pair do not communicate and the optical electron is localized. Class III is the full delocalization between the donor-accepter pair and the

optical electron is fully shared. Class II is the grey area in between Class I and Class II where the potential energy barrier to electron transfer is not so large as to prevent electron transfer but not zero so as to allow for full delocalization of the optical electron between the donor-acceptor pair.

The low temperature Co^{III} state of cobalt *bis*(dioxolene) valence tautomers is mixed valent with respect to the dioxolene ligands in which the donor-acceptor pair is the SQ-Cat ligands and the bridge is the Co^{III} metal center. In contrast to the Creutz-Taube ion the Co^{III}(SQ)(Cat) state is an interesting example of organic mixed valence in which the metal acts as the electronic coupling unit (**Figure 5.3**).

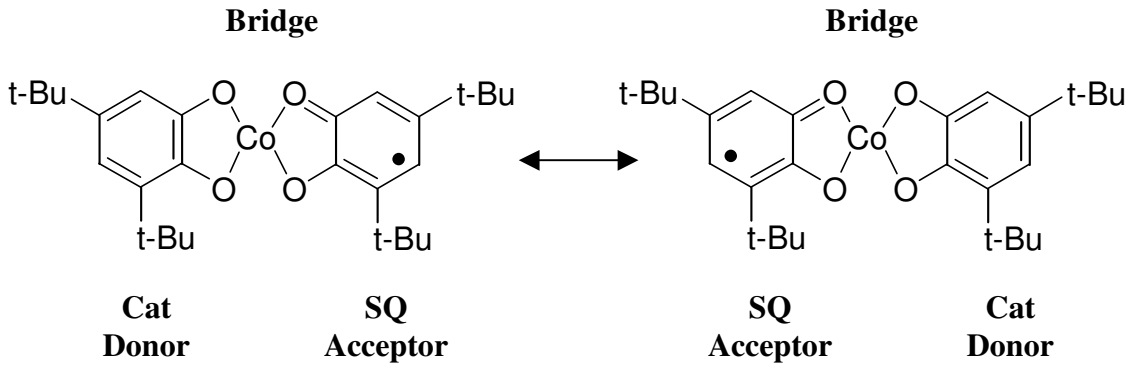

Figure 5.3. SQ and Cat as a donor-acceptor pair.

In this case the optical electron can be described as the electron that is delocalized between the SQ-Cat pair. The degree of delocalization between the SQ-Cat pair can be observed in electronic absorption spectroscopy where a light-induced electron transfer process between the SQ-Cat pair gives rise to an intervalence charge-transfer band (IVCT) in the near infrared (Chapter 3).[7] The IVCT is a function of the mixing of the

SQ-Cat ground and excited state terms and as a result the shape and intensity of the band is dependent on the overlap of the two wavefunctions.[3] The mechanism of the light-induced electron transfer process is very complex, however, a straightforward depiction can be shown qualitatively using simple MO theory (**Figure 5.4**). By ignoring the contribution of the metal bridge wavefunctions, the ground state can be constructed by simply mixing the SQ and Cat π* wavefunctions. Thus from this level of theory the optical electron populates an antibonding linear combination of the SQ-Cat orbital wavefunctions and the optical transition of the IVCT is the excitation of one of the paired electrons in the bonding linear combination to the antibonding wavefunction. Obviously the excitation energy corresponds to the difference in energy of the two combinations, which in turn is proportional to the intramolecular interaction of the SQ-Cat pair. Hence by the simple assumptions made to construct **Figure 5.4**, the level of coupling between the SQ-Cat pair ultimately determines the energy of the IVCT transition.

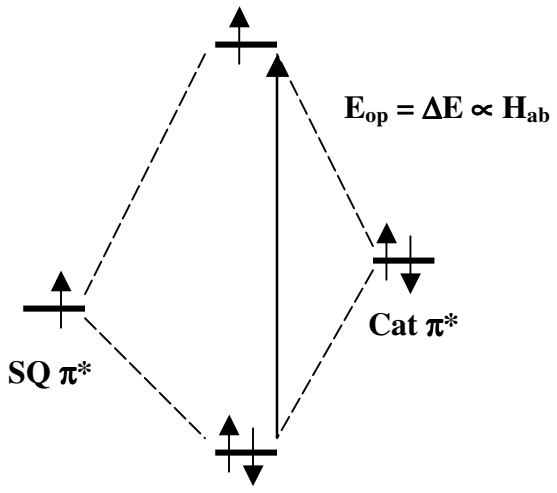

Figure 5.4. Description of the IVCT using MO theory.

Hush theory can be used to roughly correlate the bandwidth of the IVCT to the level of delocalization of the donor-acceptor pair. The following Hush relationships describe the bandwidth expected from a classical interaction between two states treated as simple harmonic oscillators and there is a symmetrical one-electron transfer:[6]

$$\frac{\Delta \nu_{1/2}^2}{\nu_{\max}} = 16kT \ln 2$$
$$\Delta \nu_{1/2} = \sqrt{16kT \ln 2 \bullet \nu_{\max}} \qquad (5.1)$$

As generally defined, if a charge-transfer band attributed to intervalence interactions is narrower than the bandwidth predicted by the Hush model, then the mixed-valent system that gives rise to the band is treated as approaching the Class II/Class III limit.[6] Bandwidths that are broader than the Hush model prediction are treated as approaching the Class II/Class I limit. Thus by treating states involved in the IVCT as a simple electron transfer process between two harmonic potentials and by ignoring other factors that may contribute to the bandwidth such as vibronic interactions and solvation, the Hush model can only be treated as a qualitative scale of the magnitude of electronic coupling in the mixed-valent system. However, despite its shortcomings the Hush relationships have successfully been applied to treat complex systems such as the Creutz-Taube ion to yield qualitatively accurate results.[1]

Even though the Robin-Day model and Hush theory do not consider the effects of the bridge that couples the donor-acceptor pair of mixed-valent molecules it is understandable to assume that the degree of electronic coupling between SQ and Cat is also *dependent* on the role of the metal wavefunctions. By using uncomplicated MO

theory the orbitals of the mixed valent interaction by including the role the metal to can be constructed (**Figure 5.5**).

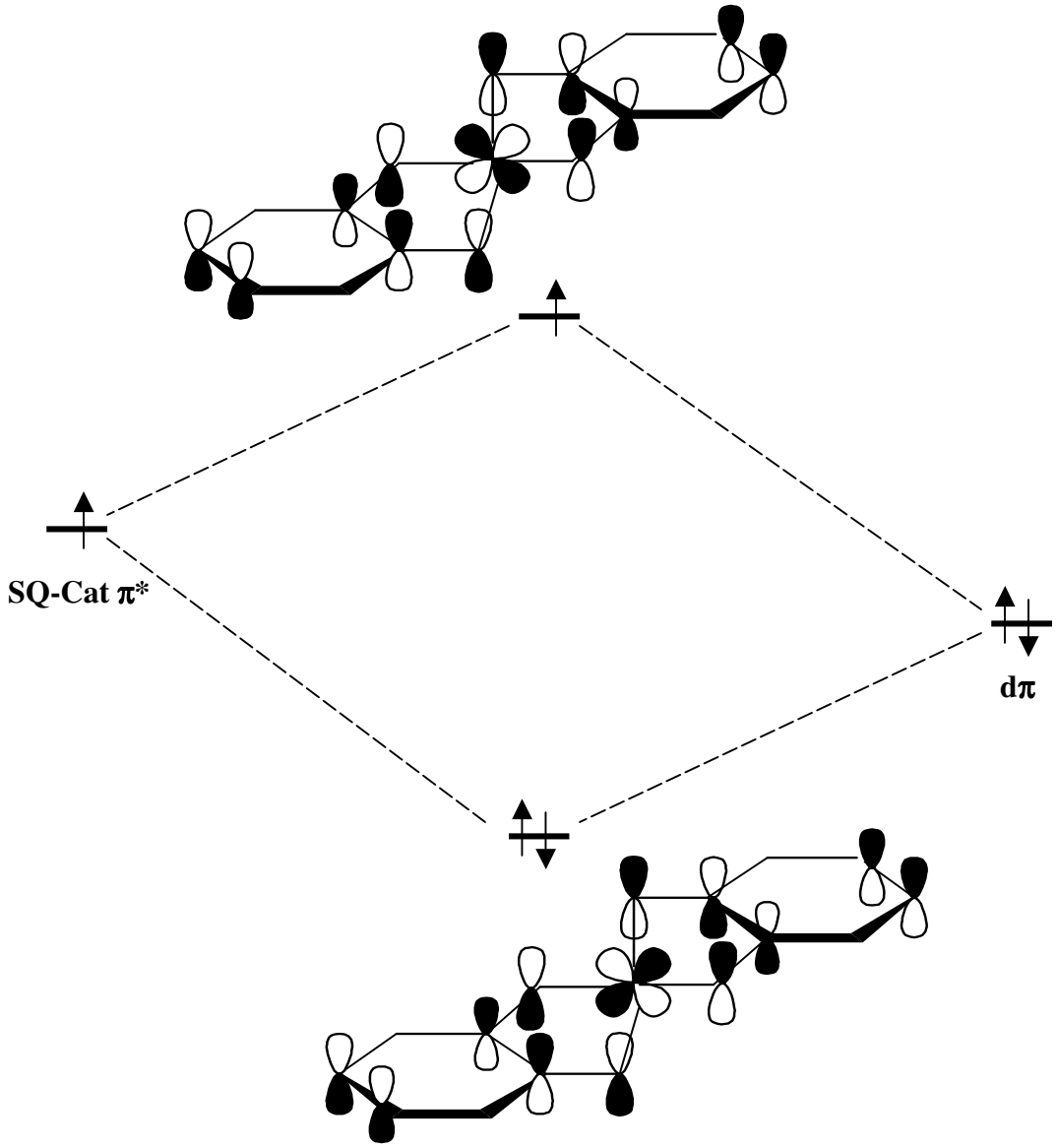

Figure 5.5. MO diagram of SQ-Cat and dπ.

In this case, to simplify the model the SQ-Cat orbital pair is treated as a single basis function consisting of the respective SQ-Cat π* with a single unpaired spin to signify the

delocalized optical electron and the Co dπ system is treated as a single filled dπ orbital. In this model the optical electron is populating an orbital that is composed of the antibonding combination of SQ-Cat and metal wavefunctions. Thus the electron can be described as being delocalized throughout the entire π-system. It is then reasonable to assume qualitatively that by varying the contribution of the metal dπ with respect to the SQ-Cat pair that the degree of delocalization of the optical electron will change. This can be performed if the metal dπ is moved closer or further away in energy with respect to the SQ-Cat pair (**Figure 5.6**).

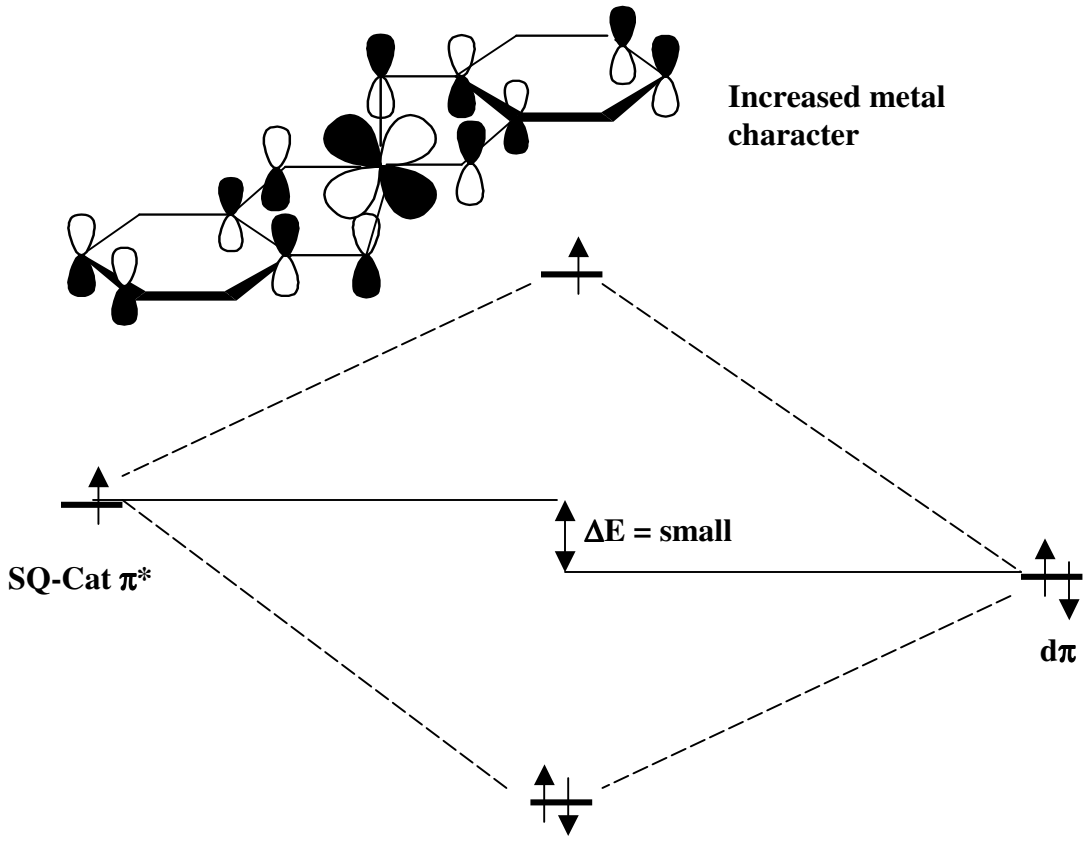

A

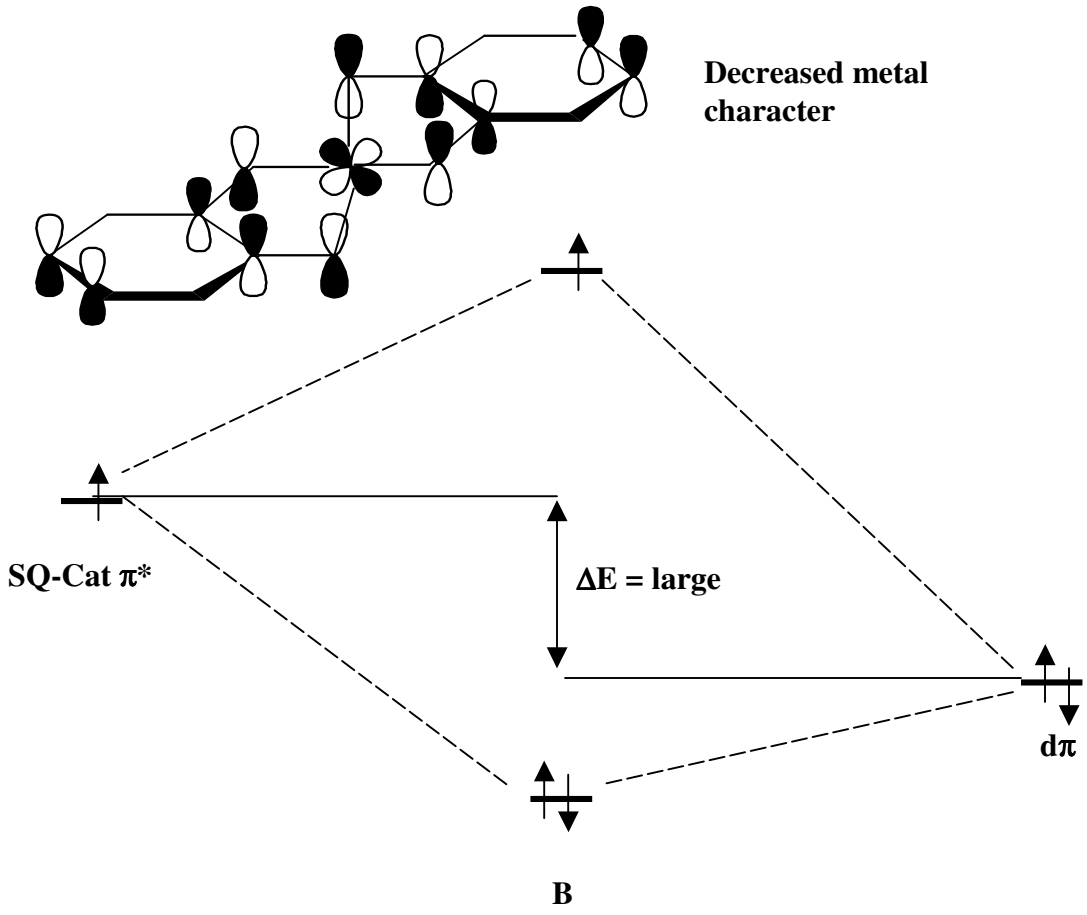

Figure 5.6. (**A**) and (**B**) Exaggerated orbital contributions of dπ to SQ-Cat π*.

By perturbing the energy difference between dπ and SQ-Cat π* orbitals, the metal orbital contribution to the delocalization of the optical electron will differ. Thus the electronic coupling between the donor-acceptor will either increasing or decreasing depending on the relative energy of dπ.

In the cobalt *bis*(dioxolene) valence tautomer the metal dπ can be perturbed by functionalizing the bipyridine counterligand with different substituents that raise or lower

the orbital eigenenergies of the bipyridine ligand orbitals. These energy perturbations can thus influence the metal orbital eigenvalues through back bonding (**Figure 5.7**).

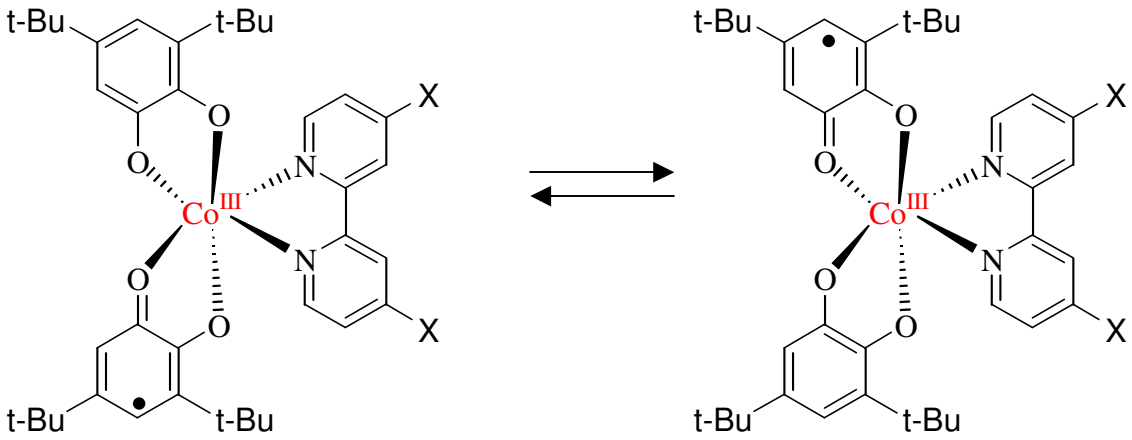

Molecule	Substituent (X)
1	$-NO_2$
2	-Br
3	-H
4	$-OCH_3$
5	$-N(CH_3)_2$

Figure 5.7. Proposed synthetic systems.

Bipyridine is a strong-field ligand because it acts as a π-acceptor through its π-symmetric LUMO (**Figure 5.7**).[8] How well bipyridine acts a π-acceptor to a particular metal center depends on the relative contribution of the bypridine π-accepting LUMO to

the coordination complex's electronic structure. It is accepted theory that the HOMO of bipyridine lies lower in energy with respect to Co^{II}/Co^{III} d-orbitals and the bipyridine LUMO is higher.[9] The LUMO energy of bipyridine can be raised or lowered by substituting the pyridine aromatic ring with electron donating and electron withdrawing groups of various strengths.

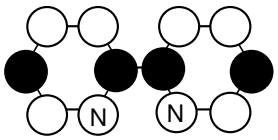

Figure 5.8. Group theory derived LUMO of bipyridine.

The degree of delocalization of the SQ-Cat group can be established qualitatively by using Hush theory. This can be done by comparing the observed IVCT with respect to the Hush prediction. The changes observed can then be correlated to a Hammett parameter to qualitatively determine the level of electronic coupling with respect to the strength of the substituent in terms of its specific perturbation on the bipyridine π-center. It is predicted that substituents that lower the LUMO of bipyridine ($-NO_2$ and –Br) will make the bipyridine counterligand behave more as a π-acid thus stabilizing the lower lying dπ away from the higher SQ-Cat π* orbitals, which would decrease the SQ-Cat interaction. Substituents such as $–OCH_3$ and $–N(CH_3)_2$ will raise the LUMO of bipyridine hence destabilizing dπ nearer to the SQ-Cat π* orbitals thus increasing the electronic coupling of the donor-acceptor pair.

5.2 Synthesis of 1.

Synthesis of **1** begins with the oxidation of bipyrdine with hydrogen peroxide to form **2**.[10] Subjecting **2** to nitric acid produces the para-nitrated product **3**.[10] **3** is then reduced with PBr_3 to form the final ligand (**4**).[10] **4** is then reacted with cobalt octacarbonyl and 3, 5 - di-tert-butyl orthoquinone to afford the final complex (**1**).

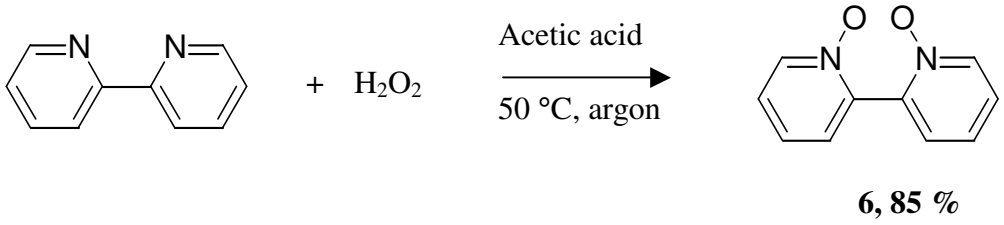

6, 85 %

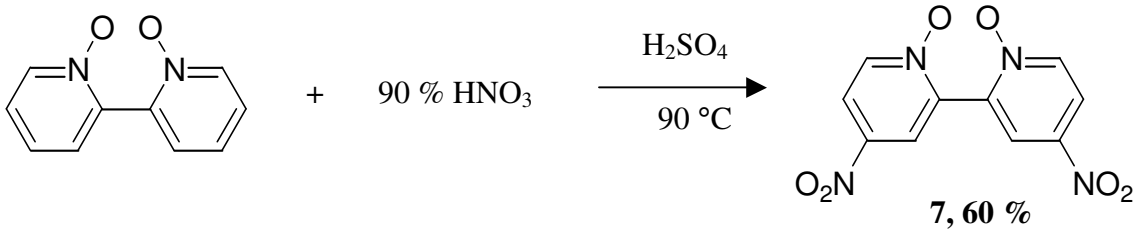

7, 60 %

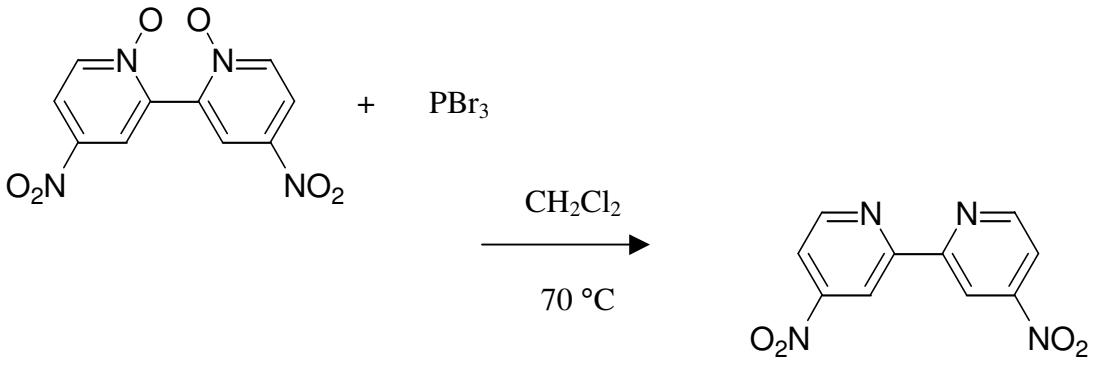

8, 44 %

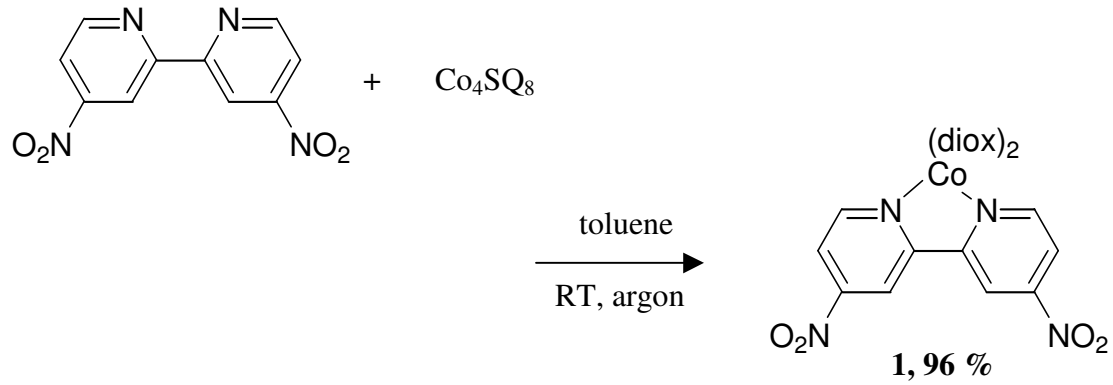

Scheme 5.1. Synthesis of **1**.

5.3 Synthesis of 2

2 is synthesized by first reacting **3** with acetyl bromide to form **5**.[10] **5** is then reduced with phosphorus tribromide to afford **6**.[10] Finally **6** is subjected to di tert-butylorthoquinone and cobalt octacarbonyl to synthesize **2**.

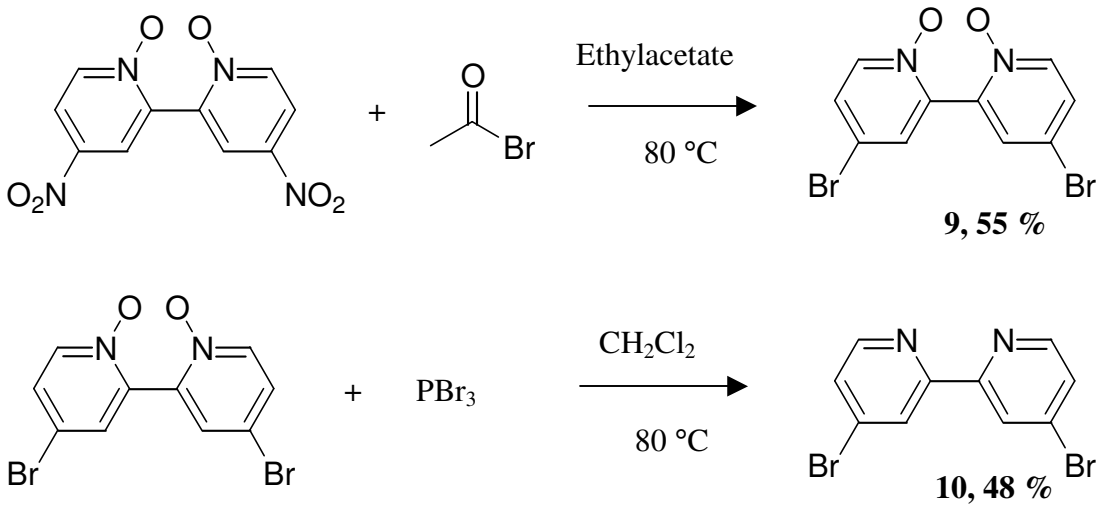

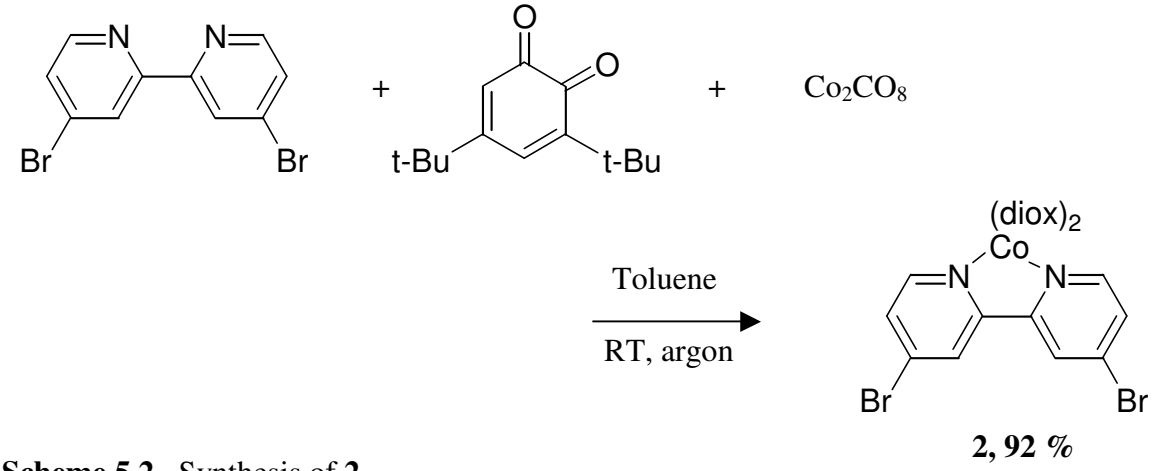

Scheme 5.2. Synthesis of **2**.

5.4 Synthesis of 4.

4 is synthesized by reacting 4,4′ -dimethoxybipridine with dicobalt octacarbonyl and 3,5-di-*tert*-butylorthoquinone.

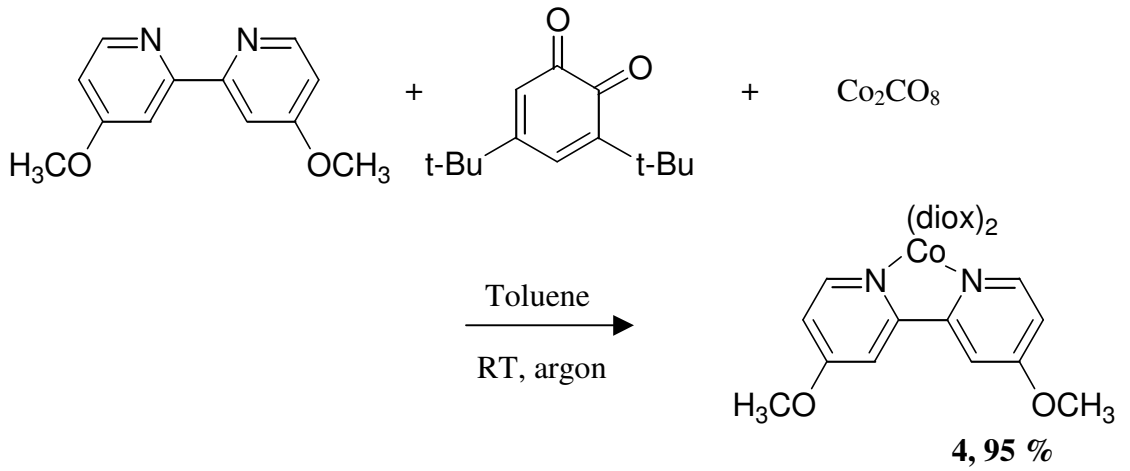

Scheme 5.3. Synthesis of **4**.

5.5 Synthesis of 5

Synthesis of **5** begins by synthesizing **9** from lithiation of 4-dimethylaminopyridine in the presence of dimethylaminoethanol and finally quenching with iodine. **10** is synthesized in the same manner with the exception of quenching with tributyl-tinchloride.[11] Both **9** and **10** and coupled via Stille reaction to synthesize **11**.[11] **11** is then reacted with orthoquinone and cobalt octacarbonyl to afford **5**.

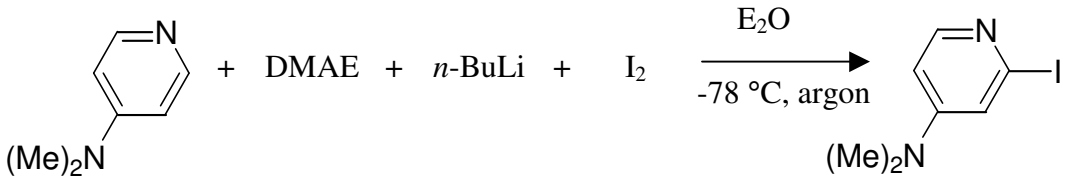

11, 60 %

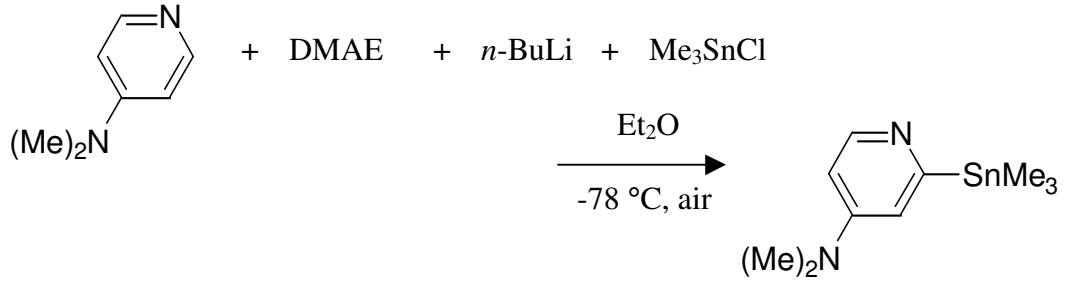

12, 60 %

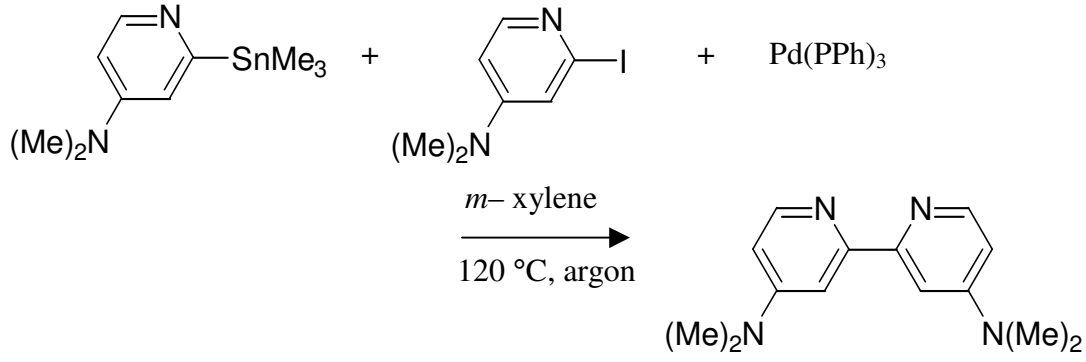

13, 60 %

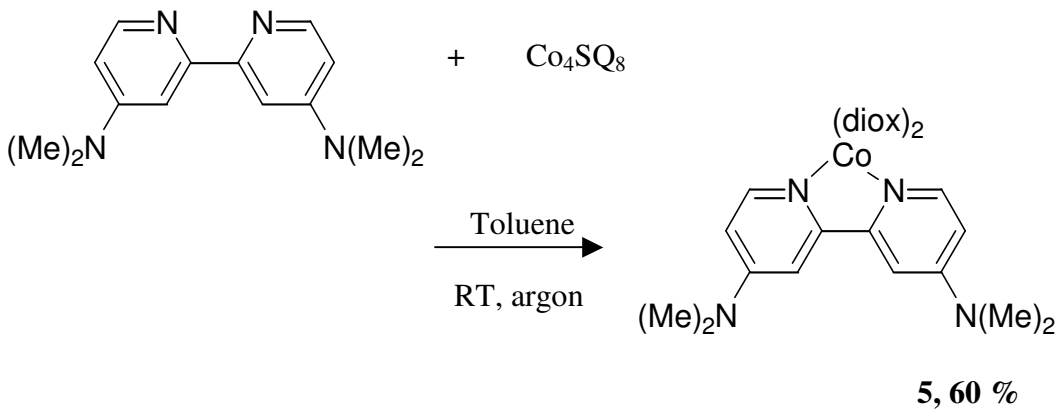

5, 60 %

Scheme 5.4. Synthesis of **5**.

5.6 Magnetic Susceptibilty Experiments

Variable temperature SQUID magnetic susceptibility experiments were performed on **1**, **2**, **4** and **5**. It has been theorized that strong π-acid interactions with the bipyridine ligand stabilizes the Co^{II} state while strong σ-donation of the counterligand stabilizes the Co^{III} state.[11] This theory is verified by the observed data in the variable temperature SQUID measurements (**Figure 5.8**). Starting from 2 K, **5** remains as the Co^{III} form throughout the temperature range. Also from 2 K, **4** remains in the Co^{III} form before beginning a sharp transition to the Co^{II} state near 350 K. The behavior of **2** and **1** are better described starting from high temperature. From 400 K **2** is in the Co^{II} form until sharply converting to the Co^{III} state between 200 – 100 K. Finally, for **1** there is a gradual depopulation of the Co^{II} form to the Co^{III} tautomer from 400 K to 2 K where there is still significant population of the Co^{II} state. The susceptibility data strongly suggest that the enthalpy difference of the Co^{III} and Co^{II} states is lowered with increasing π-accepting behavior and decreasing σ-donation of the counterligand (**Figure 5.9**). Most

interesting is that the enthalpy difference of the two states is lowered to such an extent in **1** that both Co^{III} and Co^{II} states are still populated at 2 K.

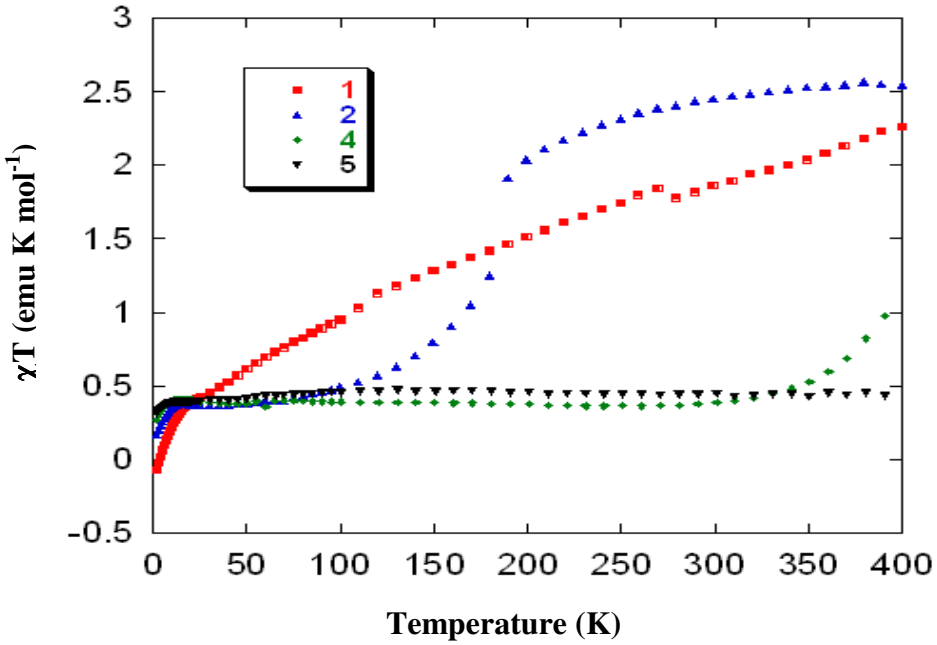

Figure 5.9. Variable temperature magnetic susceptibility of **1**, **2**, **4** and **5** (2 – 400 K).

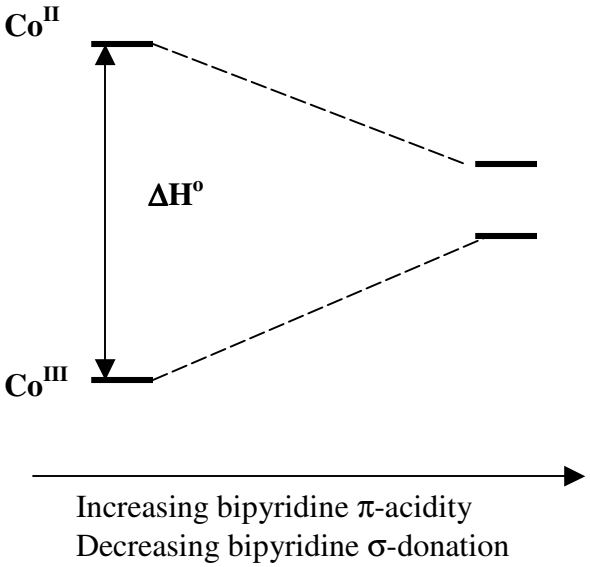

Figure 5.10. Enthalpy change with respect to π-acidity and σ-donation**.**

5.7 Variable-Temperature Infrared Spectroscopy

Variable temperature IR was used to determine the shape and intensity of the IVCT with respect to temperature (**Figure 5.10 – 5.13**). There is a startling difference in the IVCT with respect to the different substituents. Substituents like $–NO_2$ and –Br promote Gaussian band shapes to the IVCT while $–OCH_3$ and $–N(CH_3)_2$ substituents produce seemingly Lorentzian band shapes. Thus, superficially the spectroscopic data indicates that there is a strong substituent effect to the IVCT band, which is a function of the mixing of the SQ-Cat donor-acceptor pair.

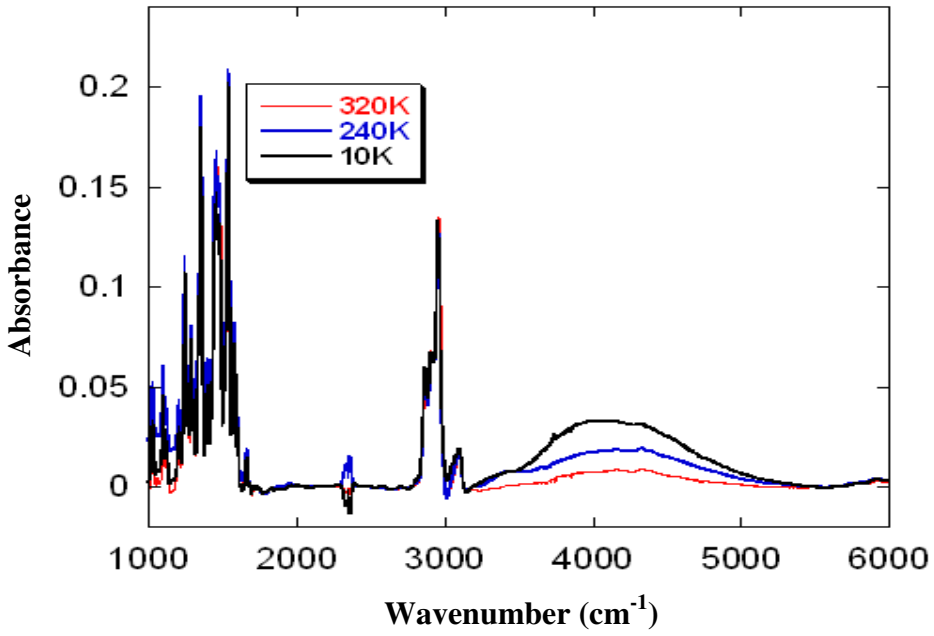

Figure 5.11. Variable temperature IR of **1** (10 – 300 K).

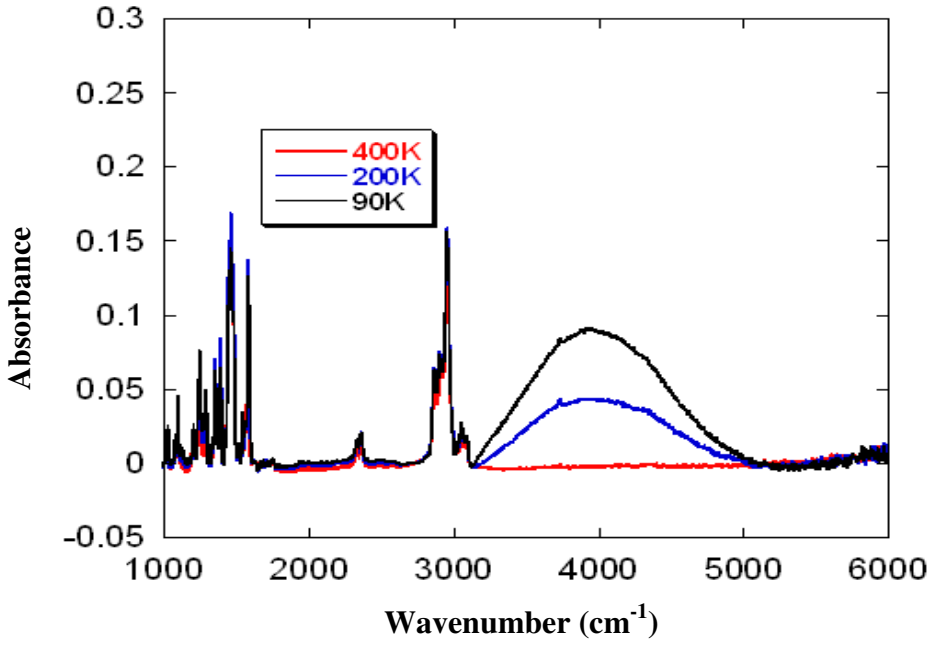

Figure 5.12. Variable temperature IR of **2** (100 – 400 K).

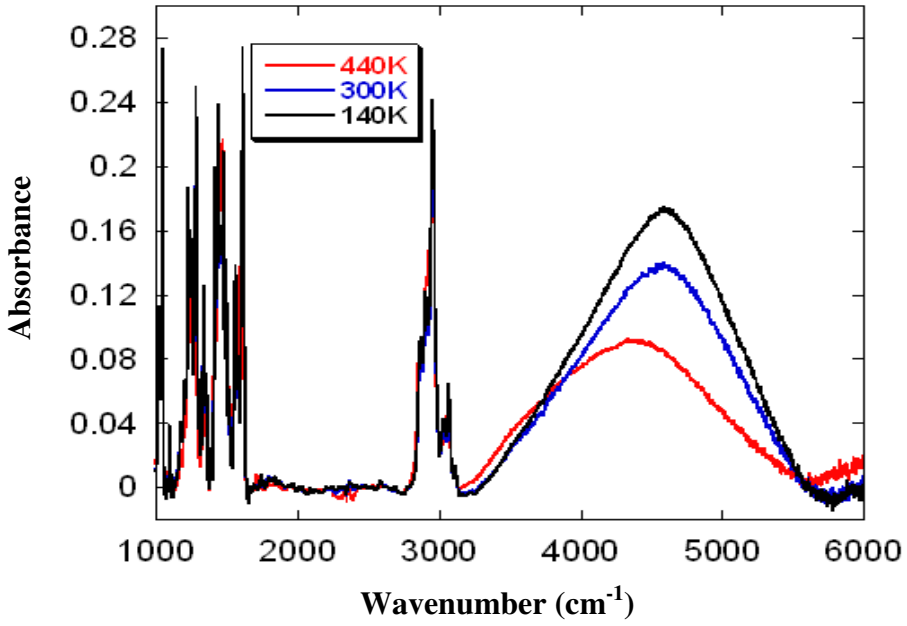

Figure 5.13. Variable temperature IR of **4** (100 – 400 K).

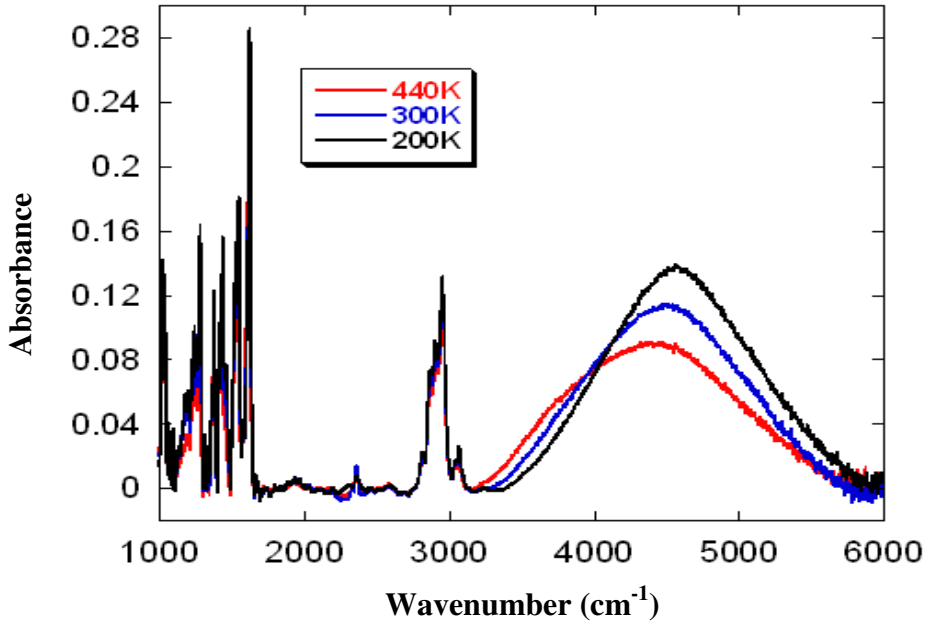

Figure 5.14. Variable temperature IR of **5** (100 – 400 K).

The spectra of **4** and **5** displays a gradual change in the absorption maximum to lower energy as the temperature increases and the IVCT gradually diminishes. This observation seems to suggest that there is a change in energy of the mixed-valent states as the temperature changes. On the other hand this phenomenon does not manisfest in **1** and **2**, which again suggest an additional difference in perturbation between the two sets of substituents. The threshold energy (E_{th}) is the energy needed to thermally populate the mixed-valent excited state (**Figure 5.14**).[6] For the compounds in this series, E_{th} can be calculated from eqn. 3.8 (**Table 5.1**). The tabulated data shows **4** and **5** have a higher E_{th} than **1** and **2**. Interestingly **3** lies in the middle of the two extremes which is where it should be if there is a trend between the perturbations produced by the substituted functional groups. The E_{th} change is consistent with a shifting of the energy of the excited state potential.

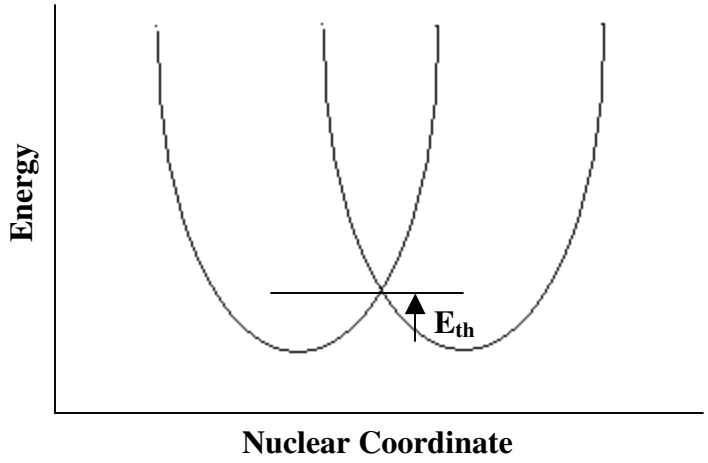

Figure 5.15. Sketch of the harmonic potentials of the ground and excited states of a mixed-valent system.

Table 5.1. E_{th} as a function of substituent.

Complex	E_{op} (cm^{-1})	E_{th} (cm^{-1})
1	4566	1013
2	4600	985
3	4250	1063
4	3941	1150
5	4050	1142

E_{th} data for **1** and **2** and respectively between **4** and **5** can be assumed to be equivalent since the E_{th} approximation is an assumption that may not be able to distinguish a smaller electronic difference between similarly behaving functional groups. To gain a greater

understanding of the electronic contributions to the threshold change, E_{th} can be plotted with respect to the Hammett parameter σ^{+}_{para} (**Figure 5.15**).

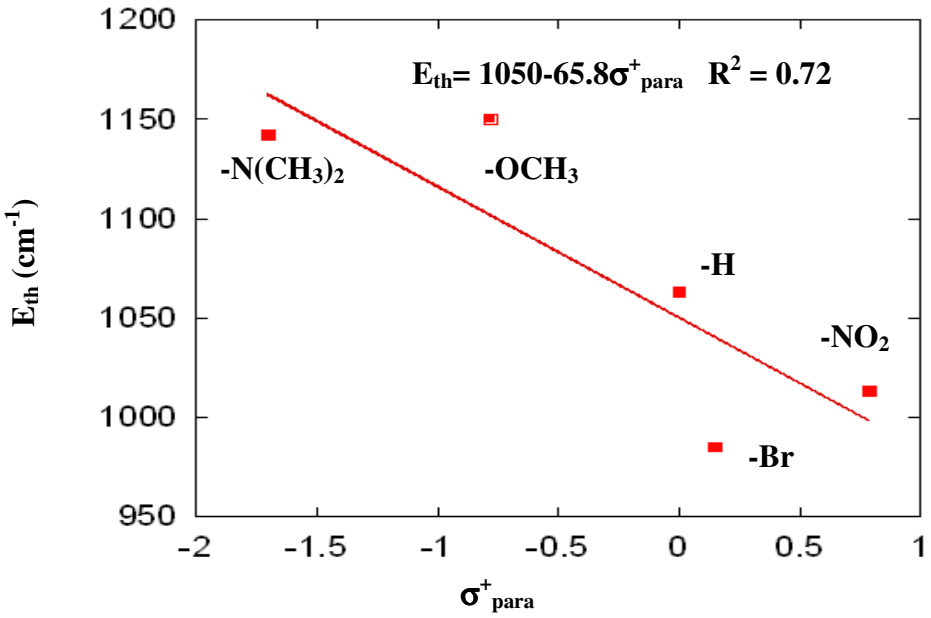

Figure 5.16. ΔE_{th} plotted as a function of σ^{+}_{para}.

It is evident from **Figure 5.15** that there is a trend between E_{th} and σ^{+}_{para}. The pressing issue is determining the meaning of the change in E_{th}. Since E_{th} is the thermal excitation barrier from the ground and excited state SQ-Cat wavefunctions, then an alteration in E_{th} suggests an adjustment in the ground and excited state energy difference which is a change in the SQ-Cat coupling. Thus an E_{th} increase implies a larger coupling interaction and with a decrease the opposite occurs. This is consistent with the hypothesis that as $d\pi$ is raised and lowered with respect to the SQ-Cat orbitals through back bonding with the bipyridine ligand and the delocalization between the SQ-Cat pair is varied by the change in the metal contribution to the mixed-valent total electronic wavefunction. The

threshold difference between the two extremes (**1** and **5**) is ~130 cm^{-1}, which implies a coupling change that is proportional to that value.

The IVCT bandwidth can also be used to qualitatively determine the level of electronic coupling. It is then straightforward to compare the actual bandwidth with respect to the Hush model. $\Delta\nu_{1/2}$ for **1, 2, 4** and **5** was determined at temperatures with the largest IVCT absorption and $\Delta E(\Delta\nu_{Hush}-\Delta\nu_{Obs})$ is the difference between the actual bandwidth at half height and the prediction made by the Hush model and $\Delta E(\Delta\nu_{Hush}-\Delta\nu_{Obs})$ was then correlated to σ^{+}_{para} (**Table 5.3**). The data indicates that there is a consistent association between ΔE and σ^{+}_{para} (**Figure 5.18**). As the strength of σ^{+}_{para} increases the SQ-Cat pair shifts consistently in the direction of the Class II/Class III limit. This suggests an enhancement in the delocalization as a function of increasing σ^{+}_{para} value of the substituent. The delocalization amplification can only come from greater mixing of the SQ-Cat wavefunctions, which in turn implies a greater contribution of the metal wavefunctions to the donor-acceptor interaction. Thus, in concurrence with the observations made with the E_{th} data, the bandwidth comparison is powerful evidence that the level of delocalization of the optical electron of the SQ-Cat pair is controlled by the d-orbital contribution through back bonding to the ancillary ligand.

Table 5.2. Calculated ΔE (Hush-Obs) values.

Molecule	Hush Prediction (cm^{-1})	Actual (cm^{-1})	ΔE (Hush-Obs) (cm^{-1})	$\sigma+_{para}$
1	1025	563	462	0.79
2	1657	1038	619	0.15
3	1813	992	821	0
4	2228	1978	1017	-0.78
5	2654	1167	1487	-1.7

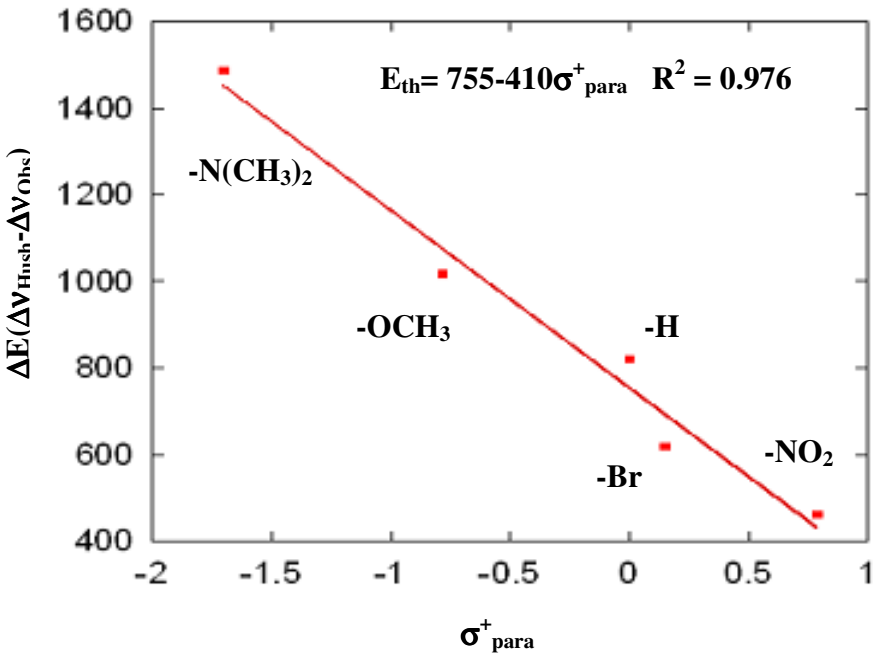

Figure 5.17. $\Delta E(\Delta\nu_{Hush}-\Delta\nu_{Obs})$ plotted as a function of σ^+_{para}.

5.8 Conclusion

The Hammett parameters were initially designed to determine the substituent contribution to the interpretation of reaction mechanisms and prediction of reaction rates and equilibria of substituted phenyl groups. Typically σ^+ describes a direct resonance interaction between the electron donor substituent and a cationic reaction center (**Figure 5.19 A**).[13] The σ^- parameter pertains to a direct resonance interaction between the substituent and an electron-rich reaction site (**Figure 5.19 B**).[13]

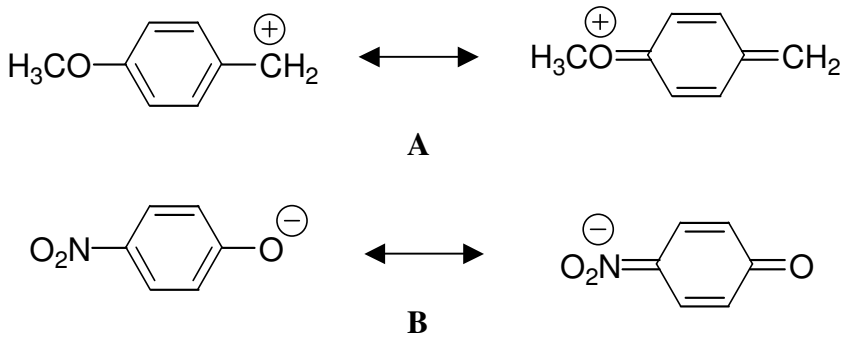

Figure 5.18. (**A**) resonance with cationic center, (**B**) resonance with anionic center.

A more complete picture is to include MO theory.[14] Theoretical calculations have shown that a more descriptive method to describe the Hammett relationship is to treat substituted phenyl groups as two distinct MO fragments consisting of the substituted phenyl MO (C_6H_4X-) and the reaction center (-Y).[15] By either donating or accepting charge the X functional group raises or lowers the energy of the phenyl MOs due to the change in inter-electron repulsion.[16-17] For an X functional group that donates charge (i.e. X's highest occupied orbital is higher than phenyl LUMO), the phenyl orbitals are raised with

respect to a cationic reaction center and the phenyl HOMO donates charge density into the reaction center LUMO.[14-18] The opposite is true for X that accepts charge that lowers the phenyl LUMO, which then accepts charge density from the HOMO of the reaction center.

The substituted valence tautomeric systems **1**, **2**, **4** and **5** are electronically complex. However, the σ^+ dependence of the E_{th} and $\Delta E(\Delta\nu_{Hush}-\Delta\nu_{Obs})$ implies that it is a resonance effect (π delocalization) that contributes to changing the bipyridine frontier orbitals with respect to the metal set in this particular set of systems. Consequently greater donation into the pyridine aromatic center destabilizes the LUMO of bipyridine to greater energy with respect to the cobalt dπ, which in turn allows for greater mixing of the metal orbitals into the SQ-Cat wavefunctions due to lesser back bonding stabilization between dπ and bipridine π^* (**Figure 5.20 A**). This process then allows for greater delocalization of the optical electron due to the increased metal contribution to the SQ-Cat wavefunction. Greater charge acceptance from the pyridine π-system stabilizes the bipyridine LUMO closer in energy to the metal dπ, which in turn stabilizes the metal orbitals to much lower energy with respect to the SQ-Cat π^* due to back bonding (**Figure 5.20 B**). The greater dπ-bipyridine π^* back bonding interaction reduces the dπ orbital contribution of the metal to the donor-acceptor pair thus reducing the coupling between the SQ-Cat pair. Despite –Br clear lack of an orbital to accept charge, –Br has precedence as a charge acceptor as evident in the literature.[19]

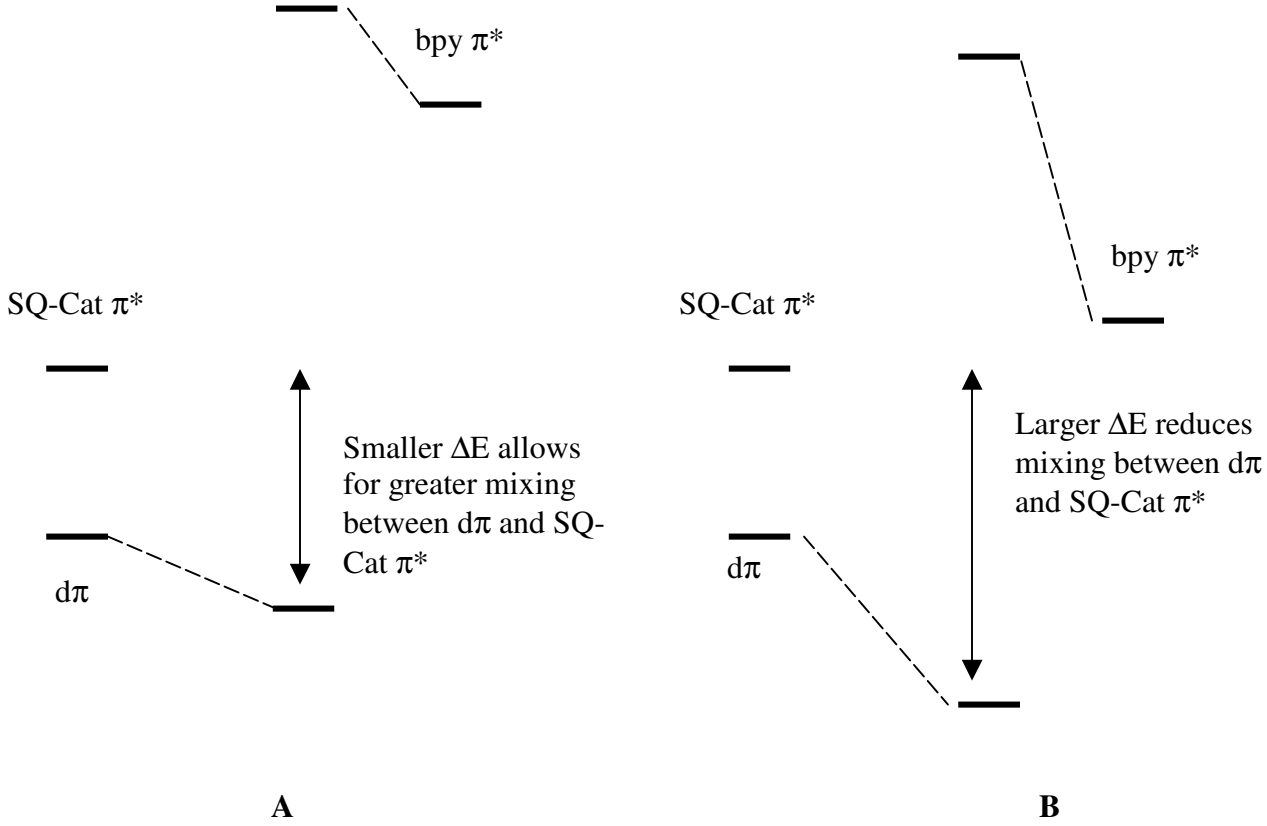

Figure 5.19. Relative mixing of dπ with SQ-Cat π* with respect to the relative energy of the bipyridne LUMO (π*).

5.9 Experimental

General. All syntheses were performed under inert conditions with anhydrous solvents unless stated otherwise. NMR spectra were recorded in *d*-chloroform at 300 MHz. Electronic absorption spectra were collected in CH_2Cl_2 on a Hewlett Packard 8452A Diode Array Scanning Spectrophotometer. IR experiments were performed on a Digilab FTS 3000 FTIR spectrometer equipped with a globar source, KBr beamsplitter and a liquid nitrogen cooled MCT detector. The spectra were the result of 64 scans at a spectral resolution of 2 cm^{-1}. The temprature dependent spectra were recorded using a helium cooled cryostat (MicrostatHe, Oxford Instruments).

Synthesis of **6**. A round bottom flask was charged with 5 g 2, 2′- bipyridine, 30 mL 30 % aqueous H_2O_2 solution and 30 mL acetic acid. The reaction mixture was heated to 50 °C for 48 hrs. Solvent was removed by distillation and impurities were washed away with acetone. Collected 3.61 g white solid. ^{1}H NMR (DMSO): δ 8.68 (d, 2H, J = 0.9 Hz); 8.58 (d, 2H, J = 7.2 Hz); 8.36 (m, 2H).

Synthesis of **7**. A 250 mLwas charged with 3.4 g of **6** and dissolved with 15 mL H_2SO_4. The reaction mixture was cooled to 0 °C. 5.7 mL fuming nitric acid was added dropwise. The reaction mixture was heated to 100 °C overnight. After allowing the reaction mixture to cool, the system was quenched with ice. Product precipitates from the reaction mixture and collected on filter frit (2.86 g, white solid). ^{1}H NMR (DMSO): δ 8.68 (d, 2H, J = 0.9 Hz); 8.58 (d, 2H, J = 7.2 Hz); 8.36 (m, 2H).

Synthesis of **8**. A 250 mL round bottom was charged with 0.5 g of **7** and 20 mL chloroform. The reaction vessel was then cooled to 0 °C. 2.56 mL phosphorus tribromide was then added dropwise and the reaction mixture was refluxed for 1 hr. Reaction mixture was quenched with ice and basicified with 6M NaOH solution. Product was collected in methylene chloride layer and recrystallized from absolute ethanol. ^{1}H NMR ($CDCl_3$): δ 9.15 (d, 2H, J = 5.4 Hz); 8.97 (s, 2H); 8.30 (d, 2H, J = 5.4).

Synthesis of **9**. A 250 mL round bottom flask was charged with 0.6 g **7** and dissolved in 10 mL acetic acid. The system was heated to 60 °C. 3.8 mL acetyl bromide was then added dropwise and the reaction mixture was heated to reflux for 2 hrs. After cooling to room temperature, the reaction mixture was quenched with ice and neutralized with 2 M Na_2CO_3 solution. Product precipitates and collected from a frit. ^{1}H NMR (DMSO): δ 8.26 (d, 2H, J = 6.9 Hz); 8.0 (s, 2H); 7.75 (m, 2H).

Synthesis of **10**. A 250 mL round bottom was charged with 1.0 g of **9** and 50 mL chloroform. The reaction vessel was then cooled to 0 °C. 4 mL phosphorus tribromide was then added dropwise and the reaction mixture was refluxed for 1 hr. Reaction mixture was quenched with ice and basicified with 6M NaOH solution. Product was collected in methylene chloride layer and recrystallized from absolute ethanol (0.78 g, white solid). ^{1}H NMR ($CDCl_3$): δ 8.60 (s, 2H); 8.48 (d, 2H, J = 5.1 Hz)); 7.51 (d, 2H, J = 2.1 Hz).

Synthesis of **11**. A schlenk flask was charged with 1.65 mL dimethyl amino ethanol and 10 mL dry diethyl ether. The reaction vessel was cooled to 0 °C. 12.3 mL of 2 M n-BuLi in hexanes was added dropwise and the reaction mixture was allowed to stir for 0.5 hrs at 0 ^{0}C. 1 g DMAP was added to reaction mix as a solid and stirred for 1 hr. The reaction mixture was then cooled to –78 °C. In a separate schlenk flask 5.2 g I_2 was dissolved in 50 mL anhydrous diethyl ether and then added to the DMAP mixture. The reaction mixture was allowed to warm to room temperature overnight. The reaction was quenched with deionized water and the product was extracted with methylene chloride and filtered through celite. The product was purified using column chromatrography in silica using a pure ethyl acetate solvent system. ^{1}H NMR ($CDCl_3$): δ 7.90 (d, 1H, J = 6.0 Hz); 6.89 (d, 1H, J = 2.4); 6.85 (q, 1H, J = 2.4); 2.97 (s, 6H).

Synthesis of **12**. A schlenk flask was charged with 0.2 mL dimethyl amino ethanol and 20 mL dry diethyl ether. The reaction vessel was cooled to 0 °C. 1.8 mL of 2 M n-BuLi in hexanes was added dropwise and the reaction mixture was allowed to stir for 0.5 hrs at 0 °C. 0.148 g DMAP was added to reaction mix as a solid and stirred for 1 hr. The reaction mixture was then cooled to –78 °C. 3 mL 1 M timethyl tin chloride was added dropwise and the reaction mixture was allowed to warm to room temperature overnight. The reaction was quenched with deionized water and the product extracted with methylene chloride. Product was purified by column chromatography in 1:5 methylene chloride/ether system. ^{1}H NMR ($CDCl_3$): δ 7.90 (d, 1H, J = 6.0 Hz); 6.89 (d, 1H, J = 2.4); 6.85 (q, 1H, J = 2.4); 2.97 (s, 6H).

Synthesis of **13**. Add 0.3 g of **11** and 0.042 g $Pd(PPh)_3$ to trimethyl tin-DMAP and dissolve in 30 mL m – xylene. Heated reaction mix to 120 °C overnight. After cooling to room temperature the reaction was quenched with 2 M NaOH solution. The product was extracted with methylene chloride and purified with column chromatography in silica using straight ethyl acetate solvent system. ^1H NMR ($CDCl_3$): δ 8.30 (d, 2H, J = 5.7 Hz); 7.68 (s, 2H); 6.54 (s, 2H,); 3.12 (s, 12H).

Synthesis of **1**. A schlenk flask is charged with 0.100 g Co_4SQ_8 and dissolved in 20 mL toluene. 0.049 g of **8** was charged in a separate flask dissolved in 10 mL toluene. The solution of **1** was cannulated to tetramer and the mixture was stirred for 10 minutes. The reaction mixture was allowed to sit overnight and the product was collected on a filter stick (0.78 g, green solid)

Synthesis of **2**. A schlenk flask was charged with 0.100 g of **10** and 0.139 g di-tert-butyl ortho benzoquinone and dissolved in 20 mL toluene. 0.054 g dicobalt octacarbonyl was added to a separate schlenk flask and dissolved in 10 mL toluene. The dibromo bipyridine mixture was cannulated to the dicobalt octacarbonyl solution and the reaction mixture was stirred for 10 minutes then allowed to sit overnight. The product precipitate was collected on a filter stick (0.82 g, green solid).

Synthesis of **4**. A schlenk flask was charged with 0.063 g **11** and 0.129 g di-tert-butyl ortho benzoquinone and dissolved in 20 mL toluene. 0.050 g dicobalt octacarbonyl was added to a separate schlenk flask and dissolved in 10 mL toluene. The dibromo

bipyridine mixture was cannulated to the dicobalt octacarbonyl solution and the reaction mixture was stirred for 10 minutes then allowed to sit overnight. The product precipitate was collected on a filter stick (0.039 g, blue solid).

Synthesis of **5**. A schlenk flask is charged with 0.056 g Co_4SQ_8 and dissolved in 20 mL THF. 0.027 g of **13** was charged in a separate flask dissolved in 10 mL toluene. The dimethylamino bipyridine solution was cannulated to tetramer and the mixture was stirred for 10 minutes. The reaction mixture was allowed to sit overnight and the product was collected on a filter stick (0.023 g, green solid).

Magnetic Measurements. Magnetic susceptibilities and saturation magnetization experiments were collected on a Quantum Design MPMS-XL7 SQUID magnetometer. Saturation magnetization experiments were performed at 2 K at a maximum applied field of 7 Tesla (**Figure 5.20 – 5.23**). All susceptibility experiments were performed at an applied field of 4000 G. Molecular diamagnetic corrections were achieved using Pascal's constants. Samples were loaded onto a Delrin sample holder and mounted directly on the sample rod. The measured magnetic susceptibility of the empty sample rod was subtracted out as background.

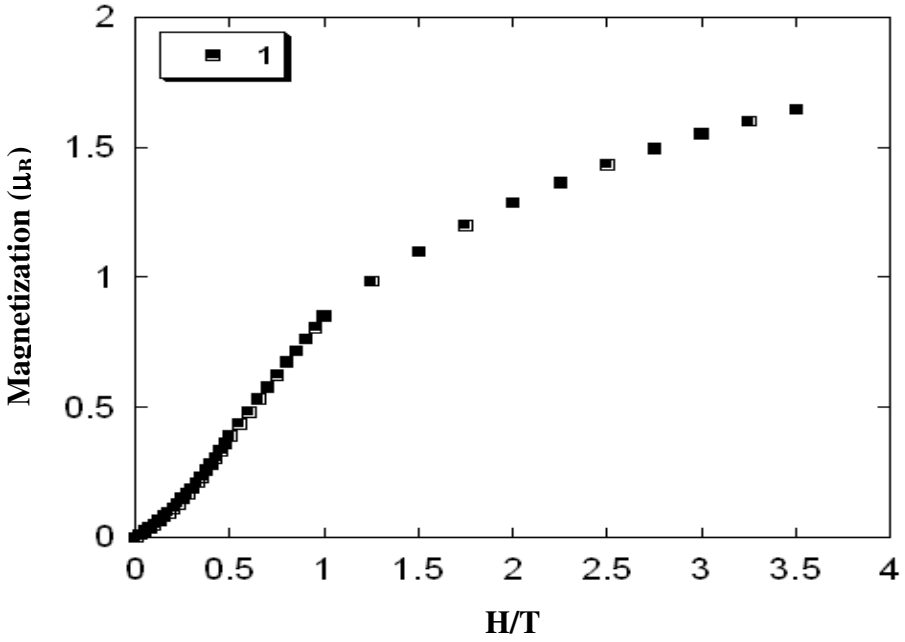

Figure 5.20. Saturation magnetization of **1**.

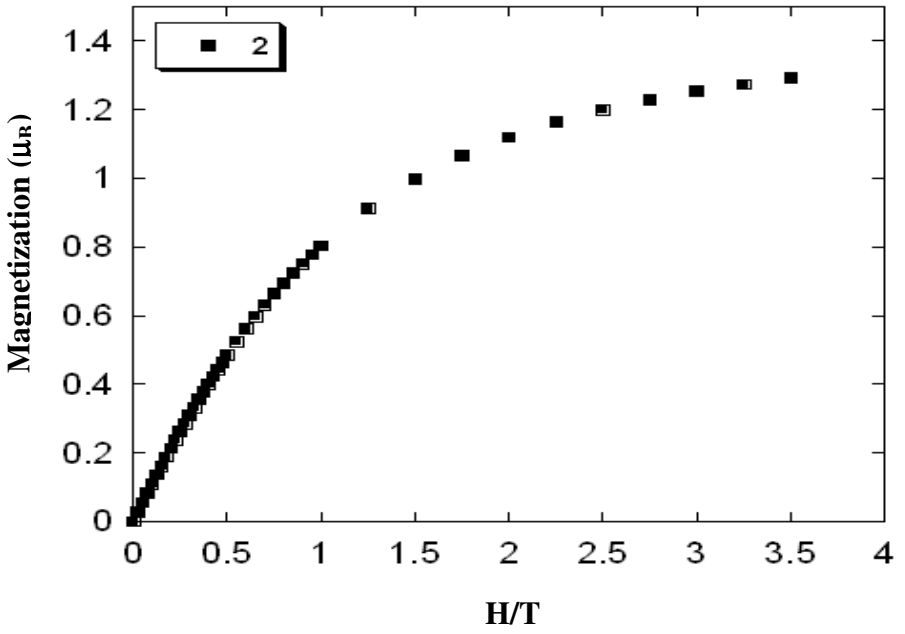

Figure 5.21. Saturation magnetization of **2**.

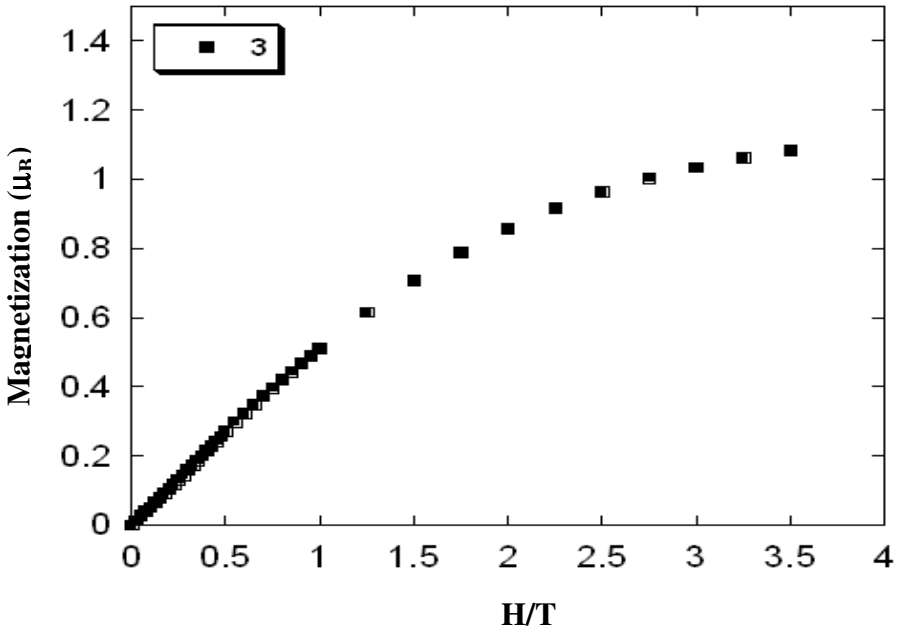

Figure 5.22. Saturation magnetization of **3**.

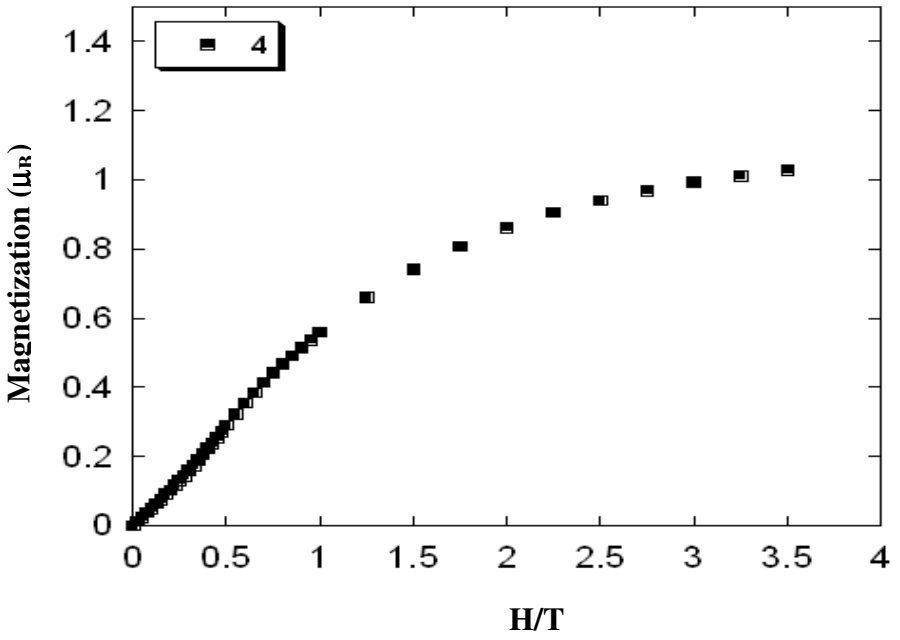

Figure 5.23. Saturation magnetization of **4**.

Structure Determination of 2. Fine dark-green needles of **2** were grown from a heptane solution at 22 deg. C. A crystal of dimensions 0.12 x 0.04 x 0.02 mm was mounted on a standard Bruker SMART CCD-based X-raydiffractometer equipped with a LT-2 low temperature device and normal focus Mo-target X-ray tube (= 0.71073 A) operated at 2000 W power (50 kV, 40 mA). The X-ray intensities were measured at 123(2) K; the detector was placed at a distance 4.980 cm from the crystal. A total of 2704 frames were collected with a scan width of 0.3 in and phi with an exposure time of 90 s/frame. The integration of the data yielded a total of 29289 reflections to a maximum 2 value of 37.12 of which 6072 were independent and 3237 were greater than 2(I). The final cell constants (Table 1) were based on the xyz centroids of 3576 reflections above 10(I). Analysis of the data showed negligible decay during data collection; the data were processed with SADABS and corrected for absorption. The structure was solved and refined with the Bruker SHELXTL (version 6.12) software package, using the space group P1bar with Z = 4 for the formula $C_{38}H_{46}N_2O_4Br_2Co\bullet(C_7H_{16})_{0.5}$. All non-hydrogen atoms were refined anisotropically with thehydrogen atoms placed in idealized positions. The heptane solvate is disordered about an inversion center in the crystal lattice and was modeled by use of the SQUEEZE subroutine of the PLATON program suite. Due to the smallcrystal size, limited resolution of the data and presence of two crystallographically independent molecules,, it was necessary to employ extensive restrains during the refinement. Full matrix least-squares refinement based on F^2 converged at R1 = 0.0821 and wR2 = 0.2039 [based on I > 2sigma(I)], R1 = 0.1540 and wR2 = 0.2299 for all data.

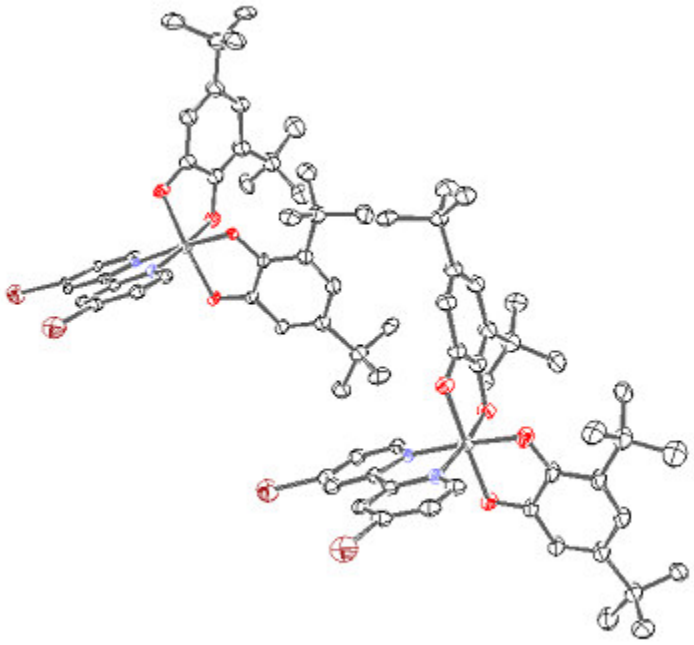

Figure 5.24. Crystal Structure of **2**.

Table 5.3. Selected bond lengths of **2**.

	Bond	Length (Å)
SQ	O1 – C11	1.278(10)
	O2 – C16	1.298(10)
	C11 – C12	1.387(11)
	C12 – C13	1.354(12)
	C13 – C14	1.468(11)
	C14 – C15	1.341(11)
	C15 – C16	1.402(11)
	C16 – C11	1.452(11)
Cat	O3 – C26	1.366(10)
	O4 – C30	1.320(10)
	C25 – C26	1.381(12)
	C25 – C27	1.394(11)
	C27 – C28	1.394(11)
	C28 – C29	1.375(12)
	C29 – C30	1.407(12)
	C26 – C30	1.438(11)
Co-O	Co1 – O1	1.915(6)
	Co1 – O2	1.909(6)
	Co1 – O3	1.841(6)
	Co1 – O4	1.877(6)

Table 5.4. Crystal data and structure refinement of **4**.

Empirical formula	$C_{39.75}\ H_{50}\ Br_2\ Co\ N_2\ O_4$
a/Å	10.1370(14)
b/Å	17.115(2)
c/Å	23.793(3)
α/deg	92.157(4)
β/deg	92.157(4)
γ/deg	97.175(4)
V/Å^3	4083.0(10)
Z	4
Formula weight	838.57
Crystal system, space group	Triclinic, P-1
T/K	123(2)
λ/Å	0.71073
ρ_{calc}/g cm^{-3}	1.364
μ/cm^{-1}	24.17
R1[d]	0.0821 [c]
wR2[b]	0.2039 [c]

[a]Quantity minimized = $R = \Sigma||F_o|-|F_c||/\Sigma|F_o|$. [b]$wR2 = \Sigma\,[w(F_o^2-F_c^2)^2]/\,\Sigma\,[(wF_o^2)^2]^{1/2}$. [c]$w = 1/[\sigma^2(F_o^2) + (0.0475P)^2 + 0.00P]$, $P = [2F_c^2 + F_o^2)]/3$.
[d]$w=1/[\sigma^2(F_o^2)+(0.1057P)^2+8.8966P]$, $P=(F_o^2+2F_c^2)/3$.

Structure Determination of 4. Blue needles of **4** were grown from a heptane/dichloromethane solution at 22 deg. C. A crystal of dimensions 0.40 x 0.06 x 0.04 mm was mounted on a standard Bruker SMART CCD-based X-ray diffractometer equipped with a LT-2 low temperature device and normal focus Mo-target X-ray tube (□ = 0.71073 A) operated at 2000 W power (50 kV, 40 mA). The X-ray intensities were measured at 123(2) K; the detector was placed at a distance 4.980 cm from the crystal. A total of 3197 frames were collected with a scan width of 0.2□ in □ and phi with an exposure time of 45 s/frame. The integration of the data yielded a total of 20498 reflections to a maximum 2□ value of 52.80□ of which 8799 were independent and 5629 were greater than 2□(I). The final cell constants (Table 1) were based on the xyz centroids of 5738 reflections above 10□(I). Analysis of the data showed negligible decay during data collection; the data were processed with SADABS and corrected for absorption. The structure was solved and refined with the Bruker SHELXTL (version 6.12) software package, using the space group P-1 with Z = 2 for the formula $C_{40}H_{52}N_2O_6Co•CH_2Cl_2$. All non-hydrogen atoms were refined anisotropically with the hydrogen atoms placed in idealized positions. Full matrix least-squares refinement based on F^2 converged at R1 = 0.0753 and wR2 = 0.2196 [based on I > 2sigma(I)], R1 = 0.1219 and wR2 = 0.2413 for all data.

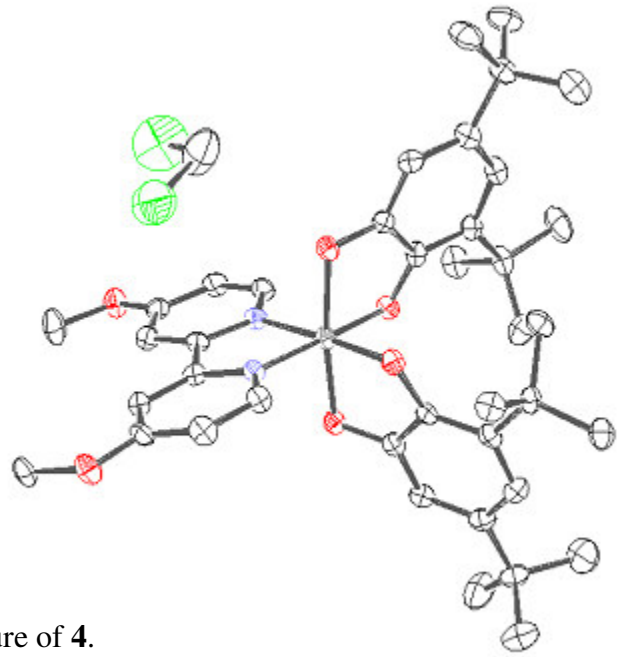

5.25 Crystal structure of **4**.

Table 5.5. Selected bond lengths of **2**.

	Bond	Length (Å)
SQ	O1 – C1	1.302(5)
	O2 – C6	1.322(5)
	C1 – C2	1.410(6)
	C2 – C3	1.371(6)
	C3 – C4	1.446(6)
	C4 – C5	1.374(6)
	C5 – C6	1.411(6)
	C6 – C1	1.454(6)
Cat	O3 – C15	1.354(5)
	O4 – C20	1.345(5)
	C15 – C16	1.396(6)
	C16 – C17	1.403(6)
	C17 – C18	1.403(7)
	C18 – C19	1.385(7)
	C19 – C20	1.395(6)
	C15 – C20	1.411(6)
Co-O	Co1 – O1	1.915(3)
	Co1 – O2	1.873(3)
	Co1 – O3	1.865(3)
	Co1 – O4	1.881(3)

Table 5.6. Crystal data and structure refinement of **4**.

Empirical formula	$C_{41}\ H_{54}\ C_{l2}\ Co\ N_2\ O_6$
a/Å	10.2100(8)
b/Å	15.7189(13)
c/Å	15.9324(15)
α/deg	66.302(6)
β/deg	71.494(4)
γ/deg	71.873(4)
V/Å^3	2170.1(3)
Z	2
Formula weight	800.69
Crystal system, space group	Triclinic, P-1
T/K	123(2)
λ/Å	0.71073
ρ_{calc}/g cm^{-3}	1.225
μ/cm^{-1}	5.63
R1[d]	0.1219 [c]
wR2[b]	0.2413 [c]

[a]Quantity minimized = $R = \Sigma||F_o|-|F_c||/\Sigma|F_o|$. [b]$wR2 = \Sigma\ [w(F_o^2-F_c^2)^2]/\ \Sigma\ [(wF_o^2)^2]^{1/2}$. [c]$w = 1/[\sigma^2(F_o^2) + (0.0475P)^2 + 0.00P]$, $P = [2F_c^2 + F_o^2)]/3$.
[d]$w=1/[\sigma^2(F_o^2)+(0.1057P)^2+8.8966P]$, $P=(F_o^2+2F_c^2)/3$.

5.10 References

1. Demadis, K. D.; Hartshorn, C. M.; Meyer, T. J. *Chem. Rev*. **2001**, *101*, 2655.
2. Geselowitz, D. A. *J. Am. Chem. Soc*. **1987**, *26*, 4135.
3. Richardson, C.; Steel, P. J.; D'Alessandro, D. M.; Junk, P. C.; Keene, R. J. *Chem. Soc. Dalton Trans*. **2002**, 2775.
4. Kaim, W.; Klein, A.; Glockle, M. *Acc. Chem. Res*. **2000**, *33*, 755.
5. Robin, M. B.; Day, P. *Adv. Inorg. Chem. Radiochem*. **1967**, *10*, 248.
6. N. S. Hush. *Prog. Inorg. Chem*. **1967**, *3*, 391.
7. Adams, D. M.; Hendrickson, D. N. *J. Am. Chem. Soc*. **1996**, *118*, 11515.
8. S. F. A. Kettle. *Physical Inorganic Chemistry: A Coordination Chemistry Approach*. Oxford University Press (New York 1998).
9. Adams, D. M.; Noodleman, L.; Hendrickson, D. N. *Inorg. Chem*. **1997**, *36*, 3966.
10. Maerker, G.; Case, F. H. *J. Am. Chem. Soc*. **1958**, *80*, 2745.
11. Wehman, P.; Dol, G. C.; Moorman, E. R.; Kamer, P. C. J.; Leeuwen, P. W. N. M. *Organometallics*. **1994**, *13*, 4856.
12. Adams, D. M.; Noodleman, L.; Hendrickson, D. N. *Inorg. Chem*. **1997**, *36*, 3966.
13. Carey, F. A.; Sundberg, R. J. *Advanced Organic Chemistry Part A: Structure and Mechanism*. Plenum Press, **1990**.
14. Topsom, R. D. *Prog. Phys. Org. Chem*. **1987**, *16*, 125.
15. Agren, H.; Bagus, P. S. *J. Am. Chem. Soc*. **1985**, *107*, 134.
16. Topsom, R. D. *Acc. Chem. Res*. **1983**, *16*, 292.
17. Reynolds, W. J.; Dais, P.; MacIntyre, D. W.; Topsom, R. D.; Marriott, S.; Taft, R. W. *J. Am. Chem. Soc*. **1983**, *105*, 378.
18. Pross, A.; Radom, L. *Prog. Phys. Org. Chem*. **1980**, *13*, 1.
19. Hansch, C.; Leo, A.; Taft, R. W. *Chem Rev*. **1991**, *91*, 165.

Chapter 6: Does Connectivity Affect Valence Tautomerism?

6.1 Introduction

The previous two chapters dealt with two important aspects of valence tautomerism: 1) intermolecular contributions to valence tautomers, and 2) donor-acceptor interactions and the role of back bonding within the low temperature mixed valent Co^{III} form. This chapter completes the discourse on valence tautomeric behavior by tackling the role of intramolecular coupling between multiple valence tautomeric units within a multinuclear valence tautomeric molecule.

Polymetallic coordination complexes display a wide variety of novel electrochemical, photochemical and photophysical behavior.[1] From a fundamental science perspective it is clear that the understanding of these behaviors depend on the fundamental intramolecular electronic coupling that occurs between the constituent metal-based chromophores. Thus, it is a simple and basic goal of science to explore the fundamental chemistry of polymetallic/multinuclear coordination complexes.

Valence tautomers are electronically labile systems and if electronically coupled, multinuclear valence tautomers can form the basis of higher order coupled metastable states. The idea of designing multinuclear valence tautomers is not entirely new. Pierpont and Jung were successful in synthesizing a polymeric cobalt valence tautomeric system where the cobalt *bis*(dioxolene) units were synthetically coupled through pyrazine molecules (**Figure 6.1**).[2] It was discovered that the polymeric system displayed a photomechanical effect in which the polymer bond lengths would change as a function of photoexciting the low temperature Co^{III} state to the Co^{II} state, which is accompanied by a

change in molecular size. The reversible molecular changes promote a distortion in the crystalline sample.

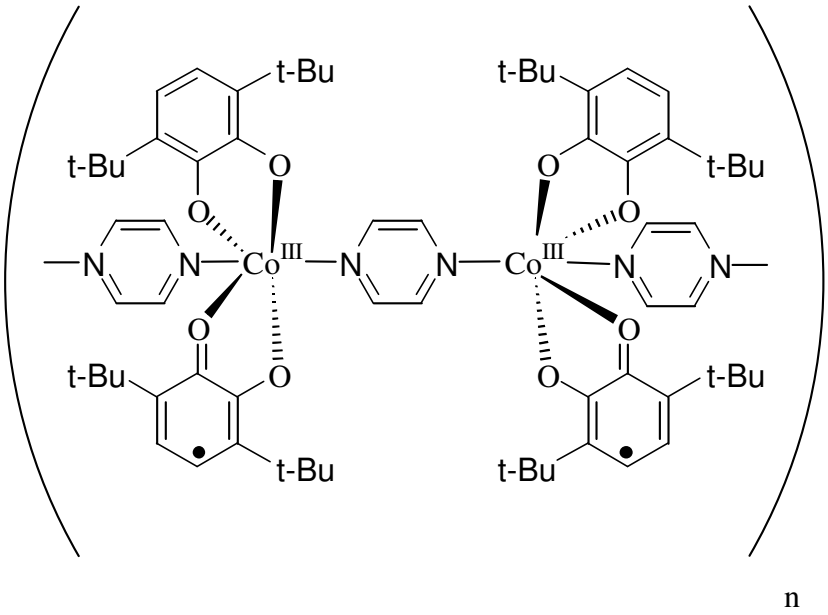

Figure 6.1. Pyrazine-bridged valence tautomer polymer.

A polymeric valence tautomer where the cobalt centers were bridged by a bis-dioxolene ligand (**Figure 6.2**) was synthesized and studied by Shultz and Dei.[3] Unlike the pyrazine bridged polymer, the dioxolene bridged polymer displays thermal hysteresis, which is a manisfestation of cooperativity.

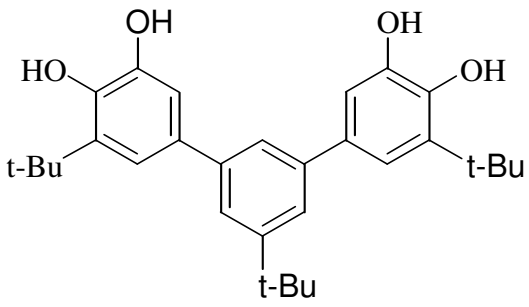

Figure 6.2. *Bis*-dioxolene ligand.

To rationally design an electronically coupled multinuclear valence tautomer, some degree of structure-property relationship must first be established for these systems. To explore the structure-property relationship it is necessary to craft molecules that possess multiple metastable states that are accessible over a desirable temperature range. In addition, the states must interact efficiently so that each state is addressable. Therefore for dinuclear cobalt *bis*(dioxolene) valence tautomers there are potentially three metastable states: $Co^{III}(SQ)(Cat)Co^{III}(SQ)(Cat)$, $Co^{III}(SQ)(Cat)Co^{II}(SQ)_2$ and $Co^{II}(SQ)_2Co^{II}(SQ)_2$. Dei and coworkers recently published a tetraoxolene-based dinuclear valence tautomer and demonstrated from EPR and magnetic susceptibility experiments that the tetraoxolene-based dinuclear valence tautomer experienced strong intramolecular electronic couping between the magnetic centers due to the interconversion between the S = 1/2 and S = 3/2 state (**Figure 6.3**).[4]

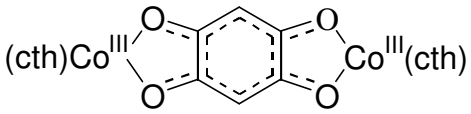

Cth = hexamethyl tetraazacyclotetradecane

Figure 6.3. Tetraoxolene dinuclear valence tautomer.

The interconversion between the two states corresponds to the population of the $Co^{III}Co^{III}$ at low temperature and the intermediate $Co^{III}Co^{II}$ electronic state at high temperature. For the $Co^{III}Co^{III}$ state the single unpaired dioxolene electron is delocalized between the two metal centers. The mixed-valent $Co^{III}Co^{II}$ form of the system occurs when the tetraoxolene bridge is oxidized by one electron. Interestingly the $Co^{II}Co^{II}$ state is not observed within a reasonable temperature range for both solution and solid-state experiments. This may be due to the fact that in order to oxidize the tetraoxolene by another electron would require oxidation from a low lying orbital, which would thus increase the enthalpy difference between the $Co^{III}Co^{II}$ and the $Co^{II}Co^{II}$ forms. Where the tetraoxolene-based valence tautomer is an attempt to couple multinuclear valence tautomeric systems through the dioxolene ligand, our effort centers on a dinuclear design through the bipyridine ligand (**Figure 6.4**). One reason why bipyridine can serve as a potential electronic coupling unit is that as shown in the previous chapter, back bonding between cobalt and bipyridine affords some degree of delocalization onto the bipyridine molecule. A reasonable first step to devise bipyridine-based dinuclear valence tautomers is to measure the effect of geometric isomers. Hence the goal of the research initiative is

to determine whether geometric ismoerism can be used to affect the thermodynamic parameters of coupled valence tautomers.

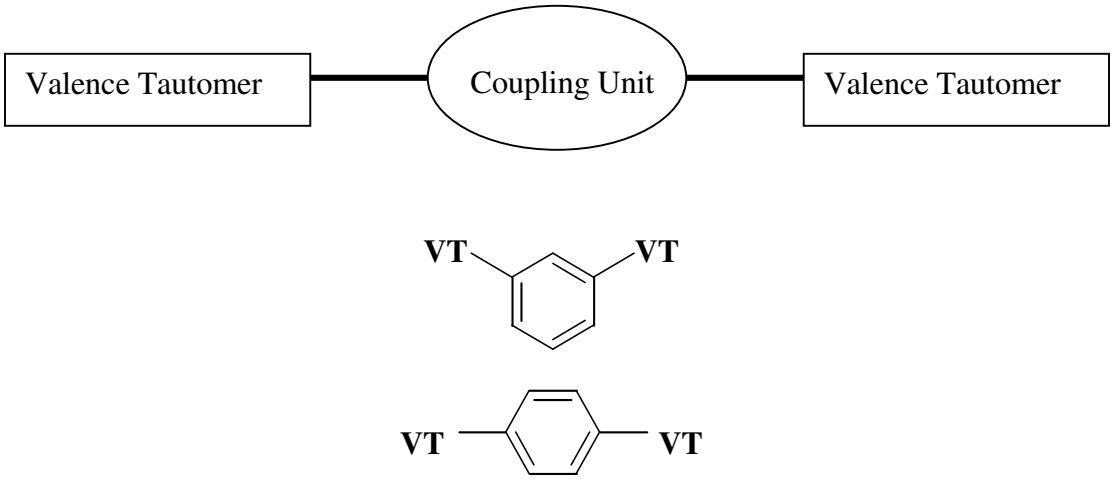

Figure 6.4. Proposed dinuclear valence tautomers.

The proposed systems are electronically very complex and any prediction of the mechanism of interaction between each metal center is challenging at best. This is because for a single valence tautomer one must account for the vibronic coupling of at least three states (Section 3.3) that are along the potential energy surface. If two valence tautomers are coupled then the number of potential electronic states is multiplied by at least two to create six different vibronically coupled interactions. Exchange coupling may also contribute to the coupling mechanism, which provides an added layer of complexity since the exchange-coupled spin state interactions would have to be accounted for. Thus, how the tautomeric units for either the para or meta-coupled systems interact depends on the type of communication that may occur through the phenylene bridge. However, for the necessary sake of formulating a hypothesis let's

assume — as experiment has indicated — that substantial spin-density is distributed on the bipyridine due to back bonding. The bipyridine ligands may then be susceptible to a spin-polarized coupled interaction through the phenylene bridge that allow for the stabilization of the metastable $Co^{III}Co^{II}$ state. The spin-polarization mechanism will differ for the differently coupled bridges due to the overlap dissimilarity. This concept was hinted at in section 2.2 where exchange coupling between organic biradicals is discussed. The biradicals of disjoint and non-disjoint systems are coupled through the molecular framework that bridges them.[5] From the exchange coupling argument in organic biradicals it is possible to extrapolate a simple rule from the Lewis dot structure that simply states, in "organic speak:" organic biradicals that are coupled conjugatively are antiferromagnetically-coupled and biradicals that are cross-conjugated are ferromagnetically-coupled. Although we are not presuming that something as simple as ferro or antiferromagnetic exchange is the mechanism of stabilizing the $Co^{III}Co^{II}$ intermediate state, we are stating that the coupling for the conjugated and cross-conjugated isomers should differ based *solely* on spin-polarization arguments. Conversely, spin-polarization is a distance dependent mechanism and the spin-density distribution may not allow for a substantial interaction between the two tautomeric centers due to the through-bond length of the two magnetic centers.

6.2 Synthesis of the Para-isomer (1)

Synthesis of the para-connected valence tautomer begins by converting commercially available 2-bromo-pyridine to **3**.[6] **3** is then coupled to 2, 5-dibromo-pyridine via Stille coupling to form **4**.[6] On a parallel route 1,4-dibromobenzene is

converted to **5**.[7] **4** and **5** are coupled via Suzuki reaction to form the **6**.[7] **6** is reacted with the cobalt semiquinone tetramer[8] to form the final dinuclear valence tautomer (**1**) (**Scheme 6.1**).

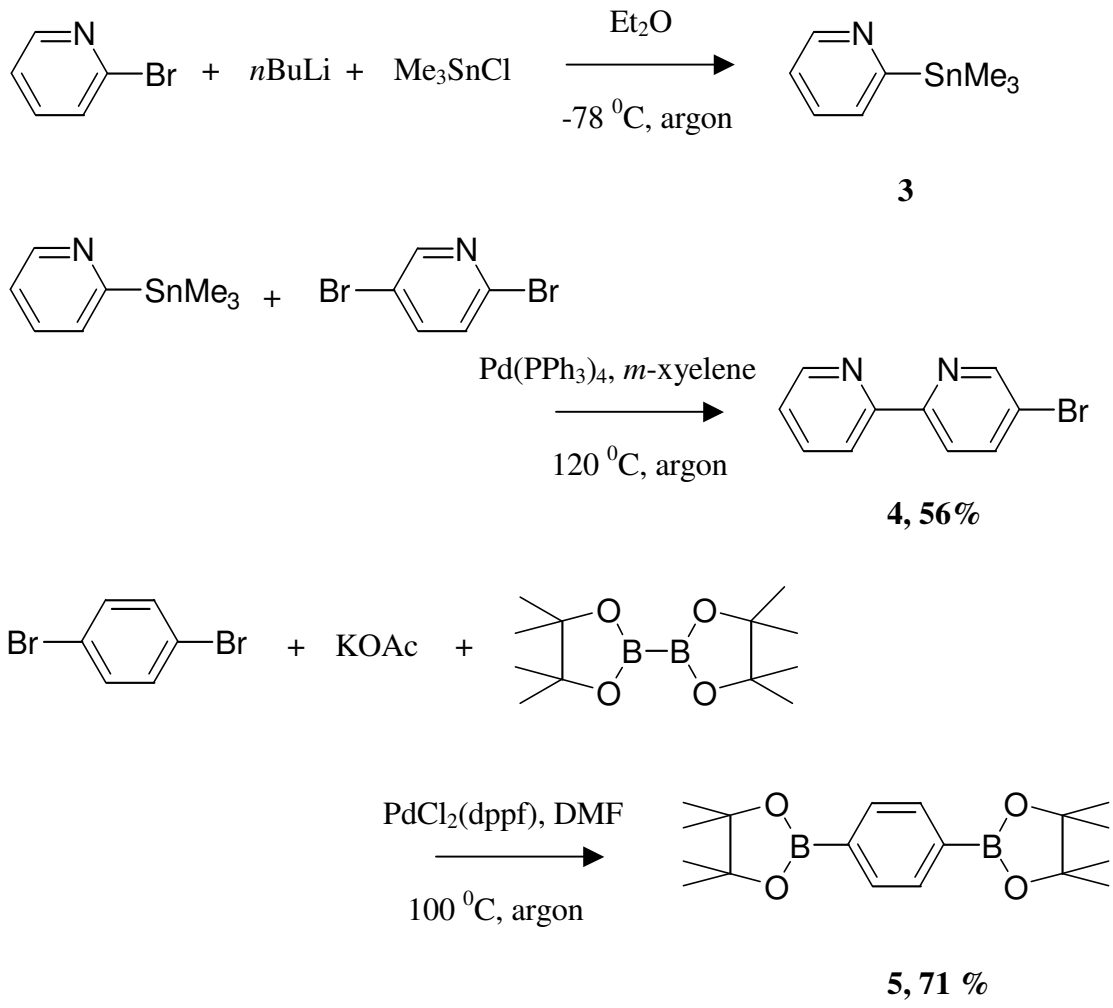

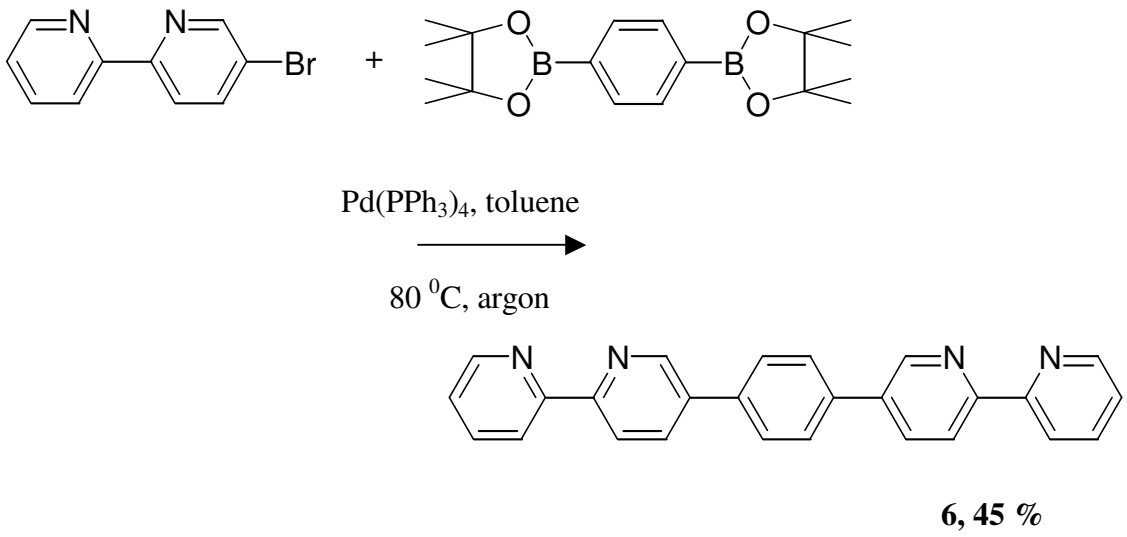

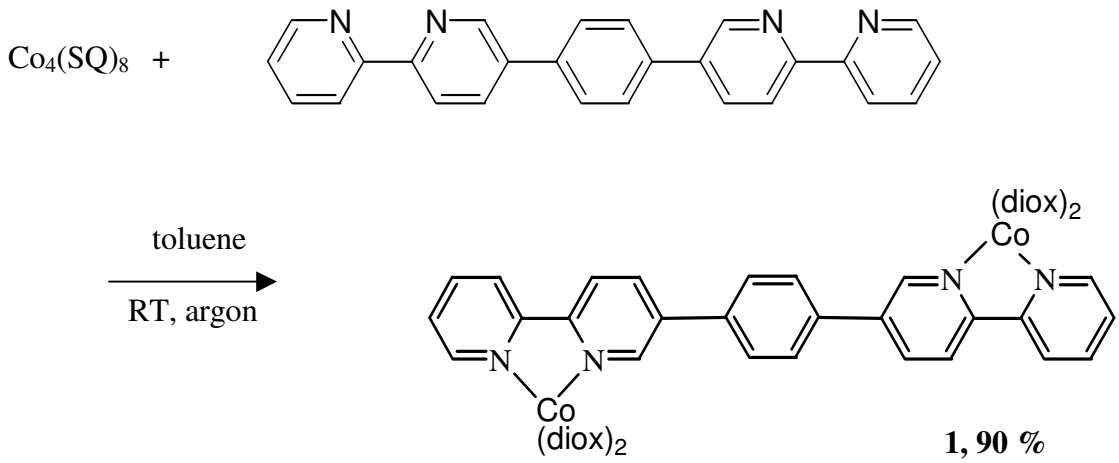

Scheme 6.1. Synthetic scheme for para-isomer.

6.3 Synthesis of the Meta-isomer (2)

Synthesis of the meta-connected valence tautomer is initiated by synthesizing (**7**) from 1, 3 -dibromo-*tert*-butyl-benzene and the dipinacol ester (**Scheme 6.2**). [9] **7** is then reacted 3-bromobipyridine by the use of a Suzuki reaction to create **8**. Finally, **8** is reacted with cobalt tetramer[8] to synthesize the final valence tautomeric complex (**2**).

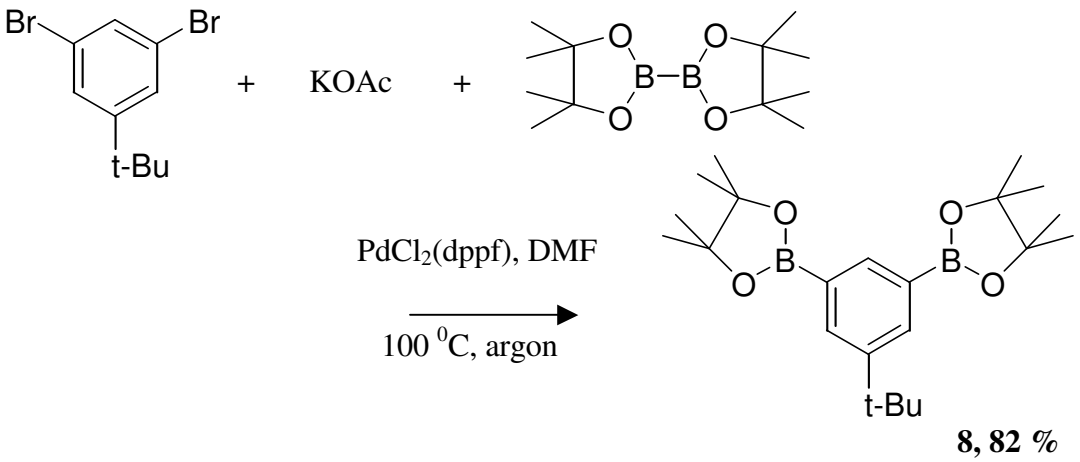

8, 82 %

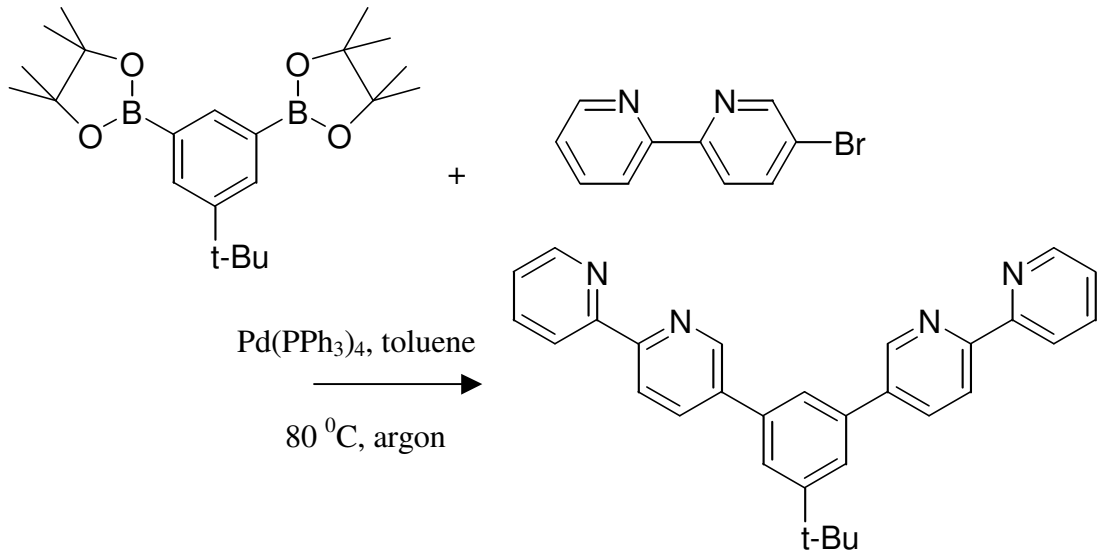

9, 48 %

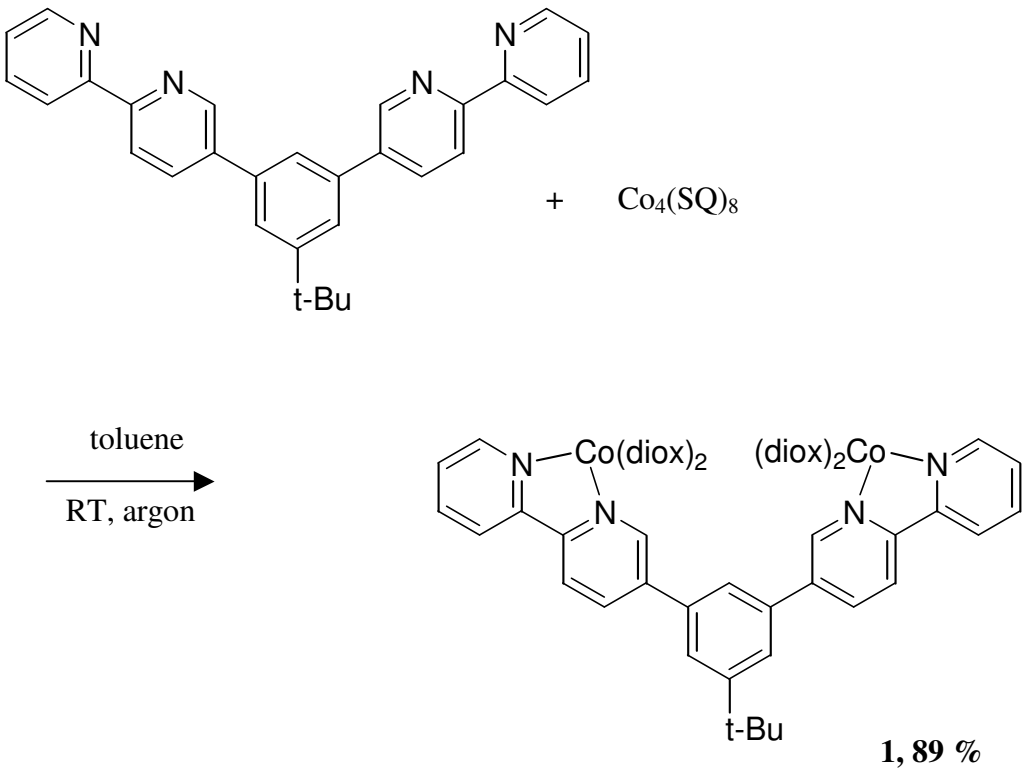

Scheme 6.2. Synthetic scheme for meta-isomer.

6.4 Magnetic Susceptibility

Crystalline samples of the valence tautomers were obtained and their respective crystal structures were determined (experimental). Variable-temperature magnetic susceptibility experiments were performed on microcrystalline samples of **1** and **2** using SQUID magnetometry at 1 Tesla applied field. At low temperature the predicted χT value for both para and meta connected valence tautomers should be 0.75 emu/K mol due to two uncorrelated semiquinone spins of the $Co^{III}(SQ)(Cat)Co^{III}(SQ)(Cat)$ state. For the intermediate $Co^{III}(SQ)(Cat)Co^{II}(SQ)_2$ state the maximum χT value is predicted to be near 2.9 emu mol^{-1} K^{-1}. Finally the estimated maximum value for the high-temperature $Co^{II}(SQ)_2Co^{II}(SQ)_2$ state is roughly 5 emu mol^{-1} K^{-1}.

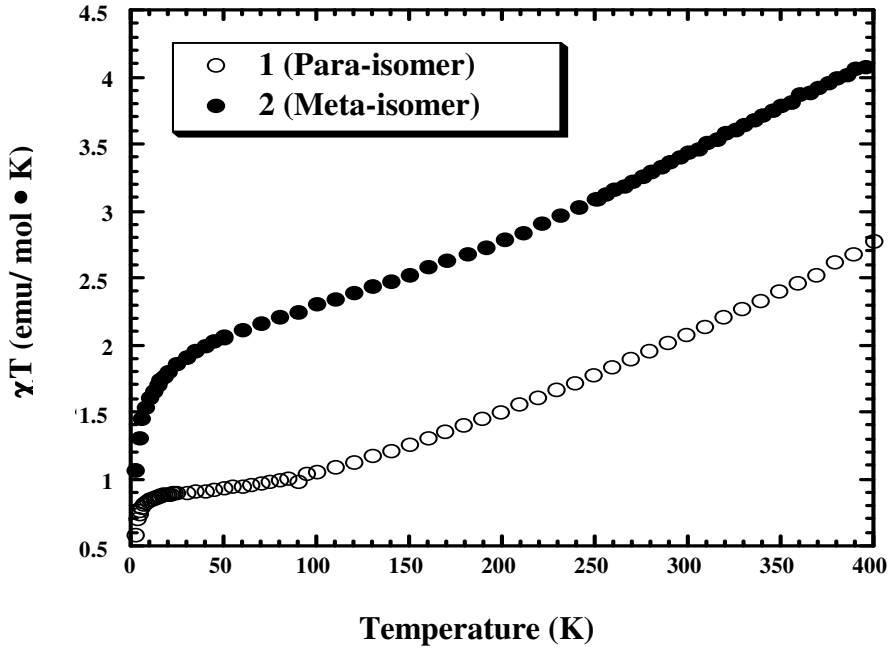

Figure 6.5. Magnetic susceptibility of para and meta isomers.

From the susceptibility data the para-compound approaches the low-temperature value (**Figure 6.5**). However, the meta-compound approaches a minimum of roughly 1.5 – 2 emu K mol^{-1} before abruptly dropping in value. The drop in susceptibility value at low temperature arises from intermolecular coupling. Thus the microcrystalline sample of the meta connected valence tautomer does not fully populate the low temperature state while the para connected sample appears to do so which can be seen from the leveling of the para χT data. At high temperature neither compound fully populates the high-temperature state due to the slow and gradual rise in the magnetic susceptibilities. The para-compound approaches the value of 2.8 emu K mol^{-1} while the meta compound approaches 4 emu K mol^{-1} at 400 K. The stabilization of the intermediate state is not observed where a step would be predicted to seen between the two temperature extremes.

It has been demonstrated that intermolecular forces play a central role in the valence tautomeric conversion.[10-12] Differences in solvation of the two valence tautomeric systems can contribute to the electronic state change. As a result the packing forces in the both compounds may likely stunt the valence tautomeric conversions, which may explain the incomplete population of the higher temperature forms. Furthermore, differences in the crystalline solvation may also explain the incomplete population of the low temperature form of the meta-compound as opposed the para valence tautomer.

6.5 Variable-Temperature IR

Variable-temperature infrared spectroscopy can be used as a spectroscopic tool to characterize the valence tautomeric conversion. The variable temperature IR data for both compounds display the signature intervalence charge-transfer band of the mixed-

valent catecholate to semiquinonate one-electron transition (**Figure 6.6** and **Figure 6.7**).[13] Furthermore both compounds are shown to be valence tautomeric due to the changes in the vibrational modes and intensity changes of the intervalence charge-transfer bands as functions of temperature in both the para and meta compounds respectively. The IVCT bands of both compounds appear identical. If a substantial amount of electronic coupling were present between the magnetic centers the IVCT bands may differ in shape and relative intensity for the two tautomeric molecules. Charge-transfer bands of mixed-valent systems that have electronically coupled chromophores can experience Davydov splitting due to changes in the relative positions of the ground and excited states.[9] From the IR data large changes in the vibrational region were observed (**Figure 6.8** and **Figure 6.9**) that correspond to the electronic conversion between the low and high temperature forms. From the SVD analysis sigmoids for both dinuclear systems can be constructed using techniques described previously (**Figure 6.10**). Unlike the crystalline samples used for the susceptibility experiments the film samples yield the near complete sigmoids for both para and meta.

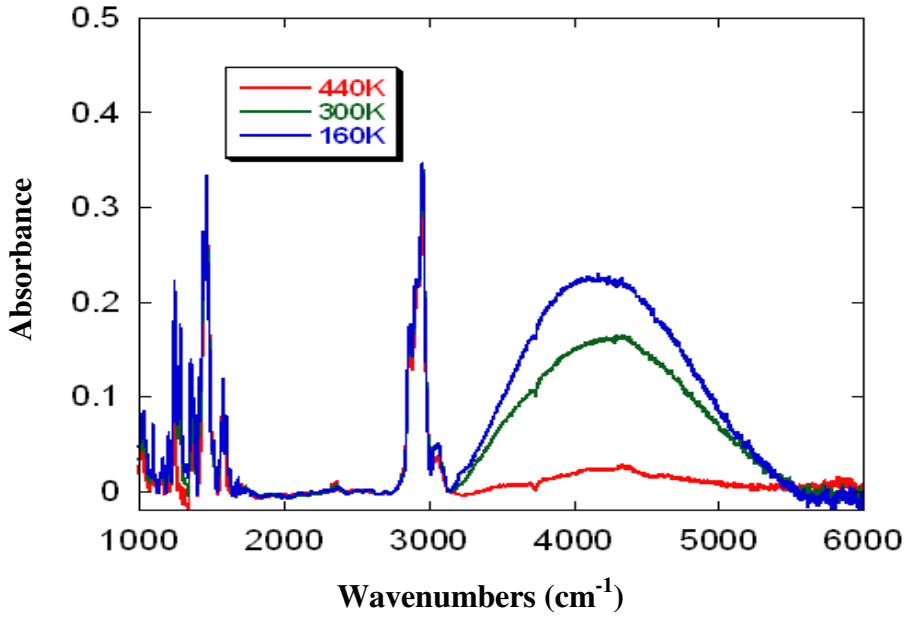

Figure 6.6. Variable Temp IR of para-isomer (100 – 400 K).

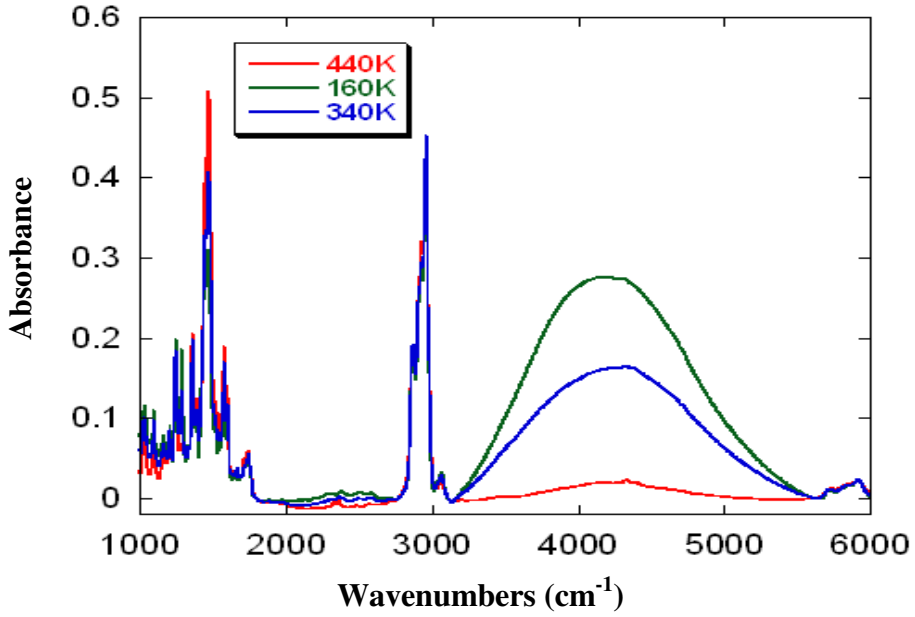

Figure 6.7. Variable-Temp IR of meta-isomer (100 – 400 K).

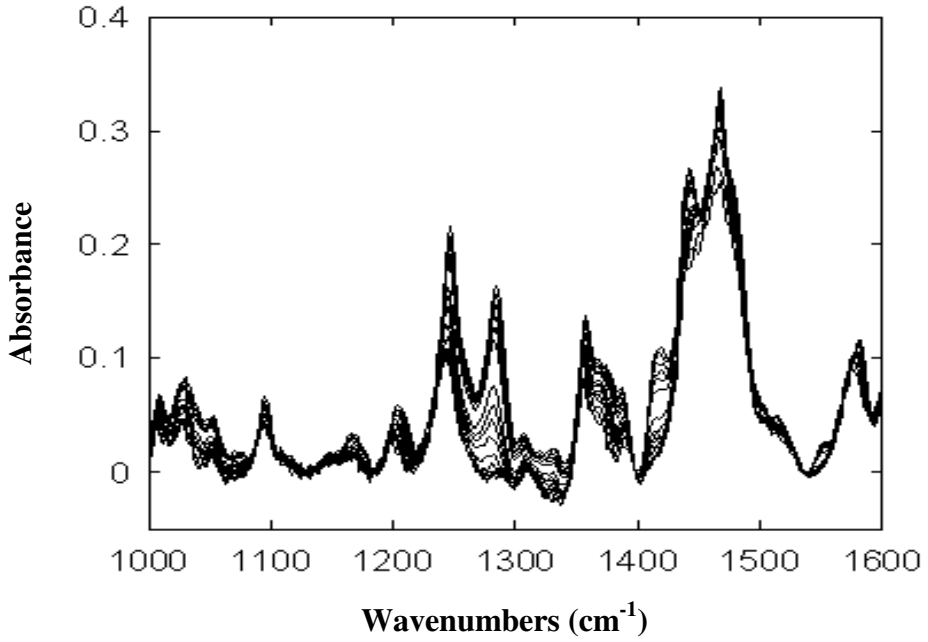

Figure 6.8. Variable Temp IR of para-isomer (100 – 400 K).

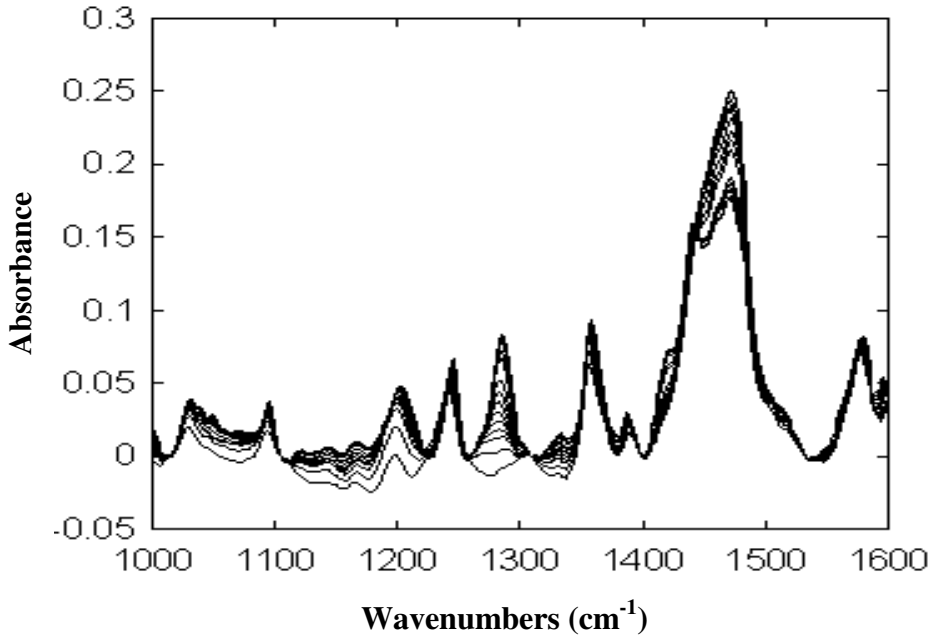

Figure 6.9. Variable Temp IR of meta-isomer (100 – 400 K).

Differences in solid state and solution based results in valence tautomeric systems have been discussed and it is not surprising that for the dinuclear valence tautomers, their behavior in the crystalline solid are different than the film. Both compounds undergo the valence tautomeric conversion near roughly the same temperature range.

The fit parameters used to model the data are identical to those utilized previously in Chapter 4. From the fit the thermodynamic changes of can be extracted (**Table 6.1**). In contrast to the magnetic susceptibility data the sigmoid fits from the SVD data indicate that there is a slight difference between the two dinuclear valence tautomers. For ΔH^0 there is a ~36 % difference between para and meta compounds and for ΔS^0 there is a ~ 18 % difference. While the susceptibility measurements were collected on crystalline samples where the individual crystalline packing of each respective valence tautomer may influence the electronic conversion, the solid-state film used for the IR experiments form "identical" amorphous sample materials. As it has been demonstrated the solid-state film results are very similar to solution data. Consequently it can reasonably be expected that both valence tautomeric samples experience similar solvations in their respective intermolecular environments. For both valence tautomers the vibrational changes indicate that there is no substantial difference for either para- or meta-connectivity. Combined with the lack of difference with the electronic IVCT bands for the two compounds, the variable temperature IR data seems to support the suggestion that the intramolecular coupling between the magnetic centers is small.

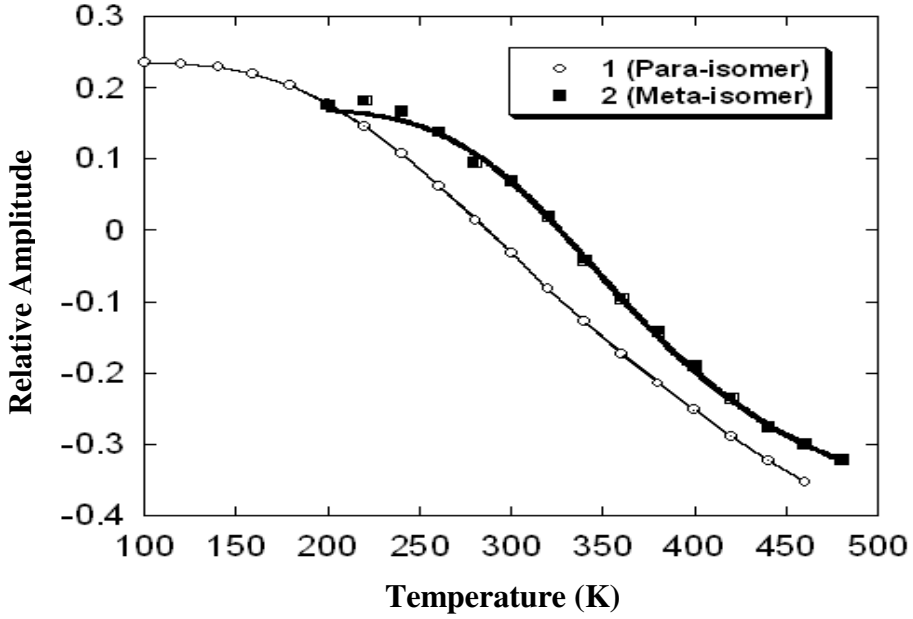

Figure 6.10. SVD analysis of para and meta isomers.

Table 6.1. Thermodynamic parameters from SVD fits of **1** and **2**.

Parameters	**Para-isomer**	**Meta-isomer**
$T_{1/2}$ (K)	458	380
ΔH^{o} (kcal/mol)	4.2	6.6
ΔS^{o} (cal/mol•K)	9.2	11.2

The intensity of the IVCT was also plotted as a function of temperature and profiles of the mole fraction of the Co^{III} ($\chi_{Co}{}^{III}$) for **1** and **2** were determined (**Figure**

6.11). The profiles were least-squares fit to eqn. 6.1 (experimental section) to obtain thermodynamic parameters.

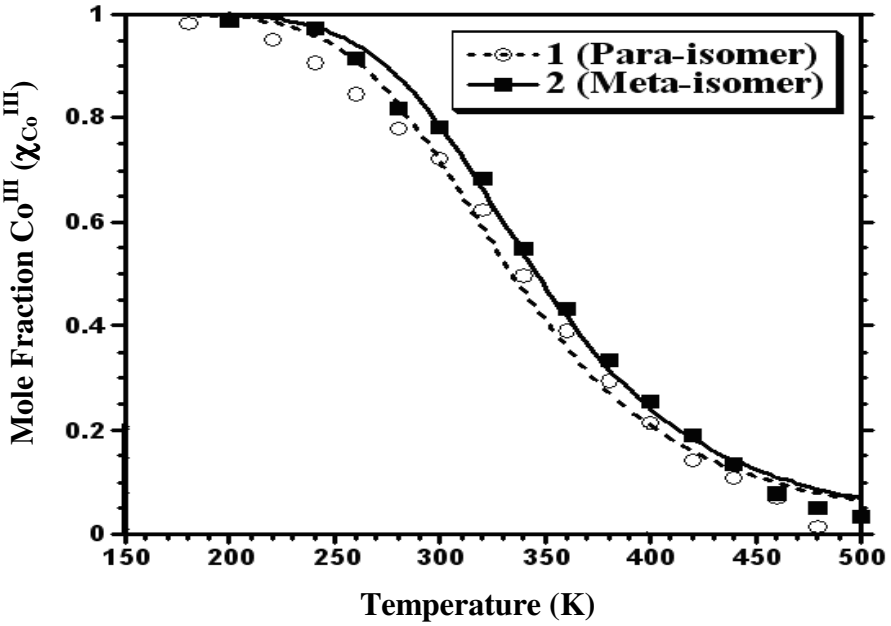

Figure 6.11. Temperature-dependences of IVCT band intensity for **1** and **2**.

Table 6.2. Thermodynamic parameters from IVCT intensity change.

Parameters	**Para-isomer**	**Meta-isomer**
$T_{1/2}$ (K)	371	375
ΔH^o (kcal/mol)	5.8	5.4
ΔS^o (cal/mol•K)	16.7	16.1

The IVCT intensity change of **1** and **2** describe two identically behaving systems, which implies that no difference in behavior between the two compounds.

6.6 Conclusion

Both IR and magnetic susceptibility data imply that there is very little intramolecular coupling in both dinuclear valence tautomeric systems. The cause of this small interaction may be two fold: 1) insufficient electron density distribution on the bipyridine ligand due to back bonding and 2) large through-bond distance between the valence tautomeric centers. Although preceding research using paramagnetic NMR has verified that backbonding[14-15] affords a significant quantity of electron density on the counterligand of the cobalt valence tautomeric bipyridine derivative, the intramolecular distance is a problem since the expanse between the cobalt centers in the para-isomer is 11 bonds and in the meta-isomer it is 10 bonds. On the other hand there is still a noticeable (albeit small) difference in the thermodynamic parameters of the two systems. The slight dissimilarity in the SVD fits between the para and meta isomers may be a combination of differing solvation environments and electronic coupling. As has been described changes in $T_{1/2}$ can be due to both back bonding and intermolecular coupling. The midpoint temperature difference of both compounds is 80 K. Using amorphous film samples for the IR experiments reduces the variation in solvation for the two systems and the thermodynamic parameters extracted may reflect a genuine electronic contribution. Yet, an electronic explanation is highly speculative without definitive evidence.

An alternative approach to designing multinuclear valence tautomeric systems is to couple the valence tautomeric centers through the dioxolene ligands.[4] Due to the extensive delocalization between the cobalt metal and the dioxolene molecule the electron density distribution can be maximized. Caution must still be exercised since too much coupling may prevent the complete conversion between the tautomeric centers

within a reasonable temperature range. For the recently published tetraoxolene dinuclear valence tautomer the magnetic susceptibility and EPR data suggest that only one of the valence tautomeric centers converts to the high-spin derivative as a function of temperature.[4] As a consequence, within a reasonable temperature for both solution and solid state samples the best that can be expected out of the tetraoxolene system is an interconversion between the $Co^{III}(Cat)(SQ)Co^{III}(Cat)(SQ)$ state and the intermediate $Co^{III}(Cat)(SQ)Co^{II}(SQ)_2$ state since the potential energy of the $Co^{II}(SQ)_2Co^{II}(SQ)_2$ state is very high relative to the first two.

6.7 Experimental

General. All reactions were performed under inert and anhydrous conditions. NMR spectra were recorded in *d*-chloroform at 300 MHz. Electronic absorption spectra were collected in CH_2Cl_2 on a Hewlett Packard 8452A Diode Array Scanning Spectrophotometer. IR experiments were performed on a Digilab FTS 3000 FTIR spectrometer equipped with a globar source, KBr beamsplitter and a liquid nitrogen cooled MCT detector. The spectra were the result of 64 scans at a spectral resolution of 2 cm^{-1}. The temperature dependent spectra were recorded using a helium cooled cryostat (MicrostatHe, Oxford Instruments). SQUID experiments were performed on a Quantum Design MPMS-XL7 SQUID magnetometer using a Delrin sample holder at an applied field of 4000G. Pascal's constants were used to calculate diamagnetic corrections.

Synthesis of 2-trimethylstannanyl-pyridine (**3**). A 250 mL schlenk flask was charged with 1 g of 2-bromopyridine and purged under argon. 20 mL diethyl ether was added and the reaction mixture was cooled to –78 °C. 3.5 ml of 2 M *n*-BuLi was added and the reaction mixture was allowed to stir for 2 hours. Finally the reaction was quenched with 7 mL of 1 M trimethylstannyl chloride and the reaction vessel was brought to room temperature overnight. Solvent was evaporated in vacuo and the crude reaction mixture was taken to the next step without purification.

Synthesis of 5-bromo-[2, 2′]bipyridinyl (**4**). Under inert atmosphere 1.65 g of 2,5-dibromopyridine and 0.073 g tetrakistriphenylphosphine was added to **3**. 20 mL of *m*-xylene was added and the reaction mixture was heated to reflux overnight. After cooling

to room temperature the reaction was quenched with 1 M NaOH solution. The product mixture was extracted with methylene chloride and rotovaped to an oil. The product was purified using alumina column chromatography in 1:5 mixture ethylacetate/petroleum ether. The collected material was further purified by recrystallization in ethanol/water mixture (2.06 g, white solid). ^{1}H-NMR: δ 8.73 (d, 1H, J = 2.4 Hz); 8.67 (m, 1H); 8.51 (d, 1H, J = 7.8); 8.32 (d, 1H, J = 8.1); 7.95 (d, 1H, J = 8.7); 7.83 (t, 1H, J = 6.0); 7.33 (m, 1H).

Synthesis of 4, 4, 5, 5, 4′, 4′, 5′,5′ – octamethyl – 2, 2' – phenyl – [2, 2']bi[1, 3, 2]dioxaborolane (**5**). A 250 mL schlenk flask was charged with 0.250 g of 1, 4 – dibromobenzene, 6.423 g diboron pinacol ester, 447.5 g potassium acetate and 0.037 g $PdCl_2$(dppf). The reactants were dissolved in 20 mL DMSO and allowed to stir at 80^0C overnight. The reaction mixture was allowed to cool and the DMSO was removed in vacuo. The product was purified by column chromatography using silica in 9:1 methylene chloride/methanol solvent system (0.22 g, white solid). ^{1}H-NMR: δ 7.80 (s, 4H); 1.35 (s, 24H).

Synthesis of 5, 5′ – phenyl – di[2, 2′]bipyridinyl (**6**). To the reaction flask containing 0.357 g of **4**, 0.2 g of **5** and 0.147 g palladium tetrakistriphenylphosphine were added. The solid reactants were dissolved in 40 mL toluene and 1 mL mL absolute ethanol and 1.6 ml 2.0 M Na_2CO_3 were added. Argon was bubbled through the reaction mixture for 30 minutes and the reaction was brought to reflux for 2 days. The reaction was then allowed to cool to room temperature and quenched with deionized water. The product

mixture was extracted using methylene chloride and purified by alumina column chromatography in 1:1 methylene chloride/pet ether solvent system (0.18 g, white solid). ^{1}H-NMR: δ 8.98 (s, 2H); 8.71 (d, 2H, J = 4.2 Hz); 8.52 (d, 2H, J = 9 Hz); 8.45 (d, 2H, J = 8.1 Hz); 8.08 (d, 1H, J = 10.5); 7.87 (m, 6H); 7.33 (t, 2H, J = 4.8 Hz).

Synthesis of 2, 2′ – (3 –tert–butyl–phenyl) –4, 4, 5, 5, 4′, 4′, 5′, 5′–octamethyl–bi[1, 3, 2]dioxoborolane (**7**). A 250 ml schlenk flask was charged with 0.293 g 1, 3–dibromo–5–tert–butyl–benzene and 0.045 g $PdCl_2$(dppf), 0.584 g diborane pinacol ester and 0.621 g potassium acetate. The reactants were dissolved in 40 mL DMSO and allowed to stir at 80 ^{0}C overnight. The reaction mixture was allowed to cool and the DMSO was removed in vacuo. Purified by column chromatography 9:1 methylene chloride/pet ether (0.228 g). ^{1}H-NMR: δ 8.02 (s, 1H); 7.92 (s, 1H); 1.337 (s, 24H).

Synthesis of 5, 5′ – (3–tert–butyl–phenyl) –bi[2, 2']bipyridinyl (**8**). To a schlenk flask 0.198 g of **3**, 0.128 g of **7** and 0.83 g tetrakis triphenylphosphine and purged with nitrogen. The reactants were dissolved in toluene and brought to reflux for 2 days. The reaction was quenched with deionized water and extracted with methylene chloride. The product was purified via chromatography 1:1 methylene chloride/ pet ether (0.156 g, white solid). ^{1}H-NMR: δ 8.79 (d, 1H, J = 0.59 Hz); 8.72 (d, 1H, J = 1.32 Hz); 8.54 (d, 1H, J = 2.7); 8.46 (d, 1H, J = 2.66 Hz); 8.11 (d, 1H, J = 6); 7.86 (t, 1H, J = 3 Hz); 7.72 (s, 2H); 7.35 (t, 1H, J = 1.7 Hz).

Synthesis of **1**. A 250 ml schlenk flask was charged with 0.100 g of **5**, purged with argon and dissolved in 15 mL toluene. In a separate flask 0.025 g of cobalt semiquinone tetramer was dissolved in 10 mL toluene. **5** was cannulated to the tetramer, allowed to stir for 20 minutes and sit under argon overnight. The product was collected on a filter stick under argon (0.58 g, green solid).

Synthesis of **2**. A 250 ml schlenk flask was charged with 0.100 g of **7**, purged with argon and dissolved in 15 ml toluene. In a separate flask 0.026 g of cobalt semiquinone tetramer was dissolved in 10 ml toluene. **7** was cannulated to the tetramer, allowed to stir for a few minutes and sit under nitrogen overnight. The product was collected on a filter stick under nitrogen (0.75 g, green solid).

The following relationship was used to fit the data in **Figure 6.11**:

$$\chi_{Co^{III}} = \frac{1}{\left[\exp\left(\frac{\Delta H^{\circ}}{RT} - \frac{\Delta S^{\circ}}{R}\right) + 1\right]} \qquad (6.1)$$

Structure Determination of 1. Purple plates of **1** were crystallized from a THF/toluene solution at 23 deg. C. A crystal of dimensions 0.14 x 0.14 x 0.06 mm was mounted on a standard Bruker SMART CCD-based X-ray diffractometer equipped with a LT-2 low temperature device and normal focus Mo-target X-ray tube (λ = 0.71073 A) operated at 2000 W power (50 kV, 40 mA). The X-ray intensities were measured at 123(2) K; the detector was placed at a distance 4.959 cm from the crystal. A total of 1808 frames were collected with a scan width of 0.3° in ω and phi with an exposure time of 120 s/frame. The frames were integrated with the Bruker SAINT software package with a narrow frame algorithm. The integration of the data yielded a total of 41930 reflections to a maximum 2θ value of 40.36° of which 9253 were independent and 4012 were greater that $2\sigma(I)$. The final cell constants (Table 6.4) were based on the xyz centroids of 721 reflections above $10\sigma(I)$. Analysis of the data showed negligible decay during data collection. The data were processed with SADABS and corrected for absorption. The structure was solved and refined with the Bruker SHELXTL (version 5.10) software package using the space group P2(1)/c with Z = 4 for the formula $C_{82}H_{98}N_4O_8Co_2$•$(tol)_2(THF)$. All non-hydrogen atoms were refined anisotropically with the hydrogen atoms placed in idealized positions. Full matrix least-squares refinement based on F^2 converged at R1 = 0.0755 and wR2 = 0.1447 [based on I > 2sigma(I)], R1 = 0.1612 and wR2 = 0.1618 for all data. The THF solvate was highly disordered and was treated by use of the PLATON/SQUEEZE subroutine.

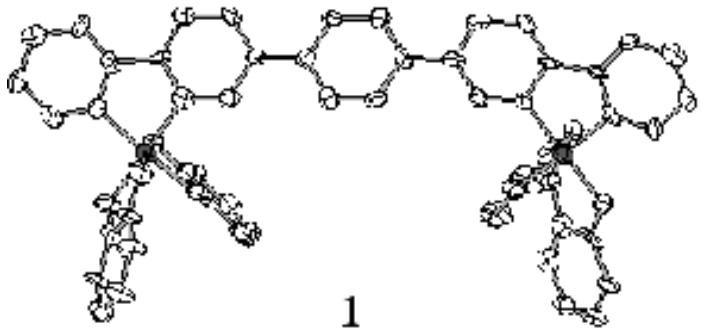

Figure 6.12. Crystal structure of **1**.

Table 6.3. Selected bond lengths of **1**.

	Bond	Length (Å)
SQ	O1 – C1	1.253(14)
	O2 – C6	1.293(13)
	C1 – C2	1.419(17)
	C2 – C3	1.397(16)
	C3 – C4	1.393(15)
	C4 – C5	1.347(15)
	C5 – C6	1.426(16)
	C6 – C1	1.435(17)
Cat	O3 – C15	1.355(13)
	O4 – C20	1.297(15)
	C15 – C16	1.366(15)
	C16 – C17	1.411(15)
	C17 – C18	1.407(15)
	C18 – C19	1.385(15)
	C19 – C20	1.428(17)
	C15 – C20	1.399(15)
Co-O	Co1 – O1	1.909(8)
	Co1 – O2	1.918(8)
	Co1 – O3	1.872(8)
	Co1 – O4	1.848(8)

Table 6.4. Crystal data and Structure Refinement of **1.**

Empirical formula	$C_{82}H_{98}N_4O_8Co_2$•(**1**•2C_7H_8)
a/Å	16.862(3)
b/Å	26.337(5)
c/Å	26.737(5)
α/deg	90
β/deg	124.136(3)
γ/deg	90
V/Å^3	9828(3)
Z	4
Formula weight	1641.88
Crystal system, space group	monoclinic, *P2$_1$/c* (purple plate)
T/K	123(2)
λ/Å	0.71073
ρ_{calc}/g cm^{-3}	1.110
μ/cm^{-1}	3.91
R1[d]	0.0755[c]
wR2[b]	0.1447[c]

[a]Quantity minimized = $R = \Sigma||F_o|-|F_c||/\Sigma|F_o|$. [b]$wR2 = \Sigma [w(F_o^2-F_c^2)^2]/ \Sigma [(wF_o^2)^2]^{1/2}$. [c]$w = 1/[\sigma^2(F_o^2) + (0.0475P)^2 + 0.00P]$, $P = [2F_c^2 + F_o^2)]/3$.
[d]$w=1/[\sigma^2(F_o^2)+(0.1057P)^2+8.8966P]$, $P=(F_o^2+2F_c^2)/3$.

Structure determination of 2. Purple block-like crystals of **2** were crystallized from a dichlorlmethane/toluene solution at 23 deg. C. A crystal of dimensions 0.12 x 0.12 x 0.08 mm was mounted on a standard Bruker SMART CCD-based X-ray diffractometer equipped with a LT-2 low temperature device and normal focus Mo-target X-ray tube (λ = 0.71073 A) operated at 2000 W power (50 kV, 40 mA). The X-rayintensities were measured at 138(2) K; the detector was placed at a distance 4.959 cm from the crystal. A total of 2527 frames were collected with a scan width of 0.3° in ω and phi with an exposure time of 90 s/frame. The frames were integrated with the Bruker SAINT software package with a narrow frame algorithm. The integration of the data yielded a total of 53173 reflections to a maximum 2θ value of 40.67° of which 9277 were independent and 4813 were greater than $2\sigma(I)$. The final cell constants (Table 6.6) were based on the xyz centroids of 3009 reflections above $10\sigma(I)$. Analysis of the data showed negligible decay during data collection. The data were processed with SADABS and corrected for absorption. The structure was solved and refined with the Bruker SHELXTL (version 5.10) software package using the space group P2(1)/n with Z = 4 for the formula $C_{86}H_{106}N_4O_8Co_2 \bullet (C_7H_8)_3$. All non-hydrogen atoms were refined anisotropically with the hydrogen atoms placed in idealized positions. Full matrix least-squares refinement based on F^2 converged at R1 = 0.0753 and wR2 = 0.1692 [based on I > 2sigma(I)], R1 = 0.1606 and wR2 = 0.2217 for all data.

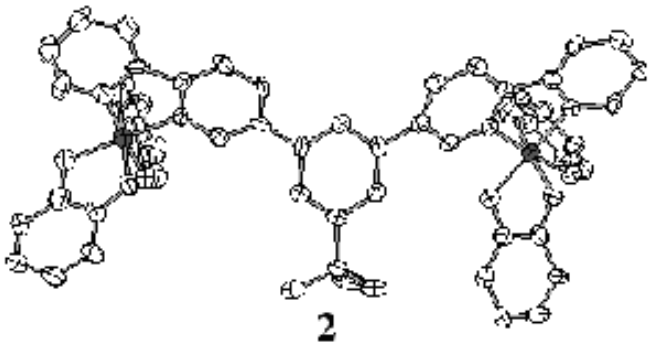

2

Figure 6.13. Crystal structure of **2**.

Table 6.5. Selected bond lengths of **2**.

	Bond	Length (Å)
SQ	O1 – C1	1.253(14)
	O2 – C6	1.293(13)
	C1 – C2	1.419(17)
	C2 – C3	1.397(16)
	C3 – C4	1.393(15)
	C4 – C5	1.347(15)
	C5 – C6	1.426(16)
	C6 – C1	1.435(17)
Cat	O3 – C15	1.355(13)
	O4 – C20	1.297(15)
	C15 – C16	1.366(15)
	C16 – C17	1.411(15)
	C17 – C18	1.407(15)
	C18 – C19	1.385(15)
	C19 – C20	1.428(17)
	C15 – C20	1.399(15)
Co-O	Co1 – O1	1.909(8)
	Co1 – O2	1.918(8)
	Co1 – O3	1.872(8)
	Co1 – O4	1.848(8)

Table 6.6. Crystal data and Structure Refinement of **2**.

Empirical formula	$C_{107}H_{130}N_4O_8Co_2$ (**2**•$3C_7H_8$)
a/Å	20.633(4)
b/Å	19.207(3)
c/Å	24.055(4)
α/deg	90
β/deg	95.452(7)
γ/deg	90
V/Å^3	9490(3)
Z	4
Formula weight	1718.01
Crystal system, space group	Monoclinic, $P2_1/n$ (purple block)
T/K	133(2)
λ/Å	0.71073
ρ_{calc}/g cm^{-3}	1.202
μ/cm^{-1}	4.08
R1[d]	0.0755[c]
wR2[b]	0.1447[c]

[a]Quantity minimized = $R = \Sigma||F_o|-|F_c||/\Sigma|F_o|$. [b]$wR2 = \Sigma [w(F_o^2-F_c^2)^2]/ \Sigma [(wF_o^2)^2]^{1/2}$. [c]$w = 1/[\sigma^2(F_o^2) + (0.0475P)^2 + 0.00P]$, $P = [2F_c^2 + F_o^2)]/3$.
[d]$w=1/[\sigma^2(F_o^2)+(0.1057P)^2+8.8966P]$, $P=(F_o^2+2F_c^2)/3$.

6.8 References

1. Balzani, V.; Juris, A.; Venturi, M.; Campagna, S.; Serroni, S. *Chem. Rev*. **1996**, *96*, 759.
2. Jung, O. – K.; Pierpont, C. G. *J. Am. Chem. Soc*. **1994**, *116*, 2229.
3. Bodnar, S. H.; Caneschi, A.; Dei, A.; Shultz, D. A. Sorace, L. *Chem. Comm*. **2001**, *20*, 2150.
4. Carbonera, C.; Dei, A.; Letard, J. – F.; Sangregorio, C.; Sorace, L. *Angew. Chem. Int. Ed*. **2004**, *43*, 3136.
5. Borden, W. T.; Davidson, E. R. *J. Am. Chem. Soc*. **1977**, *99*, 4587.
6. Schwab, P. F. H.; Fleischer, F.; Michl, J. *J. Org. Chem*. **2002**, *67*, 443.
7. Iovine, P. M.; Kellett, M. A.; Redmore, N. P.; Therien, M. J. J. Am. Chem. Soc. **2000**, *122*, 8717.
8. Wehman, P.; Dol, G. C.; Moorman, E. R.; Kamer, P. C. J.; Leeuwen, P. W. N. M. *Organometallics*. **1994**, *13*, 4856.
9. Shultz, D. A.; Lee, H. L.; Kumar, R. K.; Gwaltney, K. *J. Org. Chem*. **1999**, *64*, 9124.
10. Adams, D. M.; Dei, A.; Rheingold, A. L.; Hendrickson, D. N. *J. Am. Chem. Soc*. **1993**, *115*, 8221.
11. Bin-Salamon, S.; Brewer, S.; Feldheim, D. L.; Franzen, S.; Lappi, S.; Shultz, D. A. *J. Am. Chem. Soc*. **2005**, *127*, 5328.
12. Adams, D. M.; Noodleman, L.; Hendrickson, D. N. *Inorg. Chem*. **1997**, *36*, 3966.

General Conclusion

The research presented in Chapters 4 – 6 demonstrate discoveries in several fundamental areas of valence tautomerism. These involve the role of intermolecular interactions in valence tautomerism in a surface confined valence tautomer system, the synthetic control of the electronic delocalization of the mixed-valent $Co^{III}(SQ)(Cat)$ state and finally the rational design of strong intramolecular coupling in multinuclear valence tautomeric systems.

In the surface-attached valence tautomer, it was discovered that there is a large reduction in the thermodynamic change due to surface confinement. The experimental spectroscopic data precludes the effect of electronic coupling between the surface-confined valence tautomer and the nanoparticle surface. It was determined that the most likely cause of the thermodynamic change is the difference in the intermolecular interactions between the surface-confined valence tautomer and its free analogs. Thus surface-confinement can be used as a method to "tune" valence tautomerism.

The dinuclear valence tautomeric systems synthesized is an attempt to rationally control the intramolecular coupling between multinuclear valence tautomeric centers through the bipyridine ligand. The design parameters involved the synthesis of para and meta connected structural isomers. Unfortunately it was discovered that the connectivity changes did not matter since the intramolecular coupling between the valence tautomeric centers of either isomer was not substantial due to insufficient spin-density distribution on the bipyridine ligands and large bond-length distances between the magnetic centers. Thus, in order to rationally synthesize electronically coupled dinuclear valence tautomers through the bipyridine ligand it is necessary to either increase the spin-density

distribution on the bipyridine ligand and/or decrease the through-bond distance between the valence tautomeric centers.

Finally, it was successfully demonstrated that that the degree of electronic delocalization between the SQ-Cat donor-acceptor pair of the low-temperature mixed-valent form can be synthetically controlled by changing the orbital energies of the Co^{III} metal center through backbonding on substituted bipyridine ligands. Bipyridine ligands substituted at the para position with electron donors tend to increase the electronic delocalization of the SQ-Cat donor-acceptor pair while electron accepting substituents tend to reduce the delocalization effect. Although the exact mechanistic effect of the backbonding interaction on the delocalization is yet to be determined, the spectroscopic evidence is consistent with the very simplistic idea that the metal contribution to the SQ-Cat pair is determined by the degree of backbonding to the bipyridine π^*.

Appendix

Complete Structure Data of:

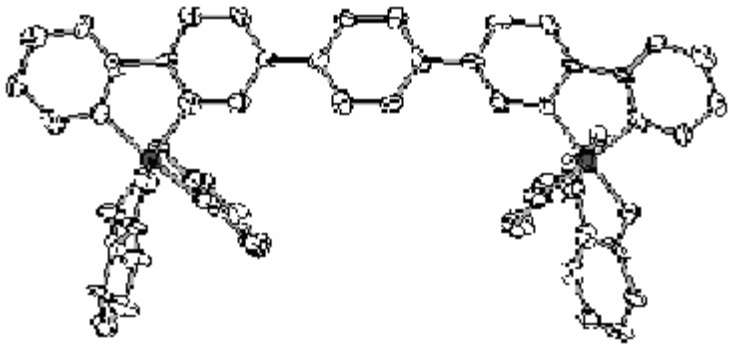

	x	y	z	U(eq)
Co(1)	7855(3)	4605(1)	3132(2)	69(1)
Co(2)	510(3)	2289(1)	681(2)	71(1)
O(1)	8049(9)	5287(4)	3122(6)	59(5)
O(2)	7772(10)	4556(6)	2410(8)	99(6)
O(3)	6542(10)	4702(5)	2672(6)	65(5)
O(4)	7842(10)	4709(5)	3842(6)	76(5)
O(5)	505(10)	2393(5)	-13(6)	64(5)
O(6)	-729(11)	2548(5)	262(7)	78(5)
O(7)	522(9)	2193(5)	1390(6)	69(5)
O(8)	1018(10)	2959(5)	966(7)	65(5)
N(1)	9181(16)	4450(6)	3629(8)	77(7)
N(2)	7771(14)	3880(6)	3182(9)	74(7)
N(3)	1732(11)	1967(6)	1070(6)	33(5)

N(4)	71(14)	1587(7)	430(9)	75(7)
C(1)	7774(14)	5435(9)	2578(11)	54(7)
C(2)	7533(15)	5929(8)	2366(10)	73(8)
C(3)	7194(17)	6002(9)	1775(12)	88(9)
C(4)	7023(15)	5629(9)	1368(11)	83(9)
C(5)	7229(17)	5164(10)	1529(12)	88(9)
C(6)	7593(17)	5009(10)	2154(13)	78(9)
C(7)	6980(20)	6573(11)	1531(14)	127(11)
C(8)	7170(20)	6958(11)	2005(14)	200(15)
C(9)	7677(19)	6701(10)	1358(12)	160(13)
C(10)	6040(20)	6604(10)	1138(13)	161(13)
C(11)	7120(30)	4709(13)	1109(16)	160(13)
C(12)	6290(20)	4363(11)	1040(14)	201(16)
C(13)	6700(20)	4925(12)	494(16)	226(18)
C(14)	8040(20)	4508(11)	1364(14)	187(14)
C(15)	6286(17)	4889(7)	3012(11)	45(7)
C(16)	5382(17)	5097(8)	2803(11)	66(7)
C(17)	5243(16)	5262(7)	3236(11)	76(8)
C(18)	5897(18)	5249(8)	3825(12)	83(8)
C(19)	6749(16)	5042(7)	4006(10)	65(7)
C(20)	6965(17)	4885(7)	3625(10)	39(7)
C(21)	4646(19)	5115(9)	2123(13)	100(9)
C(22)	4490(17)	4592(9)	1844(11)	142(11)
C(23)	3691(17)	5302(8)	1963(11)	126(10)
C(24)	5060(17)	5458(9)	1842(11)	132(11)
C(25)	5700(40)	5384(19)	4340(30)	240(20)
C(26)	4650(30)	5311(16)	4017(19)	320(30)
C(27)	6290(30)	5272(15)	4840(20)	290(30)
C(28)	5590(30)	5992(14)	4205(18)	290(20)
C(29)	-123(18)	2733(9)	-293(11)	62(8)
C(30)	-246(16)	3013(8)	-782(11)	79(8)
C(31)	-962(19)	3380(9)	-1095(11)	86(9)
C(32)	-1646(18)	3437(8)	-991(11)	90(9)
C(33)	-1593(16)	3174(8)	-497(10)	68(8)
C(34)	-790(17)	2824(8)	-177(10)	49(7)
C(35)	-1190(30)	3658(12)	-1725(16)	153(13)
C(36)	-460(30)	4128(14)	-1346(17)	280(20)
C(37)	-2050(30)	3973(15)	-2035(19)	300(20)
C(38)	-610(30)	3438(13)	-1877(16)	260(20)
C(39)	-2300(20)	3251(10)	-323(13)	113(10)
C(40)	-2841(15)	2745(8)	-417(10)	111(9)
C(41)	-3062(19)	3646(10)	-769(12)	164(13)
C(42)	-1823(17)	3407(8)	310(11)	125(11)
C(43)	651(17)	2645(11)	1637(12)	84(9)
C(44)	492(15)	2692(9)	2079(10)	87(8)
C(45)	683(17)	3182(10)	2313(11)	95(9)

C(46)	947(17)	3587(10)	2080(12)	105(10)
C(47)	1093(17)	3554(9)	1637(12)	82(8)
C(48)	899(15)	3039(9)	1396(11)	51(8)
C(49)	570(30)	3327(15)	2907(18)	192(16)
C(50)	1580(30)	3470(12)	3435(17)	244(19)
C(51)	420(20)	2863(11)	3119(14)	199(16)
C(52)	-180(20)	3725(11)	2613(15)	202(16)
C(53)	1313(19)	3974(10)	1375(12)	97(9)
C(54)	2293(17)	3820(9)	1463(11)	142(12)
C(55)	1630(20)	4482(11)	1836(14)	193(15)
C(56)	589(18)	4078(9)	716(12)	144(12)
C(57)	9864(18)	4769(9)	3792(11)	80(9)
C(58)	10806(16)	4605(9)	4219(10)	83(8)
C(59)	11004(17)	4119(9)	4423(10)	91(9)
C(60)	10317(16)	3775(8)	4242(10)	73(8)
C(61)	9399(16)	3998(9)	3858(10)	50(7)
C(62)	8595(19)	3636(9)	3597(12)	76(9)
C(63)	8595(16)	3117(8)	3671(10)	71(8)
C(64)	7771(16)	2881(8)	3371(10)	70(8)
C(65)	6904(19)	3079(9)	2950(11)	84(8)
C(66)	6949(16)	3610(8)	2908(10)	63(8)
C(67)	5992(18)	2835(8)	2626(11)	70(8)
C(68)	5980(20)	2330(11)	2820(14)	145(12)
C(69)	5140(20)	2080(11)	2480(15)	151(12)
C(70)	4306(17)	2262(9)	1995(11)	71(8)
C(71)	4290(20)	2769(10)	1799(12)	122(10)
C(72)	5140(20)	3018(10)	2132(13)	122(10)
C(73)	3439(17)	1980(8)	1684(10)	60(7)
C(74)	3388(16)	1445(8)	1628(10)	71(8)
C(75)	2517(18)	1202(9)	1280(10)	84(9)
C(76)	1700(20)	1439(10)	1018(11)	77(8)
C(77)	2528(16)	2204(8)	1375(10)	59(8)
C(78)	733(19)	1277(9)	709(11)	59(8)
C(79)	579(17)	749(8)	552(10)	76(8)
C(80)	-336(16)	632(8)	185(10)	71(8)
C(81)	-1063(16)	978(8)	-79(10)	76(8)
C(82)	-837(17)	1481(8)	92(10)	58(8)
C(83)	-2100(30)	-28(11)	1640(20)	930(100)
C(84)	-1489(17)	375(7)	1674(12)	236(17)
C(85)	-1862(12)	746(10)	1236(9)	235(18)
C(86)	-1290(20)	1127(8)	1263(10)	330(20)
C(87)	-340(19)	1138(8)	1728(13)	186(15)
C(88)	33(12)	767(11)	2165(10)	241(18)
C(89)	-541(19)	386(8)	2138(9)	210(16)
C(90)	2610(30)	2224(8)	45(13)	480(40)
C(91)	2954(15)	2744(7)	190(7)	248(18)

C(92)	2376(12)	3126(10)	155(9)	194(15)
C(93)	2708(19)	3616(8)	292(10)	380(30)
C(94)	3620(20)	3724(8)	464(9)	234(18)
C(95)	4196(13)	3342(11)	498(9)	280(20)
C(96)	3864(14)	2851(9)	361(9)	252(19)

Table 3. Bond lengths [A] and angles [deg] for rk480ht.

Co(1)-O(1)	1.851(12)
Co(1)-O(2)	1.880(18)
Co(1)-O(3)	1.886(14)
Co(1)-N(1)	1.93(2)
Co(1)-N(2)	1.948(17)
Co(1)-O(4)	1.952(16)
Co(2)-O(5)	1.892(14)
Co(2)-O(6)	1.894(16)
Co(2)-O(7)	1.923(15)
Co(2)-N(3)	1.943(15)
Co(2)-O(8)	1.947(14)
Co(2)-N(4)	1.990(18)
Co(2)-C(29)	2.51(3)
O(1)-C(1)	1.33(2)
O(2)-C(6)	1.34(2)
O(3)-C(15)	1.32(2)
O(4)-C(20)	1.36(2)
O(5)-C(29)	1.28(2)
O(6)-C(34)	1.35(2)
O(7)-C(43)	1.34(3)
O(8)-C(48)	1.30(2)
N(1)-C(57)	1.31(2)
N(1)-C(61)	1.31(2)
N(2)-C(66)	1.38(2)
N(2)-C(62)	1.38(2)
N(3)-C(77)	1.30(2)
N(3)-C(76)	1.41(2)
N(4)-C(78)	1.26(2)
N(4)-C(82)	1.32(2)
C(1)-C(2)	1.40(2)
C(1)-C(6)	1.52(3)
C(2)-C(3)	1.37(3)
C(3)-C(4)	1.39(3)
C(3)-C(7)	1.61(3)
C(4)-C(5)	1.29(2)
C(5)-C(6)	1.49(3)
C(5)-C(11)	1.60(3)
C(7)-C(10)	1.36(3)

C(7)-C(8)	1.53(3)
C(7)-C(9)	1.55(3)
C(11)-C(14)	1.42(3)
C(11)-C(13)	1.51(4)
C(11)-C(12)	1.61(3)
C(15)-C(20)	1.39(2)
C(15)-C(16)	1.43(2)
C(16)-C(17)	1.39(2)
C(16)-C(21)	1.54(3)
C(17)-C(18)	1.34(3)
C(18)-C(19)	1.37(2)
C(18)-C(25)	1.64(5)
C(19)-C(20)	1.34(2)
C(21)-C(23)	1.53(3)
C(21)-C(22)	1.54(3)
C(21)-C(24)	1.59(3)
C(25)-C(27)	1.19(6)
C(25)-C(26)	1.50(5)
C(25)-C(28)	1.65(5)
C(29)-C(34)	1.37(2)
C(29)-C(30)	1.43(3)
C(30)-C(31)	1.42(3)
C(31)-C(32)	1.36(3)
C(31)-C(35)	1.69(4)
C(32)-C(33)	1.46(3)
C(33)-C(34)	1.48(2)
C(33)-C(39)	1.55(3)
C(35)-C(38)	1.41(4)
C(35)-C(37)	1.48(4)
C(35)-C(36)	1.66(4)
C(39)-C(42)	1.48(3)
C(39)-C(40)	1.57(3)
C(39)-C(41)	1.58(3)
C(43)-C(44)	1.37(3)
C(43)-C(48)	1.42(3)
C(44)-C(45)	1.41(3)
C(45)-C(46)	1.45(3)
C(45)-C(49)	1.77(4)
C(46)-C(47)	1.36(3)
C(47)-C(48)	1.48(3)
C(47)-C(53)	1.48(3)
C(49)-C(51)	1.44(4)
C(49)-C(52)	1.51(4)
C(49)-C(50)	1.56(4)
C(53)-C(56)	1.52(3)
C(53)-C(54)	1.62(3)

C(53)-C(55)	1.71(3)
C(57)-C(58)	1.43(3)
C(58)-C(59)	1.37(2)
C(59)-C(60)	1.35(2)
C(60)-C(61)	1.44(2)
C(61)-C(62)	1.50(3)
C(62)-C(63)	1.40(2)
C(63)-C(64)	1.33(2)
C(64)-C(65)	1.37(3)
C(65)-C(66)	1.43(2)
C(65)-C(67)	1.45(3)
C(67)-C(72)	1.40(3)
C(67)-C(68)	1.45(3)
C(68)-C(69)	1.37(3)
C(69)-C(70)	1.37(3)
C(70)-C(73)	1.45(2)
C(70)-C(71)	1.45(3)
C(71)-C(72)	1.38(3)
C(73)-C(77)	1.43(2)
C(73)-C(74)	1.43(2)
C(74)-C(75)	1.40(3)
C(75)-C(76)	1.33(3)
C(76)-C(78)	1.45(3)
C(78)-C(79)	1.45(2)
C(79)-C(80)	1.34(2)
C(80)-C(81)	1.38(2)
C(81)-C(82)	1.40(2)
C(83)-C(84)	1.474(7)
C(84)-C(85)	1.3900
C(84)-C(89)	1.3900
C(85)-C(86)	1.3900
C(86)-C(87)	1.3900
C(87)-C(88)	1.3900
C(88)-C(89)	1.3900
C(90)-C(91)	1.471(6)
C(91)-C(92)	1.3900
C(91)-C(96)	1.3900
C(92)-C(93)	1.3900
C(93)-C(94)	1.3900
C(94)-C(95)	1.3900
C(95)-C(96)	1.3900

O(1)-Co(1)-O(2)	87.8(7)
O(1)-Co(1)-O(3)	90.9(6)
O(2)-Co(1)-O(3)	87.7(7)
O(1)-Co(1)-N(1)	93.9(7)

O(2)-Co(1)-N(1)	94.4(7)
O(3)-Co(1)-N(1)	174.8(7)
O(1)-Co(1)-N(2)	174.9(8)
O(2)-Co(1)-N(2)	92.1(8)
O(3)-Co(1)-N(2)	94.2(7)
N(1)-Co(1)-N(2)	81.0(8)
O(1)-Co(1)-O(4)	88.7(6)
O(2)-Co(1)-O(4)	174.2(7)
O(3)-Co(1)-O(4)	87.6(6)
N(1)-Co(1)-O(4)	90.5(7)
N(2)-Co(1)-O(4)	91.7(7)
O(5)-Co(2)-O(6)	88.7(7)
O(5)-Co(2)-O(7)	179.2(6)
O(6)-Co(2)-O(7)	91.3(7)
O(5)-Co(2)-N(3)	90.2(7)
O(6)-Co(2)-N(3)	174.7(6)
O(7)-Co(2)-N(3)	89.9(6)
O(5)-Co(2)-O(8)	90.6(6)
O(6)-Co(2)-O(8)	90.3(6)
O(7)-Co(2)-O(8)	88.6(6)
N(3)-Co(2)-O(8)	94.8(6)
O(5)-Co(2)-N(4)	90.6(7)
O(6)-Co(2)-N(4)	93.2(7)
O(7)-Co(2)-N(4)	90.2(7)
N(3)-Co(2)-N(4)	81.7(8)
O(8)-Co(2)-N(4)	176.3(8)
O(5)-Co(2)-C(29)	29.9(6)
O(6)-Co(2)-C(29)	61.5(7)
O(7)-Co(2)-C(29)	149.8(8)
N(3)-Co(2)-C(29)	118.5(8)
O(8)-Co(2)-C(29)	79.5(7)
N(4)-Co(2)-C(29)	103.2(8)
C(1)-O(1)-Co(1)	110.7(14)
C(6)-O(2)-Co(1)	109.6(16)
C(15)-O(3)-Co(1)	109.7(14)
C(20)-O(4)-Co(1)	104.3(14)
C(29)-O(5)-Co(2)	102.8(16)
C(34)-O(6)-Co(2)	103.2(14)
C(43)-O(7)-Co(2)	106.5(16)
C(48)-O(8)-Co(2)	104.0(14)
C(57)-N(1)-C(61)	118(2)
C(57)-N(1)-Co(1)	125.4(16)
C(61)-N(1)-Co(1)	115.9(17)
C(66)-N(2)-C(62)	118(2)
C(66)-N(2)-Co(1)	125.2(17)
C(62)-N(2)-Co(1)	116.3(16)

C(77)-N(3)-C(76)	121(2)
C(77)-N(3)-Co(2)	124.3(14)
C(76)-N(3)-Co(2)	114.6(16)
C(78)-N(4)-C(82)	126(2)
C(78)-N(4)-Co(2)	111.9(17)
C(82)-N(4)-Co(2)	120.7(17)
O(1)-C(1)-C(2)	125(2)
O(1)-C(1)-C(6)	114(2)
C(2)-C(1)-C(6)	120(3)
C(3)-C(2)-C(1)	116(2)
C(2)-C(3)-C(4)	126(3)
C(2)-C(3)-C(7)	117(3)
C(4)-C(3)-C(7)	117(2)
C(5)-C(4)-C(3)	122(3)
C(4)-C(5)-C(6)	120(3)
C(4)-C(5)-C(11)	126(3)
C(6)-C(5)-C(11)	114(2)
O(2)-C(6)-C(5)	132(3)
O(2)-C(6)-C(1)	113(2)
C(5)-C(6)-C(1)	115(3)
C(10)-C(7)-C(8)	102(3)
C(10)-C(7)-C(9)	123(3)
C(8)-C(7)-C(9)	105(2)
C(10)-C(7)-C(3)	106(3)
C(8)-C(7)-C(3)	113(3)
C(9)-C(7)-C(3)	107(2)
C(14)-C(11)-C(13)	113(3)
C(14)-C(11)-C(5)	107(3)
C(13)-C(11)-C(5)	107(3)
C(14)-C(11)-C(12)	120(3)
C(13)-C(11)-C(12)	104(3)
C(5)-C(11)-C(12)	105(3)
O(3)-C(15)-C(20)	116(2)
O(3)-C(15)-C(16)	126(2)
C(20)-C(15)-C(16)	118(3)
C(17)-C(16)-C(15)	117(2)
C(17)-C(16)-C(21)	125(2)
C(15)-C(16)-C(21)	118(2)
C(18)-C(17)-C(16)	124(3)
C(17)-C(18)-C(19)	117(3)
C(17)-C(18)-C(25)	124(3)
C(19)-C(18)-C(25)	118(3)
C(20)-C(19)-C(18)	123(3)
C(19)-C(20)-O(4)	120(2)
C(19)-C(20)-C(15)	120(3)
O(4)-C(20)-C(15)	120(2)

C(23)-C(21)-C(22)	107(2)
C(23)-C(21)-C(16)	112(2)
C(22)-C(21)-C(16)	111(2)
C(23)-C(21)-C(24)	112(2)
C(22)-C(21)-C(24)	107(2)
C(16)-C(21)-C(24)	107(2)
C(27)-C(25)-C(26)	127(6)
C(27)-C(25)-C(18)	117(5)
C(26)-C(25)-C(18)	104(4)
C(27)-C(25)-C(28)	114(5)
C(26)-C(25)-C(28)	93(4)
C(18)-C(25)-C(28)	95(4)
O(5)-C(29)-C(34)	122(3)
O(5)-C(29)-C(30)	124(3)
C(34)-C(29)-C(30)	114(3)
O(5)-C(29)-Co(2)	47.3(12)
C(34)-C(29)-Co(2)	76.6(16)
C(30)-C(29)-Co(2)	166(2)
C(31)-C(30)-C(29)	123(3)
C(32)-C(31)-C(30)	121(3)
C(32)-C(31)-C(35)	115(3)
C(30)-C(31)-C(35)	122(3)
C(31)-C(32)-C(33)	121(2)
C(32)-C(33)-C(34)	113(2)
C(32)-C(33)-C(39)	124(2)
C(34)-C(33)-C(39)	123(2)
O(6)-C(34)-C(29)	116(2)
O(6)-C(34)-C(33)	116(2)
C(29)-C(34)-C(33)	127(3)
C(38)-C(35)-C(37)	136(4)
C(38)-C(35)-C(36)	94(3)
C(37)-C(35)-C(36)	95(3)
C(38)-C(35)-C(31)	108(3)
C(37)-C(35)-C(31)	114(3)
C(36)-C(35)-C(31)	92(2)
C(42)-C(39)-C(33)	112(2)
C(42)-C(39)-C(40)	109(2)
C(33)-C(39)-C(40)	109(2)
C(42)-C(39)-C(41)	112(2)
C(33)-C(39)-C(41)	108(2)
C(40)-C(39)-C(41)	107(2)
O(7)-C(43)-C(44)	117(3)
O(7)-C(43)-C(48)	116(2)
C(44)-C(43)-C(48)	126(3)
C(43)-C(44)-C(45)	111(3)
C(44)-C(45)-C(46)	123(3)

C(44)-C(45)-C(49)	120(3)
C(46)-C(45)-C(49)	117(3)
C(47)-C(46)-C(45)	127(3)
C(46)-C(47)-C(48)	110(3)
C(46)-C(47)-C(53)	127(3)
C(48)-C(47)-C(53)	123(3)
O(8)-C(48)-C(43)	122(2)
O(8)-C(48)-C(47)	116(2)
C(43)-C(48)-C(47)	122(3)
C(51)-C(49)-C(52)	122(3)
C(51)-C(49)-C(50)	102(3)
C(52)-C(49)-C(50)	120(3)
C(51)-C(49)-C(45)	108(3)
C(52)-C(49)-C(45)	100(3)
C(50)-C(49)-C(45)	104(3)
C(47)-C(53)-C(56)	116(2)
C(47)-C(53)-C(54)	105(2)
C(56)-C(53)-C(54)	109(2)
C(47)-C(53)-C(55)	108(2)
C(56)-C(53)-C(55)	115(2)
C(54)-C(53)-C(55)	103(2)
N(1)-C(57)-C(58)	118(2)
C(59)-C(58)-C(57)	122(2)
C(60)-C(59)-C(58)	122(2)
C(59)-C(60)-C(61)	111(2)
N(1)-C(61)-C(60)	129(2)
N(1)-C(61)-C(62)	115(2)
C(60)-C(61)-C(62)	115(2)
N(2)-C(62)-C(63)	120(2)
N(2)-C(62)-C(61)	109(2)
C(63)-C(62)-C(61)	130(3)
C(64)-C(63)-C(62)	118(2)
C(63)-C(64)-C(65)	128(2)
C(64)-C(65)-C(66)	111(2)
C(64)-C(65)-C(67)	129(2)
C(66)-C(65)-C(67)	119(3)
N(2)-C(66)-C(65)	124(2)
C(72)-C(67)-C(65)	128(2)
C(72)-C(67)-C(68)	117(3)
C(65)-C(67)-C(68)	116(3)
C(69)-C(68)-C(67)	116(3)
C(70)-C(69)-C(68)	127(3)
C(69)-C(70)-C(73)	123(3)
C(69)-C(70)-C(71)	118(3)
C(73)-C(70)-C(71)	118(2)
C(72)-C(71)-C(70)	115(3)

C(71)-C(72)-C(67)	127(3)
C(77)-C(73)-C(74)	112(2)
C(77)-C(73)-C(70)	124(2)
C(74)-C(73)-C(70)	124(2)
C(75)-C(74)-C(73)	121(2)
C(76)-C(75)-C(74)	123(3)
C(75)-C(76)-N(3)	117(3)
C(75)-C(76)-C(78)	134(3)
N(3)-C(76)-C(78)	109(2)
N(3)-C(77)-C(73)	126(2)
N(4)-C(78)-C(76)	121(2)
N(4)-C(78)-C(79)	121(2)
C(76)-C(78)-C(79)	115(3)
C(80)-C(79)-C(78)	113(2)
C(79)-C(80)-C(81)	125(2)
C(80)-C(81)-C(82)	118(2)
N(4)-C(82)-C(81)	116(2)
C(85)-C(84)-C(89)	120.0
C(85)-C(84)-C(83)	119.9(6)
C(89)-C(84)-C(83)	120.1(6)
C(86)-C(85)-C(84)	120.0
C(85)-C(86)-C(87)	120.0
C(86)-C(87)-C(88)	120.0
C(89)-C(88)-C(87)	120.0
C(88)-C(89)-C(84)	120.0
C(92)-C(91)-C(96)	120.0
C(92)-C(91)-C(90)	120.2(6)
C(96)-C(91)-C(90)	119.8(6)
C(91)-C(92)-C(93)	120.0
C(94)-C(93)-C(92)	120.0
C(93)-C(94)-C(95)	120.0
C(96)-C(95)-C(94)	120.0
C(95)-C(96)-C(91)	120.0

Table 4. Anisotropic displacement parameters (A^2 x 10^3) for rk480ht.

The anisotropic displacement factor exponent takes the form:

-2 pi^2 [h^2 a*^2 U11 + ... + 2 h k a* b* U12]

	U11	U22	U33	U23	U13	U12
Co(1)	68(3)	55(3)	75(3)	-2(3)	33(3)	1(2)
Co(2)	81(3)	51(3)	78(3)	3(2)	43(3)	1(3)
O(1)	95(13)	33(9)	50(11)	7(9)	42(10)	11(9)
O(2)	85(14)	77(13)	121(18)	0(13)	50(13)	16(11)
O(3)	76(13)	48(10)	34(10)	2(9)	10(10)	4(9)
O(4)	62(13)	74(11)	77(14)	23(10)	30(11)	11(10)
O(5)	92(13)	35(9)	64(13)	17(9)	42(11)	8(10)
O(6)	107(15)	69(11)	96(14)	-25(11)	81(13)	-46(11)
O(7)	69(12)	71(12)	67(13)	-15(10)	38(11)	-35(10)
O(8)	88(13)	62(11)	72(13)	6(10)	62(12)	14(9)
N(1)	160(20)	27(13)	75(17)	3(12)	85(18)	-28(14)
N(2)	66(16)	83(15)	75(17)	7(14)	41(15)	-42(14)
N(3)	37(13)	35(11)	16(11)	0(10)	7(10)	-2(11)
N(4)	49(16)	85(16)	67(17)	4(14)	17(14)	-2(14)

Table 5. Hydrogen coordinates (x 10^4) and isotropic displacement parameters (A^2 x 10^3) for rk480ht.

	x	y	z	U(eq)
H(2)	7600	6193	2613	87
H(4)	6753	5714	970	99
H(8A)	7337	7274	1915	299
H(8B)	7685	6844	2391	299
H(8C)	6622	6999	2007	299
H(9A)	7545	6494	1029	240
H(9B)	8309	6641	1694	240
H(9C)	7608	7048	1245	240
H(10A)	5856	6950	1049	241
H(10B)	5734	6454	1311	241
H(10C)	5852	6430	777	241
H(12A)	6555	4050	1241	302
H(12B)	5828	4303	624	302
H(12C)	6010	4532	1214	302
H(13A)	6143	5112	378	338
H(13B)	6534	4657	214	338
H(13C)	7146	5142	497	338
H(14A)	8486	4777	1509	281
H(14B)	8053	4322	1066	281
H(14C)	8193	4290	1690	281
H(17)	4656	5391	3107	91
H(19)	7201	5009	4414	78
H(22A)	3935	4595	1444	214
H(22B)	4415	4351	2079	214
H(22C)	5023	4501	1836	214
H(23A)	3531	5134	2208	189
H(23B)	3221	5231	1549	189
H(23C)	3720	5657	2030	189
H(24A)	4574	5531	1433	198

H(24B)	5564	5285	1860	198
H(24C)	5292	5766	2064	198
H(26A)	4478	5356	4294	474
H(26B)	4488	4978	3854	474
H(26C)	4329	5552	3700	474
H(27A)	6640	5565	5053	430
H(27B)	6699	5028	4840	430
H(27C)	5997	5133	5024	430
H(28A)	5354	6051	3794	432
H(28B)	6187	6151	4458	432
H(28C)	5153	6129	4287	432
H(30)	159	2953	-901	95
H(32)	-2155	3646	-1237	108
H(36A)	-752	4361	-1230	417
H(36B)	-302	4294	-1595	417
H(36C)	105	3999	-996	417
H(37A)	-2596	3762	-2259	450
H(37B)	-2029	4201	-2301	450
H(37C)	-2088	4159	-1744	450
H(38A)	-611	3081	-1839	383
H(38B)	22	3562	-1614	383
H(38C)	-837	3523	-2283	383
H(40A)	-3377	2724	-824	166
H(40B)	-3047	2736	-153	166
H(40C)	-2429	2467	-332	166
H(41A)	-2772	3887	-881	247
H(41B)	-3317	3815	-577	247
H(41C)	-3557	3476	-1120	247
H(42A)	-1647	3754	349	188
H(42B)	-1270	3206	555	188
H(42C)	-2241	3362	436	188
H(44)	284	2433	2208	104
H(46)	1024	3901	2250	126
H(50A)	1914	3173	3653	366
H(50B)	1552	3700	3696	366
H(50C)	1908	3625	3280	366
H(51A)	583	2909	3519	298
H(51B)	814	2606	3119	298
H(51C)	-225	2766	2861	298
H(52A)	-786	3569	2358	304
H(52B)	-63	3942	2380	304
H(52C)	-179	3918	2915	304
H(54A)	2185	3756	1080	213
H(54B)	2539	3524	1706	213
H(54C)	2736	4090	1657	213
H(55A)	1805	4753	1685	289

H(55B)	2147	4395	2231	289
H(55C)	1104	4584	1850	289
H(56A)	609	3815	481	216
H(56B)	726	4393	610	216
H(56C)	-27	4091	641	216
H(57)	9740	5092	3636	96
H(58)	11297	4832	4361	100
H(59)	11627	4024	4692	109
H(60)	10422	3438	4352	87
H(63)	9152	2942	3923	85
H(64)	7783	2542	3455	84
H(66)	6385	3785	2681	76
H(68)	6501	2184	3154	174
H(69)	5126	1750	2590	181
H(71)	3755	2916	1476	146
H(72)	5156	3344	2014	147
H(74)	3939	1257	1824	86
H(75)	2512	856	1231	101
H(77)	2503	2551	1394	70
H(79)	1062	517	689	91
H(80)	-493	295	103	86
H(81)	-1680	879	-359	91
H(82)	-1296	1725	-26	70
H(83A)	-2649	116	1597	1400
H(83B)	-1763	-222	2006	1400
H(83C)	-2285	-242	1309	1400
H(85)	-2495	738	925	282
H(86)	-1537	1375	971	394
H(87)	44	1393	1746	223
H(88)	667	774	2476	289
H(89)	-292	138	2431	251
H(90A)	2529	2125	-321	716
H(90B)	2014	2203	1	716
H(90C)	3052	2006	362	716
H(92)	1767	3054	41	232
H(93)	2321	3872	269	458
H(94)	3840	4052	555	280
H(95)	4805	3414	612	336
H(96)	4251	2596	384	302

Complete Structure Data of:

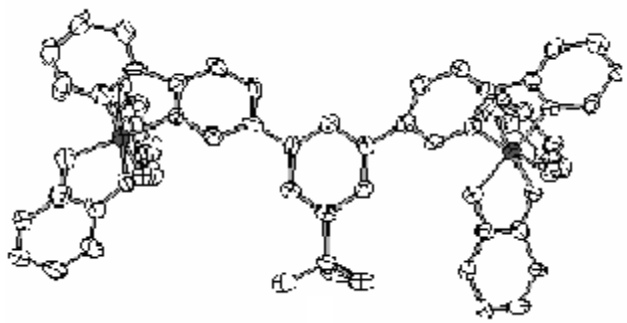

	x	y	z	U(eq)
Co(1)	4375(1)	-1522(1)	3817(1)	78(1)
Co(2)	5351(1)	-620(1)	9033(1)	92(1)
N(1)	4889(5)	-996(5)	3348(6)	80(3)
N(2)	4964(5)	-1136(6)	4407(5)	73(3)
N(3)	6027(5)	-12(5)	9308(6)	84(3)
N(4)	5704(6)	-517(7)	8342(5)	81(3)
O(1)	3930(4)	-2070(5)	4299(3)	90(3)
O(2)	4858(3)	-2335(5)	3723(3)	82(2)
O(3)	3850(4)	-766(4)	3895(3)	85(2)
O(4)	3820(4)	-1825(4)	3230(3)	87(3)
O(5)	5045(4)	-753(5)	9723(3)	101(3)
O(6)	5830(4)	-1431(4)	9175(3)	98(3)
O(7)	4845(5)	157(4)	8888(3)	93(3)
O(8)	4689(5)	-1162(4)	8697(3)	94(3)
C(1)	4061(7)	-2689(9)	4228(5)	86(4)
C(2)	3755(6)	-3259(11)	4448(5)	106(5)
C(3)	3917(8)	-3934(8)	4329(7)	103(5)
C(4)	4415(8)	-4037(8)	4012(6)	98(4)
C(5)	4730(7)	-3540(10)	3772(5)	82(4)

C(6)	4562(9)	-2854(9)	3903(6)	93(5)
C(7)	3565(10)	-4517(9)	4592(8)	143(6)
C(8)	4003(12)	-4903(13)	4980(10)	329(19)
C(9)	2994(11)	-4323(8)	4839(11)	302(18)
C(10)	3375(11)	-5002(11)	4141(10)	291(14)
C(11)	5232(8)	-3718(7)	3393(7)	110(4)
C(12)	5298(7)	-4486(7)	3303(6)	152(6)
C(13)	5856(7)	-3442(8)	3636(7)	164(7)
C(14)	5039(7)	-3432(7)	2830(5)	160(7)
C(15)	3318(8)	-892(9)	3553(6)	74(4)
C(16)	2826(10)	-446(7)	3561(5)	88(4)
C(17)	2266(8)	-533(8)	3201(7)	87(4)
C(18)	2236(7)	-1127(10)	2869(5)	92(4)
C(19)	2723(9)	-1597(7)	2875(6)	84(4)
C(20)	3303(9)	-1473(8)	3212(6)	80(4)
C(21)	1718(9)	-50(8)	3129(8)	125(5)
C(22)	1084(9)	-315(9)	3053(11)	280(15)
C(23)	1768(13)	491(17)	3489(14)	420(30)
C(24)	1713(12)	359(14)	2587(13)	360(20)
C(25)	2660(7)	-2284(8)	2551(6)	103(4)
C(26)	3160(7)	-2297(6)	2152(5)	132(5)
C(27)	2016(7)	-2341(7)	2186(7)	182(7)
C(28)	2769(7)	-2883(6)	2972(5)	134(5)
C(29)	5246(7)	-1341(9)	9909(6)	98(4)
C(30)	5058(7)	-1640(10)	10423(7)	125(5)
C(31)	5249(7)	-2261(10)	10603(7)	107(5)
C(32)	5659(8)	-2618(7)	10276(7)	115(5)
C(33)	5870(7)	-2396(9)	9789(7)	108(4)
C(34)	5669(7)	-1720(8)	9611(6)	86(4)
C(35)	5089(12)	-2576(10)	11141(8)	158(7)
C(36)	4734(10)	-2110(9)	11468(7)	229(11)
C(37)	5736(12)	-2653(14)	11518(9)	303(16)
C(38)	4862(11)	-3240(11)	11099(7)	259(14)
C(39)	6331(9)	-2801(8)	9444(7)	117(5)
C(40)	6958(8)	-2417(8)	9478(7)	161(6)
C(41)	6463(7)	-3527(7)	9686(6)	173(7)
C(42)	6040(8)	-2859(8)	8848(7)	178(7)
C(43)	4262(9)	-74(14)	8698(5)	103(6)
C(44)	3795(11)	433(10)	8612(5)	110(5)
C(45)	3192(13)	265(11)	8410(7)	135(9)
C(46)	3080(8)	-438(17)	8326(6)	147(8)
C(47)	3555(13)	-976(11)	8411(6)	114(6)
C(48)	4164(12)	-774(12)	8604(6)	105(6)
C(49)	2611(10)	778(15)	8330(12)	194(10)
C(50)	2709(11)	1119(13)	7834(12)	315(18)
C(51)	1987(10)	394(11)	8256(12)	317(18)

C(52)	2659(11)	1270(14)	8792(11)	326(19)
C(53)	3451(9)	-1745(13)	8345(9)	158(7)
C(54)	2761(9)	-1932(10)	8151(9)	248(11)
C(55)	3852(8)	-2026(8)	7903(7)	191(8)
C(56)	3623(10)	-2157(8)	8882(9)	203(9)
C(57)	4844(7)	-978(7)	2796(7)	92(4)
C(58)	5232(8)	-607(8)	2509(6)	93(4)
C(59)	5681(8)	-201(8)	2785(8)	106(5)
C(60)	5731(6)	-207(7)	3374(7)	99(4)
C(61)	5325(7)	-604(8)	3640(6)	78(4)
C(62)	5376(7)	-660(8)	4266(6)	83(4)
C(63)	5782(6)	-335(6)	4658(8)	93(4)
C(64)	5793(6)	-526(7)	5204(6)	93(4)
C(65)	5397(7)	-1043(8)	5364(6)	81(4)
C(66)	4975(6)	-1311(6)	4941(8)	82(4)
C(67)	6126(9)	183(9)	9853(8)	117(5)
C(68)	6555(10)	665(11)	10012(7)	135(6)
C(69)	6871(8)	990(7)	9632(9)	120(5)
C(70)	6778(8)	783(10)	9078(8)	118(5)
C(71)	6361(8)	263(8)	8918(7)	94(5)
C(72)	6178(9)	-67(8)	8362(6)	89(4)
C(73)	6503(6)	60(7)	7900(8)	96(4)
C(74)	6326(8)	-304(9)	7440(6)	92(4)
C(75)	5848(8)	-772(8)	7414(6)	83(4)
C(76)	5549(6)	-869(6)	7885(8)	89(4)
C(77)	5418(5)	-1326(9)	5934(6)	75(3)
C(78)	5633(5)	-916(6)	6385(8)	78(3)
C(79)	5637(6)	-1193(9)	6926(6)	77(3)
C(80)	5441(6)	-1874(9)	6974(5)	86(4)
C(81)	5240(5)	-2289(7)	6536(7)	75(4)
C(82)	5236(5)	-2003(8)	6027(6)	85(4)
C(83)	5025(8)	-3019(7)	6588(6)	103(4)
C(84)	4343(8)	-3094(8)	6370(9)	237(12)
C(85)	5430(9)	-3485(7)	6301(7)	188(8)
C(86)	5093(9)	-3266(7)	7175(7)	191(8)

Table 3. Bond lengths [A] and angles [deg] for kp15ht.

Co(1)-O(4)	1.848(8)
Co(1)-O(3)	1.872(8)
Co(1)-O(1)	1.909(8)
Co(1)-O(2)	1.918(8)
Co(1)-N(2)	1.947(9)
Co(1)-N(1)	1.955(9)
Co(2)-O(7)	1.872(8)
Co(2)-O(8)	1.878(9)
Co(2)-O(5)	1.879(8)
Co(2)-O(6)	1.891(8)
Co(2)-N(4)	1.922(10)
Co(2)-N(3)	1.929(10)
N(1)-C(57)	1.331(13)
N(1)-C(61)	1.345(13)
N(2)-C(66)	1.337(13)
N(2)-C(62)	1.349(12)
N(3)-C(71)	1.355(13)
N(3)-C(67)	1.368(15)
N(4)-C(76)	1.313(12)
N(4)-C(72)	1.337(15)
O(1)-C(1)	1.253(14)
O(2)-C(6)	1.293(13)
O(3)-C(15)	1.355(13)
O(4)-C(20)	1.297(15)
O(5)-C(29)	1.287(14)
O(6)-C(34)	1.278(13)
O(7)-C(43)	1.358(17)
O(8)-C(48)	1.351(17)
C(1)-C(2)	1.419(17)
C(1)-C(6)	1.435(17)
C(2)-C(3)	1.397(16)
C(3)-C(4)	1.393(15)
C(3)-C(7)	1.540(18)
C(4)-C(5)	1.347(15)
C(5)-C(6)	1.426(16)
C(5)-C(11)	1.526(16)
C(7)-C(8)	1.46(2)
C(7)-C(9)	1.47(2)

C(7)-C(10)	1.47(2)
C(11)-C(14)	1.489(16)
C(11)-C(13)	1.497(16)
C(11)-C(12)	1.521(15)
C(15)-C(16)	1.366(15)
C(15)-C(20)	1.399(15)
C(16)-C(17)	1.411(15)
C(17)-C(18)	1.407(15)
C(17)-C(21)	1.498(17)
C(18)-C(19)	1.385(15)
C(19)-C(20)	1.428(17)
C(19)-C(25)	1.550(16)
C(21)-C(23)	1.37(2)
C(21)-C(22)	1.442(18)
C(21)-C(24)	1.54(2)
C(25)-C(26)	1.517(15)
C(25)-C(28)	1.551(15)
C(25)-C(27)	1.557(16)
C(29)-C(34)	1.421(16)
C(29)-C(30)	1.470(17)
C(30)-C(31)	1.334(15)
C(31)-C(32)	1.427(16)
C(31)-C(35)	1.513(19)
C(32)-C(33)	1.378(16)
C(33)-C(34)	1.436(15)
C(33)-C(39)	1.572(18)
C(35)-C(38)	1.38(2)
C(35)-C(36)	1.47(2)
C(35)-C(37)	1.58(2)
C(39)-C(42)	1.513(17)
C(39)-C(40)	1.528(17)
C(39)-C(41)	1.543(16)
C(43)-C(48)	1.39(2)
C(43)-C(44)	1.403(19)
C(44)-C(45)	1.37(2)
C(45)-C(46)	1.40(2)
C(45)-C(49)	1.59(3)
C(46)-C(47)	1.46(2)
C(47)-C(48)	1.39(2)
C(47)-C(53)	1.52(2)
C(49)-C(50)	1.41(2)
C(49)-C(52)	1.47(3)
C(49)-C(51)	1.52(3)
C(53)-C(56)	1.54(2)
C(53)-C(55)	1.543(18)
C(53)-C(54)	1.54(2)

C(57)-C(58)	1.349(14)
C(58)-C(59)	1.361(15)
C(59)-C(60)	1.419(15)
C(60)-C(61)	1.375(14)
C(61)-C(62)	1.511(16)
C(62)-C(63)	1.368(14)
C(63)-C(64)	1.373(14)
C(64)-C(65)	1.396(14)
C(65)-C(66)	1.391(14)
C(65)-C(77)	1.483(15)
C(67)-C(68)	1.339(18)
C(68)-C(69)	1.357(17)
C(69)-C(70)	1.393(17)
C(70)-C(71)	1.376(17)
C(71)-C(72)	1.505(18)
C(72)-C(73)	1.401(16)
C(73)-C(74)	1.340(14)
C(74)-C(75)	1.365(15)
C(75)-C(76)	1.380(14)
C(75)-C(79)	1.469(16)
C(77)-C(78)	1.390(13)
C(77)-C(82)	1.399(14)
C(78)-C(79)	1.415(14)
C(79)-C(80)	1.400(14)
C(80)-C(81)	1.364(14)
C(81)-C(82)	1.352(13)
C(81)-C(83)	1.504(15)
C(83)-C(85)	1.478(16)
C(83)-C(86)	1.494(16)
C(83)-C(84)	1.502(17)
O(4)-Co(1)-O(3)	89.3(4)
O(4)-Co(1)-O(1)	88.3(3)
O(3)-Co(1)-O(1)	92.0(4)
O(4)-Co(1)-O(2)	87.3(4)
O(3)-Co(1)-O(2)	175.8(4)
O(1)-Co(1)-O(2)	85.5(4)
O(4)-Co(1)-N(2)	175.7(5)
O(3)-Co(1)-N(2)	88.3(4)
O(1)-Co(1)-N(2)	95.3(5)
O(2)-Co(1)-N(2)	95.3(3)
O(4)-Co(1)-N(1)	94.2(5)
O(3)-Co(1)-N(1)	91.7(3)
O(1)-Co(1)-N(1)	175.6(4)
O(2)-Co(1)-N(1)	91.0(4)
N(2)-Co(1)-N(1)	82.3(6)
O(7)-Co(2)-O(8)	88.8(4)

O(7)-Co(2)-O(5)	91.6(4)
O(8)-Co(2)-O(5)	89.4(3)
O(7)-Co(2)-O(6)	177.5(4)
O(8)-Co(2)-O(6)	88.7(4)
O(5)-Co(2)-O(6)	87.6(4)
O(7)-Co(2)-N(4)	91.4(4)
O(8)-Co(2)-N(4)	91.7(6)
O(5)-Co(2)-N(4)	176.8(4)
O(6)-Co(2)-N(4)	89.4(4)
O(7)-Co(2)-N(3)	87.9(4)
O(8)-Co(2)-N(3)	174.1(5)
O(5)-Co(2)-N(3)	95.6(6)
O(6)-Co(2)-N(3)	94.5(4)
N(4)-Co(2)-N(3)	83.4(7)
C(57)-N(1)-C(61)	119.0(11)
C(57)-N(1)-Co(1)	127.9(13)
C(61)-N(1)-Co(1)	113.0(11)
C(66)-N(2)-C(62)	118.4(11)
C(66)-N(2)-Co(1)	123.7(12)
C(62)-N(2)-Co(1)	117.9(12)
C(71)-N(3)-C(67)	121.6(14)
C(71)-N(3)-Co(2)	115.7(12)
C(67)-N(3)-Co(2)	122.4(15)
C(76)-N(4)-C(72)	119.6(11)
C(76)-N(4)-Co(2)	126.3(13)
C(72)-N(4)-Co(2)	113.9(13)
C(1)-O(1)-Co(1)	108.8(9)
C(6)-O(2)-Co(1)	108.4(10)
C(15)-O(3)-Co(1)	105.6(9)
C(20)-O(4)-Co(1)	109.2(8)
C(29)-O(5)-Co(2)	107.2(8)
C(34)-O(6)-Co(2)	109.2(9)
C(43)-O(7)-Co(2)	106.6(12)
C(48)-O(8)-Co(2)	109.3(12)
O(1)-C(1)-C(2)	125.6(16)
O(1)-C(1)-C(6)	118.7(16)
C(2)-C(1)-C(6)	115.7(14)
C(3)-C(2)-C(1)	121.5(13)
C(4)-C(3)-C(2)	118.1(13)
C(4)-C(3)-C(7)	124.1(17)
C(2)-C(3)-C(7)	117.7(18)
C(5)-C(4)-C(3)	125.7(13)
C(4)-C(5)-C(6)	115.2(13)
C(4)-C(5)-C(11)	121.0(16)
C(6)-C(5)-C(11)	123.8(16)
O(2)-C(6)-C(5)	120.8(18)

O(2)-C(6)-C(1)	115.6(16)
C(5)-C(6)-C(1)	123.6(14)
C(8)-C(7)-C(9)	112.0(19)
C(8)-C(7)-C(10)	104.8(18)
C(9)-C(7)-C(10)	107.2(19)
C(8)-C(7)-C(3)	109.7(17)
C(9)-C(7)-C(3)	116.5(16)
C(10)-C(7)-C(3)	105.9(15)
C(14)-C(11)-C(13)	111.9(13)
C(14)-C(11)-C(12)	104.9(13)
C(13)-C(11)-C(12)	108.4(13)
C(14)-C(11)-C(5)	108.9(12)
C(13)-C(11)-C(5)	109.7(13)
C(12)-C(11)-C(5)	113.0(13)
O(3)-C(15)-C(16)	118.2(16)
O(3)-C(15)-C(20)	118.1(16)
C(16)-C(15)-C(20)	123.6(15)
C(15)-C(16)-C(17)	121.2(13)
C(18)-C(17)-C(16)	115.7(12)
C(18)-C(17)-C(21)	117.5(18)
C(16)-C(17)-C(21)	126.7(18)
C(19)-C(18)-C(17)	123.3(13)
C(18)-C(19)-C(20)	120.0(14)
C(18)-C(19)-C(25)	122.7(17)
C(20)-C(19)-C(25)	117.2(15)
O(4)-C(20)-C(15)	116.3(16)
O(4)-C(20)-C(19)	127.8(14)
C(15)-C(20)-C(19)	115.9(15)
C(23)-C(21)-C(22)	111(2)
C(23)-C(21)-C(17)	113.8(17)
C(22)-C(21)-C(17)	120.2(14)
C(23)-C(21)-C(24)	98.0(19)
C(22)-C(21)-C(24)	99.1(17)
C(17)-C(21)-C(24)	111.0(16)
C(26)-C(25)-C(28)	109.9(12)
C(26)-C(25)-C(19)	108.1(11)
C(28)-C(25)-C(19)	108.5(11)
C(26)-C(25)-C(27)	106.2(12)
C(28)-C(25)-C(27)	112.3(12)
C(19)-C(25)-C(27)	111.9(13)
O(5)-C(29)-C(34)	119.5(14)
O(5)-C(29)-C(30)	122.3(16)
C(34)-C(29)-C(30)	118.2(14)
C(31)-C(30)-C(29)	122.3(14)
C(30)-C(31)-C(32)	116.3(14)
C(30)-C(31)-C(35)	124.1(17)

C(32)-C(31)-C(35)	119.4(18)
C(33)-C(32)-C(31)	127.0(13)
C(32)-C(33)-C(34)	115.4(14)
C(32)-C(33)-C(39)	125.5(16)
C(34)-C(33)-C(39)	119.0(15)
O(6)-C(34)-C(29)	115.7(14)
O(6)-C(34)-C(33)	123.6(15)
C(29)-C(34)-C(33)	120.7(14)
C(38)-C(35)-C(36)	114.8(19)
C(38)-C(35)-C(31)	115.2(17)
C(36)-C(35)-C(31)	113.1(16)
C(38)-C(35)-C(37)	103.5(19)
C(36)-C(35)-C(37)	102.6(18)
C(31)-C(35)-C(37)	105.7(18)
C(42)-C(39)-C(40)	110.8(14)
C(42)-C(39)-C(41)	109.5(14)
C(40)-C(39)-C(41)	107.7(13)
C(42)-C(39)-C(33)	109.1(13)
C(40)-C(39)-C(33)	108.8(13)
C(41)-C(39)-C(33)	110.8(13)
O(7)-C(43)-C(48)	120(2)
O(7)-C(43)-C(44)	115(2)
C(48)-C(43)-C(44)	124.9(18)
C(45)-C(44)-C(43)	120.8(18)
C(44)-C(45)-C(46)	115(2)
C(44)-C(45)-C(49)	126(2)
C(46)-C(45)-C(49)	118(2)
C(45)-C(46)-C(47)	125.2(19)
C(48)-C(47)-C(46)	117.1(17)
C(48)-C(47)-C(53)	116(2)
C(46)-C(47)-C(53)	127(2)
O(8)-C(48)-C(47)	129(2)
O(8)-C(48)-C(43)	114(2)
C(47)-C(48)-C(43)	116.7(18)
C(50)-C(49)-C(52)	110(3)
C(50)-C(49)-C(51)	110(2)
C(52)-C(49)-C(51)	113(2)
C(50)-C(49)-C(45)	102.3(19)
C(52)-C(49)-C(45)	109(2)
C(51)-C(49)-C(45)	112(2)
C(47)-C(53)-C(56)	114.0(16)
C(47)-C(53)-C(55)	109.6(16)
C(56)-C(53)-C(55)	107.6(18)
C(47)-C(53)-C(54)	113(2)
C(56)-C(53)-C(54)	105.6(17)
C(55)-C(53)-C(54)	106.8(16)

N(1)-C(57)-C(58)	123.4(12)
C(57)-C(58)-C(59)	119.9(13)
C(58)-C(59)-C(60)	117.5(12)
C(61)-C(60)-C(59)	119.6(12)
N(1)-C(61)-C(60)	120.5(11)
N(1)-C(61)-C(62)	117.3(14)
C(60)-C(61)-C(62)	122.0(17)
N(2)-C(62)-C(63)	121.6(11)
N(2)-C(62)-C(61)	108.9(15)
C(63)-C(62)-C(61)	129.3(16)
C(62)-C(63)-C(64)	119.1(12)
C(63)-C(64)-C(65)	121.1(12)
C(66)-C(65)-C(64)	115.4(12)
C(66)-C(65)-C(77)	119.9(15)
C(64)-C(65)-C(77)	124.7(16)
N(2)-C(66)-C(65)	124.1(11)
C(68)-C(67)-N(3)	120.1(17)
C(67)-C(68)-C(69)	120.5(18)
C(68)-C(69)-C(70)	119.3(16)
C(71)-C(70)-C(69)	120.3(15)
N(3)-C(71)-C(70)	118.0(15)
N(3)-C(71)-C(72)	110.5(17)
C(70)-C(71)-C(72)	131.5(17)
N(4)-C(72)-C(73)	121.7(11)
N(4)-C(72)-C(71)	115.7(18)
C(73)-C(72)-C(71)	123(2)
C(74)-C(73)-C(72)	116.9(12)
C(73)-C(74)-C(75)	122.1(13)
C(74)-C(75)-C(76)	117.8(13)
C(74)-C(75)-C(79)	124.8(16)
C(76)-C(75)-C(79)	117.4(18)
N(4)-C(76)-C(75)	121.9(12)
C(78)-C(77)-C(82)	119.3(11)
C(78)-C(77)-C(65)	119.4(16)
C(82)-C(77)-C(65)	121.3(15)
C(77)-C(78)-C(79)	118.4(11)
C(80)-C(79)-C(78)	117.8(12)
C(80)-C(79)-C(75)	121.9(15)
C(78)-C(79)-C(75)	120.2(16)
C(81)-C(80)-C(79)	124.5(12)
C(82)-C(81)-C(80)	115.9(11)
C(82)-C(81)-C(83)	119.5(15)
C(80)-C(81)-C(83)	124.6(14)
C(81)-C(82)-C(77)	124.0(12)
C(85)-C(83)-C(86)	104.4(13)
C(85)-C(83)-C(81)	109.9(12)

C(86)-C(83)-C(81)	112.6(12)
C(85)-C(83)-C(84)	111.8(14)
C(86)-C(83)-C(84)	107.1(14)
C(81)-C(83)-C(84)	110.9(12)

Table 4. Anisotropic displacement parameters (A^2 x 10^3) for kp15ht.

The anisotropic displacement factor exponent takes the form:

-2 pi^2 [h^2 a*^2 U11 + ... + 2 h k a* b* U12]

	U11	U22	U33	U23	U13	U12
Co(1)	98(1)	76(1)	60(1)	-2(1)	9(1)	-9(1)
Co(2)	126(2)	94(1)	60(1)	4(1)	24(1)	14(1)
N(1)	89(8)	70(7)	79(10)	4(7)	1(7)	-24(6)
N(2)	75(8)	90(8)	53(9)	0(6)	4(6)	-5(7)
N(3)	104(9)	81(8)	63(8)	-23(8)	-10(8)	9(7)
N(4)	102(9)	78(8)	66(10)	5(7)	16(7)	-9(7)
O(1)	123(7)	73(6)	76(6)	-5(5)	25(5)	0(6)
O(2)	84(6)	87(6)	75(6)	6(5)	14(5)	1(5)
O(3)	99(7)	78(6)	76(6)	-21(5)	0(5)	-6(5)
O(4)	86(7)	91(7)	81(6)	-17(5)	-2(5)	10(5)
O(5)	134(8)	105(7)	68(6)	10(6)	32(5)	41(6)
O(6)	140(7)	103(7)	56(5)	11(5)	28(5)	24(5)
O(7)	124(8)	77(6)	77(6)	-3(5)	5(6)	18(6)
O(8)	116(8)	89(7)	82(6)	-9(5)	30(6)	-7(6)
C(1)	88(11)	118(16)	57(9)	6(11)	34(8)	9(12)
C(2)	111(12)	148(16)	66(9)	-11(11)	39(8)	-28(13)
C(3)	121(14)	66(12)	125(13)	-13(10)	27(11)	-8(10)
C(4)	100(12)	89(13)	109(11)	-2(10)	33(9)	21(10)
C(5)	94(11)	82(13)	73(9)	24(10)	21(8)	-6(11)
C(6)	136(16)	68(14)	69(10)	25(9)	-16(11)	-19(12)
C(7)	189(18)	98(13)	150(16)	-6(13)	53(14)	-50(14)
C(8)	360(40)	300(30)	300(30)	220(30)	-90(30)	-110(30)
C(9)	370(30)	103(14)	510(40)	-9(17)	370(30)	-17(16)
C(10)	360(30)	230(20)	310(30)	-60(20)	140(30)	-210(20)

C(11)	120(14)	87(12)	129(14)	11(10)	41(12)	4(10)
C(12)	187(16)	117(13)	160(14)	11(11)	49(12)	44(11)
C(13)	88(12)	153(14)	260(20)	-20(14)	53(13)	-2(11)
C(14)	245(18)	170(14)	78(10)	36(11)	72(11)	78(13)
C(15)	73(13)	77(12)	76(12)	15(11)	22(9)	3(11)
C(16)	100(13)	82(12)	83(11)	-3(8)	17(11)	-33(12)
C(17)	90(14)	56(11)	115(12)	5(10)	18(11)	14(10)
C(18)	85(12)	94(12)	97(11)	5(10)	11(8)	-10(11)
C(19)	93(12)	78(12)	84(11)	3(10)	19(11)	4(12)
C(20)	124(18)	70(13)	48(9)	-14(9)	11(11)	-26(12)
C(21)	134(16)	70(11)	168(16)	-2(11)	1(12)	19(12)
C(22)	103(16)	145(17)	590(50)	-30(20)	30(20)	0(14)
C(23)	330(30)	400(40)	490(50)	-300(40)	-200(30)	290(30)
C(24)	300(30)	320(30)	490(50)	290(40)	170(30)	180(30)
C(25)	102(13)	111(13)	98(11)	-37(11)	28(10)	-11(10)
C(26)	173(15)	118(12)	102(11)	-36(9)	5(11)	-11(10)
C(27)	116(13)	168(15)	246(19)	-82(14)	-48(14)	-4(11)
C(28)	214(16)	81(10)	112(11)	6(9)	40(11)	-10(10)
C(29)	127(13)	106(13)	62(12)	-9(12)	19(9)	8(11)
C(30)	192(16)	99(13)	91(13)	-6(11)	52(11)	15(12)
C(31)	124(13)	106(14)	99(14)	-10(13)	51(10)	7(10)
C(32)	170(15)	88(11)	88(11)	44(11)	21(11)	-1(11)
C(33)	142(14)	81(13)	102(14)	16(10)	17(11)	7(10)
C(34)	122(12)	82(13)	55(10)	1(10)	17(9)	6(9)
C(35)	250(20)	151(17)	91(13)	46(13)	83(16)	-8(16)
C(36)	380(30)	196(18)	144(16)	58(14)	180(20)	77(19)
C(37)	270(30)	470(50)	160(20)	140(20)	0(20)	-70(30)
C(38)	430(40)	190(20)	175(19)	-3(16)	140(20)	-180(20)
C(39)	133(15)	112(13)	109(13)	1(11)	27(12)	34(12)
C(40)	140(15)	162(15)	188(17)	24(12)	46(13)	15(13)
C(41)	243(19)	108(12)	184(16)	43(12)	98(14)	77(12)
C(42)	250(20)	162(15)	134(16)	-47(13)	61(15)	26(14)
C(43)	97(16)	170(20)	42(9)	11(12)	10(9)	28(19)
C(44)	86(13)	158(18)	83(11)	-6(10)	2(9)	-35(16)
C(45)	200(30)	100(14)	118(14)	-5(12)	59(16)	-47(18)
C(46)	69(13)	260(30)	119(13)	26(17)	25(10)	26(19)
C(47)	103(17)	140(20)	101(11)	9(11)	7(11)	-47(17)
C(48)	140(30)	92(17)	86(12)	-4(11)	39(13)	11(17)
C(49)	124(19)	230(30)	230(30)	40(20)	33(18)	100(20)
C(50)	280(30)	330(30)	360(40)	200(30)	130(30)	190(30)
C(51)	92(16)	220(20)	640(60)	0(30)	40(20)	20(16)
C(52)	280(30)	370(40)	340(40)	-170(30)	90(30)	100(30)
C(53)	123(17)	170(20)	190(20)	-46(17)	75(15)	-58(15)
C(54)	154(19)	240(20)	350(30)	-110(20)	33(19)	-70(17)
C(55)	188(18)	179(16)	219(19)	-70(15)	74(16)	-56(14)
C(56)	280(30)	121(14)	220(20)	-4(15)	103(19)	-48(15)

C(57)	122(13)	107(11)	43(10)	-15(9)	-16(9)	7(10)
C(58)	106(12)	107(11)	69(10)	31(10)	30(11)	-6(9)
C(59)	117(13)	110(12)	91(15)	30(10)	8(10)	-22(10)
C(60)	92(11)	124(12)	81(12)	-3(9)	8(10)	-34(9)
C(61)	75(10)	93(10)	71(13)	10(10)	28(10)	-14(9)
C(62)	88(11)	89(10)	77(14)	18(10)	25(10)	-25(9)
C(63)	114(12)	87(10)	75(12)	-13(10)	-9(10)	-37(8)
C(64)	123(12)	108(12)	47(11)	6(8)	2(8)	-26(10)
C(65)	94(11)	86(11)	65(13)	-2(11)	10(11)	-6(9)
C(66)	92(11)	94(10)	62(10)	2(10)	20(9)	-9(8)
C(67)	136(16)	124(14)	90(17)	-21(11)	11(11)	21(11)
C(68)	167(19)	163(19)	79(13)	0(14)	31(14)	18(14)
C(69)	151(15)	111(12)	91(13)	-37(13)	-21(12)	7(11)
C(70)	124(13)	117(14)	114(17)	-10(11)	22(11)	-15(11)
C(71)	109(13)	78(11)	100(16)	39(12)	39(13)	10(10)
C(72)	130(14)	95(12)	36(12)	-19(10)	-23(11)	9(11)
C(73)	132(12)	98(11)	59(10)	5(11)	16(11)	-13(9)
C(74)	133(14)	113(12)	34(11)	-16(9)	21(9)	-7(11)
C(75)	122(13)	87(12)	43(13)	4(10)	17(10)	13(10)
C(76)	154(13)	66(9)	46(9)	-18(9)	3(11)	-24(8)
C(77)	77(9)	100(13)	47(11)	2(12)	-3(7)	7(8)
C(78)	96(10)	68(9)	70(11)	1(10)	11(8)	-20(7)
C(79)	104(10)	77(12)	53(12)	-10(10)	27(8)	16(9)
C(80)	134(12)	70(11)	57(11)	2(10)	25(8)	12(9)
C(81)	105(10)	70(11)	53(10)	8(11)	22(8)	9(8)
C(82)	120(11)	73(11)	62(12)	4(9)	7(8)	-14(8)
C(83)	172(16)	54(10)	85(11)	21(9)	18(10)	-16(10)
C(84)	150(16)	122(14)	410(30)	86(17)	-101(19)	-83(13)
C(85)	300(20)	69(10)	216(19)	-24(12)	126(17)	-10(13)
C(86)	310(20)	120(13)	146(16)	54(12)	23(15)	-48(14)

Table 5. Hydrogen coordinates (x 10^4) and isotropic displacement parameters (A^2 x 10^3) for kp15ht.

	x	y	z	U(eq)
H(2A)	3440	-3180	4677	127
H(4A)	4539	-4488	3961	117
H(8A)	4165	-4608	5280	494
H(8B)	4344	-5070	4790	494
H(8C)	3788	-5285	5125	494
H(9A)	3101	-4009	5139	453
H(9B)	2804	-4727	4977	453
H(9C)	2703	-4108	4562	453
H(10A)	3160	-5385	4284	437
H(10B)	3742	-5163	3984	437
H(10C)	3099	-4776	3859	437
H(12A)	4899	-4673	3155	228
H(12B)	5434	-4704	3651	228
H(12C)	5603	-4567	3047	228
H(13A)	5820	-2959	3703	247
H(13B)	6163	-3519	3381	247
H(13C)	5986	-3673	3979	247
H(14A)	4986	-2944	2856	241
H(14B)	4649	-3638	2681	241
H(14C)	5358	-3531	2591	241
H(16A)	2860	-79	3808	105
H(18A)	1870	-1209	2634	110
H(22A)	977	-501	3397	421
H(22B)	1055	-670	2776	421
H(22C)	798	50	2935	421
H(23A)	1819	322	3864	636
H(23B)	1394	767	3433	636
H(23C)	2126	765	3425	636

H(24A)	1628	54	2276	540
H(24B)	2116	573	2572	540
H(24C)	1392	706	2573	540
H(26A)	3112	-1902	1913	198
H(26B)	3114	-2707	1931	198
H(26C)	3569	-2290	2358	198
H(27A)	1978	-1974	1920	272
H(27B)	1681	-2310	2419	272
H(27C)	1992	-2774	1996	272
H(28A)	2438	-2887	3210	201
H(28B)	3167	-2823	3192	201
H(28C)	2770	-3311	2775	201
H(30A)	4797	-1387	10629	150
H(32A)	5800	-3047	10405	138
H(36A)	4676	-2321	11817	343
H(36B)	4330	-2016	11268	343
H(36C)	4962	-1688	11533	343
H(37A)	5662	-2843	11871	455
H(37B)	5930	-2210	11573	455
H(37C)	6008	-2952	11339	455
H(38A)	4801	-3408	11462	389
H(38B)	5159	-3527	10939	389
H(38C)	4468	-3245	10867	389
H(40A)	6886	-1954	9349	242
H(40B)	7234	-2645	9250	242
H(40C)	7147	-2411	9856	242
H(41A)	6639	-3490	10067	259
H(41B)	6755	-3759	9477	259
H(41C)	6077	-3782	9665	259
H(42A)	5969	-2407	8694	267
H(42B)	5647	-3099	8836	267
H(42C)	6320	-3106	8635	267
H(44A)	3897	889	8693	132
H(46A)	2670	-573	8207	176
H(50A)	2363	1423	7729	472
H(50B)	2740	787	7545	472
H(50C)	3092	1380	7889	472
H(51A)	1652	711	8145	476
H(51B)	1913	181	8601	476
H(51C)	2001	47	7976	476
H(52A)	2334	1609	8726	490
H(52B)	3063	1490	8820	490
H(52C)	2612	1031	9132	490
H(54A)	2723	-2422	8109	372
H(54B)	2635	-1714	7801	372
H(54C)	2496	-1778	8421	372

H(55A)	3760	-2504	7841	287
H(55B)	4290	-1971	8031	287
H(55C)	3754	-1777	7563	287
H(56A)	3526	-2633	8815	304
H(56B)	3387	-1987	9168	304
H(56C)	4065	-2108	8998	304
H(57A)	4528	-1234	2597	111
H(58A)	5194	-628	2123	111
H(59A)	5945	70	2595	127
H(60A)	6038	56	3579	119
H(63A)	6046	11	4555	112
H(64A)	6068	-308	5472	112
H(66A)	4683	-1631	5036	99
H(67A)	5896	-20	10114	140
H(68A)	6638	777	10386	162
H(69A)	7145	1348	9739	144
H(70A)	6999	996	8816	141
H(73A)	6825	381	7912	115
H(74A)	6535	-235	7127	111
H(76A)	5228	-1193	7879	107
H(78A)	5770	-469	6333	94
H(80A)	5448	-2057	7329	103
H(82A)	5104	-2273	5720	102
H(84A)	4219	-3565	6398	356
H(84B)	4283	-2953	5988	356
H(84C)	4092	-2811	6584	356
H(85A)	5290	-3950	6336	282
H(85B)	5857	-3444	6466	282
H(85C)	5405	-3363	5916	282
H(86A)	4963	-3737	7186	286
H(86B)	4835	-2991	7390	286
H(86C)	5525	-3228	7329	286

Complete Structure Data of:

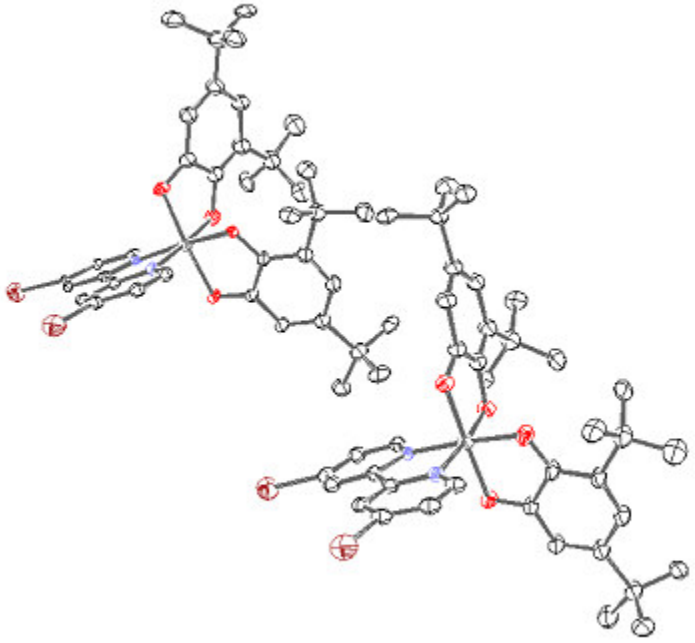

	x	y	z	U(eq)
Co(1)	7981(1)	1243(1)	3198(1)	19(1)
O(1)	7163(3)	757(2)	2601(2)	21(1)
O(2)	8593(3)	2076(2)	1995(2)	21(1)
O(3)	6281(3)	2125(2)	3319(2)	22(1)
O(4)	8703(3)	1868(2)	3686(2)	21(1)
O(5)	13574(3)	-1589(2)	3299(2)	29(1)
O(6)	6919(3)	-1492(2)	7185(2)	27(1)
Cl(1)	9983(3)	-1918(2)	2373(2)	114(1)
Cl(2)	7508(3)	-1834(2)	3874(2)	83(1)
N(1)	9742(4)	310(3)	3154(2)	20(1)
N(2)	7513(4)	339(3)	4441(2)	18(1)
C(1)	7030(4)	1402(3)	1788(3)	19(1)
C(2)	6185(5)	1413(3)	1233(3)	22(1)
C(3)	6140(5)	2099(3)	368(3)	25(1)
C(4)	6996(5)	2801(3)	26(3)	24(1)
C(5)	7846(5)	2835(3)	525(3)	22(1)
C(6)	7841(5)	2139(3)	1425(3)	19(1)
C(7)	5223(5)	2176(4)	-266(3)	26(1)

C(8)	4354(6)	1388(4)	195(4)	39(1)
C(9)	6157(6)	2079(4)	-1202(4)	39(1)
C(10)	4197(5)	3133(4)	-459(4)	36(1)
C(11)	8749(5)	3601(3)	143(3)	25(1)
C(12)	8301(6)	4180(4)	807(4)	34(1)
C(13)	8582(7)	4277(4)	-835(4)	44(2)
C(14)	10312(5)	3104(4)	87(4)	34(1)
C(15)	6563(5)	2898(3)	3349(3)	18(1)
C(16)	5646(5)	3787(3)	3219(3)	22(1)
C(17)	6085(5)	4505(3)	3303(3)	24(1)
C(18)	7406(5)	4368(3)	3486(3)	25(1)
C(19)	8307(5)	3484(3)	3600(3)	22(1)
C(20)	7892(5)	2750(3)	3537(3)	21(1)
C(21)	4190(5)	3958(3)	2993(3)	21(1)
C(22)	4415(5)	3779(4)	2083(3)	27(1)
C(23)	3314(5)	3273(4)	3805(3)	28(1)
C(24)	3349(5)	4983(3)	2885(4)	29(1)
C(25)	7802(5)	5203(4)	3565(4)	28(1)
C(26)	7549(7)	6130(4)	2689(4)	48(2)
C(27)	6850(7)	5412(4)	4424(4)	45(2)
C(28)	9347(6)	5014(4)	3583(5)	50(2)
C(29)	10853(5)	361(3)	2397(3)	24(1)
C(30)	12116(5)	-277(3)	2457(3)	25(1)
C(31)	12278(5)	-1001(3)	3300(3)	22(1)
C(32)	11132(5)	-1073(3)	4078(3)	22(1)
C(33)	9892(5)	-407(3)	3971(3)	19(1)
C(34)	8591(4)	-383(3)	4734(3)	18(1)
C(35)	8461(5)	-1020(3)	5631(3)	20(1)
C(36)	7170(5)	-925(3)	6271(3)	22(1)
C(37)	6057(5)	-207(3)	5975(3)	25(1)
C(38)	6258(5)	421(3)	5065(3)	23(1)
C(39)	13800(6)	-2359(4)	4155(4)	40(1)
C(40)	8058(5)	-2261(3)	7509(3)	27(1)
C(41)	8191(9)	-1405(5)	2660(5)	72(2)

Table 3. Bond lengths [A] and angles [deg] for sbsb.

Co(1)-O(3)	1.865(3)
Co(1)-O(2)	1.873(3)
Co(1)-O(4)	1.881(3)
Co(1)-O(1)	1.915(3)
Co(1)-N(2)	1.931(4)
Co(1)-N(1)	1.937(4)
O(1)-C(1)	1.302(5)
O(2)-C(6)	1.322(5)
O(3)-C(15)	1.354(5)
O(4)-C(20)	1.345(5)
O(5)-C(31)	1.358(5)
O(5)-C(39)	1.441(6)
O(6)-C(36)	1.357(5)
O(6)-C(40)	1.444(6)
Cl(1)-C(41)	1.748(8)
Cl(2)-C(41)	1.753(8)
N(1)-C(33)	1.352(6)
N(1)-C(29)	1.363(6)
N(2)-C(38)	1.356(6)
N(2)-C(34)	1.357(6)
C(1)-C(2)	1.410(6)
C(1)-C(6)	1.454(6)
C(2)-C(3)	1.371(6)
C(3)-C(4)	1.446(6)
C(3)-C(7)	1.531(6)
C(4)-C(5)	1.374(6)
C(5)-C(6)	1.411(6)
C(5)-C(11)	1.554(6)
C(7)-C(10)	1.519(7)
C(7)-C(9)	1.533(7)
C(7)-C(8)	1.549(7)
C(11)-C(13)	1.521(7)
C(11)-C(14)	1.535(7)
C(11)-C(12)	1.537(7)
C(15)-C(16)	1.396(6)
C(15)-C(20)	1.411(6)
C(16)-C(17)	1.403(6)
C(16)-C(21)	1.557(6)
C(17)-C(18)	1.403(7)
C(18)-C(19)	1.385(7)
C(18)-C(25)	1.548(6)
C(19)-C(20)	1.395(6)

C(21)-C(22)	1.521(6)
C(21)-C(24)	1.540(6)
C(21)-C(23)	1.542(6)
C(25)-C(27)	1.499(7)
C(25)-C(28)	1.519(7)
C(25)-C(26)	1.580(7)
C(29)-C(30)	1.369(7)
C(30)-C(31)	1.386(6)
C(31)-C(32)	1.402(6)
C(32)-C(33)	1.377(6)
C(33)-C(34)	1.491(6)
C(34)-C(35)	1.368(6)
C(35)-C(36)	1.396(6)
C(36)-C(37)	1.379(6)
C(37)-C(38)	1.381(6)

O(3)-Co(1)-O(2)	89.17(13)
O(3)-Co(1)-O(4)	87.61(13)
O(2)-Co(1)-O(4)	88.27(13)
O(3)-Co(1)-O(1)	87.73(13)
O(2)-Co(1)-O(1)	86.53(13)
O(4)-Co(1)-O(1)	173.06(13)
O(3)-Co(1)-N(2)	95.19(14)
O(2)-Co(1)-N(2)	175.22(14)
O(4)-Co(1)-N(2)	89.94(14)
O(1)-Co(1)-N(2)	95.59(14)
O(3)-Co(1)-N(1)	176.42(14)
O(2)-Co(1)-N(1)	93.64(14)
O(4)-Co(1)-N(1)	90.24(14)
O(1)-Co(1)-N(1)	94.66(14)
N(2)-Co(1)-N(1)	81.94(15)
C(1)-O(1)-Co(1)	107.1(3)
C(6)-O(2)-Co(1)	109.6(3)
C(15)-O(3)-Co(1)	107.9(3)
C(20)-O(4)-Co(1)	106.3(3)
C(31)-O(5)-C(39)	118.2(4)
C(36)-O(6)-C(40)	117.6(4)
C(33)-N(1)-C(29)	118.6(4)
C(33)-N(1)-Co(1)	115.8(3)
C(29)-N(1)-Co(1)	125.4(3)
C(38)-N(2)-C(34)	118.1(4)
C(38)-N(2)-Co(1)	125.6(3)
C(34)-N(2)-Co(1)	115.9(3)
O(1)-C(1)-C(2)	124.2(4)
O(1)-C(1)-C(6)	117.3(4)
C(2)-C(1)-C(6)	118.5(4)

C(3)-C(2)-C(1)	120.6(4)
C(2)-C(3)-C(4)	118.8(4)
C(2)-C(3)-C(7)	123.9(4)
C(4)-C(3)-C(7)	117.3(4)
C(5)-C(4)-C(3)	123.9(4)
C(4)-C(5)-C(6)	116.2(4)
C(4)-C(5)-C(11)	122.8(4)
C(6)-C(5)-C(11)	121.0(4)
O(2)-C(6)-C(5)	123.8(4)
O(2)-C(6)-C(1)	114.3(4)
C(5)-C(6)-C(1)	121.9(4)
C(10)-C(7)-C(3)	110.1(4)
C(10)-C(7)-C(9)	108.9(4)
C(3)-C(7)-C(9)	110.1(4)
C(10)-C(7)-C(8)	108.1(4)
C(3)-C(7)-C(8)	111.6(4)
C(9)-C(7)-C(8)	108.1(4)
C(13)-C(11)-C(14)	108.1(4)
C(13)-C(11)-C(12)	108.8(4)
C(14)-C(11)-C(12)	109.5(4)
C(13)-C(11)-C(5)	111.7(4)
C(14)-C(11)-C(5)	108.9(4)
C(12)-C(11)-C(5)	109.7(4)
O(3)-C(15)-C(16)	124.9(4)
O(3)-C(15)-C(20)	114.9(4)
C(16)-C(15)-C(20)	120.2(4)
C(15)-C(16)-C(17)	117.6(4)
C(15)-C(16)-C(21)	120.4(4)
C(17)-C(16)-C(21)	122.0(4)
C(18)-C(17)-C(16)	122.7(4)
C(19)-C(18)-C(17)	118.7(4)
C(19)-C(18)-C(25)	122.2(4)
C(17)-C(18)-C(25)	119.1(4)
C(18)-C(19)-C(20)	120.0(4)
O(4)-C(20)-C(19)	122.2(4)
O(4)-C(20)-C(15)	117.1(4)
C(19)-C(20)-C(15)	120.7(4)
C(22)-C(21)-C(24)	108.6(4)
C(22)-C(21)-C(23)	109.6(4)
C(24)-C(21)-C(23)	108.2(4)
C(22)-C(21)-C(16)	109.6(4)
C(24)-C(21)-C(16)	111.6(4)
C(23)-C(21)-C(16)	109.1(4)
C(27)-C(25)-C(28)	111.1(5)
C(27)-C(25)-C(18)	108.4(4)
C(28)-C(25)-C(18)	113.2(4)

C(27)-C(25)-C(26)	107.5(5)
C(28)-C(25)-C(26)	105.9(4)
C(18)-C(25)-C(26)	110.5(4)
N(1)-C(29)-C(30)	121.5(4)
C(29)-C(30)-C(31)	119.8(4)
O(5)-C(31)-C(30)	115.8(4)
O(5)-C(31)-C(32)	125.1(4)
C(30)-C(31)-C(32)	119.1(4)
C(33)-C(32)-C(31)	118.1(4)
N(1)-C(33)-C(32)	122.7(4)
N(1)-C(33)-C(34)	112.9(4)
C(32)-C(33)-C(34)	124.4(4)
N(2)-C(34)-C(35)	122.6(4)
N(2)-C(34)-C(33)	112.5(4)
C(35)-C(34)-C(33)	124.9(4)
C(34)-C(35)-C(36)	118.9(4)
O(6)-C(36)-C(37)	116.5(4)
O(6)-C(36)-C(35)	124.5(4)
C(37)-C(36)-C(35)	119.0(4)
C(36)-C(37)-C(38)	119.4(4)
N(2)-C(38)-C(37)	121.9(4)
Cl(1)-C(41)-Cl(2)	111.1(5)

Symmetry transformations used to generate equivalent atoms:

Table 4. Anisotropic displacement parameters (A^2 x 10^3) for sbsb.
The anisotropic displacement factor exponent takes the form:
-2 pi^2 [h^2 a*^2 U11 + ... + 2 h k a* b* U12]

	U11	U22	U33	U23	U13	U12
Co(1)	18(1)	20(1)	17(1)	-4(1)	-2(1)	-4(1)
O(1)	20(2)	23(2)	18(2)	-4(1)	-3(1)	-6(1)
O(2)	19(2)	25(2)	19(2)	-5(1)	-4(1)	-7(1)
O(3)	17(2)	24(2)	23(2)	-6(1)	-6(1)	-4(1)
O(4)	16(2)	24(2)	23(2)	-7(1)	-6(1)	-2(1)
O(5)	20(2)	31(2)	24(2)	-8(2)	3(1)	2(1)
O(6)	24(2)	34(2)	14(2)	-2(1)	2(1)	-9(2)
Cl(1)	83(2)	132(2)	122(2)	-50(2)	5(2)	-36(2)
Cl(2)	108(2)	75(1)	66(1)	-20(1)	-6(1)	-38(1)
N(1)	21(2)	25(2)	14(2)	-6(2)	3(2)	-10(2)
N(2)	16(2)	21(2)	16(2)	-6(2)	-3(2)	-4(2)
C(1)	16(2)	20(2)	17(2)	-8(2)	2(2)	-3(2)
C(2)	21(2)	26(2)	22(2)	-9(2)	1(2)	-11(2)
C(3)	18(2)	32(3)	23(3)	-10(2)	1(2)	-8(2)
C(4)	18(2)	28(3)	19(2)	-4(2)	-1(2)	-4(2)
C(5)	17(2)	22(2)	23(2)	-6(2)	-2(2)	-2(2)
C(6)	15(2)	19(2)	18(2)	-4(2)	1(2)	-4(2)
C(7)	20(2)	36(3)	23(2)	-8(2)	-5(2)	-10(2)
C(8)	44(3)	49(3)	34(3)	-9(3)	-16(3)	-24(3)
C(9)	35(3)	60(4)	28(3)	-25(3)	-4(2)	-8(3)
C(10)	23(3)	49(3)	32(3)	-9(3)	-4(2)	-9(2)
C(11)	15(2)	27(3)	25(3)	2(2)	-4(2)	-10(2)
C(12)	33(3)	26(3)	38(3)	-8(2)	-1(2)	-12(2)
C(13)	48(4)	43(3)	33(3)	12(3)	-17(3)	-26(3)
C(14)	22(3)	38(3)	30(3)	-4(2)	3(2)	-13(2)
C(15)	18(2)	23(2)	14(2)	-5(2)	-4(2)	-6(2)
C(16)	19(2)	27(2)	16(2)	-5(2)	-1(2)	-5(2)
C(17)	19(2)	23(2)	26(3)	-10(2)	2(2)	-6(2)
C(18)	26(3)	29(3)	22(2)	-11(2)	1(2)	-11(2)
C(19)	15(2)	30(3)	21(2)	-9(2)	0(2)	-8(2)
C(20)	15(2)	26(2)	17(2)	-7(2)	0(2)	-3(2)
C(21)	14(2)	22(2)	24(2)	-7(2)	-4(2)	-1(2)
C(22)	20(3)	38(3)	25(3)	-10(2)	-7(2)	-6(2)
C(23)	20(3)	35(3)	30(3)	-11(2)	-1(2)	-10(2)

C(24)	21(3)	29(3)	34(3)	-8(2)	-9(2)	-2(2)
C(25)	27(3)	33(3)	31(3)	-16(2)	-2(2)	-11(2)
C(26)	54(4)	41(3)	48(4)	-8(3)	-9(3)	-21(3)
C(27)	48(4)	49(4)	48(4)	-29(3)	1(3)	-16(3)
C(28)	39(4)	38(3)	82(5)	-24(3)	-21(3)	-7(3)
C(29)	28(3)	26(2)	16(2)	-6(2)	-1(2)	-10(2)
C(30)	21(2)	32(3)	19(2)	-13(2)	7(2)	-7(2)
C(31)	20(2)	24(2)	23(2)	-11(2)	-4(2)	-3(2)
C(32)	21(2)	24(2)	18(2)	-7(2)	2(2)	-6(2)
C(33)	17(2)	23(2)	15(2)	-8(2)	1(2)	-6(2)
C(34)	15(2)	21(2)	18(2)	-8(2)	0(2)	-6(2)
C(35)	17(2)	20(2)	20(2)	-5(2)	-3(2)	-5(2)
C(36)	26(3)	26(2)	15(2)	-4(2)	-5(2)	-11(2)
C(37)	14(2)	33(3)	25(3)	-9(2)	1(2)	-7(2)
C(38)	17(2)	27(2)	22(2)	-8(2)	-2(2)	-3(2)
C(39)	29(3)	37(3)	32(3)	-1(2)	-4(2)	8(2)
C(40)	29(3)	29(3)	14(2)	0(2)	-4(2)	-6(2)
C(41)	83(6)	47(4)	70(5)	-17(4)	3(4)	-15(4)

Table 5. Hydrogen coordinates (x 10^4) and isotropic displacement parameters (A^2 x 10^3) for sbsb.

	x	y	z	U(eq)
H(2A)	5642	941	1461	26
H(4A)	6968	3266	-579	29
H(8A)	3782	1418	810	58
H(8B)	4997	765	275	58
H(8C)	3733	1484	-209	58
H(9A)	5558	2170	-1619	58
H(9B)	6772	1444	-1089	58
H(9C)	6737	2560	-1498	58
H(10A)	3615	3210	138	55
H(10B)	3587	3165	-842	55
H(10C)	4727	3642	-797	55
H(12A)	8853	4674	553	51
H(12B)	8470	3758	1428	51
H(12C)	7294	4477	861	51
H(13A)	7611	4649	-804	66
H(13B)	8791	3911	-1253	66
H(13C)	9239	4706	-1080	66
H(14A)	10584	2708	-309	51
H(14B)	10457	2705	720	51
H(14C)	10894	3584	-185	51
H(17A)	5462	5109	3234	28
H(19A)	9208	3377	3722	26
H(22A)	3496	3874	1950	41
H(22B)	4935	3125	2146	41
H(22C)	4958	4222	1566	41
H(23A)	2370	3409	3689	43
H(23B)	3229	3358	4398	43
H(23C)	3786	2616	3843	43
H(24A)	3881	5430	2364	44
H(24B)	3197	5108	3468	44
H(24C)	2434	5062	2755	44
H(26A)	6532	6375	2728	72
H(26B)	7988	5977	2109	72
H(26C)	7971	6612	2686	72
H(27A)	7064	4878	4987	68
H(27B)	5863	5505	4407	68
H(27C)	7002	5990	4442	68

H(28A)	9556	5588	3571	75
H(28B)	9945	4843	3033	75
H(28C)	9537	4491	4158	75
H(29A)	10749	851	1815	29
H(30A)	12879	-225	1921	30
H(32A)	11210	-1567	4662	27
H(35A)	9237	-1519	5814	24
H(37A)	5159	-145	6394	30
H(38A)	5496	926	4870	28
H(39A)	13542	-2107	4671	61
H(39B)	14799	-2682	4074	61
H(39C)	13215	-2812	4301	61
H(40A)	8275	-2723	7189	40
H(40B)	7775	-2574	8189	40
H(40C)	8898	-2009	7368	40
H(41A)	7660	-1550	2329	87
H(41B)	8067	-706	2447	87

Complete Structure Data of:

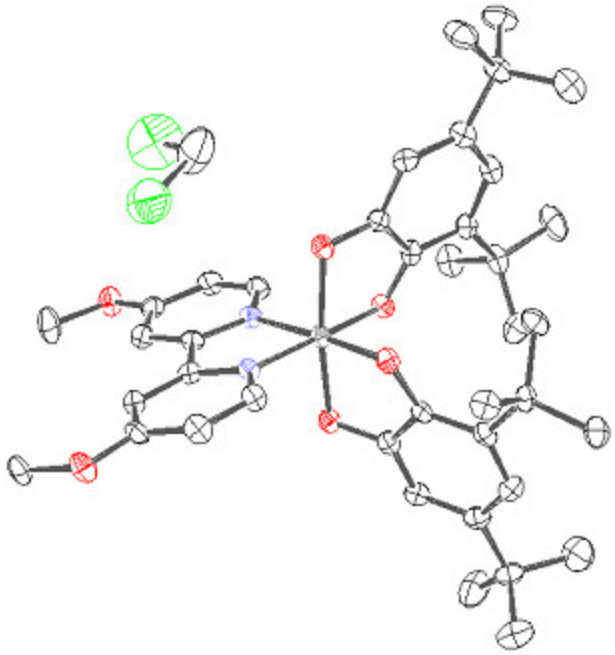

	x	y	z	U(eq)
Co(1)	2974(1)	1476(1)	1619(1)	24(1)
Br(1)	6861(1)	-1095(1)	819(1)	42(1)
Br(2)	2087(1)	-1380(1)	3371(1)	39(1)
N(1)	4062(7)	739(4)	1314(3)	23(1)
N(2)	2656(7)	680(4)	2157(3)	16(1)
O(1)	1429(6)	1017(4)	1161(3)	22(2)
O(2)	3259(7)	2191(4)	1029(3)	29(2)
O(3)	1994(6)	2153(4)	1980(3)	24(2)
O(4)	4516(6)	1958(4)	2035(3)	24(2)
C(1)	4786(9)	800(6)	860(4)	26(2)
C(2)	5612(10)	279(5)	704(4)	26(2)
C(3)	5727(9)	-360(5)	1035(4)	26(2)
C(4)	5035(9)	-456(6)	1507(4)	23(2)
C(5)	4163(9)	86(5)	1631(4)	21(1)

C(6)	3338(9)	58(5)	2117(4)	19(1)
C(7)	3184(9)	-552(6)	2469(4)	23(2)
C(8)	2251(9)	-520(5)	2864(4)	24(2)
C(9)	1562(10)	89(5)	2930(4)	25(2)
C(10)	1795(9)	692(6)	2563(4)	21(2)
C(11)	1308(9)	1402(6)	715(4)	22(1)
C(12)	232(9)	1208(6)	324(4)	24(2)
C(13)	118(8)	1631(6)	-142(4)	26(1)
C(14)	1180(9)	2271(6)	-230(4)	27(2)
C(15)	2241(9)	2478(5)	135(4)	27(1)
C(16)	2307(9)	2066(6)	633(4)	26(1)
C(17)	-1018(9)	1481(5)	-618(4)	30(2)
C(18)	-2186(10)	874(6)	-400(5)	41(3)
C(19)	-561(11)	1120(7)	-1134(4)	37(3)
C(20)	-1630(10)	2253(5)	-734(5)	32(3)
C(21)	3333(9)	3203(5)	61(4)	33(2)
C(22)	4708(9)	2917(7)	89(5)	40(3)
C(23)	3102(12)	3557(7)	-512(4)	48(3)
C(24)	3261(12)	3811(6)	520(4)	36(3)
C(25)	2411(8)	3228(5)	2705(4)	29(1)
C(26)	2802(8)	2647(5)	2357(4)	26(1)
C(27)	3366(8)	3673(6)	3073(4)	28(2)
C(28)	4708(8)	3564(6)	3102(4)	29(1)
C(29)	5105(10)	3031(6)	2721(4)	29(2)
C(30)	4188(8)	2547(6)	2349(4)	26(1)
C(31)	954(8)	3384(5)	2700(4)	32(2)
C(32)	-5(10)	2615(5)	2802(5)	27(3)
C(33)	560(11)	3649(7)	2112(4)	37(3)
C(34)	680(11)	4007(6)	3142(5)	36(3)
C(35)	5748(9)	4036(5)	3513(4)	32(2)
C(36)	6791(10)	4541(7)	3186(5)	40(3)
C(37)	5187(11)	4554(6)	3926(5)	40(3)
C(38)	6495(11)	3441(6)	3843(5)	45(3)
Co(2)	2822(2)	883(1)	6900(1)	26(1)
Br(3)	6705(1)	-1722(1)	6152(1)	40(1)
Br(4)	1846(1)	-1940(1)	8667(1)	35(1)
N(3)	3921(7)	140(4)	6610(3)	20(1)
N(4)	2403(7)	47(4)	7423(3)	17(1)
O(5)	1300(6)	505(4)	6398(3)	21(2)
O(6)	3277(6)	1607(4)	6351(3)	19(2)
O(7)	1847(6)	1599(4)	7228(3)	29(2)
O(8)	4291(6)	1337(4)	7382(3)	28(2)
C(39)	4694(9)	214(6)	6168(4)	21(2)
C(40)	5526(10)	-311(5)	6027(4)	21(2)
C(41)	5577(9)	-973(5)	6339(4)	21(2)
C(42)	4749(9)	-1101(6)	6767(4)	20(2)

C(43)	3936(9)	-533(5)	6902(4)	19(1)
C(44)	3073(9)	-562(5)	7374(4)	17(1)
C(45)	2922(9)	-1166(5)	7733(4)	13(1)
C(46)	2056(9)	-1125(5)	8151(4)	10(1)
C(47)	1325(9)	-506(5)	8201(4)	14(1)
C(48)	1538(9)	95(6)	7821(4)	16(2)
C(49)	1225(9)	992(6)	6002(4)	23(1)
C(50)	144(10)	946(6)	5605(4)	25(2)
C(51)	84(9)	1496(6)	5212(4)	30(1)
C(52)	1199(9)	2121(6)	5202(4)	29(2)
C(53)	2282(9)	2174(6)	5551(4)	28(1)
C(54)	2302(9)	1616(5)	5970(4)	23(1)
C(55)	-1068(9)	1522(6)	4752(4)	34(2)
C(56)	-2223(10)	815(6)	4843(5)	35(3)
C(57)	-697(12)	1449(7)	4163(4)	42(3)
C(58)	-1686(11)	2293(6)	4880(5)	43(3)
C(59)	3491(9)	2851(6)	5550(4)	33(2)
C(60)	4727(10)	2461(7)	5435(5)	37(3)
C(61)	3289(12)	3410(6)	5080(5)	37(3)
C(62)	3705(12)	3325(7)	6101(4)	38(3)
C(64)	2397(8)	2968(5)	7605(5)	33(1)
C(63)	2699(9)	2225(5)	7458(5)	32(1)
C(65)	3438(9)	3535(6)	7818(5)	33(2)
C(66)	4772(9)	3413(5)	7870(5)	34(1)
C(67)	5057(10)	2673(5)	7721(5)	33(2)
C(68)	4059(9)	2057(5)	7517(5)	31(1)
C(69)	965(9)	3171(6)	7526(4)	35(2)
C(70)	6(10)	2593(6)	7855(5)	34(3)
C(71)	524(11)	3077(7)	6899(4)	38(3)
C(72)	799(12)	4004(6)	7738(5)	46(3)
C(73)	5876(10)	4073(6)	8046(4)	39(2)
C(74)	6763(11)	4215(7)	7540(5)	44(3)
C(75)	5443(11)	4836(6)	8231(5)	43(3)
C(76)	6772(11)	3791(7)	8522(5)	48(3)

Table 3. Bond lengths [A] and angles [deg] for sbse.

Co(1)-O(3)	1.841(6)
Co(1)-O(4)	1.877(6)
Co(1)-O(2)	1.909(6)
Co(1)-O(1)	1.915(6)
Co(1)-N(2)	1.916(7)
Co(1)-N(1)	1.927(7)
Br(1)-C(3)	1.886(9)
Br(2)-C(8)	1.936(9)
N(1)-C(1)	1.344(11)
N(1)-C(5)	1.382(10)
N(2)-C(6)	1.344(10)
N(2)-C(10)	1.345(10)
O(1)-C(11)	1.278(10)
O(2)-C(16)	1.298(10)
O(3)-C(26)	1.366(10)
O(4)-C(30)	1.320(10)
C(1)-C(2)	1.355(12)
C(2)-C(3)	1.383(12)
C(3)-C(4)	1.366(12)
C(4)-C(5)	1.396(12)
C(5)-C(6)	1.468(11)
C(6)-C(7)	1.362(11)
C(7)-C(8)	1.380(12)
C(8)-C(9)	1.335(12)
C(9)-C(10)	1.385(12)
C(11)-C(12)	1.387(11)
C(11)-C(16)	1.452(11)
C(12)-C(13)	1.354(12)
C(13)-C(14)	1.468(11)
C(13)-C(17)	1.552(11)
C(14)-C(15)	1.341(11)
C(15)-C(16)	1.402(11)
C(15)-C(21)	1.581(11)
C(17)-C(19)	1.481(12)
C(17)-C(20)	1.555(12)
C(17)-C(18)	1.601(12)
C(21)-C(24)	1.491(12)
C(21)-C(23)	1.529(12)
C(21)-C(22)	1.533(12)
C(25)-C(26)	1.381(12)
C(25)-C(27)	1.394(11)
C(25)-C(31)	1.532(11)

C(26)-C(30)	1.438(11)
C(27)-C(28)	1.394(11)
C(28)-C(29)	1.375(12)
C(28)-C(35)	1.522(11)
C(29)-C(30)	1.407(12)
C(31)-C(33)	1.531(12)
C(31)-C(34)	1.533(12)
C(31)-C(32)	1.571(12)
C(35)-C(37)	1.487(13)
C(35)-C(36)	1.550(12)
C(35)-C(38)	1.551(13)
Co(2)-O(7)	1.849(7)
Co(2)-O(6)	1.874(6)
Co(2)-O(8)	1.887(6)
Co(2)-O(5)	1.919(6)
Co(2)-N(3)	1.929(7)
Co(2)-N(4)	1.956(7)
Br(3)-C(41)	1.880(9)
Br(4)-C(46)	1.894(8)
N(3)-C(39)	1.353(11)
N(3)-C(43)	1.367(11)
N(4)-C(44)	1.319(10)
N(4)-C(48)	1.339(11)
O(5)-C(49)	1.286(10)
O(6)-C(54)	1.300(10)
O(7)-C(63)	1.363(10)
O(8)-C(68)	1.315(10)
C(39)-C(40)	1.353(12)
C(40)-C(41)	1.381(12)
C(41)-C(42)	1.368(12)
C(42)-C(43)	1.392(12)
C(43)-C(44)	1.466(12)
C(44)-C(45)	1.363(11)
C(45)-C(46)	1.375(11)
C(46)-C(47)	1.372(11)
C(47)-C(48)	1.398(12)
C(49)-C(50)	1.392(12)
C(49)-C(54)	1.437(11)
C(50)-C(51)	1.355(12)
C(51)-C(52)	1.459(12)
C(51)-C(55)	1.554(12)
C(52)-C(53)	1.325(12)
C(53)-C(54)	1.407(12)
C(53)-C(59)	1.577(12)
C(55)-C(57)	1.481(13)
C(55)-C(58)	1.558(13)

C(55)-C(56)	1.606(12)
C(59)-C(62)	1.505(12)
C(59)-C(61)	1.520(13)
C(59)-C(60)	1.526(13)
C(64)-C(63)	1.383(12)
C(64)-C(65)	1.396(12)
C(64)-C(69)	1.537(12)
C(63)-C(68)	1.442(12)
C(65)-C(66)	1.392(12)
C(66)-C(67)	1.373(12)
C(66)-C(73)	1.513(12)
C(67)-C(68)	1.416(12)
C(69)-C(71)	1.527(13)
C(69)-C(72)	1.527(13)
C(69)-C(70)	1.567(12)
C(73)-C(75)	1.489(13)
C(73)-C(76)	1.537(13)
C(73)-C(74)	1.557(13)

O(3)-Co(1)-O(4)	89.4(3)
O(3)-Co(1)-O(2)	90.7(3)
O(4)-Co(1)-O(2)	91.2(3)
O(3)-Co(1)-O(1)	91.1(3)
O(4)-Co(1)-O(1)	177.0(3)
O(2)-Co(1)-O(1)	85.8(3)
O(3)-Co(1)-N(2)	93.2(3)
O(4)-Co(1)-N(2)	92.5(3)
O(2)-Co(1)-N(2)	174.6(3)
O(1)-Co(1)-N(2)	90.4(3)
O(3)-Co(1)-N(1)	174.3(3)
O(4)-Co(1)-N(1)	87.3(3)
O(2)-Co(1)-N(1)	93.9(3)
O(1)-Co(1)-N(1)	92.4(3)
N(2)-Co(1)-N(1)	82.4(3)
C(1)-N(1)-C(5)	116.6(8)
C(1)-N(1)-Co(1)	128.8(6)
C(5)-N(1)-Co(1)	114.4(6)
C(6)-N(2)-C(10)	117.9(7)
C(6)-N(2)-Co(1)	117.0(6)
C(10)-N(2)-Co(1)	125.1(6)
C(11)-O(1)-Co(1)	109.7(5)
C(16)-O(2)-Co(1)	111.3(6)
C(26)-O(3)-Co(1)	110.2(5)
C(30)-O(4)-Co(1)	108.3(5)
N(1)-C(1)-C(2)	124.5(9)
C(1)-C(2)-C(3)	118.0(9)

C(4)-C(3)-C(2)	120.8(9)
C(4)-C(3)-Br(1)	120.8(7)
C(2)-C(3)-Br(1)	118.4(7)
C(3)-C(4)-C(5)	118.2(9)
N(1)-C(5)-C(4)	121.7(8)
N(1)-C(5)-C(6)	113.4(7)
C(4)-C(5)-C(6)	124.8(8)
N(2)-C(6)-C(7)	122.6(8)
N(2)-C(6)-C(5)	112.5(7)
C(7)-C(6)-C(5)	124.8(8)
C(6)-C(7)-C(8)	116.9(9)
C(9)-C(8)-C(7)	123.1(9)
C(9)-C(8)-Br(2)	120.7(7)
C(7)-C(8)-Br(2)	116.0(7)
C(8)-C(9)-C(10)	116.4(9)
N(2)-C(10)-C(9)	123.1(9)
O(1)-C(11)-C(12)	121.1(8)
O(1)-C(11)-C(16)	118.5(7)
C(12)-C(11)-C(16)	120.4(8)
C(13)-C(12)-C(11)	120.0(9)
C(12)-C(13)-C(14)	118.4(8)
C(12)-C(13)-C(17)	125.9(8)
C(14)-C(13)-C(17)	115.7(8)
C(15)-C(14)-C(13)	123.6(9)
C(14)-C(15)-C(16)	117.4(8)
C(14)-C(15)-C(21)	123.5(8)
C(16)-C(15)-C(21)	118.8(7)
O(2)-C(16)-C(15)	125.3(8)
O(2)-C(16)-C(11)	114.6(8)
C(15)-C(16)-C(11)	120.0(8)
C(19)-C(17)-C(13)	111.6(8)
C(19)-C(17)-C(20)	112.3(8)
C(13)-C(17)-C(20)	110.5(8)
C(19)-C(17)-C(18)	107.6(8)
C(13)-C(17)-C(18)	108.1(7)
C(20)-C(17)-C(18)	106.4(8)
C(24)-C(21)-C(23)	109.7(8)
C(24)-C(21)-C(22)	110.6(8)
C(23)-C(21)-C(22)	108.4(8)
C(24)-C(21)-C(15)	108.8(8)
C(23)-C(21)-C(15)	110.6(7)
C(22)-C(21)-C(15)	108.7(8)
C(26)-C(25)-C(27)	118.9(8)
C(26)-C(25)-C(31)	121.5(7)
C(27)-C(25)-C(31)	119.6(8)
O(3)-C(26)-C(25)	126.4(7)

O(3)-C(26)-C(30)	113.5(8)
C(25)-C(26)-C(30)	120.0(8)
C(25)-C(27)-C(28)	122.8(9)
C(29)-C(28)-C(27)	117.8(8)
C(29)-C(28)-C(35)	119.2(8)
C(27)-C(28)-C(35)	122.9(8)
C(28)-C(29)-C(30)	122.2(9)
O(4)-C(30)-C(29)	123.4(8)
O(4)-C(30)-C(26)	118.3(7)
C(29)-C(30)-C(26)	118.0(8)
C(33)-C(31)-C(25)	107.5(8)
C(33)-C(31)-C(34)	109.0(8)
C(25)-C(31)-C(34)	114.6(8)
C(33)-C(31)-C(32)	107.3(8)
C(25)-C(31)-C(32)	111.7(8)
C(34)-C(31)-C(32)	106.4(8)
C(37)-C(35)-C(28)	114.2(8)
C(37)-C(35)-C(36)	109.2(8)
C(28)-C(35)-C(36)	110.1(8)
C(37)-C(35)-C(38)	108.3(8)
C(28)-C(35)-C(38)	107.7(8)
C(36)-C(35)-C(38)	107.2(8)
O(7)-Co(2)-O(6)	89.3(3)
O(7)-Co(2)-O(8)	87.2(3)
O(6)-Co(2)-O(8)	90.8(3)
O(7)-Co(2)-O(5)	89.5(3)
O(6)-Co(2)-O(5)	86.0(3)
O(8)-Co(2)-O(5)	175.4(3)
O(7)-Co(2)-N(3)	175.7(3)
O(6)-Co(2)-N(3)	92.9(3)
O(8)-Co(2)-N(3)	89.0(3)
O(5)-Co(2)-N(3)	94.4(3)
O(7)-Co(2)-N(4)	96.2(3)
O(6)-Co(2)-N(4)	174.3(3)
O(8)-Co(2)-N(4)	91.1(3)
O(5)-Co(2)-N(4)	92.4(3)
N(3)-Co(2)-N(4)	81.8(3)
C(39)-N(3)-C(43)	116.9(8)
C(39)-N(3)-Co(2)	128.0(6)
C(43)-N(3)-Co(2)	115.1(6)
C(44)-N(4)-C(48)	121.5(8)
C(44)-N(4)-Co(2)	115.5(6)
C(48)-N(4)-Co(2)	123.0(6)
C(49)-O(5)-Co(2)	108.3(5)
C(54)-O(6)-Co(2)	111.3(5)
C(63)-O(7)-Co(2)	109.0(6)

C(68)-O(8)-Co(2)	106.3(6)
N(3)-C(39)-C(40)	123.6(9)
C(39)-C(40)-C(41)	119.2(9)
C(42)-C(41)-C(40)	119.4(9)
C(42)-C(41)-Br(3)	120.1(7)
C(40)-C(41)-Br(3)	120.4(7)
C(41)-C(42)-C(43)	119.0(9)
N(3)-C(43)-C(42)	121.8(8)
N(3)-C(43)-C(44)	113.2(8)
C(42)-C(43)-C(44)	125.0(8)
N(4)-C(44)-C(45)	121.2(8)
N(4)-C(44)-C(43)	114.2(8)
C(45)-C(44)-C(43)	124.6(8)
C(44)-C(45)-C(46)	118.4(8)
C(47)-C(46)-C(45)	121.2(8)
C(47)-C(46)-Br(4)	119.1(7)
C(45)-C(46)-Br(4)	119.7(7)
C(46)-C(47)-C(48)	117.2(9)
N(4)-C(48)-C(47)	120.4(9)
O(5)-C(49)-C(50)	123.1(8)
O(5)-C(49)-C(54)	118.4(8)
C(50)-C(49)-C(54)	118.4(8)
C(51)-C(50)-C(49)	120.8(9)
C(50)-C(51)-C(52)	118.5(8)
C(50)-C(51)-C(55)	126.1(8)
C(52)-C(51)-C(55)	115.5(8)
C(53)-C(52)-C(51)	123.5(9)
C(52)-C(53)-C(54)	117.1(8)
C(52)-C(53)-C(59)	124.2(9)
C(54)-C(53)-C(59)	118.6(8)
O(6)-C(54)-C(53)	124.1(8)
O(6)-C(54)-C(49)	114.3(8)
C(53)-C(54)-C(49)	121.6(8)
C(57)-C(55)-C(51)	115.4(9)
C(57)-C(55)-C(58)	112.7(9)
C(51)-C(55)-C(58)	106.5(8)
C(57)-C(55)-C(56)	107.8(8)
C(51)-C(55)-C(56)	108.5(8)
C(58)-C(55)-C(56)	105.4(8)
C(62)-C(59)-C(61)	108.3(8)
C(62)-C(59)-C(60)	110.3(9)
C(61)-C(59)-C(60)	107.3(9)
C(62)-C(59)-C(53)	111.9(8)
C(61)-C(59)-C(53)	111.6(8)
C(60)-C(59)-C(53)	107.4(8)
C(63)-C(64)-C(65)	118.0(8)

C(63)-C(64)-C(69)	121.1(8)
C(65)-C(64)-C(69)	120.9(8)
O(7)-C(63)-C(64)	127.4(8)
O(7)-C(63)-C(68)	112.5(8)
C(64)-C(63)-C(68)	120.0(8)
C(66)-C(65)-C(64)	124.4(9)
C(67)-C(66)-C(65)	116.9(9)
C(67)-C(66)-C(73)	120.9(8)
C(65)-C(66)-C(73)	122.2(9)
C(66)-C(67)-C(68)	122.4(9)
O(8)-C(68)-C(67)	124.1(8)
O(8)-C(68)-C(63)	117.7(8)
C(67)-C(68)-C(63)	118.2(9)
C(71)-C(69)-C(72)	108.8(9)
C(71)-C(69)-C(64)	108.3(8)
C(72)-C(69)-C(64)	114.1(8)
C(71)-C(69)-C(70)	108.8(8)
C(72)-C(69)-C(70)	106.6(8)
C(64)-C(69)-C(70)	110.1(8)
C(75)-C(73)-C(66)	116.0(9)
C(75)-C(73)-C(76)	109.0(9)
C(66)-C(73)-C(76)	108.5(8)
C(75)-C(73)-C(74)	108.7(9)
C(66)-C(73)-C(74)	107.9(9)
C(76)-C(73)-C(74)	106.2(9)

Table 4. Anisotropic displacement parameters (A^2 x 10^3) for sbse.
The anisotropic displacement factor exponent takes the form:
-2 pi^2 [h^2 a*^2 U11 + ... + 2 h k a* b* U12]

	U11	U22	U33	U23	U13	U12
Co(1)	6(1)	28(1)	36(1)	3(1)	-5(1)	-2(1)
Br(1)	20(1)	53(1)	56(1)	-9(1)	4(1)	12(1)
Br(2)	22(1)	39(1)	54(1)	10(1)	1(1)	-7(1)
N(1)	19(2)	23(2)	26(2)	-3(2)	-3(2)	-1(2)
N(2)	12(2)	14(2)	21(2)	-1(2)	-2(2)	4(2)
O(1)	9(3)	29(3)	27(3)	5(2)	-3(2)	-5(2)
O(2)	22(3)	36(3)	30(3)	7(2)	-3(2)	3(2)
O(3)	13(3)	24(3)	34(3)	1(2)	0(2)	-1(2)
O(4)	10(3)	27(3)	33(3)	1(2)	-1(2)	-2(2)
C(1)	21(2)	25(2)	28(3)	-5(2)	0(2)	-3(2)
C(2)	21(3)	28(3)	29(3)	-5(2)	1(2)	-2(2)
C(3)	19(2)	27(3)	29(3)	-5(2)	1(2)	-1(2)
C(4)	18(2)	23(2)	26(2)	-2(2)	-2(2)	0(2)
C(5)	18(2)	20(2)	24(2)	-4(2)	-3(2)	0(2)
C(6)	16(2)	18(2)	24(2)	-1(2)	-4(2)	5(2)
C(7)	18(2)	25(2)	25(2)	-2(2)	-3(2)	1(2)
C(8)	20(2)	26(3)	25(3)	-1(2)	-4(2)	1(2)
C(9)	20(3)	27(3)	27(3)	-1(2)	-3(2)	0(2)
C(10)	17(3)	21(3)	24(3)	-3(2)	-2(2)	6(2)
C(11)	10(2)	29(2)	28(2)	9(2)	-3(2)	-2(2)
C(12)	11(3)	29(3)	32(3)	8(3)	-1(2)	-2(2)
C(13)	14(2)	30(2)	35(2)	7(2)	-4(2)	2(2)
C(14)	15(3)	30(3)	34(3)	8(3)	-4(2)	4(2)
C(15)	16(2)	32(2)	34(2)	10(2)	-5(2)	3(2)
C(16)	15(2)	32(2)	29(2)	10(2)	-4(2)	1(2)
C(17)	17(3)	31(3)	40(3)	6(3)	-8(3)	0(3)
C(18)	27(5)	41(6)	49(6)	11(5)	-12(5)	-7(5)
C(19)	21(5)	39(6)	47(6)	-3(5)	-12(5)	-4(5)
C(20)	25(5)	27(5)	42(6)	2(5)	-10(5)	-1(5)
C(21)	20(3)	39(3)	39(3)	13(3)	-5(3)	-4(3)
C(22)	19(5)	52(6)	43(6)	14(5)	-4(5)	-17(5)
C(23)	26(5)	58(6)	55(6)	19(5)	-2(5)	-20(5)
C(24)	32(5)	29(5)	42(5)	15(4)	-2(4)	-13(4)
C(25)	16(2)	27(2)	43(2)	2(2)	-1(2)	0(2)

C(26)	15(2)	26(2)	37(2)	4(2)	-2(2)	-3(2)
C(27)	16(3)	24(3)	42(3)	1(3)	-2(3)	-1(2)
C(28)	15(2)	25(2)	42(2)	2(2)	-6(2)	-6(2)
C(29)	14(3)	28(3)	41(3)	3(3)	-4(3)	-7(3)
C(30)	13(2)	27(2)	36(2)	4(2)	-2(2)	-5(2)
C(31)	17(3)	30(3)	50(3)	0(3)	-2(3)	5(3)
C(32)	13(4)	25(4)	45(5)	0(4)	0(4)	14(4)
C(33)	18(5)	32(5)	61(6)	9(5)	-7(5)	6(5)
C(34)	10(5)	39(6)	60(6)	-9(5)	-5(5)	10(5)
C(35)	19(3)	28(3)	46(3)	2(3)	-11(3)	-6(3)
C(36)	24(5)	35(6)	56(6)	6(5)	-13(5)	-8(5)
C(37)	21(5)	40(6)	53(6)	-3(5)	-12(5)	-7(5)
C(38)	35(6)	35(6)	56(6)	3(5)	-25(5)	-13(5)
Co(2)	9(1)	25(1)	40(1)	6(1)	-6(1)	-4(1)
Br(3)	19(1)	44(1)	56(1)	-7(1)	4(1)	5(1)
Br(4)	23(1)	30(1)	51(1)	9(1)	3(1)	-4(1)
N(3)	14(2)	19(2)	23(2)	2(2)	0(2)	-5(2)
N(4)	11(2)	18(2)	19(2)	0(2)	-4(2)	-6(2)
O(5)	12(3)	22(3)	27(3)	3(2)	-7(2)	1(2)
O(6)	16(3)	13(3)	25(3)	5(2)	-6(2)	-6(2)
O(7)	20(3)	28(3)	38(3)	3(2)	-4(2)	2(2)
O(8)	17(3)	27(3)	36(3)	-3(2)	-11(2)	0(2)
C(39)	18(2)	21(2)	23(3)	1(2)	0(2)	-3(2)
C(40)	19(2)	22(3)	22(3)	1(2)	2(2)	-2(2)
C(41)	19(2)	20(2)	23(3)	0(2)	2(2)	-2(2)
C(42)	18(2)	19(2)	22(2)	0(2)	-1(2)	-4(2)
C(43)	14(2)	19(2)	21(2)	1(2)	-2(2)	-4(2)
C(44)	12(2)	17(2)	20(2)	0(2)	-5(2)	-5(2)
C(45)	8(2)	10(2)	20(2)	1(2)	-5(2)	2(2)
C(46)	6(2)	6(2)	18(2)	4(2)	-4(2)	-1(2)
C(47)	7(2)	12(2)	22(2)	1(2)	-4(2)	1(2)
C(48)	9(3)	16(3)	21(3)	-1(2)	-5(2)	-4(2)
C(49)	14(2)	22(2)	30(2)	6(2)	-7(2)	-1(2)
C(50)	18(3)	24(3)	32(3)	7(3)	-7(2)	-1(2)
C(51)	22(2)	27(2)	38(2)	5(2)	-7(2)	-1(2)
C(52)	23(3)	26(3)	38(3)	7(3)	-5(3)	-1(2)
C(53)	21(2)	25(2)	36(2)	8(2)	-4(2)	-2(2)
C(54)	17(2)	20(2)	30(2)	8(2)	-5(2)	-3(2)
C(55)	24(3)	32(3)	43(3)	1(3)	-9(3)	0(3)
C(56)	23(5)	30(6)	51(6)	0(5)	-6(5)	-3(5)
C(57)	25(5)	46(6)	50(6)	-3(5)	-14(5)	-12(5)
C(58)	30(5)	46(6)	49(6)	-5(5)	-25(5)	10(5)
C(59)	24(3)	32(3)	40(3)	7(3)	-2(3)	-8(3)
C(60)	22(5)	32(6)	50(6)	3(5)	0(5)	-18(5)
C(61)	28(5)	33(6)	48(6)	15(5)	-1(5)	-5(5)
C(62)	35(6)	33(6)	41(6)	10(5)	4(5)	-15(5)

C(64)	20(2)	30(2)	47(2)	6(2)	-3(2)	-3(2)
C(63)	20(2)	30(2)	43(2)	4(2)	-5(2)	0(2)
C(65)	21(3)	29(3)	47(3)	1(3)	-6(3)	-3(3)
C(66)	24(2)	28(2)	49(2)	0(2)	-5(2)	-2(2)
C(67)	22(3)	27(3)	46(3)	1(3)	-7(3)	0(3)
C(68)	19(2)	28(2)	43(2)	2(2)	-8(2)	-1(2)
C(69)	17(3)	30(3)	56(3)	10(3)	1(3)	-2(3)
C(70)	23(5)	27(5)	55(6)	16(5)	6(5)	2(5)
C(71)	10(5)	33(6)	69(6)	14(5)	3(5)	-6(5)
C(72)	24(5)	42(6)	73(6)	8(6)	3(5)	1(5)
C(73)	29(3)	30(3)	55(3)	-1(3)	-5(3)	-5(3)
C(74)	33(6)	32(6)	62(6)	-1(5)	-1(5)	-5(5)
C(75)	31(6)	33(6)	60(6)	-9(5)	-16(5)	-12(5)
C(76)	40(6)	41(6)	57(6)	0(6)	-6(5)	-19(5)

Table 5. Hydrogen coordinates (x 10^4) and isotropic displacement parameters (A^2 x 10^3) for sbse.

	x	y	z	U(eq)
H(1A)	4713	1240	633	31
H(2A)	6097	350	377	32
H(4A)	5145	-881	1745	27
H(7A)	3694	-980	2443	28
H(9A)	945	107	3213	30
H(10A)	1324	1136	2601	25
H(12A)	-425	778	383	29
H(14A)	1113	2555	-564	32
H(18A)	-2914	768	-695	61
H(18B)	-2519	1101	-61	61
H(18C)	-1840	380	-311	61
H(19A)	235	1445	-1248	55
H(19B)	-1269	1088	-1438	55
H(19C)	-347	590	-1059	55
H(20A)	-954	2642	-877	48
H(20B)	-1936	2464	-384	48
H(20C)	-2387	2140	-1015	48
H(22A)	5393	3360	35	60
H(22B)	4729	2507	-208	60
H(22C)	4883	2700	458	60
H(23A)	2172	3656	-566	72
H(23B)	3296	3188	-812	72
H(23C)	3691	4055	-527	72
H(24A)	3843	4293	447	53
H(24B)	3552	3612	882	53
H(24C)	2341	3928	532	53
H(27A)	3090	4066	3316	34
H(29A)	6028	2987	2709	35
H(32A)	-932	2713	2732	40
H(32B)	142	2466	3192	40
H(32C)	176	2187	2545	40
H(33A)	-406	3660	2073	55
H(33B)	814	3280	1826	55
H(33C)	1020	4178	2062	55
H(34A)	1196	4514	3072	55
H(34B)	940	3844	3519	55
H(34C)	-272	4063	3116	55

H(36A)	6387	4979	3021	60
H(36B)	7091	4214	2884	60
H(36C)	7555	4751	3444	60
H(37A)	4804	4974	3728	60
H(37B)	5897	4788	4203	60
H(37C)	4491	4242	4120	60
H(38A)	6937	3702	4191	67
H(38B)	7163	3251	3611	67
H(38C)	5857	2994	3937	67
H(39A)	4651	658	5943	25
H(40A)	6068	-225	5719	26
H(42A)	4729	-1570	6969	24
H(45A)	3404	-1604	7694	15
H(47A)	701	-486	8480	17
H(48A)	1066	539	7847	20
H(50A)	-559	524	5609	30
H(52A)	1146	2511	4931	35
H(56A)	-2956	822	4554	53
H(56B)	-2554	881	5218	53
H(56C)	-1865	310	4811	53
H(57A)	41	1857	4102	64
H(57B)	-1465	1512	3905	64
H(57C)	-419	928	4091	64
H(58A)	-1026	2750	4830	64
H(58B)	-1949	2301	5269	64
H(58C)	-2471	2312	4621	64
H(60A)	5489	2868	5411	55
H(60B)	4569	2147	5079	55
H(60C)	4917	2118	5743	55
H(61A)	2424	3605	5104	55
H(61B)	3311	3131	4714	55
H(61C)	4001	3856	5118	55
H(62A)	4515	3702	6098	56
H(62B)	3798	2971	6411	56
H(62C)	2939	3612	6152	56
H(65A)	3221	4037	7935	40
H(67A)	5958	2571	7757	39
H(70A)	-920	2668	7752	52
H(70B)	199	2700	8261	52
H(70C)	138	2048	7757	52
H(71A)	-382	3215	6839	57
H(71B)	540	2529	6767	57
H(71C)	1133	3426	6687	57
H(72A)	1248	4388	7496	70
H(72B)	1194	4096	8126	70
H(72C)	-151	4063	7730	70

H(74A)	6254	4433	7232	65
H(74B)	7038	3714	7408	65
H(74C)	7554	4588	7660	65
H(75A)	4934	5042	7918	65
H(75B)	6228	5215	8348	65
H(75C)	4880	4753	8549	65
H(76A)	7539	4193	8617	72
H(76B)	7086	3298	8399	72
H(76C)	6263	3702	8856	72